Full Release

ORNL-3900

(600)

ANNUAL REPORT 1964

65025

OAK RIDGE NATIONAL LABORATORY

ChemRisk Document No. 1006

ANNUAL REPORT

1964

OAK RIDGE NATIONAL LABORATORY

OPERATED BY UNION CARBIDE CORPORATION • FOR THE U.S. ATOMIC ENERGY COMMISSION

ORNL-3900

CONTRACT NO. W-7405-ENG-26

ABOUT THE COVER

The pale blue glow shown in the cover picture is produced by a beam of high-energy deuterons emerging from the beam port of the Oak Ridge Isochronous Cyclotron. This 76-inch sector-focusing cyclotron is one of the forerunners of a new generation of resonance accelerators in which a very carefully designed magnetic field focuses the ions throughout their acceleration and also compensates for the phase drift that would occur in a classical cyclotron as the particles approach relativistic velocities (i.e., becoming heavier due to increasing kinetic energy). The ORIC also accelerates protons, alpha particles, and helium-3 and carbon-12 particles to a range of energies between 10 and 100 Mev. Since November 1964 the cyclotron has been in use on a 24-hours-a-day, seven-days-a-week schedule, accomplishing a wide variety of experiments in nuclear physics, nuclear chemistry, biology, and space instrumentation. To obtain the photograph of the beam, the camera shutter was opened in the totally darkened cyclotron vault, the shield doors were closed, and the cyclotron was operated for 90 minutes with about a quarter of a microampere of deuterons emerging from the beam port through a thin aluminum window. The exposure was made using professional color negative film; the camera stop was set at *f* 4.5, and at the end a single flash bulb was set off to illuminate the external beam equipment. This 34-Mev deuteron beam is believed to be the highest-energy external beam ever photographed. The full range of the beam, close to 20 feet, is not quite fully shown, as the beam was intercepted at the wall, which was only 19 feet away. The pink glow at the left is light emitted from concrete blocks being struck by scattered deuterons close to the end of their range.

CONTENTS

REACTOR DEVELOPMENT

Gas-Cooled Reactor Program 4
- Experimental Gas-Cooled Reactor 4
  - EGCR Control-Rod Environmental Test 4
  - Irradiation Testing of the EGCR Fuel Element 5
  - Engineering Mechanics 6
- Testing of Fueled-Graphite Spheres 6
- Impact Resistance of Fueled Graphite Spheres for Pebble-Bed Reactors 9
- Properties of Pyrolytic Carbon Coatings on Nuclear Fuel Particles 11
- Diffusion of Fuel Metals in Pyrocarbons 11
- Fission-Gas Release from Uranium Dioxide 11
- Creep of Graphite Under Irradiation 13
- Fission Product Transport and Deposition 13
- Reactor Analysis 14

Studies and Evaluations 15
- Fuel Shipment Studies 15
  - Computer Codes for Fuel Cycle Economics Studies 15
  - Shipping Containers 15

Applied and Basic Reactor Physics 17
- Reactor Shielding 17
  - Fast-Neutron Penetration and Scattering Experiments 17
  - Shielding Studies for SNAP Systems 18
  - Studies of Shielding Against Nuclear Weapons Radiation 20
  - Radiation Shielding Information Center 21
- Criticality Safety 21
  - Critical Dimensions of Arrays of Aqueous Uranyl Fluoride Solutions Containing Uranium Enriched to 5% in ^{235}U 22
  - Critical Experiments with SPERT-D Fuel Elements 23
- Basic Reactor Physics 26
  - Measurement of α as a Function of Energy 26
  - Neutron Cross-Section Studies 27
  - Pulsed-Neutron Measurements of Diffusion Parameters in Ordinary Ice as a Function of Temperature 28
  - Monte Carlo Calculations and Experiments with Enriched Uranium Metal Systems 30
- Reactor Theory 31

Reactor Fuels and Materials 32
High-Temperature Containment of Liquid Metals 32
SNAP-8 Corrosion Program 32
SNAP-50 Corrosion Test Loop 32
Forced-Circulation Boiling-Potassium Corrosion Loops 32
Fabrication of High-Temperature Materials from Vapors 32
Diffusion in Metals 39
Zirconium Metallurgy 39
Analysis of Complex Stresses in Zircaloy-2 39
Stress-Oriented Precipitation of Hydrides in Zircaloy-2 39
Determination of the (0001) Pole Figures in Zircaloy-2 by Quantitative Metallography 40
Zone-Refined and Single-Crystal Zirconium 40
Nondestructive Test Development 40
Use of X-Ray Television to Observe Hidden Motions 40
Radiography of Highly Radioactive Materials 40
Nondestructive Determination of Fuel Assay 40
Vibrating Eddy-Current Probe 41
Radiation Stability of Structural Metals 42
Atomic Rearrangements in Irradiated Alloys 42

Reactor Components 44
Reactor Controls Development 44
Measurement of Shutdown Reactivity 44
Coincidence Magnet for Reactor Safety Systems 44

Engineering Research 48
Heat Transfer and Fluid Mechanics 48

Power Reactor Fuel Processing 50
Chemical Analysis of Advanced Reactor Fuels 50
Head-End Processes for Power Reactor Fuels 50
Fuel Recovery Processes for Graphite-Type Fuels 50
Chop-Leach Process for Reactor Fuel Recovery 51
Thorium Reactor Fuel Processing 52
Fluoride Volatility Processing 52

Thorium Utilization Program 53
Extension of the Sol-Gel Process to the Preparation of Microspheres Containing Thorium 53
Molten-Salt Reactor Program 54
Introduction 54
Molten-Salt Reactor Experiment 54
Construction 54
Operation 55
Component Development 56
Sampler-Enricher 56
Oxygen-Removal Unit 58
Control Rod 58

Heaters 59
Fuel and Coolant Pumps 59

Chemical Development 61
Production of Fuel and Coolant Salts 61
Compatibility of Fuels and Materials 61

Fuel Processing 61
MSRE Processing Facility 61
Distillation of Molten Salts 62

Reactor Evaluations 63
Reactor Analysis 63
Advanced Converter Reactors 63
^{233}U Fuel Value Study 63
Thorium Breeder Reactor Study 64
Other Activities 64

Engineering Evaluations 65
Advanced Converter Study 65

Space Reactor Studies 66
Medium Power Reactor Experiment 66
Development of the Boiling Potassium Reactor System 66
MPRE Facility 67
Engineering Development 68

Nuclear Desalting Program 69
Dual-Purpose Reactors 69

System Studies 69

Low-Temperature Reactors 69

High Flux Isotope Reactor 71
Mechanical Design 71

Development and Testing 72

Nuclear Design 72

Safety Experiments with the High Flux Isotope Reactor Fuel Element 73

Nuclear Safety 74
Nuclear Safety Pilot Plant 74

Behavior of Fission Products on In-Pile Destruction of Reactor Fuels 75

Properties of Fission Product Aerosols Produced by Overheated Reactor Fuels 76

Nuclear Safety Information Center 76

Technical Progress Review "Nuclear Safety" 77

Reactor Containment Handbook 77

Radioactive Waste Disposal 78
Environmental Studies 78
Clinch River Study 78

Low-Level Radioactive Waste Disposal 78

Incorporation of Intermediate-Level Radioactive Waste in Asphalt 78

High-Level Radioactive Waste Disposal 79
Disposal in Geologic Formations 80
Disposal in Natural Salt Formations 80

PHYSICAL RESEARCH

Physics and Mathematics 83
Shielding Against High-Energy Radiations 83
Channeling of Fast Heavy Ions by an Ordered Crystal Lattice 84
Study of the Electrical Charge Distribution in Metallic Alloys Through the Use of the Mössbauer Effect 84
New Technique for Use in Nuclear and Solid-State Physics 86
Binding Energies of Nuclei 86
Analog States 87
Evidence for a Lambda-Nucleon Resonance 88
Fission Studies, Including New Energy Determinations Based on Measurements of High-Energy Bromine and Iodine Ions 89
Gamma-Ray Spectroscopy with Lithium-Drifted Germanium Detectors 90
The Explosion of Multicharged Molecular Ions 92
Polarized Proton Experiment 92
Nuclear Data Processed in 20,000-Channel Analyzers 94
Pickup Reactions 95
Oak Ridge Isochronous Cyclotron 95
The Separated-Orbit Cyclotron 97
Instrumentation and Controls Development 98
National Laboratory Instrument Modules 98
Electronic Circuitry 98
Computer Technology 98
Data Handling Techniques 99
Temperature Measurement 99
Gas Chromatography 101
Mathematics and Programming Research 101

Chemistry 103
Analytical Chemistry Research 103
Analytical Instrumentation 103
X-Ray and Spectrochemical Analyses 103
Mass Spectrometry 103
Isotopic Composition of Atmospheric Neon 104
Optical and Electron Microscopy 105
Special Research and Development Problems 105
Analytical Biochemistry 105
Effects of Radiation on Analytical Methods 105
Low-Cost Radiochemical Analyses by Gamma-Ray Spectrum Resolution 106
Mechanism of Radiation Corrosion of Zirconium Alloys 107

Chemical Engineering Research 107
Prediction of the Flow Capacity of Pulsed Columns 107
Effect of Ionizing Radiation on Coalescence Rates in Liquid-Liquid Systems 107
Separations Process Development 108
New Solvent Extraction Separations 108
Thorium Recovery from Granitic Rock 109
Separation of Transfer Ribonucleic Acids 109
Waste Streams from Plants Processing Uranium Ores 110
Fundamental Principles of Solvent Extraction 110
Preparation and Properties of Actinide-Element Oxides 111
Protactinium Chemistry 111
Irradiation Effects on Gas-Solid Systems 113
Surface Chemistry 113
Solubility of Magnetic Iron Oxide in High-Temperature Water 114
Physical Chemistry of Molten Salts 114
Crystal Studies 114
UF_4-UF_3 Equilibria 115
Viscosity of Molten Fluoride Mixtures 115
Gaseous Diffusion 116
Analytical Studies of Molten-Salt Systems 116
Chemical Research Related to the Desalination of Water 117
Properties of Solutions and Phase Studies 117
Concentration Polarization at Phase Boundaries 119
Periodic Phenomena in Flowing Suspensions 120
Reactions and Transport Phenomena at Surfaces 121
Corrosion Studies 122
Hyperfiltration (Reverse Osmosis) and Membrane Studies 124
Paramagnetic Resonance Studies of Short-Lived Free Radicals in Liquids 125
Stripping Processes in Chemically Reactive Collisions 126
Stereoscopic Crystal-Structure Illustrations Plotted by Computer Program 126
Solutions of Metals in Molten Salts 128
Transuranium-Element Processing 129
Development of Separation Processes 130
Metallurgy and Materials 132
Technical Accomplishments of the Pure Materials Program 132
Crystal Structure of Calcium Beryllate 133
Growth of Uranium Dioxide Single Crystals 133
Structure of Thin Films 134
Corrosion of Aluminum-Base Alloys 134
Oxidation of Refractory Metals 134
Metallurgical Application of the Mössbauer Effect 134
Direct Observation of Lattice Defects 134
Prediction of Thermal Conductivity 135

Effect of Fabrication Method on Metal Structure 136

Fundamental Investigation of Radiation Damage in Solids 136
Semiconductor Research 136
Effect of Ionizing Radiation on Ionic Crystals 137
Light Absorption and Emission by Alkali Halide Crystals 137
Neutron Spectrometer Facility 138
Channeling of Energetic Atoms in Solids 138
Neutron Diffraction 138
X-Ray Observations of Defects in Nearly Perfect Copper Crystals 140

Controlled Thermonuclear Research 142
Injection-Accumulation Program 142
General 142
The DCX-1 Experiment 143
DCX-2 144

Injection into a Hot-Electron Plasma 144

Ion Heating by Beam-Plasma Interaction 145

Flute Suppression on the Hydrogen Arc 147

Ion Sound Waves: Velocity Measurements by Time-of-Flight 148

The Magnet Laboratory 148

The Atomic and Molecular Processes Information Center 149

BIOLOGY AND MEDICINE

Somatic Effects of Radiation 151
Statistical Services and Research 151

Pathology and Physiology 151
Radiation-Induced Myeloid Leukemia 151

Radiation Genetics 153
Cytology and Genetics 153
Studies on Reparable Premutational Lesions with Alkylating Agents 153
Repair of Damage Induced in DNA by Ultraviolet Radiation 153
Are Sister Chromatid Exchanges Sister Strand Crossovers or Radiation-Induced Exchanges? 154
X-Ray-Induced Forward Mutation Rates for Mutants in the *ad-3* Region of *Neurospora* 154
Mammalian Cytology and Cytogenetic Effects of Radiation 155

Drosophila Cytology and Genetics 156
Distributive Pairing and Aneuploidy in Man 156

Mammalian Genetics 157
Induction of Mutations by Neutrons 157

Cooperative NIH-AEC Co-Carcinogenesis Program 158

Combating Detrimental Effects of Radiation 159
Mammalian Recovery 159
Effect of AET on Acute Lethality from Dimethylnitrosamine 159

Radiation Immunology 159

Aging and the Immune Mechanism 159

AEC-NASA Space Biology Program 160
Dosimetry of Beta-Ray Irradiation Device for Radiation–Space-Flight Interaction Experiment 160
Gemini III Experiment 160

Molecular- and Cellular-Level Studies 161
Cytochemistry and Cell Reproduction 161
Mutagenic Action During Meiosis and Antimutagenic Action During Mitosis by 5-Aminoacridine in Yeast 161

Cell Growth and Differentiation 161
Epigenetic Control of Genes 161

Radiation Microbiology 162
Postirradiation Growth, Division, and Recovery in Bacteria 162

Cell Physiology 163
Freezing of Multicellular Systems 163

Subcellular and Viral Physiology 163
Isolation of Rat Macroglobulin in the Zonal Centrifuge 163

Nucleic Acid Enzymology 164
Mechanism of Breakage and Rejoining of Bacteriophage T2 DNA 164

Enzymology 164
Protein Synthesis 164

Plant Physiology and Photosynthesis 165
Studies of Normal and Abnormal Development in Histologically Simple Structures During Growth Without Cell Division 165
Photosynthesis 166

Biophysics 166
UV Photoproducts Produced in Bacterial Spores 166
Re-Pairing of Long-Lived Free Radicals 166
Mechanism of DNA Transfer in Bacterial Mating 167

NIH-AEC Development of an Ultracentrifuge 167

Physics of Tissue Damage 168
Tracer Studies of Vacuum Pump Oil Deposition 168
Optical Studies of Graphite 168
Mean Free Paths of Low-Energy Electrons in Solids 168

Terrestrial and Freshwater Ecology 169

Radiological Physics, Health Physics, and Radiation Instrumentation 170
Radiation Physics 170
Atomic and Molecular Radiation Physics 170
Polarization Studies in the Vacuum Ultraviolet 171
Transition Radiation and Low-Energy Bremsstrahlung 171

Internal Dose Estimation 172

Health Physics Technology 172

HPRR Operations and Special Projects 173

Basic Instrumentation 173
Lithium-Drifted Germanium Detectors 173

Charge-Sensitive Preamplifier 176
Instrumentation for Photosynthesis Studies 176

Nuclear Energy Civil Effects 177
Dose Distribution Functions for Nuclear Weapons Radiation in Japanese Dwellings 177

Accelerator for Operation HENRE 177

Civil Defense 177

ISOTOPE DEVELOPMENT

Isotope Development 183

Nuclear and Radiochemical Analyses 183

Radioisotope Applied Research 183
Reactor-Produced ^{33}P 184
Radioisotope Generators 184
The (n,γ) Burnup of ^{146}Pm in ^{147}Pm 184
Other Radioisotope Production Studies 184
Computer Programming for Isotopes Calculations 184
Cyclotron-Produced Radioisotopes 185

Radioisotope Technology 185
Carbon-14 Process Improvement 185
Xenon-133, Iodine-131 Process Improvement 185
Krypton-85 Enrichment System 185
Technetium-99 Source Preparation 185
Americium-Beryllium-Curium Source 186
Iridium-192 Sources 186
Promethium-147 Source 188
Phosphorus-32 Sources 188
Simulation of Space Radiation Using the 86-Inch Cyclotron 188
Cooperative Programs with Industry 188
Fission Products Development Laboratory Operations 189

Radioisotope Safety 189
Source Classification System 189
Evaluation of Test Methods 189

Isotopes Information and Quarterly Review 190

Target Preparation 190

Electromagnetic Isotope Separations 191

TRAINING, EDUCATION, AND INFORMATION

University Relations 195

Oak Ridge School of Reactor Technology 196
Formal Programs at ORSORT 196

Assistance to Educational Institutions 196

Information Centers 198

Aging and the Immune Mechanism 159
AEC-NASA Space Biology Program 160
Dosimetry of Beta-Ray Irradiation Device for Radiation–Space-Flight

PHOTO 66931

ART WORK - NO NUMBER

REACTOR DEVELOPMENT

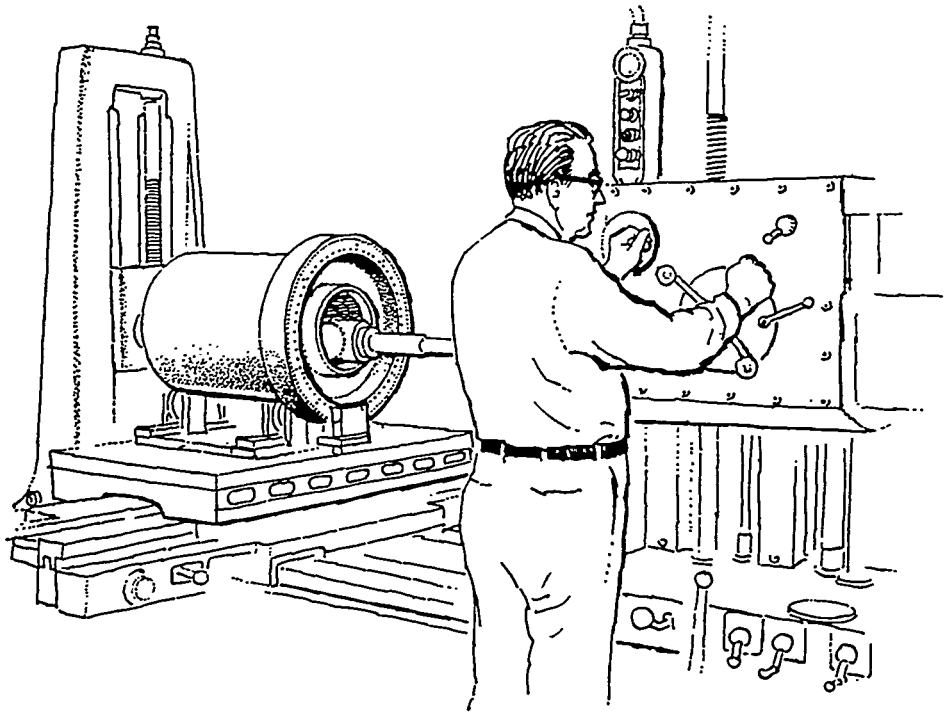

With the ending of 1964, economic nuclear power has become a reality. Consistent with this, much of the Oak Ridge National Laboratory's reactor development program is aimed at longer-range goals: thermal breeding, advanced reactors for space applications, and inexpensive energy sources for water desalination. The molten-salt reactor, which shows great promise as a thermal breeder, had its origin in the Aircraft Nuclear Propulsion Program. Among the many advantages of the molten-salt reactor are low inventory of fissionable material, good thermal efficiency at the high operating temperatures that are achieved, good compatibility of the fuel with existing materials of construction, and utilization of thorium as a fertile material. The use of a fluid fuel simplifies the reprocessing and fuel fabrication steps, and very low fuel cycle costs are predicted.

During the past year, attention was focused on one of the more difficult present-day problems: development of a light-weight, low-power reactor for space applications. The approach taken to this problem is strikingly simple: a reactor boils potassium, and the resulting potassium vapor operates a turbine in a direct cycle. Present indications are that the system is stable and that potassium cycles may even find use in commercial power production.

Perhaps the most exciting development of 1964 has been the acceptance of the belief that very large nuclear reactors may be used to desalt water inexpensively. Although the role of ORNL in the program is not yet well defined, evaporator technology and system studies seem to be two areas where need for additional work and Laboratory capability converge.

In addition to these main-line reactor programs, much research and development in support of the AEC's broader reactor program was carried out. For example, ORNL had a major responsibility for the instrumentation and control system and the fuel elements for the AEC's Experimental Gas-Cooled Reactor. The Laboratory also served as advisor to the AEC in the review of EGCR designs and in solving special problems which arose. With the fulfilling of some of these obligations in 1964, effort was diverted to the problems of advanced gas-cooled reactors, in particular to those related to fuel development. The Laboratory also assisted in solving some of the very difficult materials problems of certain of the AEC space reactors and carried out a comprehensive program on the evaluations of power reactor types, fuel cycles, and related problems. Many of these studies were made at the request of the USAEC, while others were made to guide the reactor development effort of the Laboratory.

GAS-COOLED REACTOR PROGRAM

EXPERIMENTAL GAS-COOLED REACTOR

EGCR Control-Rod Environmental Test

A test facility was constructed in which it has been possible to mock up the core graphite configuration of the EGCR control-rod channel and to simulate the helium coolant conditions with respect to temperature, pressure, and flow rate (Fig. 1). A prototype of the EGCR control-rod drive was tested to determine the normal operating characteristics and the scram characteristics in a straight control-rod channel and, also, in a bowed channel (Fig. 2). The mechanism was operated for over 900 hr, during which time the control rod was scrammed more than 2700 times. Abnormal conditions encountered during the testing resulted in corrections to the control-rod drives that are to be used in the reactor. Before installation in the EGCR, one of the drives will be performance tested as previously described, and then the rod will be subjected to an endurance test.

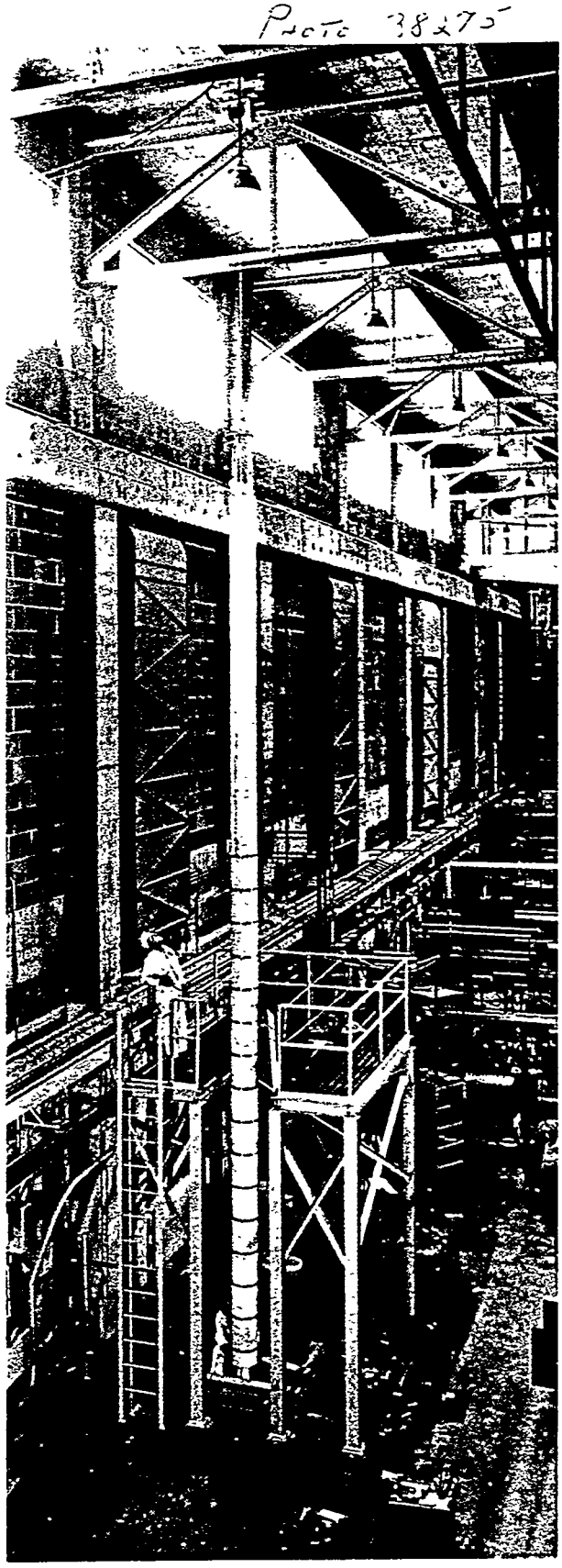

Fig. 1. Control-Rod Drive Test Facility. A mockup of one core channel of the EGCR is being inserted preparatory to testing the control-rod drive mechanism. From such tests, curves have been plotted to show the position of the control rod as a function of time during a reactor scram.

65-2858

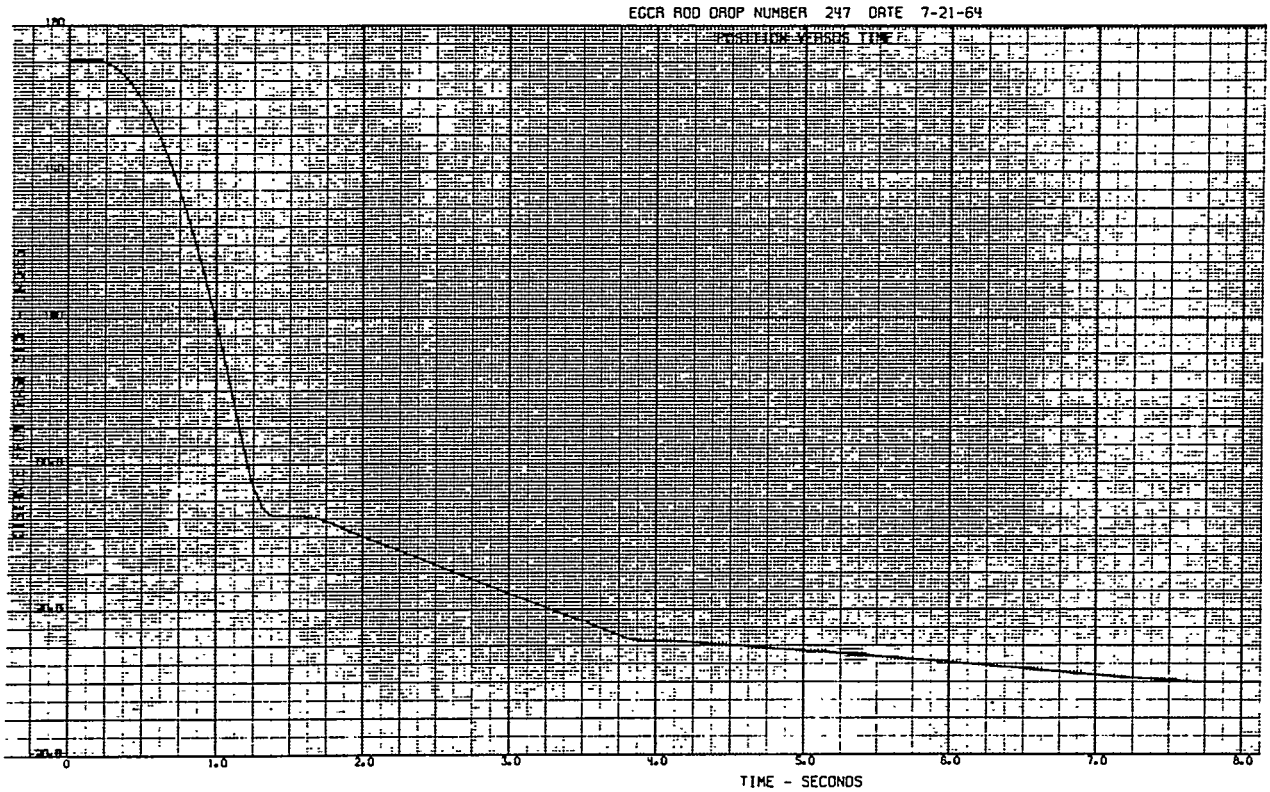

Fig. 2. Typical Data from the EGCR Control-Rod Drive Test. The position of the control rod is shown as a function of time during a scram.

Irradiation Testing of the EGCR Fuel Element

An extensive program of irradiation testing of the EGCR fuel element is nearing completion. The last 3 of 17 EGCR prototype capsules were removed from the ETR. Of the 13 ETR capsules examined thus far, 4 had cladding failures. However, each of these was considerably overpowered or was fueled with UO_2 that was relatively high in nitrogen – conditions outside the EGCR design. The expansion of overheated UO_2 imposed on nitride-embrittled cladding caused the failures.

Two capsules continue to be irradiated in the ORR. These are the last in a series to evaluate fuel and cladding materials taken from the production run for the EGCR core. Previous tests of production-run materials have indicated satisfactory performance up to 5000 Mwd/ton burnup, although one cladding failure occurred as a result of nitriding of the capsule vessel wall by the nitrogen gas used for temperature control. We intend to irradiate the remaining two capsules during 1965 and 1966 to demonstrate the capability of EGCR core materials for achieving a burnup of 10,000 Mwd per metric ton of uranium.

Engineering Mechanics

Although during 1964 most of our work involved graphite mechanics, we also devoted some effort to other stress analysis problems. In one study, for example, we made a three-way comparison between experimental data from a nozzle–spherical-vessel system and theoretical predictions using the CERL II code and the USA code. CERL II is an ORNL revision and enlargement of a British computer code originally developed by the Central Electrical Research Laboratory in London, and USA is a more generally applicable code developed at ORNL. Both theoretical codes predicted maximum stresses well, but CERL could not be used in some cases; and in some regions of lower stress, neither code predicted the experimental stress well.

During 1964, the principal effort of the graphite mechanics program was spent in completing the experimental work on EGCR-type AGOT graphite, in attempting to interpret the results in usable mathematical form, and in developing theoretical methods of using the resulting generalizations.

We improved techniques for tensile and compressive testing of graphite to the point where bending, torsion, and other extraneous effects became negligible. This resulted in considerably higher measured values of the strength. We also found that the more recent values correlated well with the results obtained in bend tests, provided the bend data included the shift in neutral axis due to the difference between the tensile and compressive stress-strain relationships. We developed digital and analog computer techniques for computing the location of the neutral axis, so that strain data from the extreme surfaces could be plotted directly as stress-strain curves for tension and compression.

Our measurements of strain ratio imply that a useful approximate failure criterion is a tensile strain, either direct or induced, of 0.15%. Our strain ratio tests also indicated that in graphite, unlike many other materials, volume changes are associated with the nonlinear parts of the stress-strain relationship. This implies that the nonlinear behavior is affected by the hydrostatic pressure. We have achieved some success in attempts to match the uniaxial test data by analytical relationships based on creep and plasticity models.

We began statistical studies to catalog the variations in the experimental data, and found a rough correlation between position in the original log and strength. The uncorrelated scatter was still high, however.

We completed development of the Non-Homogeneous Biharmonic Code (NBC). This code permits stress and strain solutions for any prismatic shape assuming plane stress or plane strain. We assume, in this calculation, that the material is elastic and isotropic in the transverse plane.

Using this code, we solved the case of a thick-walled cylinder with nonuniform neutron dosage, and with a modification, we analyzed a thick-walled elastoplastic cylinder.

TESTING OF FUELED-GRAPHITE SPHERES

As part of the continuing search to develop more efficient and more economical fuels for nuclear power reactors, prospective fuels are subjected to intensive irradiation testing to observe their behavior under conditions that closely match or exceed those expected in reactor service. We have recently completed a series of such tests that demonstrated the performance characteristics of an all-ceramic fuel element developed for high-temperature gas-cooled reactors. These tests employed specially designed containers or capsules that permitted the fuel to be held at a controlled high temperature (up to 2800°F) during irradiation in a low-temperature test reactor. One type of irradiation capsule used is shown in Fig. 3.

63-3061

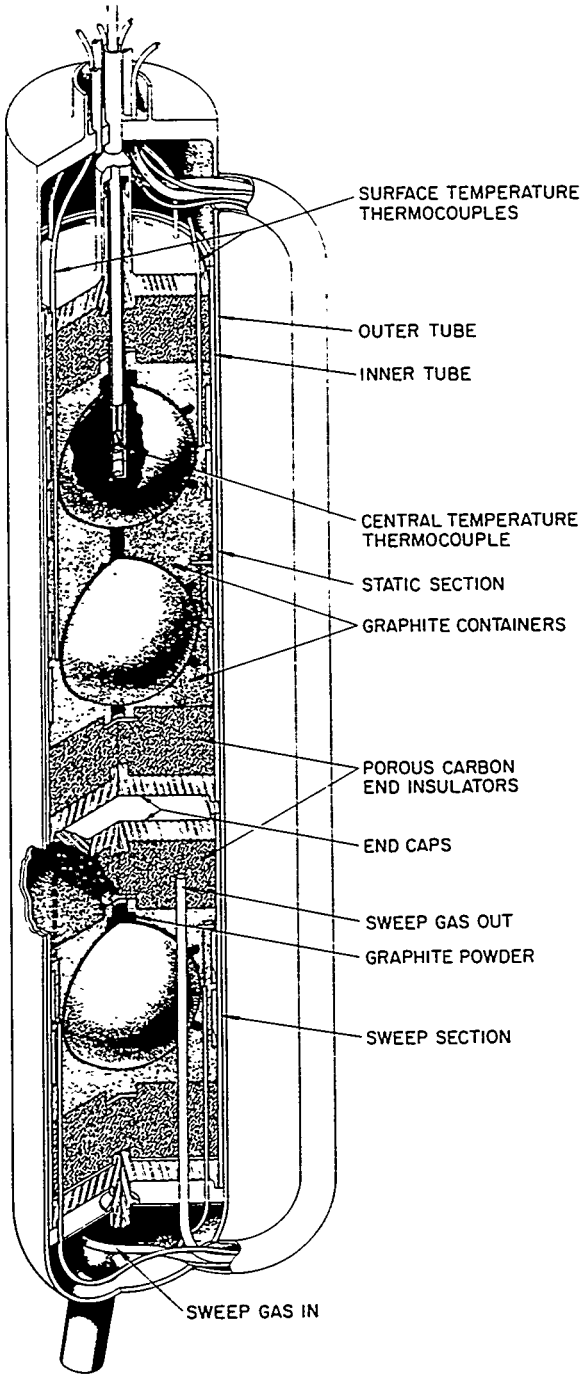

Fig. 3. Sweep Capsule Assembly for Irradiation of 6-cm-diam Spherical Fuel Elements in the ORR Poolside Facility. Three fuel spheres, held in graphite inside of metal cans, are irradiated simultaneously. One sphere is canned separately, and a small flow of inert gas is passed through the can to continuously sweep out and permit measurement of any radioactive gases that escape from the fuel. Thermocouples measure the surface temperatures of all spheres and the central temperature of one. Temperatures are controlled by adjusting the composition of gas in a small annulus between the inner and outer tubes as well as by positioning the capsule relative to the test reactor core.

The fuel is in the form of fueled-graphite spheres, approximately $2\frac{1}{2}$ in. in diameter, made up of an outer shell of pure graphite and an inner core of graphite containing a dispersion of small particles of uranium-thorium carbide that have been coated with pyrolytic carbon to form a barrier against the release of radioactive fission products. Many tests were performed to evaluate fuels made by different processes and by several manufacturers.

The ORR Eight-Ball Facility permits the simultaneous irradiation of eight $1\frac{1}{2}$-in. spheres in the core of the ORR. After a series of short experiments, which indicated the general mechanical and chemical stability of spherical fuel elements, a long-duration experiment was conducted to investigate the effects of high burnup and high fast-neutron exposure. This test contained fuel spheres from three vendors and specimens of pyrolytic-carbon-coated B_4C. The irradiation extended for nine months at a power density of 30 to 35 w per cubic centimeter of sphere and at sphere surface temperatures of 1500°F. The fast-neutron exposure (energy above 0.18 Mev) exceeded 1×10^{21} neutrons/cm^2, and 38 to 47% of the heavy-metal atoms were fissioned.

Eight capsules were irradiated in the ORR poolside facility to evaluate 6-cm fueled spheres of the reference design for the German AVR reactor. Each capsule (Fig. 3) contains three fueled spheres, one of which is swept continuously with a small flow of helium for determination of

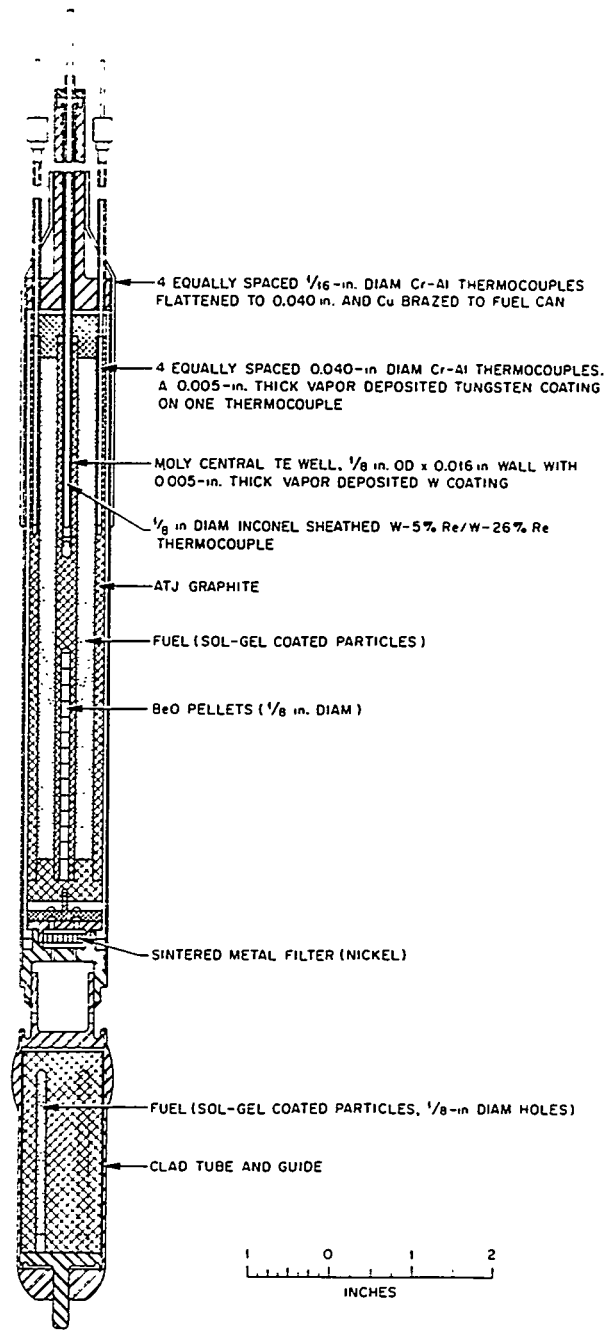

Fig. 4. Fuel Assembly for Experiment 14 in ORR Loop No. 1.

fission-gas release. The other two are in a sealed container; the central temperature of one of these is continuously measured. The last capsule in this series is still being irradiated and contains prototype AVR fuel spheres supplied by the vendor who is fabricating the initial AVR core loading.

Screening tests of loose coated fuel particles were conducted in miniature capsules in the LITR. These capsules have four isolated specimen containers in a vertical tandem arrangement. Fuel center temperatures are measured in the top and bottom containers. The fuel container material was changed from tantalum to graphite to permit tests at higher temperature.

A significant experiment has been under way for five months in ORR in-pile loop No. 1. The test fuel assembly (Fig. 4) has a vented tubular graphite fuel element containing a blend of loose pyrolytic-carbon-coated UO_2-ThO_2 particles produced by the sol-gel process. This is the first severe test of sol-gel oxide particles at high-temperature gas-cooled reactor conditions. The test element simulates one fueled hole of the reference design fuel for the TARGET reactor. It also includes a central graphite core containing BeO pellets for compatibility studies and a thermocouple for temperature measurement. We have been able to maintain the central temperature at 2500°F by adding neon to the helium coolant despite the consumption of one-third of the initial ^{235}U atoms. A second element containing similar fuel in a sealed container is an attached part of the test assembly and is operating at about 1200°F. The results of the test give considerable confidence that this fuel would perform satisfactorily in a nuclear reactor – the release of fission products was quite low (less than 0.01% of the xenon and krypton isotopes formed by the fission process escaped from the spheres), and the strength of the spheres was largely unaffected. A manufacturer in the United States is now furnishing a full core loading of similar fuel for the German AVR reactor.

PHOTO 63172

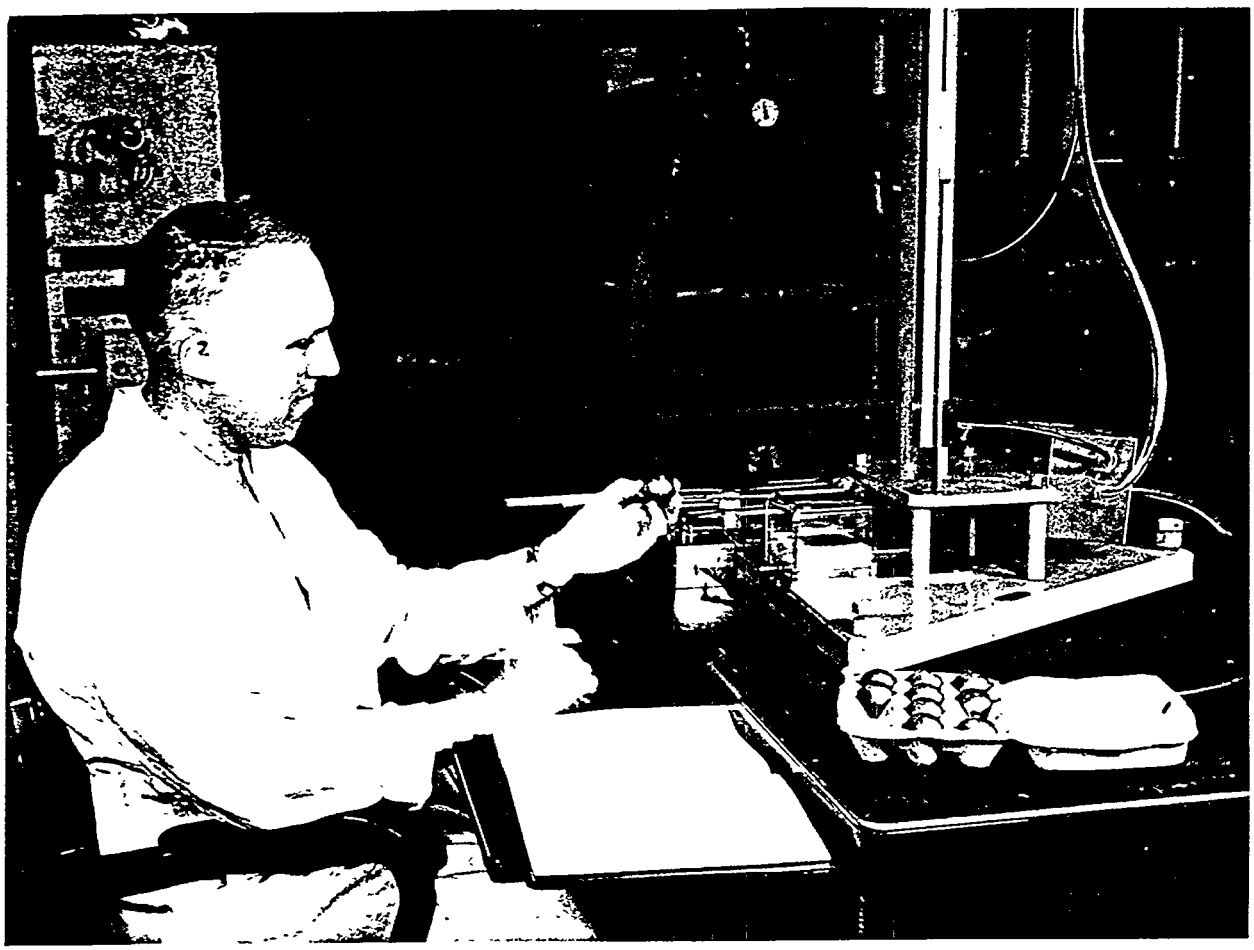

Fig. 5. Apparatus Used in Drop-Weight Testing of 1.5-in.-diam Graphite Spheres. The spheres are placed on a steel plate, and a weight is dropped onto the sphere from a controlled height. The kinetic energy of the dropped weight at impact is the same as that of the sphere in the free-drop test. Although the free-drop test better simulates operating conditions, this drop-weight test is more easily applied to irradiated specimens during hot-cell examination.

IMPACT RESISTANCE OF FUELED GRAPHITE SPHERES FOR PEBBLE-BED REACTORS

Fueled graphite spheres for high-temperature gas-cooled reactors of the pebble-bed type must withstand repeated dropping because of the continual remote reloading of fuel during operation of the reactor. We have studied the impact resistance of spheres of artificial graphite 1.5 and 2.36 in. in diameter.

The results from solid graphite spheres indicated that a fine-grained molded grade (grade ATJ) was the best of eight grades tested. Further impact tests were then performed on simulated fueled spheres, which consisted of machined ATJ shells containing solid spherical inserts that represented the fuel. Spheres having the inserts completely cemented in place were definitely superior to those with uncemented inserts. The minimum shell thickness needed to withstand the repeated free-drop tests was also determined.

The test spheres were dropped onto a bed of graphite spheres or onto a steel plate. The latter provided a much more severe test. A typical sphere having the recommended design features would survive 75 drops from 4 m onto the spheres followed by at least one drop from 4 m onto a steel plate. In supplementary experiments, we dropped weights onto the test spheres, using the apparatus shown in Fig. 5.

Photo 68161A

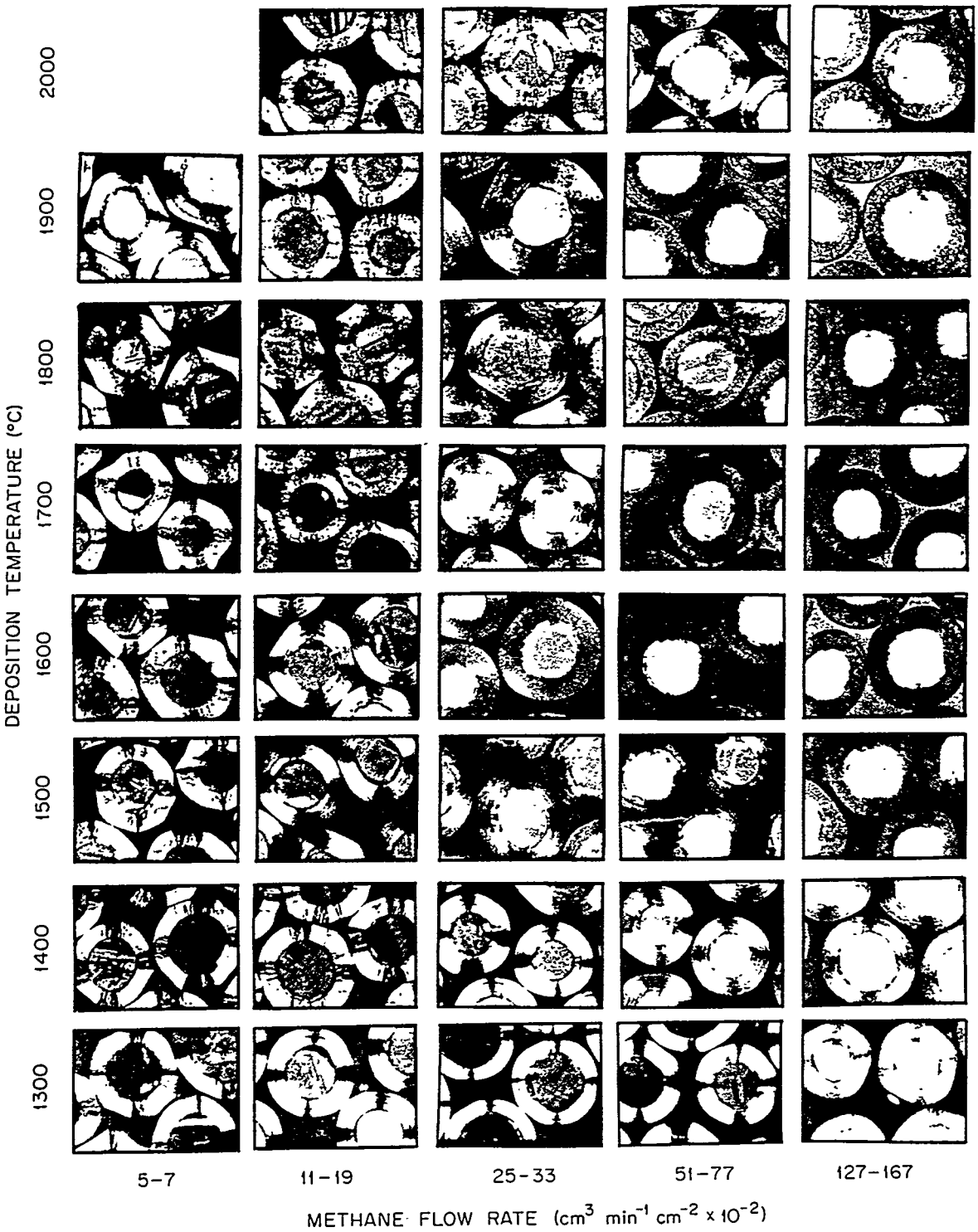

Fig. 6. Effect of the Environment in the Coating Furnace on the Structure of Pyrolytic Carbon Coatings. The fuel particles are UC_2 microspheres 0.010 in. in diameter, which were coated by the decomposition of methane in a fluidized bed. Coatings deposited at high flow rates have a featureless structure, which appears almost uniformly dark in polarized light. The structure of coatings deposited at the lower flow rates is either highly laminated or granular, and both types show typical dark and light crosses when viewed in polarized light.

Spheres having small differences in design or tightness of the threaded plug, or in which different cements were used to hold the insert, differed little, if any, in impact resistance. The tests clearly showed that the size of the gap between the insert and the shell is very important. This gap may vary because of the dimensional variations normally tolerated in manufacturing. The gap is normally filled with cement, but if the original gap is 0.02 in. instead of 0.010 in., the shell must be increased in thickness from 0.315 to 0.394 in.

PROPERTIES OF PYROLYTIC CARBON COATINGS ON NUCLEAR FUEL PARTICLES

Graphite fuel elements show great potential for high-temperature gas-cooled power reactors, particularly in that they will retain a very large fraction of the highly radioactive products from fissioning when a continuous low-permeability carbon coating is provided on all particles of the fuel material. We have been studying the properties of fuel-particle coatings that determine their integrity.

The carbon coating must withstand severe temperatures and intense radiation without breaking. Such coatings are usually applied on 0.010-in.-diam fuel particles by the decomposition of methane in a fluidized bed. A thorough study of the properties of coatings deposited on particles at various temperatures and flow rates of methane was recently completed. Properties such as density, hardness, and orientation of the crystallites in the coatings varied systematically with the set of deposition conditions.

The differences in properties of the coatings are illustrated in Fig. 6, which demonstrates the effect of deposition temperature and methane flow rate in the fluidized bed on the microstructure of the coatings. Polished cross sections of the coated fuel particles, when viewed by polarized light under a microscope, display features such as the darkened cross and the granular or laminar structure, which are closely related to other physical and mechanical properties of the coatings. Correlations of this type provide a basis for controlling the properties of coatings, so that the types of coatings that successfully withstand irradiation testing may be specified and reproduced.

DIFFUSION OF FUEL METALS IN PYROCARBONS

The movement of uranium and thorium in pyrocarbons is of practical interest in gas-cooled reactor technology, since low fuel mobility at high temperatures is most desirable. We are concerned with the localization of these fuel metals within assigned reactor regions by the use of pyrocarbon coatings, formed by the pyrolysis of natural gas at temperatures between 1200 and 2000°C. Our studies of the structure of pyrocarbons reveal the presence of many imperfections, as compared with the structure of graphite. In fact, surfaces of specimens, even when very smooth, remind one of cauliflower (see photos in Fig. 7). This appearance stems from defects initiated at the atomic level, which are, in turn, reflected up through larger structural units – including those visible to the naked eye. Comparisons of the photos and radiographs demonstrate that the migration patterns of fuel metals are directly related to the large-scale imperfections of pyrocarbon specimens. One may see also that the patterns observed when the direction of diffusion is the direction of growth of the deposited coating turn "inside out" when the direction of diffusion is reversed. If the pyrocarbon is baked at 3000°C before the metal is introduced, one observes little or no movement of metal at the usual experimental temperatures, because rapid rearrangements of carbon atoms at 3000°C erase many of the defects upon which the movement depends. In fact, the structure improves and approaches the structure of graphite. Most of the improvement occurs in primitive structural units; thus defects at all levels of magnification influence fuel migration.

FISSION-GAS RELEASE FROM URANIUM DIOXIDE

Much of the radiation damage that limits the lifetime of reactor fuels is caused by the creation of the noble gases krypton and xenon during fissioning of the fuel. We are studying the release of fission gas from uranium dioxide at temperatures up to 1400°C; the experiments are conducted in a reactor, so that the effect of fissioning will be taken into account. It has been shown that the

PHOTO 66588

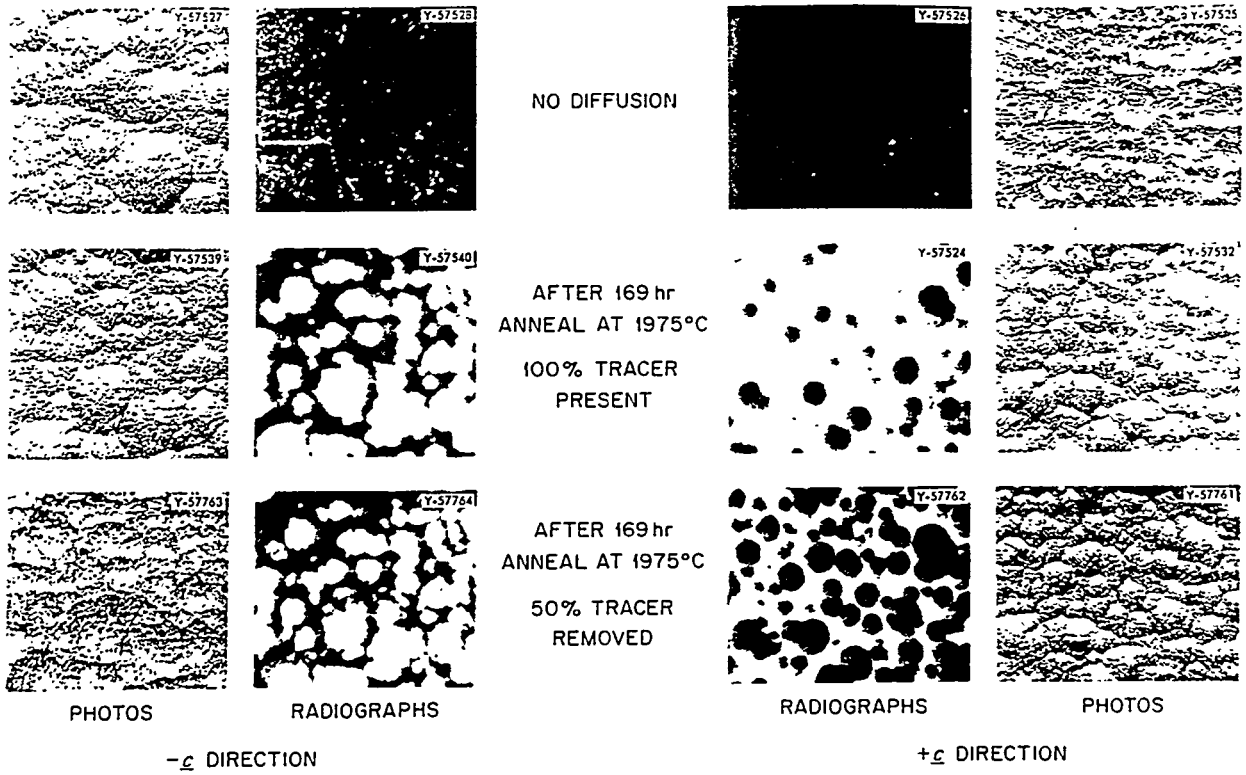

Fig. 7. Photographs Showing the Appearance of Pyrocarbon Specimens and Radiographs Indicating Thorium Positions After Diffusion at High Temperature. Specimens are 0.25 in. on an edge; the +c direction corresponds to the direction in which the pyrocarbon "grows" during the deposition process. The thorium tracer is concentrated at positions corresponding to the dark regions of the radiographs. Although we are interested in the diffusion perpendicular to the surfaces, most of the movement takes place laterally over these surfaces. Notice the uniformity of tracer before movement and the persistence of the tracer positions after movement, even when the surfaces are ground to remove tracer.

release of fission gas at high temperatures is not controlled by a diffusion process, as once believed, but by a trapping process. The release rate is therefore much lower than expected. As a result of these studies, we have developed new theories of the behavior of fission gas. The experimental data, as well as the theory, suggest the possibility of a longer useful life for fuel elements and cheaper production of nuclear power than had been anticipated.

Below about 600 to 700°C the fission gas does not escape from the fuel except through fissions on the surface. At higher temperatures the trapped gas will begin to escape. The escape rate of fission gas appears to depend on the number of traps, the type of traps, and the temperature. The fissioning of the fuel not only produces fission gas but also produces traps, which to a large extent retard the escape of the fission gas. As a consequence, the rate of release of fission gas from UO_2 at high temperature is not materially affected by the rate of fission. The small traps in the fuel may either migrate to form larger traps, capture a fission product atom, or anneal and vanish. Grain boundaries and imperfections in the fuel structure will also act as traps. This is confirmed by the fact that the rate of release of fission gas from polycrystalline specimens (with grain boundaries) is much lower than the corresponding rate of release from single crystals (without grain boundaries) of the same geometric dimensions. The amount of trapping depends on the fuel structure, irradiation history, fission rate, and temperature.

CREEP OF GRAPHITE UNDER IRRADIATION

Artificial graphite, which is used to support the core of high-temperature gas-cooled reactors, loses very little of its strength at high temperatures but will break if stretched as much as 0.2%.

Three grades of artificial graphite were tested under bending loads while exposed to high-intensity neutron radiation in the core of the ORR. These tests showed that artificial graphite would stretch slowly under irradiation and would not fail until deformed as much as three times the amount that would break the material in normal tests. The stretching consisted of two stages. The first or primary stage constituted a large part of the total amount of stretching and was about the same at the three temperatures tested: 150, 270, and 330°C. The second stage consisted of stretching at a slow uniform rate, which was greatest at the lowest temperature.

FISSION PRODUCT TRANSPORT AND DEPOSITION

With higher core temperatures being proposed for advanced gas-cooled reactors, retention of fission products within a reactor core will become increasingly difficult. The consequences of permitting a release of some or all of the fission products into the primary system of the reactor are under investigation. In one phase of that program the transport and deposition behavior of fission products are being determined. An out-of-pile loop was fabricated in which individual fission products or groups of selected isotopes can be injected into a gas system that simulates the coolant conditions of a reactor. The deposition of fission products downstream from the injector is measured as a function of deposition geometry and coolant conditions (Fig. 8). From such evaluations information can be developed for analytical

65-661

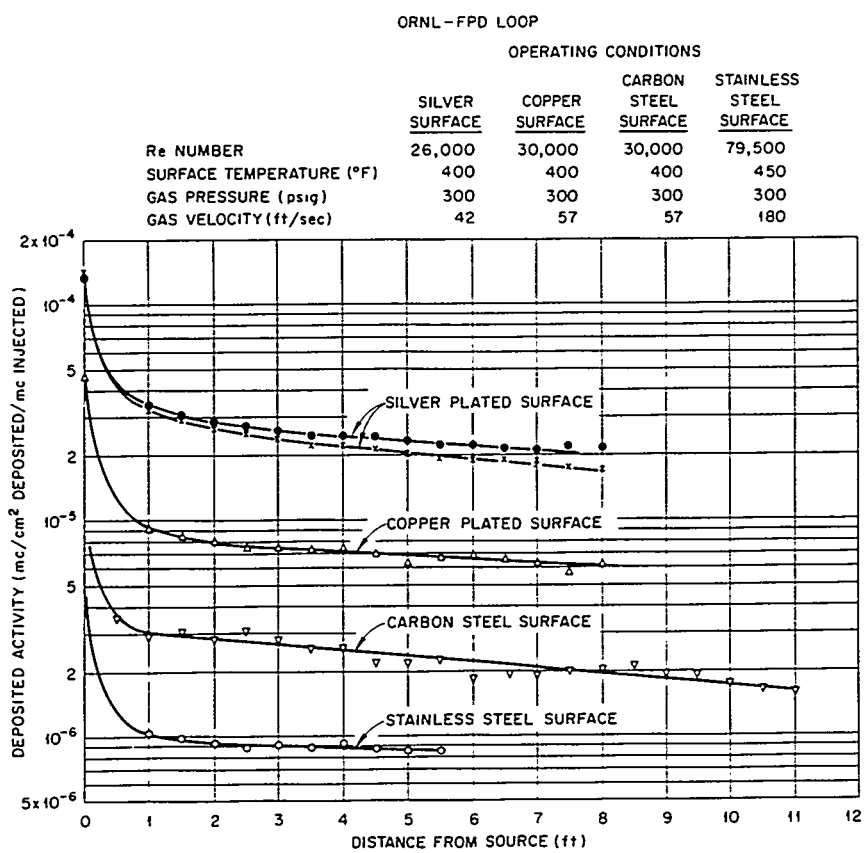

Fig. 8. Fission Product Deposition. The quantities of fission products deposited on four different surfaces plotted vs distance from the source.

models directed toward prediction of fission product deposition in actual reactor components.

REACTOR ANALYSIS

Previous planning for high-temperature gas-cooled reactors has been largely based on the assumption that such reactors would operate best on the thorium cycle, in which the principal fissionable material is the ^{233}U produced from the thorium, and only enough highly enriched ^{235}U is used to make up the breeding deficiency. The economic advantage of the thorium-^{233}U fuel lies in the good neutron economy of ^{233}U in a thermal spectrum, leading to a fuel cycle in which the burnup can be very high or the conversion ratio can be near unity. On the other hand, the price of low-enrichment uranium is considerably less per gram of fissionable material than it is for highly enriched uranium, and also it is possible that plutonium may become available in large quantities at a reasonable price. These facts have led us to do a series of studies to determine those economic conditions under which it would be advantageous to operate a high-temperature gas-cooled reactor with one of the alternative fuels.

We calculated the burnup, conversion ratio, and fuel-cycle cost for a wide variety of fuel compositions. For the case of a fully developed industry of 15,000 Mw (electrical) (and hence low fabrication and processing costs), we found that the thorium-uranium recycled fuel gave lower fuel-cycle costs, as well as higher conversion ratios, than the low-enrichment uranium fuel in semihomogeneous core arrangements.

However, for a smaller industry (with fuel fabrication costs above $165 per kilogram of heavy metal), the low-enrichment uranium fuel on a "throwaway" cycle gave lower fuel costs than the thorium-uranium fuel. Designs in which the low-enrichment uranium fuel was lumped in heterogeneous lattices to reduce the required enrichment did not yield any advantage in fuel-cycle costs and required unreasonably low power densities.

We also investigated the use of plutonium (from uranium irradiated to 20,000 Mwd/ton) instead of highly enriched uranium as makeup fuel in a thorium-uranium recycle fuel cycle. Here we obtained reasonably high conversion ratios (up to 0.9) and interesting fuel-cycle costs for calculations assuming a large industry. Under the ground rules of the study, plutonium at any price under $11.00 per gram of fissionable material would be competitive with highly enriched uranium at $12.00.

discharge through chemical processing. This code also has provisions for calculating the cost of shipping gamma-active recycled fresh fuels, such as ^{233}U and ^{241}Pu.

More recently, the TASCO code has been developed for the calculation of waste disposal costs in chemical processing, for the case in which the waste liquid is held in underground storage tanks for a lengthy period. TASCO can be used to determine the optimal storage tank size for a given waste production rate.

STUDIES AND EVALUATIONS

FUEL SHIPMENT STUDIES

Computer Codes for Fuel Cycle Economics Studies

Reactor fuel cycle economic studies have been considerably aided by the development of several computer codes for optimizing various portions of the fuel cycle. The first phase of this work involved the development and testing of the MYRA code for spent reactor fuel shipping cost studies. This code uses as input the fuel dimensions, nuclear characteristics, and decay time. It designs a shipping cask that meets the requirements of shielding, heat removal, and allowable weight. For each cask design, it calculates the associated shipping costs, which include amortization of the cask, freight charges, handling costs, and insurance against damage. It also calculates the inventory charges for the cooling period. By doing this for several decay times, the optimal cooling time can be found.

In the second phase of the study, the range of the MYRA code was extended so that a greater portion of the fuel cycle might be considered during the optimization process. This phase resulted in the development of the NORA code, which extends the optimization through the chemical reprocessing of the spent fuel. NORA determines the optimal cooling time and optimal shipping conditions for minimizing the total of shipping costs, chemical processing costs, and fuel use charges. This covers the period from reactor

Shipping Containers

In the shipment of radioactive materials, utmost care must be exercised to prevent the escape of the contained material either in normal handling or as the result of accidents. To provide a sound basis for optimizing the design of containers for these materials, various dynamic tests have been conducted on typical containers to assess the amount of damage under simulated accident conditions. Previous tests with heavy multiton lead-shielded casks for shipping highly radioactive fuel elements from nuclear reactors to a fuel processing plant are summarized in ORNL-TM-681, *Guide to the Design of Shipping Casks for the Transportation of Radioactive Materials.*

More recently, drop tests have been conducted with containers for the shipment of unirradiated highly enriched ^{235}U and plutonium solutions. The containers are used in shipping these solutions from a nuclear reactor fuel processing plant to a fuel fabrication plant. Each container contains several gallons of fuel solution and must be separated from adjacent containers by some form of barrier to prevent the initiation of a nuclear chain reaction by interaction of the fuel in the group of containers. The containers tested (Fig. 1) were 8-in.-diam closed steel pipes 24 in. long centered in a 55-gal steel drum; the container was restrained in the drum by 12 spokes. This type of container was able to withstand a free-fall drop from 30 ft in a horizontal attitude onto a piece of armor plate embedded in a 5-ft-thick concrete slab. Since this test is considered to be equivalent to a severe transportation accident, the container design tested was deemed to be structurally safe.

PHOTO 65463

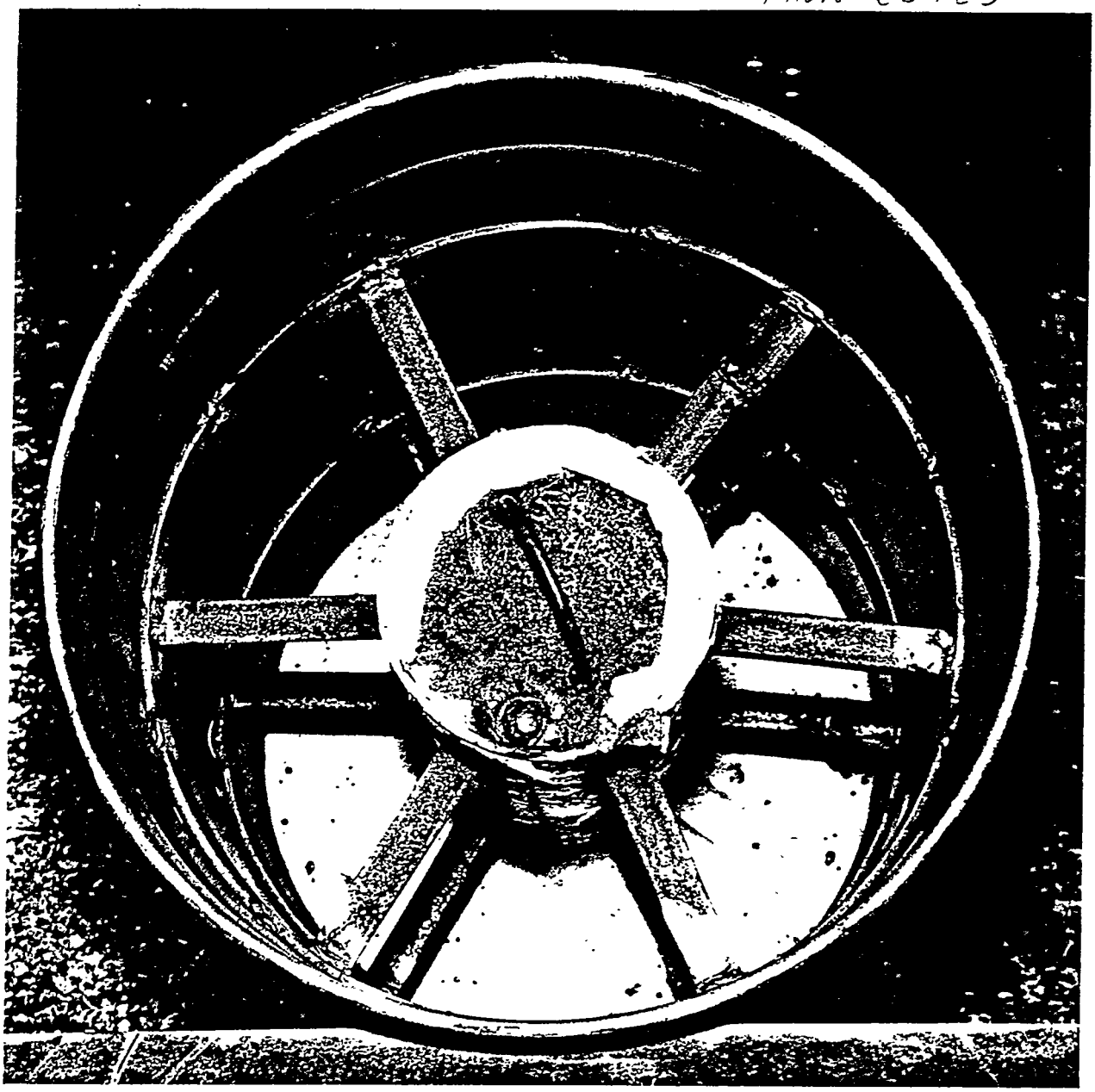

Fig. 1. Fuel Solution Shipping Container. Highly enriched ^{235}U nitrate and plutonium nitrate are shipped in stainless steel or plastic bottles, which are placed in the 8-in. steel tube in the center of the 55-gal drum. The surrounding drum acts as a spacer between bottles to prevent a nuclear chain reaction from occurring.

APPLIED AND BASIC REACTOR PHYSICS

REACTOR SHIELDING

The major portion of the 1964 reactor shielding program was directed toward the development of calculational techniques for predicting neutron and gamma-ray dose levels at the payload of SNAP-type spacecraft and within structures designed for protection against nuclear weapons radiation. A few basic shielding experiments were performed on the transmission and scattering of fast neutrons by various shielding materials, and several studies were carried out to support the development of a fast-neutron spectrometer. The remainder of the shielding effort was centered in the Radiation Shielding Information Center (RSIC), which broadened its scope to include weapons radiation and radiations occurring in space and also to serve an international community.

Fast-Neutron Penetration and Scattering Experiments

Reactor and other fast-neutron shielding problems now depend upon digital computer computations of penetration and scattering. Since prudence demands that the most promising of these methods be tested against experimental results, there are continuing programs at the Laboratory for generating tests as opportunities arise. The experimental arrangement for one such test, which was performed by ORNL at the General Atomic Linear Electron Accelerator, is shown in Fig. 1. In this experiment the spectra of photoneutrons scattered from cylinders of lithium hydride, graphite, concrete, aluminum, and steel were measured. Flight-time spectroscopy using liquid organic scintillation detectors was employed, and both the spectrum of primary photoneutrons incident on the cylinders and the spectra of photoneutrons scattered at several angles were obtained. The results were in every case compared with those from a penetration analysis performed with the standard O5R Monte Carlo program, the differences between the measured and calculated values being less than 20%. This study showed that the cross sections employed in the Monte Carlo program had reasonable validity over the 0.5- to 10-Mev energy range and, to a lesser extent, that the program could follow neutron scattering through the samples.

To support fast-neutron spectroscopy studies of this type, considerable effort was expended in studying both the light output and the neutron detection efficiency of liquid organic scintillators as a function of neutron energy in the 0.2- to 14-Mev range. These detectors offer high efficiency and the opportunity for the experimenter to discriminate between pulses originating from gamma rays and neutrons, although the differential pulse-height response of the scintillators to monoenergetic fast neutrons continues to rise as the pulse height decreases from maximum to zero. Extensive measurements and computations have been completed to elucidate the details of this response for spectrometers operating in the 0.5- to 20-Mev range. A result is the knowledge of the efficiency of the standard detectors studied for any stated "bias" threshold, which is necessary for flight-time experiments such as those described above. When these computed responses are combined with the advanced data analysis ("unscrambling") techniques which are considered as part of the experimental instrument, the pulse-height spectra themselves may be analyzed to yield a neutron flux spectrum. Figure 2 illustrates this process for neutrons from the $^{9}Be(\alpha,n)^{12}C$ reaction, the hatched area indicating the region of uncertainty in the result.

2-01-058-990 R

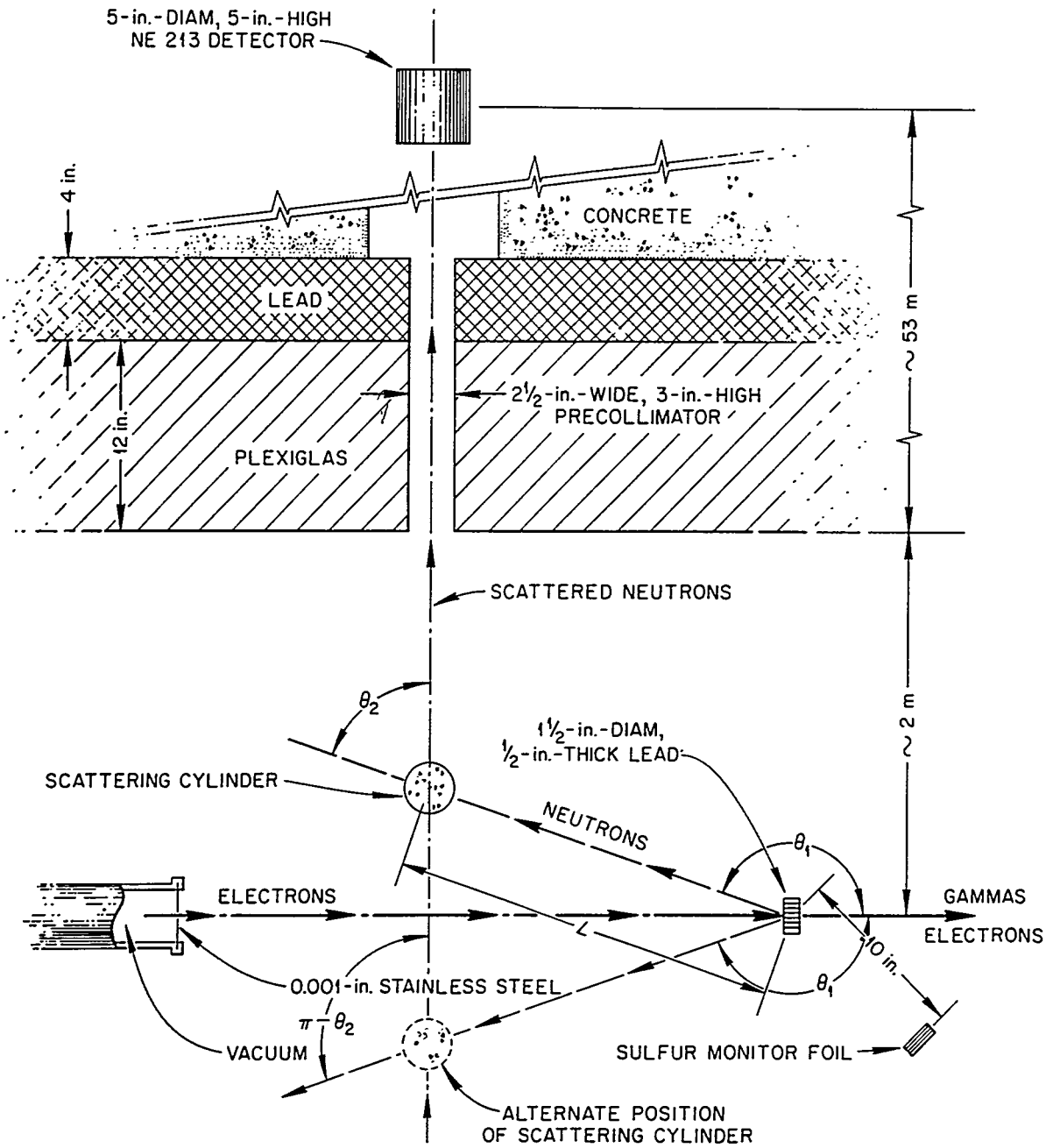

Fig. 1. Fast-Neutron Penetration and Scattering Experiment.

Shielding Studies for SNAP Systems

A development program is continuing for shields to be used on space vehicles whose auxiliary power is generated by nuclear reactors. The scope of the program has been increased from that reported previously[1] to include applications to missions in which part of the payload will be human beings. Since the permissible radiation dose level that a man can tolerate over an extended

[1] *Oak Ridge National Laboratory, 1963.* ORNL-3650, p. 56.

64-11082

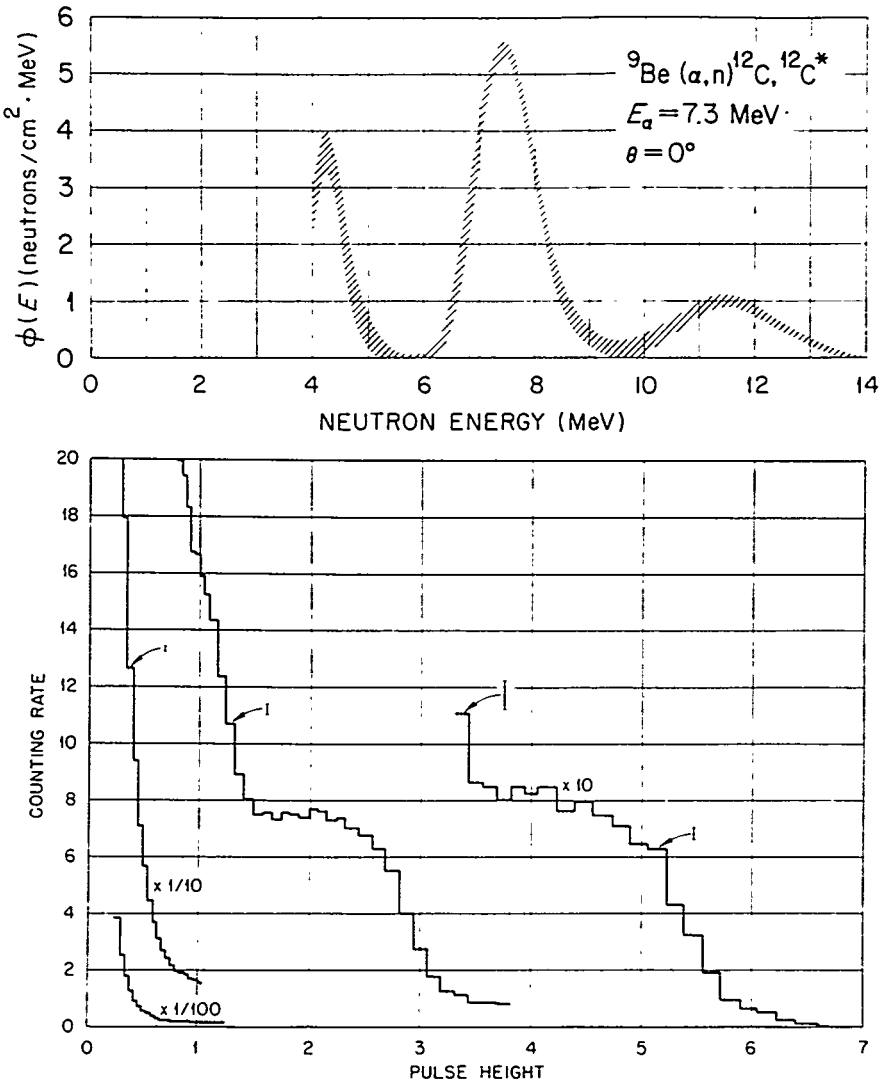

Fig. 2. Pulse-Height Distribution and Unfolded Neutron Spectrum for the $^9Be(\alpha,n)^{12}C$ Reaction.

period of time is very much less than the dose level that can be tolerated by electronic systems, the problem of designing such a shield is somewhat more difficult. For example, the shield would have to be very much thicker and, therefore, very much heavier than a shield for an unmanned vehicle and could weigh as much as 20,000 to 30,000 lb. It is therefore imperative that accurate methods of shield design and of shield optimization with respect to weight be developed in order to reduce to a minimum the overall weight of the system to be put into orbit.

The development program includes experimental studies of the transmission of radiation from a uranium-zirconium hydride SNAP-10 prototype reactor. The experimental work is supported by theoretical studies aimed at designing a meaningful experiment that can be performed in the earth's atmosphere, the primary difficulty being to reduce to tolerable levels unwanted background radiation from neutrons either scattered around the shield by the atmosphere or scattered in structural materials in the immediate environment of the reactor. The theoretical effort is also concerned with

developing advanced Monte Carlo techniques for making accurate predictions of the radiation transmitted through any shield, no matter how complicated the geometry.

In manned systems the gamma-ray dose level particularly must be reduced to a much lower level than for unmanned systems, and since a large fraction of the total gamma-ray dose is due to secondary gamma rays produced in the shield itself, an optimum arrangement is attained by dividing the metal gamma-ray shield into several shaped layers. The development program for manned systems thus requires the ability to calculate the production of secondary gamma rays in the several layers of the gamma-ray shield, as well as the transmission of both the secondary and the primary (reactor) gamma rays. Since the production of these secondary gamma rays results from the capture of very low-energy neutrons, studies have been made on the feasibility of combining Monte Carlo calculations with two-dimensional multigroup transport methods. It has been determined that these two techniques can be coupled, which greatly increases the efficiency of machine calculations of the neutron capture rates within the shield. A Monte Carlo code with flexible geometry has been developed for calculating the gamma-ray dose emitted from the shield.

A significant effort has been made to adapt a prototype SNAP reactor for use in the experimental program at the Tower Shielding Facility. A heat-rejection system consisting of a liquid-metal-to-air radiator was designed for the reactor along with some modifications to the control system to render the reactor compatible to the TSF. Facilities for storing and handling the unshielded reactor were designed, as well as a system of collimators to be used with the detectors in making experimental measurements of the various radiations leaking from the reactor and shields.

Studies of Shielding Against Nuclear Weapons Radiation

Shielding studies for civilian and military defense programs continued with the analysis of the experimental results for shielded complex structures tested at the Tower Shielding Facility and the development of calculational techniques. Calculations of the dose within the shielded bunkers[2] and circular holes[3] agreed within 25% with the measurements and showed the relative importance of the various components of the radiation which contribute to the dose, such as the uncollided flux, the shield-scattered flux, the wall-scattered flux, and secondary gamma rays produced in the walls of the structure. Wall scattering was found to contribute up to 40% of the fast-neutron dose rate at positions deep within the structure. Thermal-neutron capture in the concrete shield accounted for as much as 90% of the gamma-ray dose rate for the heavily shielded structures.

Simplified methods were developed for calculating most of the components contributing to the dose in the structures. Direct-beam transmission factors were obtained from Monte Carlo calculations as a function of the angle and energy of the incident radiation, and the wall-scattered contribution was calculated utilizing the albedo concept, where the angular distribution for the scattered radiation was obtained from a fit to previous Monte Carlo calculations. No new machine programs were required during the course of the work, and considerable attention was given to the analysis and systemization of parametric data applicable to radiation shielding calculations of protected structures.

The 1964 experimental program and additional theoretical work were aimed at the measurement and calculation of the differential neutron albedo from concrete. A very detailed Monte Carlo calculation was completed of the neutron albedo differentiated with respect to five variables: energy of incidence, polar angle of incidence, polar and azimuthal angles of emergence, energy of emergence, and distance of emerging neutron from the point of entry, all as a function of depth in the shield. These results were compared with experiments done at the TSF where a tightly collimated beam of neutrons was incident on a large concrete slab. Both the shield and the detector could be revolved about the point of incidence of the neutron beam to cover the angular variations obtained in the calculations. The spectrum of the incident neutron beam was determined, and the scattered neutron dose was measured for a large number of combinations of the

[2] *Oak Ridge National Laboratory, 1963*, ORNL-3650, p. 57.

[3] *Oak Ridge National Laboratory, 1962*, ORNL-3350, p. 99.

polar angle of incidence and the polar and azimuthal angles of emergence. The average deviation between the results of the calculations and the experiments was approximately 5%.

The calculated differential albedo data have been utilized in a simplified Monte Carlo calculation for neutron transmission through passageways having up to three bends. Each collision with the wall is treated as a single event, and the probable neutron direction and energy are selected from the albedo data. This treatment allows the neutron distribution in a passageway with three bends to be calculated with good accuracy in approximately 1/2 hr of machine time. The passageway transmission has been compared with experimental results for a 3-ft-square concrete-walled duct at the TSF.

Radiation Shielding Information Center

The Radiation Shielding Information Center (RSIC) now serves an international shielding community and has broadened its scope to include not only reactor shielding but also shielding against weapons radiation and shielding against radiations occurring in space.

The computer-oriented system for storing and retrieving bibliographic information has been in operation for two years and has been used to produce many literature searches and bibliographies automatically. During the latter part of 1964, the system was modified to include a routine for selective dissemination of information (the SDI routine). The purpose of SDI is to inform individual scientists of literature which RSIC has incorporated into its system in the interval between issuances of comprehensive bibliographies. This is accomplished by the computer program which updates the system. The program searches for a match between the scientist's interest profile and the subject categories assigned to the literature specimen. If a match occurs, the scientist is sent a sheet of paper on which are printed his name and address, the bibliographic information, and an abstract.

The collection, examination, and dissemination of useful digital computer codes written to perform shielding calculations has become one of RSIC's most important services. An intensive effort is made to collect interesting codes, acquire complete documentation, obtain the programming language versions, and acquire sample problems from the originator. This collection consists presently of 70 code packages in various stages of completion. RSIC operates these codes on the computers at ORNL, disseminates the code packages upon request, and answers technical questions regarding the operation of the codes.

The members of the Center's staff have written several reports, including one which presents a survey of methods for calculating gamma-ray heating (ORNL-RSIC-8), another which compares methods for calculating neutron distributions in shields (ORNL-RSIC-3), and others which give compilations of useful data (ORNL-RSIC-4, ORNL-RSIC-7). It is this effort that makes RSIC different from a specialized library or a data center, since it acts as a shunt for sending essential information to the scientist, and he is relieved of performing an arduous literature search.

Communication with the shielding community is aided by the regular distribution of a newsletter. This newsletter is sent to 480 persons throughout the world and is used as a vehicle for conveying to the shielding community information related to RSIC activities and activities of other organizations interested in shielding.

CRITICALITY SAFETY

An integral part of any complete reactor development and operation program is the safe and economic handling of the fissile materials outside the reactor. For a number of years the Oak Ridge National Laboratory has been engaged in an extensive experimental effort to establish the critical parameters for fissile isotopes, primarily ^{235}U, in a variety of nonreactor environments. The results of many experiments have been directly applicable to casting of metal and fabrication of reactor fuels, to their storage and transport, and to chemical plants for reprocessing after use. Through applicable calculational methods, appropriate experimental data can be extrapolated into areas not directly measured. In general, the studies are made with common materials in simple geometry in order that data of most general applicability will be obtained. As demand requires, these measurements are supplemented by tests representative of specific items of equipment.

Critical Dimensions of Arrays of Aqueous Uranyl Fluoride Solutions Containing Uranium Enriched to 5% in ^{235}U

In addition to establishing the critical dimensions of single units of fissile material, we have more recently combined numbers of units, each individually quite subcritical, into assemblies that were critical. Earlier assemblies used units of aqueous uranium solution and of uranium metal of high (93%) ^{235}U enrichment. Operations connected with the nuclear power reactor program have given impetus to similar studies of assemblies of units of low (less than 5%) enrichment. These studies are concerned with an aqueous solution of uranium, enriched to only 5% in ^{235}U, at a concentration of 900 g of U per liter. As many as 25 cylinders of solution, 24 cm in diameter and of varying but common height, have been arranged in critical planar assemblies without reflectors (Fig. 3). When the cylinder height was 142 cm it was observed that the centers of the cylinders, set in a triangular pattern, were separated 39.5 cm. Calculational models which will adequately describe such assemblies are being investigated.

PHOTO 71552

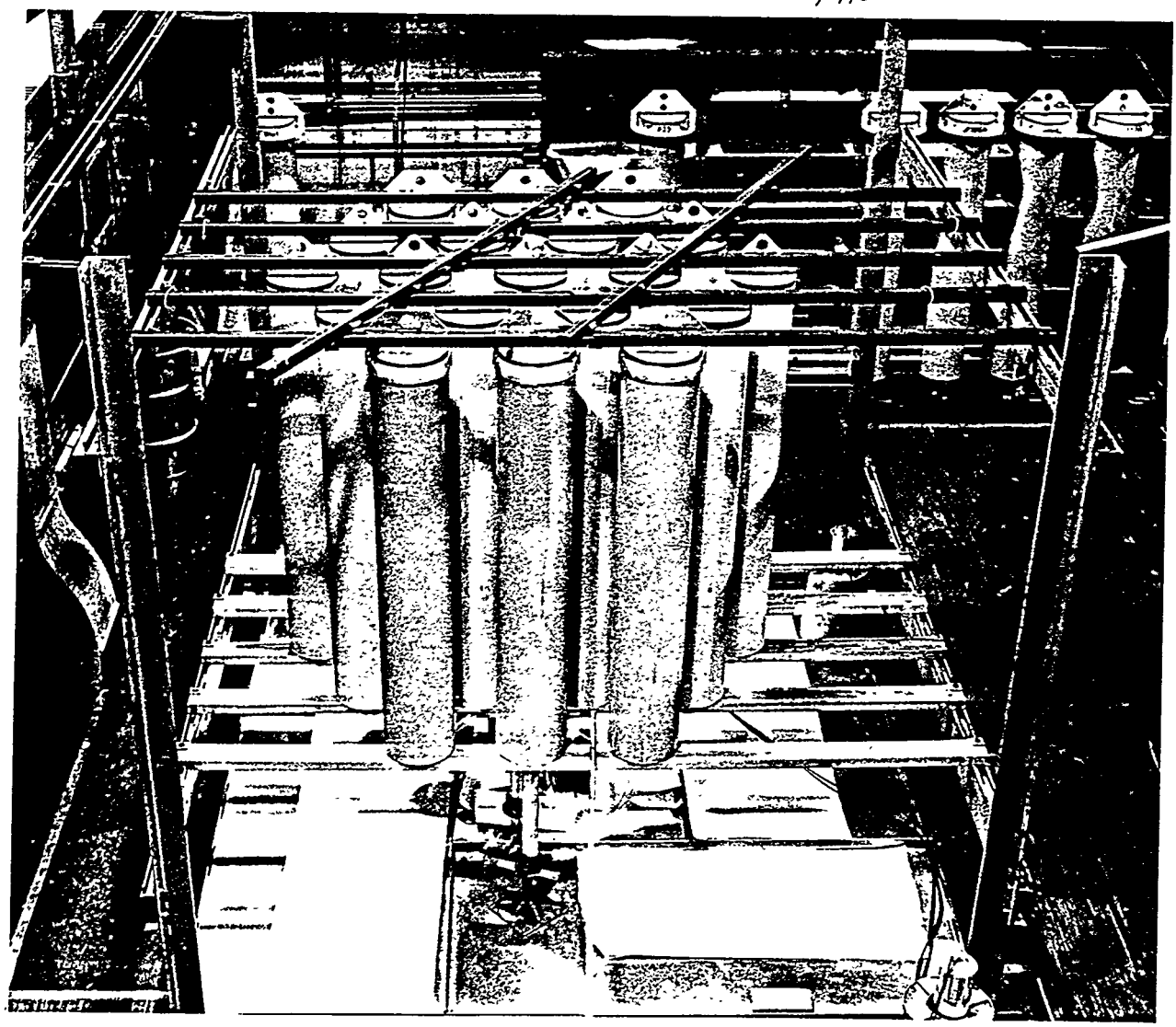

Fig. 3. Typical Array of Cylinders Containing Aqueous Solutions of Uranium Enriched to 5% in ^{235}U.

In other experiments, critical arrays have been assembled in which the uranyl fluoride solution was contained in 10.75-in.-diam polyethylene bottles having a capacity of about 25 liters (Fig. 4). Since these bottles are used for storage and intraplant transport of uranium solutions of low enrichment, the results of these experiments form bases for safe and economic handling criteria. It was shown, for example, that an infinitely long single line of these bottles in contact was not critical even when completely surrounded by a hydrogenous reflector. The relative effects of materials such as concrete, wood, Plexiglas, foamed plastic, and Foamglas as reflectors for this enrichment were determined.

Critical Experiments with SPERT-D Fuel Elements

The critical dimensions of lattices of SPERT-D fuel elements in several nonreactor environments were determined to establish specifications for use in storage, transportation, and chemical processing operations. Each fuel element contained about 300 g of ^{235}U in 22 aluminum-clad flat plates. In addition to lattices with water moderator and reflector, a dilute aqueous solution of uranyl nitrate was used in some experiments to simulate a dissolver. In still other experiments, varying amounts of boron were added to the uranyl nitrate solution to determine its effect as a soluble neutron absorber in chemical process equipment.

It was shown, for example, that a minimum of about 3.5 kg of ^{235}U is required in a critical lattice moderated and reflected by water. This mass is reduced to 2.8 kg (contained in the elements) when uranyl nitrate solution (enrichment 92.6%) having a ^{235}U concentration of 3.99 g/liter is substituted for water (Fig. 5). It is increased to 13.6 kg when 1.110 g of natural boron is added to each liter of the uranyl nitrate solution (Fig. 6).

PHOTO 71991

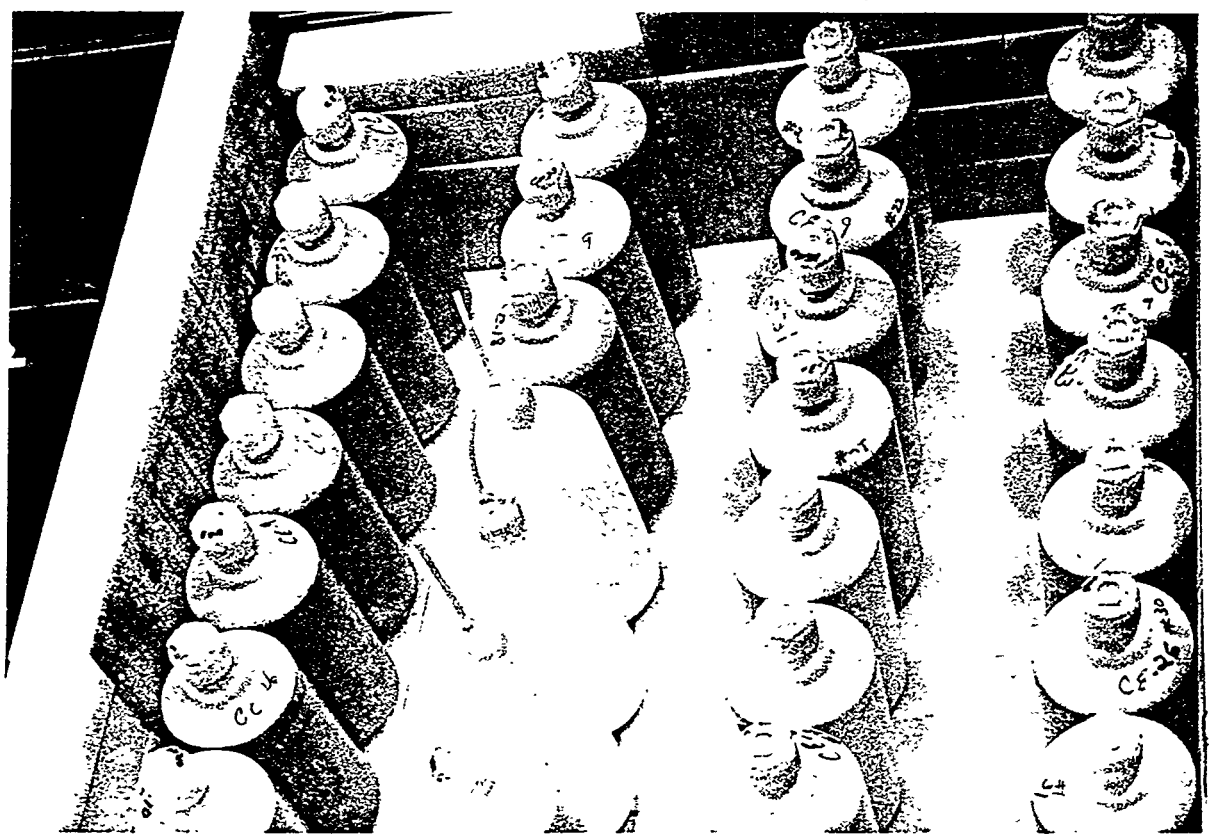

Fig. 4. Typical Array of Polyethylene Bottles Containing Aqueous Solutions of Uranium Enriched to 5% in ^{235}U.

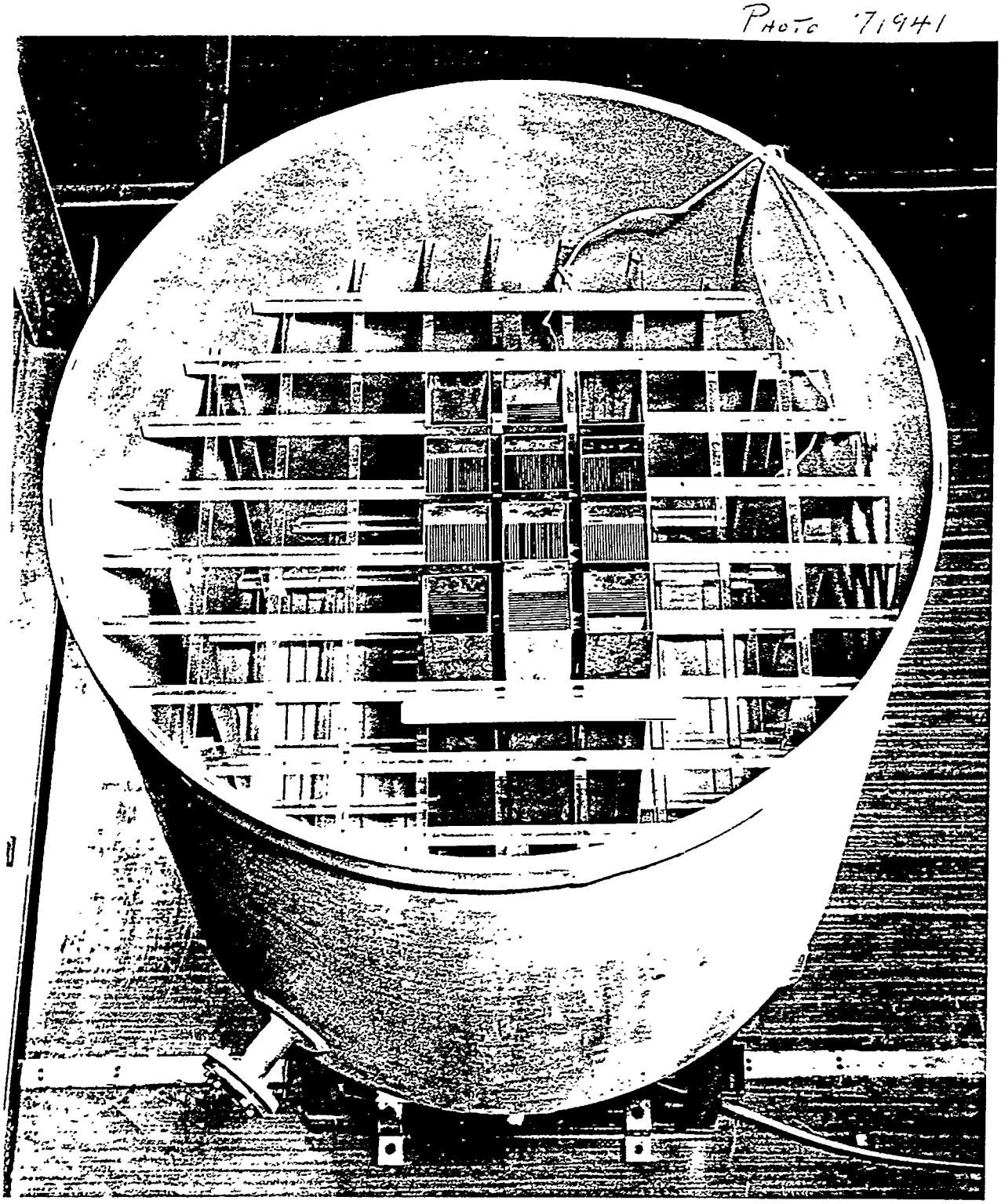

Fig. 5. Configuration of SPERT-D Fuel Elements That Is Critical when Immersed in a Solution Containing Enriched Uranium.

PHOTO 71921

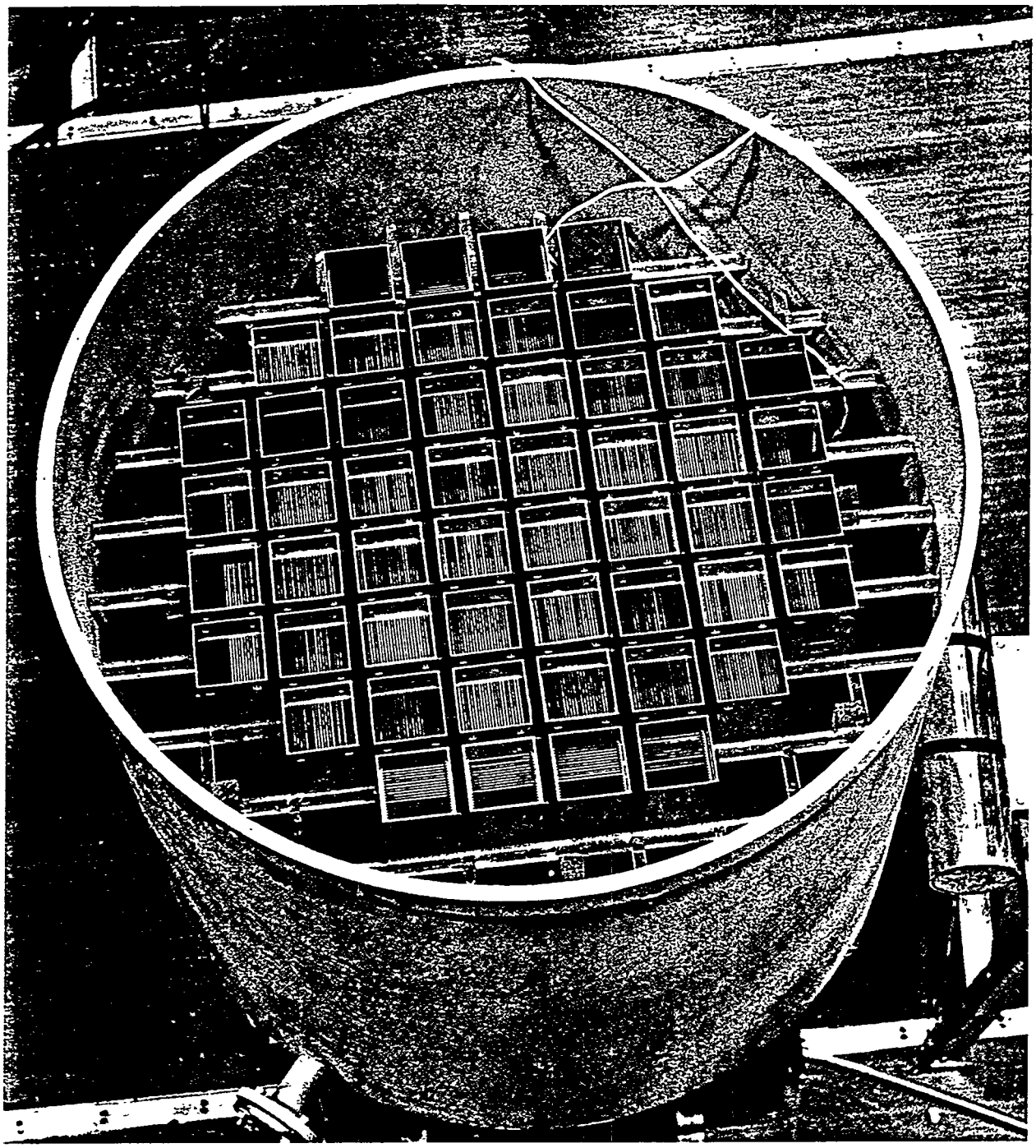

Fig. 6. Configuration of SPERT-D Fuel Elements That Is Critical when Immersed in a Solution Containing Enriched Uranium and Boron.

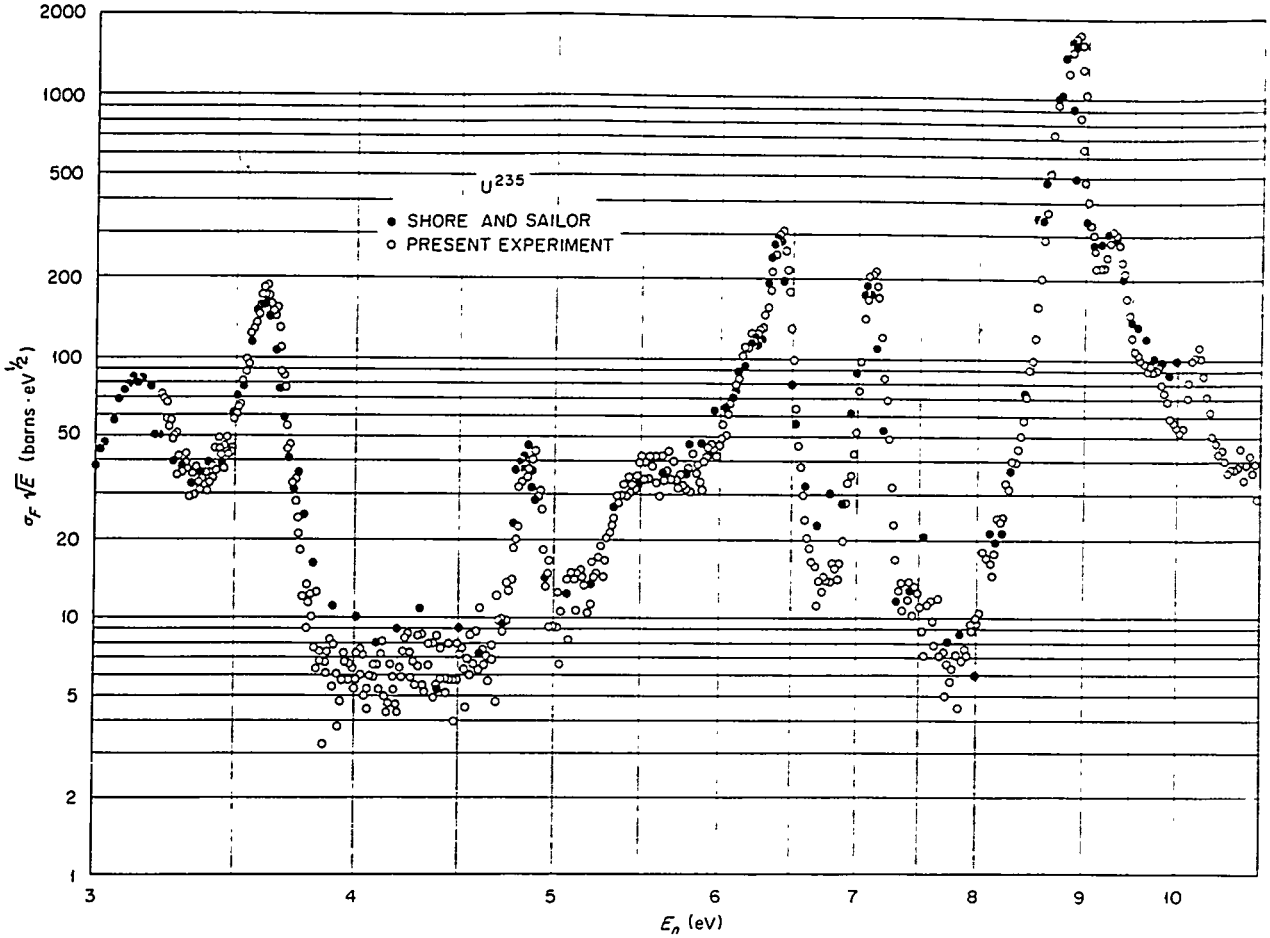

Fig. 7. Comparison of ^{235}U Fission Cross Section Obtained from ORNL Measurements with That Obtained from Brookhaven Measurements (Shore and Sailor).

BASIC REACTOR PHYSICS

The aim of the basic reactor physics program continues to be the generation of information that will facilitate the design and use of many types of reactors. The measurements to determine the neutron capture and fission cross sections for the three principal reactor fuels and those to study the nuclear reaction mechanisms whereby neutrons scatter from various nuclei were extended, and an experiment to investigate the diffusion of D-D neutrons pulsed into ice was completed. Critical experiments with various arrangements of 93%-^{235}U-enriched uranium metal have also been continued.

Measurement of α as a Function of Energy

The techniques used to measure α as a function of energy for the three isotopes ^{233}U, ^{235}U, and ^{239}Pu were discussed previously.[4] The measurements performed for ^{235}U in the spring of 1963 have now been analyzed to obtain the fission and capture cross sections, as well as α, in the energy range from 3 to 25 ev. Figure 7 shows a comparison of the fission cross section obtained from this analysis with that from a more standard measurement by Shore and Sailor of Brookhaven National

[4] *Oak Ridge National Laboratory, 1963*, ORNL-3650, p. 63.

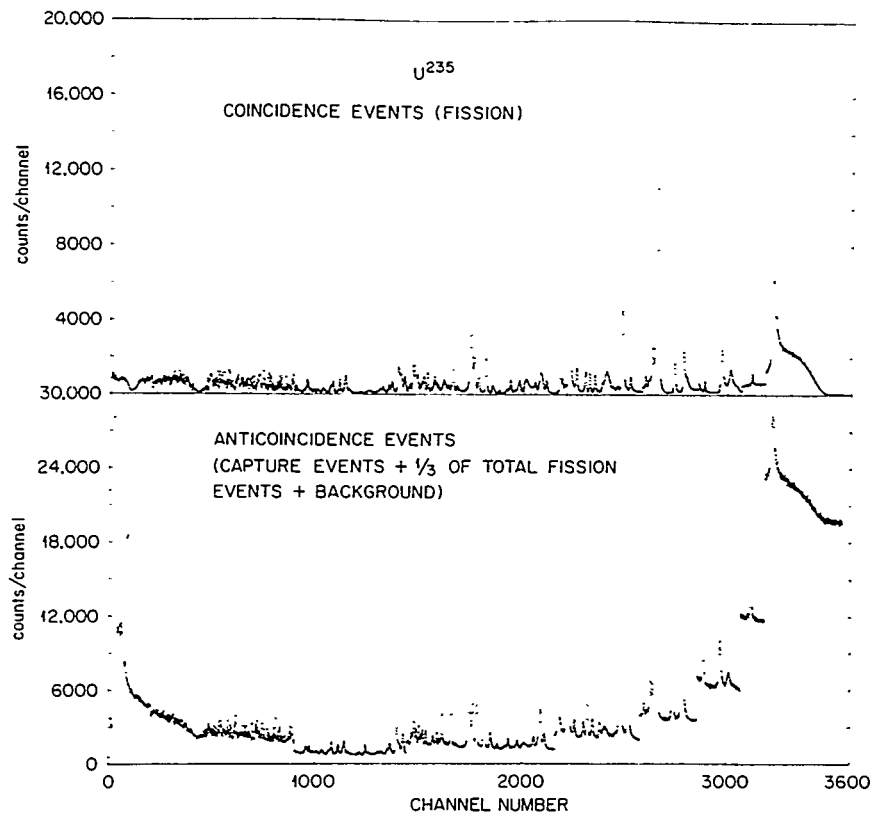

Fig. 8. Typical Time-of-Flight Spectra Obtained in ^{235}U Cross-Section Measurements at Rensselaer.

Laboratory. The agreement between the two sets of results is quite good and gives confidence in our technique.

Further ^{235}U measurements were performed with the Rensselaer Polytechnic Institute linear accelerator in November 1964. These measurements utilized a small computer (DEC PDP4) which allowed the collection of data over a wide energy range (from 0.1 ev to a few kev). Typical time-of-flight spectra obtained by this technique are shown in Fig. 8. The data are now being reduced to obtain fission and capture cross sections and α. Some data on ^{239}Pu were also collected at RPI, but further measurements on this isotope will be required to improve the precision of the results. Measurements at RPI on ^{233}U will be initiated shortly.

Measurements will be made at the ORNL 3-Mev Van de Graaff to determine α of ^{233}U and ^{239}Pu in the energy range from 20 kev to 1 Mev. Earlier measurements for ^{235}U in the kev energy range have now been published.[5]

Neutron Cross-Section Studies

Studies of neutron cross sections required for accurate reactor and shielding calculations are being continued. The program involves both experimental and theoretical nuclear physics, with the experiments designed to test various theoretical aspects of nuclear reaction mechanisms. A better understanding of these mechanisms is required if we are to make reliable predictions

[5] L. W. Weston, G. deSaussure, and R. Gwin, *Nucl. Sci. Eng.* 20, 80 (1964).

of differential and total cross sections for nuclear reactions. To develop confidence in the predictions, a systematic study that compares theoretical predictions with experimental data for a wide range of target nuclei, incident nucleons, incident energies, and nuclear reactions is being carried out.

In the experimental program, which is performed at the various Laboratory accelerators, we have been concentrating on developing an experimental system to measure elastic and inelastic neutron differential cross sections for incident neutron energies above 4 Mev. The required pulsed beams have been obtained, and the experimental equipment has been built and tested. This equipment is operational, but we will continue to develop new techniques and improve the system as a whole. Data have been obtained for the scattering of 5-Mev neutrons by silicon. We anticipate that the data acquired from this experimental system will complement the higher-energy charged-particle data in the understanding of the theory.

In the theoretical program we are continuing our study of the optical-model method of describing elastic scattering. Experimental data in the few-Mev incident-energy range, where the compound nucleus contributions to the scattering are thought to be important, are being studied by a method which combines the shape-elastic scattering predictions of the optical model with the compound-elastic scattering predictions obtained from a generalized Hauser-Feshbach formalism modified to include spin-orbit coupling (Fig. 9). A computer code has been written which is capable of searching on and analyzing several angular distributions, elastic and inelastic, and at different energies, simultaneously.

The excellent approximation to the nonlocal potential reported previously[6] was proved rigorously mathematically correct. The same mathematical formalism was used to derive an expression approximating the finite range contribution required in distorted-wave reaction calculations; the resulting approximation was found to be in good agreement with the exact calculation. In addition, this mathematical formalism was applied to Weinberg's second fundamental theorem to extend it to nonhomogeneous nuclear systems.

[6] *Oak Ridge National Laboratory, 1963,* ORNL-3650, p. 61.

Pulsed-Neutron Measurements of Diffusion Parameters in Ordinary Ice as a Function of Temperature

The parameters λ_a, D, and C in the familar equation[7]

$$\lambda = \lambda_a + DB^2(1 - CB^2)$$

have been measured for ice over the buckling range 0.039 to 0.738 cm^{-2}. The classical pulsed-neutron method was used with the ice contained in an absorber-lined cryostat at temperatures down to −85°C. Special techniques were developed for producing accurately shaped ice cylinders of uniform density.

A 300-kev deuteron accelerator, both pre- and postacceleration-pulsed, was used to produce 20- to 200-μsec bursts of D-D neutrons which impinged on the ice cylinders [D-T neutrons could not be used, despite intensity advantages, because they caused a high quasi-flat background due to photoneutrons from the decay of 7.35-sec ^{16}N produced by the $^{16}O(n,p)^{16}N$ reaction]. Each of 65 decays was measured with at least 10^6 counts in an 18-channel time analyzer, after waiting times ranging from 533 μsec (largest cylinder) to 140 μsec (smallest cylinder).

The results were analyzed by a nonlinear least-squares fitting to a two-exponential decay model. A small-amplitude accelerator-derived component of $(6.5 \pm 2.5) \times 10^{-3}$ sec^{-1} was found and corrected for. The corrected data had slopes constant within 1.5% over the time observed.

The results show that the absorption cross section has a $1/v$ dependence over the measured temperature range, making λ_a a constant and yielding an average value of 331.5 ± 3.1 mb for σ_a(H); vD may be fitted to a linear temperature relation, yielding

$$vD = (3.30 + 0.0123T) \times 10^4 \text{ cm}^2/\text{sec} ,$$

where T is the temperature (°C). The diffusion cooling coefficient, C, has large uncertainties but fits a linear temperature dependence:

$$C = (4.55 + 0.025T) \times 10^3 \text{ cm}^4/\text{sec} .$$

[7] K. H. Beckurts, *Nucl. Instr. Methods* 11, 144 (1961).

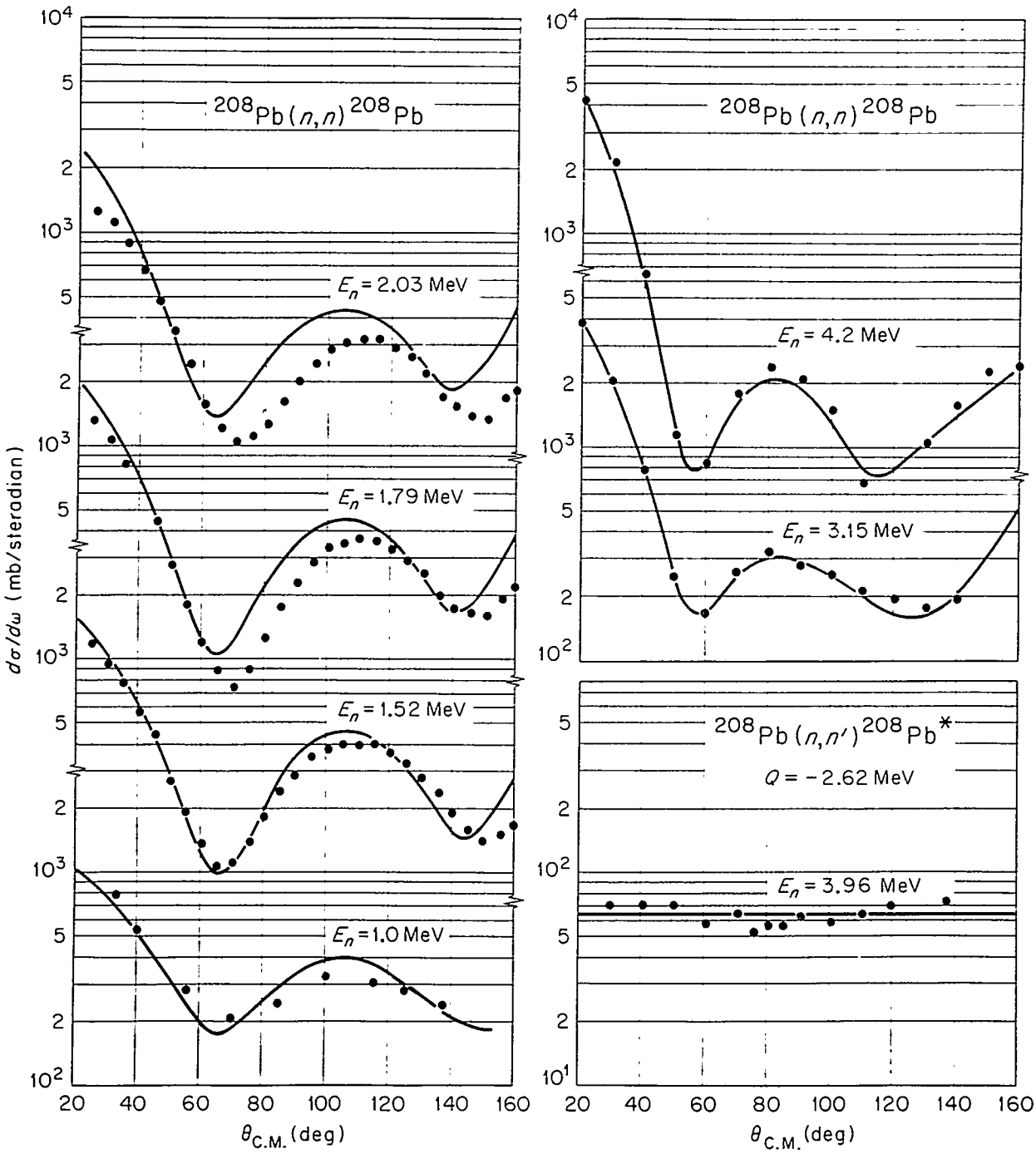

Fig. 9. Neutron Scattering Cross Sections for ^{208}Pb. The differential elastic and inelastic scattering cross sections are compared with predictions based on a model combining the optical model with the compound nucleus (Hauser-Feshbach). All the data shown were searched on simultaneously to obtain one set of parameters.

Photo 66028

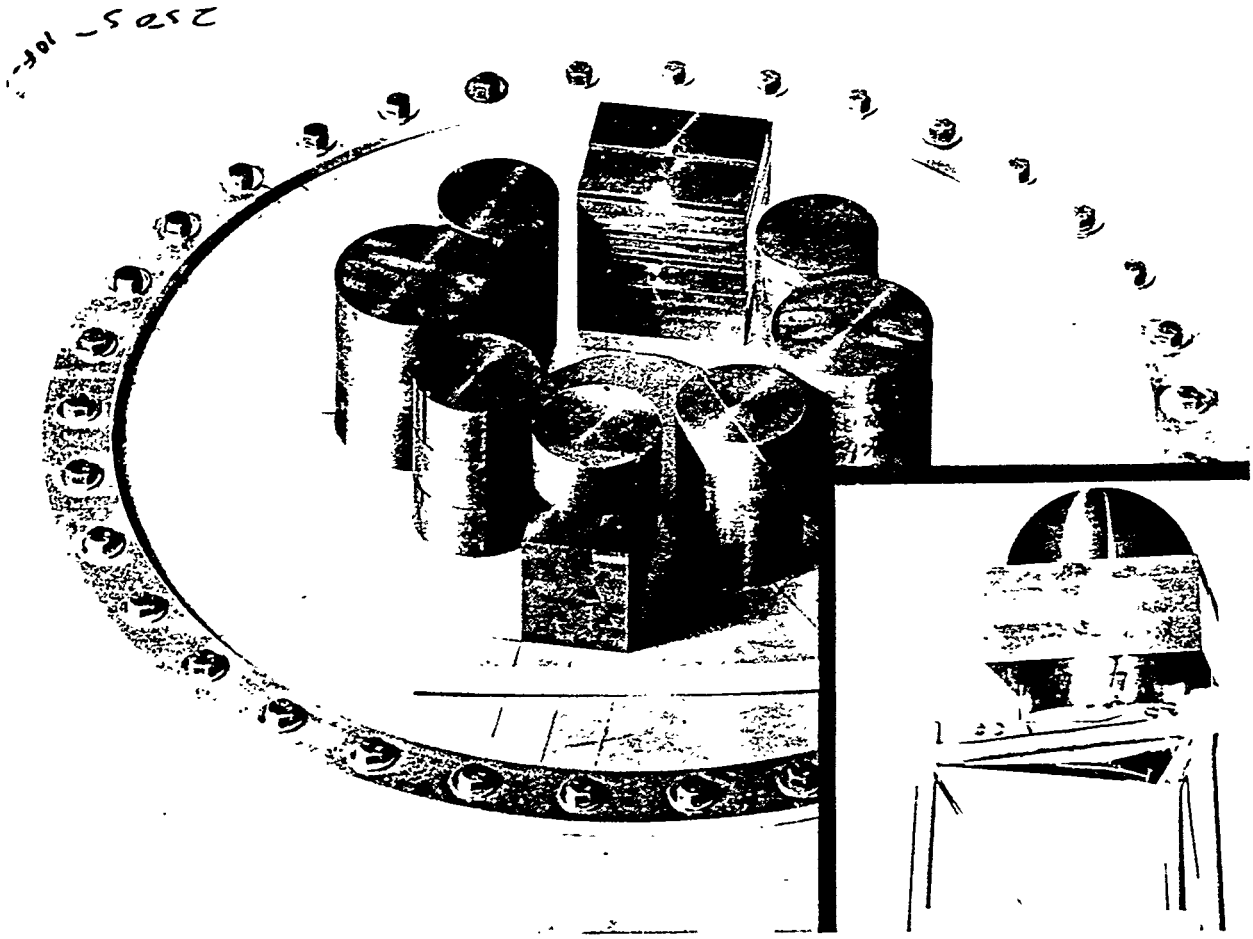

Fig. 10. Critical Configuration of Uranium Metal Pieces Enriched to 93.2% in ^{235}U. The inset shows an irregularly shaped unit which is raised through the center of the other unit to achieve criticality.

Monte Carlo Calculations and Experiments with Enriched Uranium Metal Systems

A program of considerable significance, embodying both experiments and theoretical analyses, has been carried on in the study of nuclear chain reactions. Self-sustaining chain-reacting (critical) assemblies have been constructed from pieces of uranium metal of which about 93% was the fissile ^{235}U isotope. These pieces were of a variety of shapes – cylinders, disks, rectangular parallelepipeds, and one hemisphere. In a particular assembly, these pieces, each individually highly subcritical, were arranged so that in combination criticality was established. The uranium was unmoderated and unreflected. The experiments were carried out with equipment, described in the preceding report of this series,[8] whereby the upper section of the assembly was supported on a thin sheet of steel and the lower section was brought into position by a remotely operated vertical lift device (Fig. 10).

The neutron multiplication factor of these assemblies was calculated by a Monte Carlo method which follows the neutrons, collision by collision, until they produce other neutrons by fission or are lost from the assembly. The nuclear properties used in the calculations were taken from the published reports of other experiments. The agreement between the experimental neutron multiplication factor of unity and the calculated values for five assemblies was satisfactory, and, in fact,

[8] *Oak Ridge National Laboratory, 1963,* ORNL-3650, p. 64.

the small differences may be due largely to uncertainties in the nuclear properties of the uranium.

In addition to the neutron multiplication factors, the Monte Carlo calculation evaluates the lifetime of the prompt neutrons in the assembly and the neutron flux distribution.

A simplification of the Monte Carlo calculation has been developed whereby only the neutron multiplication factor can be calculated but much more readily than with the complete method. In this modification characteristic nuclear properties of the material making up the assembly are established from two or more experiments with single critical units of the material. The properties are those displayed to neutrons of a single "average" energy. The method is known as "one-velocity" Monte Carlo calculations. The multiplication factors of the assemblies mentioned above have been calculated by this simplified method, and the agreement with experiment was satisfactory in these comparisons also.

REACTOR THEORY

We continued with studies seeking improved methods for obtaining numerical solutions to the neutron transport equation. The present approach differs from existing techniques in that the difference equations are constructed considering neutron rays through the system and has shown good success in problems with slab geometry. The more difficult problem of cylindrical geometry has now been considered, and encouraging results have been obtained. The angular fluxes are given quite accurately for purely absorbing cylinders, and success in more difficult problems seems now to depend on the introduction of new and specialized forms of quadrature, which are presently being developed.

Analytical studies of space-time reactor transients have concentrated on the transients associated with several common reactor experiments. Pulsed-source transients were studied in detail for highly reflected cores, and certain problems of space dependence for the $k\beta/l$ and source-jerk experiments (for reactivity measurements) were clarified. For the source-jerk experiment, an exact theory was developed which involves the spatial integration of experimental measurements. The space-time transient associated with rod-drop experiments was studied for large reactivity changes in order to assess the limits of usefulness for this technique.

REACTOR FUELS AND MATERIALS

HIGH-TEMPERATURE CONTAINMENT OF LIQUID METALS

Compact light-weight nuclear power sources are needed for the systematic exploration of outer space. Power generation will use boiling alkali metals rather than water as the working fluid. We are studying corrosion by these high-temperature liquids and have demonstrated that certain alloys of niobium resist them adequately. A niobium-base alloy containing zirconium has successfully contained boiling potassium at 1200°C for periods up to 5000 hr. Since niobium will rapidly burn in air at these temperatures, the apparatus must be contained in large vacuum chambers, as shown in Fig. 1.

SNAP-8 CORROSION PROGRAM

The SNAP-8 corrosion program has been in progress for the past year and a half. The purpose of the program is to study corrosion in scaled-down loops (Fig. 2) which simulate the NaK-cooled reactor circuit of the SNAP-8 reactor system. The corrosion program is designed to observe the effects of two different oxygen levels (below 30 and about 80 ppm), hydrogen addition, operating time, and maximum temperatures of 1300, 1400, and 1450°F. Ten corrosion loops have completed operation, and metallographic examinations are in progress.

SNAP-50 CORROSION TEST LOOP

A test loop (Fig. 3) designed for studying the nature and extent of corrosion and dissimilar-metal interactions in an alkali-metal heat-rejection circuit was built and was operated approximately 3000 hr at a heater outlet temperature of 1257°F. Removable Nb–1% Zr alloy specimens and type 316 stainless steel specimens were shown, in metallurgical examinations, to experience minor transfer of carbon and nitrogen to the Nb–1% Zr alloy, and a very thin layer of NbC and NbN was found on the surface of the alloy.

FORCED-CIRCULATION BOILING-POTASSIUM CORROSION LOOPS

A series of forced-circulation boiling-potassium loops was operated to determine the effects of high-velocity potassium vapor of varying quality and temperature on potential power-plant structural materials and potential turbine nozzle and blade materials (Fig. 4). Loops fabricated from type 316 stainless steel were used to investigate the effects of potassium vapor up to 870°C, and refractory-metal loops designed for operation under a vacuum are providing an analysis of vapor effects up to 1100°C. Samples of type 316 stainless steel, Haynes alloy No. 25, and molybdenum alloy (TZM) were tested in the stainless steel loops. In addition, a 3000-hr test of an Nb–1% Zr test piece was completed in an Nb–1% Zr loop system (Fig. 5). A second refractory-metal loop was assembled for the purpose of evaluating the corrosion-erosion resistance of a nozzle–turbine-blade assembly fabricated of TZM.

FABRICATION OF HIGH-TEMPERATURE MATERIALS FROM VAPORS

We are preparing reactor fuels and other high-temperature materials by deposition from chemically reacting vapors. Although the ultimate goal of producing complete fuel elements from vapors has not been achieved, several improved materials and fabricated pieces have emerged from this program. The more recent accomplishments include the one-step production of uranium dioxide

Photo 39755

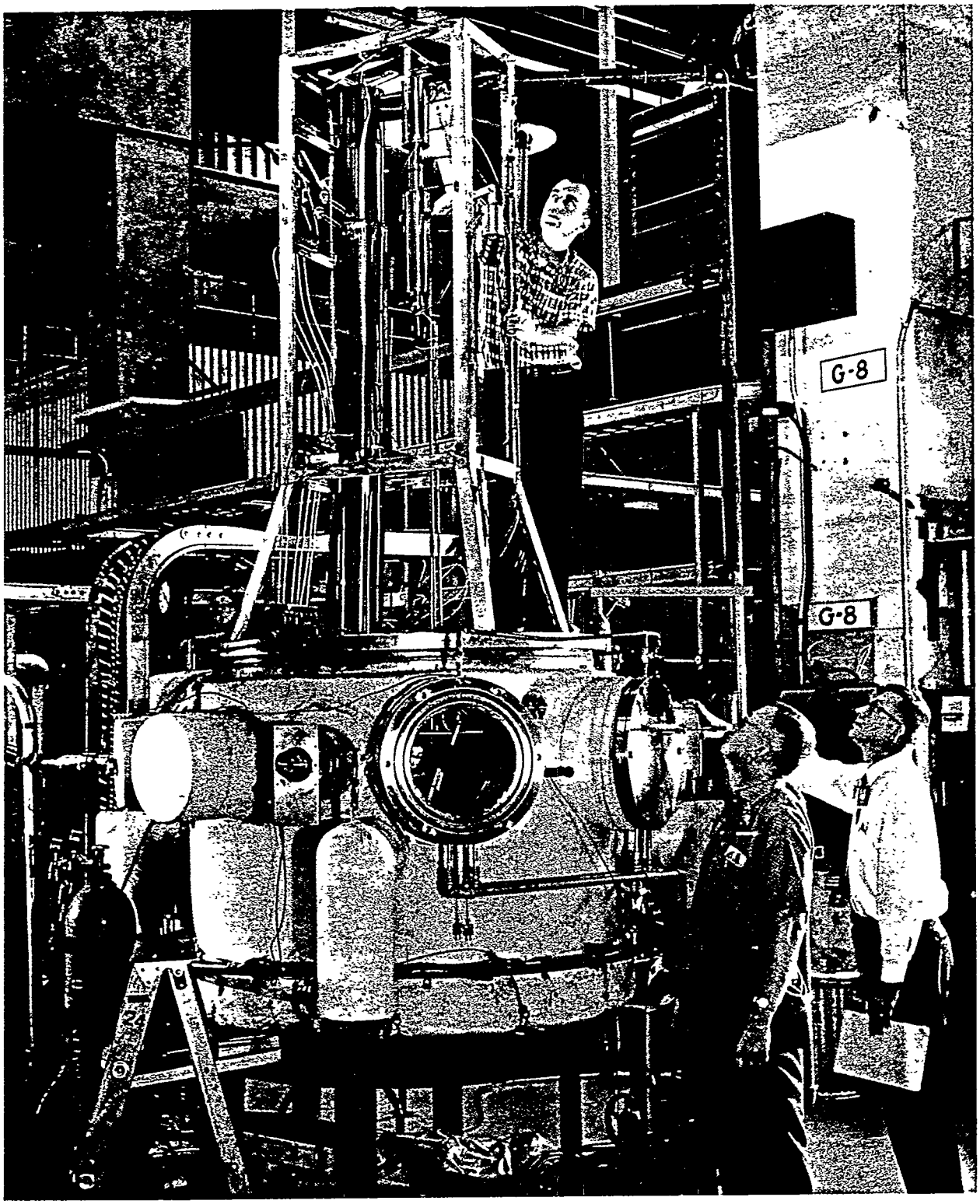

Fig. 1. Loop for Studying Corrosion by Boiling Potassium. Since this loop was fabricated from a niobium alloy, it operated in a large vacuum chamber for protection from the atmosphere. In the photograph, the top bell of the chamber is removed.

Photo 70710

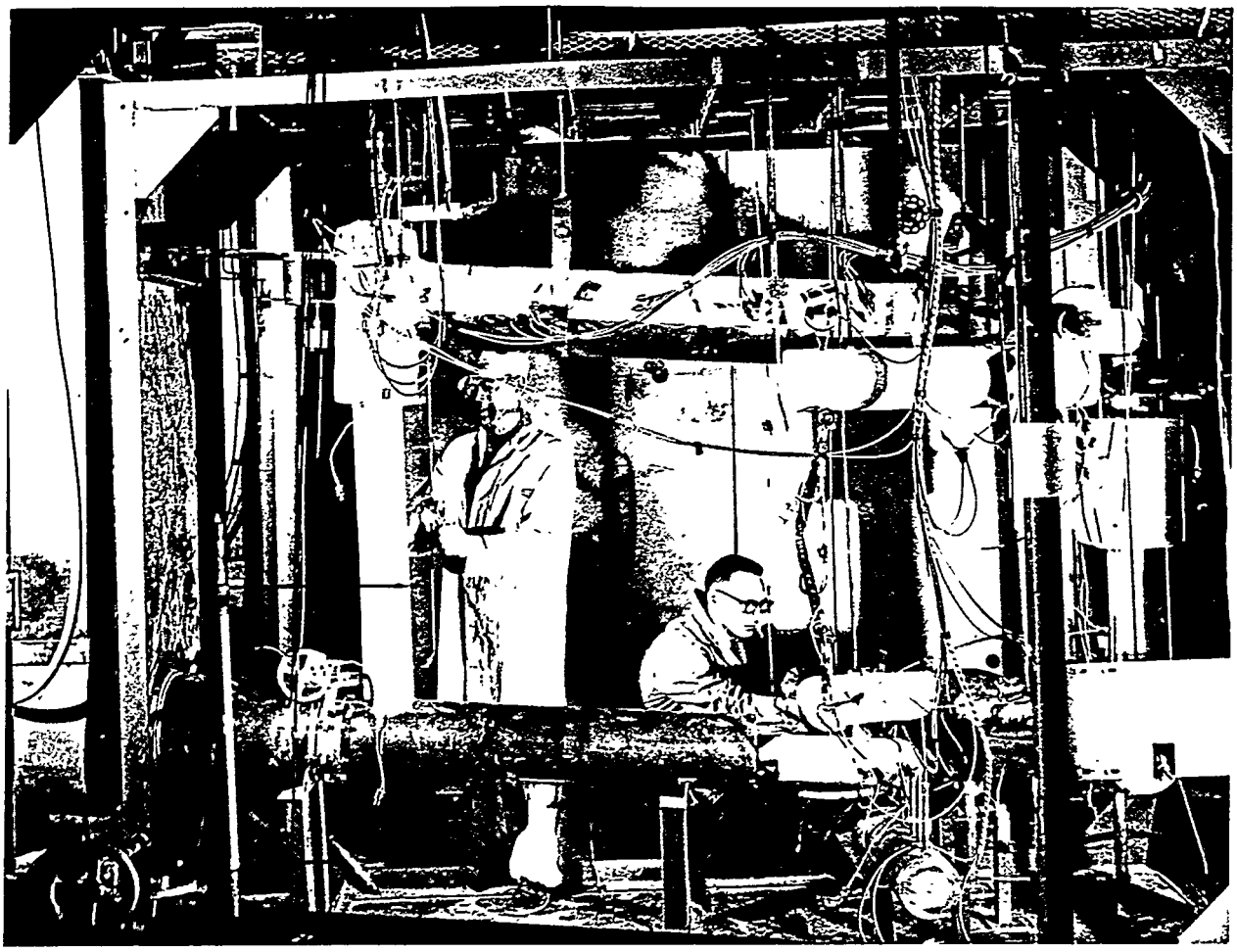

Fig. 2. SNAP-8 Corrosion Test Loop. One of a series of loops that have been assembled and operated to simulate the NaK-cooled reactor circuit of the SNAP-8 space power plant. Ten corrosion loops have completed operation, and metallographic examinations are in progress.

in several forms from uranium hexafluoride and the production of tungsten-rhenium alloy tubing from the hexafluorides of these metals.

Tungsten alloyed with rhenium is very strong at the very high temperatures of some space applications. Its fabrication is very difficult and expensive because of the high temperatures required (e.g., 1800°C for extrusion), the tendency to form a brittle sigma phase during alloying, and the poor recovery of the expensive rhenium. These difficulties are avoided by our method of reducing a mixture of tungsten and rhenium hexafluorides with hydrogen at 450 to 700°C. Since the rhenium compound is much more easily reduced than the tungsten compound, uniformity requires careful selection and control of deposition conditions. A uniform 7-in.-long tube of W–12% Re, shown in Fig. 6, was prepared at 600°C with the reacting gases diluted with argon.

Pyrolytic production of uranium dioxide from uranium hexafluoride permits production of reactor fuel (possibly even fabricated fuel pieces) from gaseous-diffusion product in one operation. As seen in Fig. 7, the product may be fine powder, coarse dendritic crystallites, or a uniformly thick theoretically dense (i.e., nonporous) massive solid, depending on reaction pressure, temperature, and gas-mixing techniques. The oxygen-to-uranium ratio of the massive solid may be varied from 2.004 to 2.156 by adjusting the ratios of the reactants. These products are formed from reaction of uranium hexafluoride with hydrogen and

PHOTO 71226

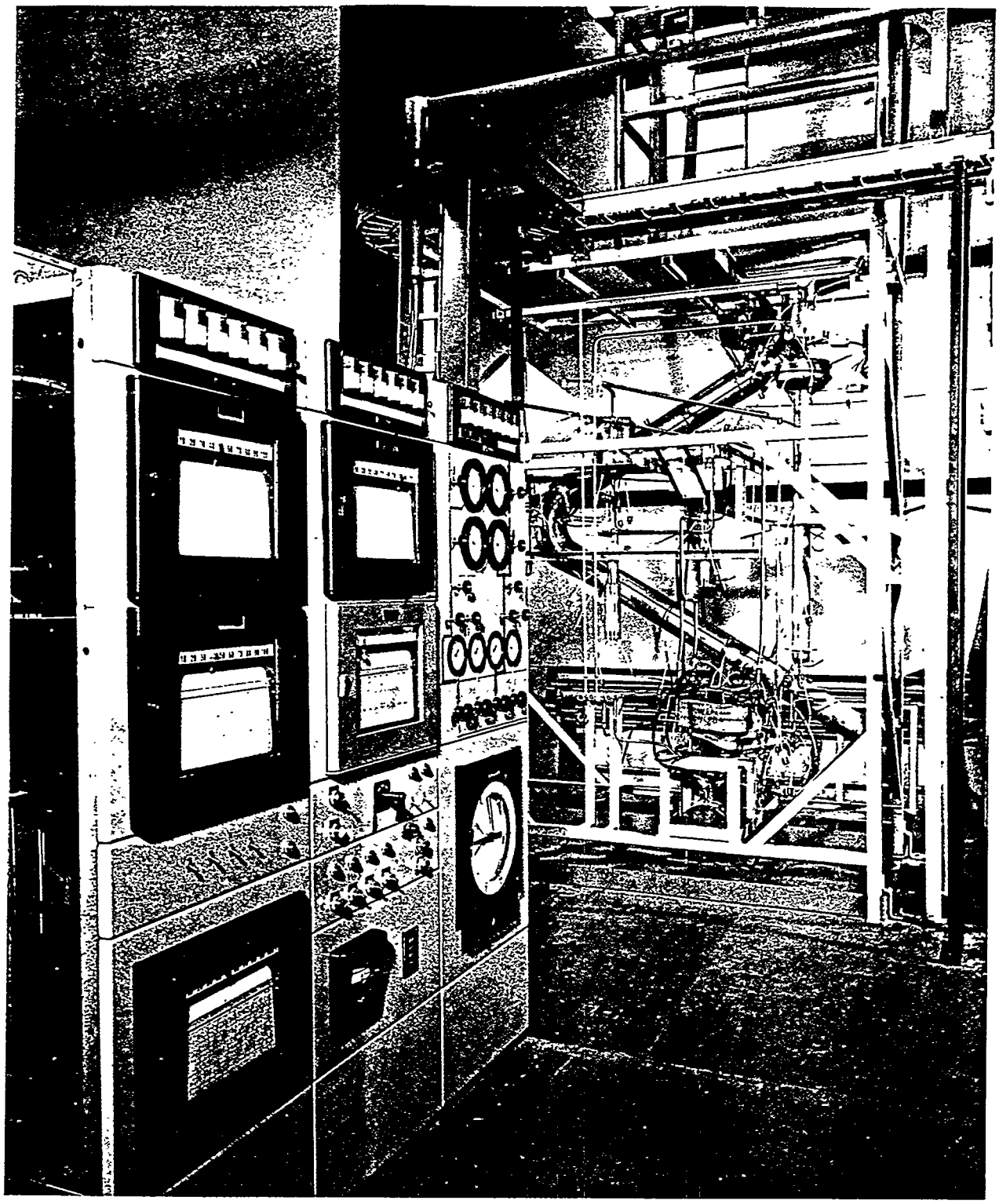

Fig. 3. SNAP-50 Corrosion Test Loop. The loop is shown prior to the addition of thermal insulation. This loop simulates a heat-rejection system of a space reactor power plant in which a sodium-potassium alloy is circulated through components that are all type 316 stainless steel except the condenser, which is Nb–1% Zr alloy.

Photo 70964

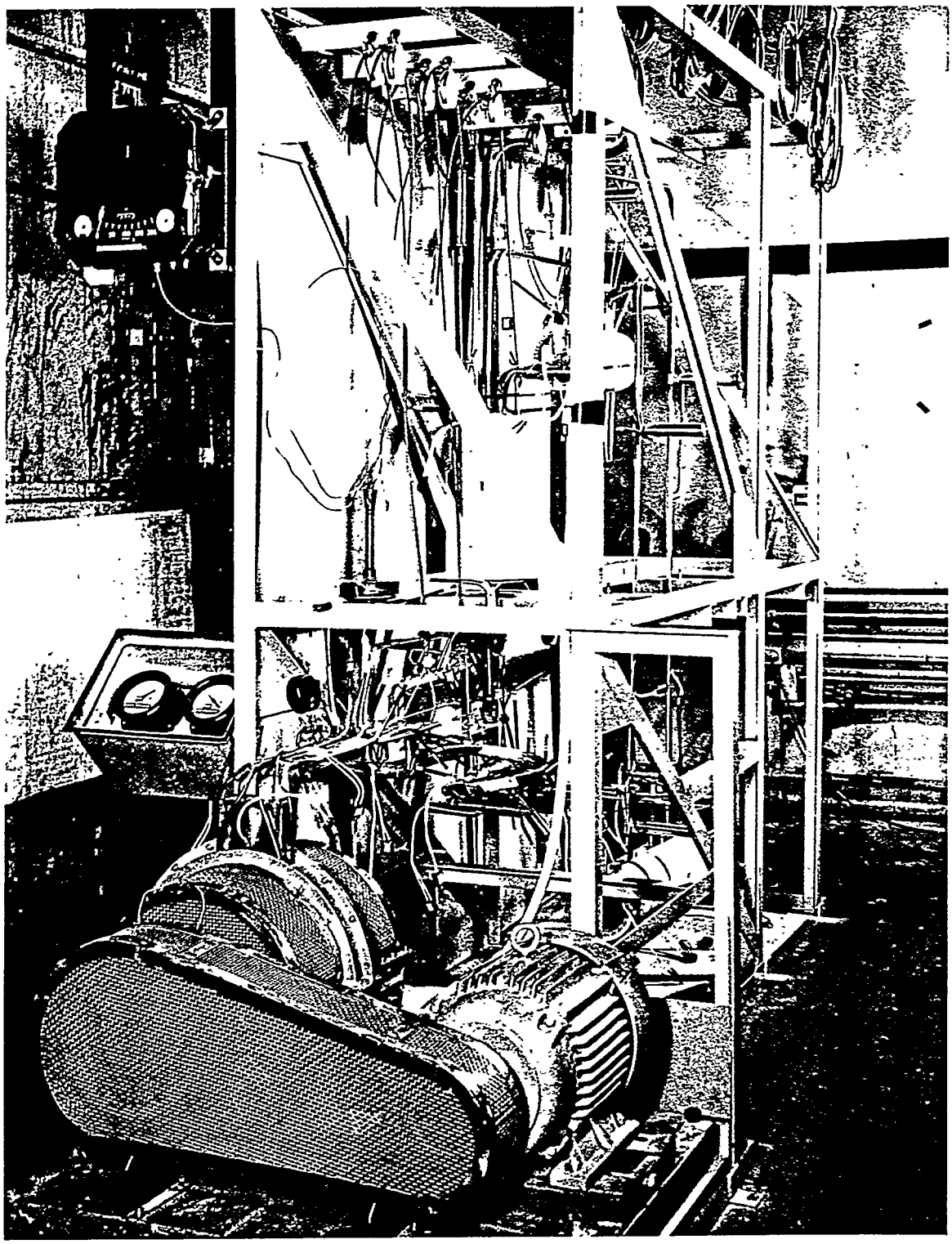

Fig. 4. Boiling-Potassium Corrosion Loop. This facility was built for the purpose of testing electrodynamic pumps that circulate liquid metals in high-temperature materials experiments. The stainless steel pump shown here was operated in potassium at 1750 rpm without detectable damage. A pump having an Nb–1% Zr cell is under development.

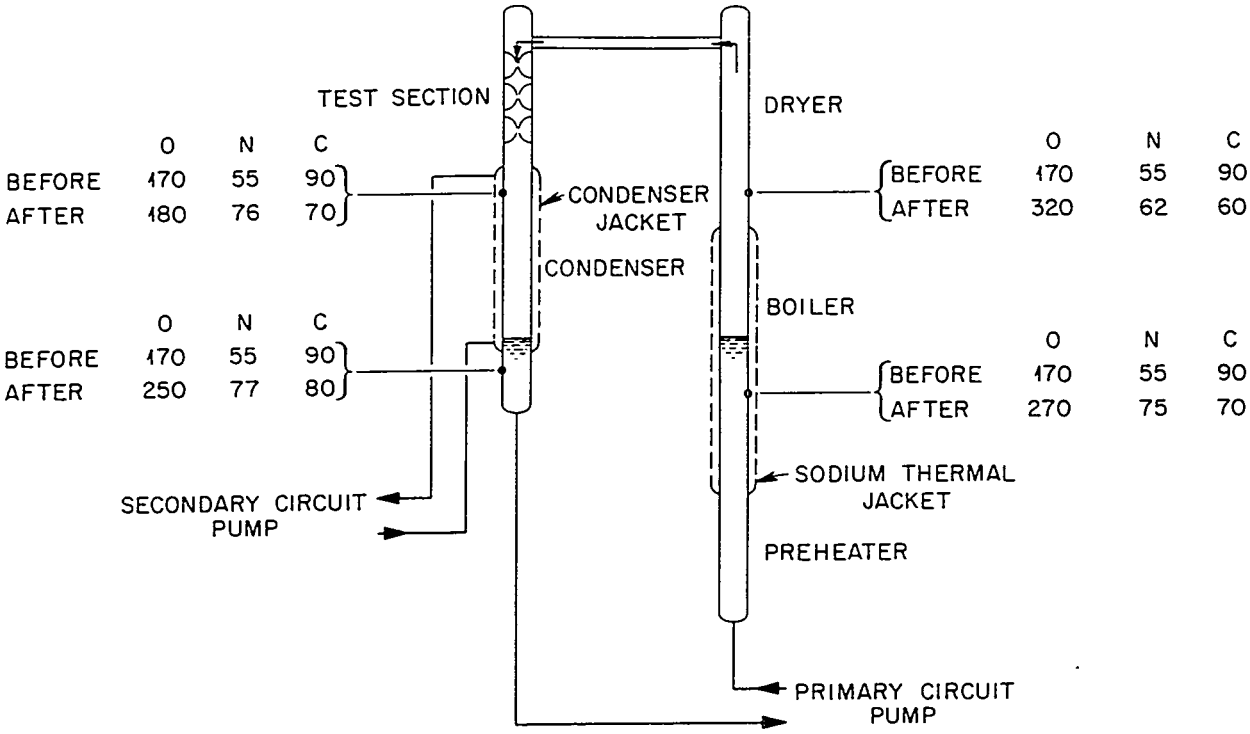

Fig. 5. Boiling-Potassium Corrosion Test. This diagram shows the results from analyses of total wall cross sections at various locations before and after forced circulation of boiling potassium for 3000 hr.

Y-58939

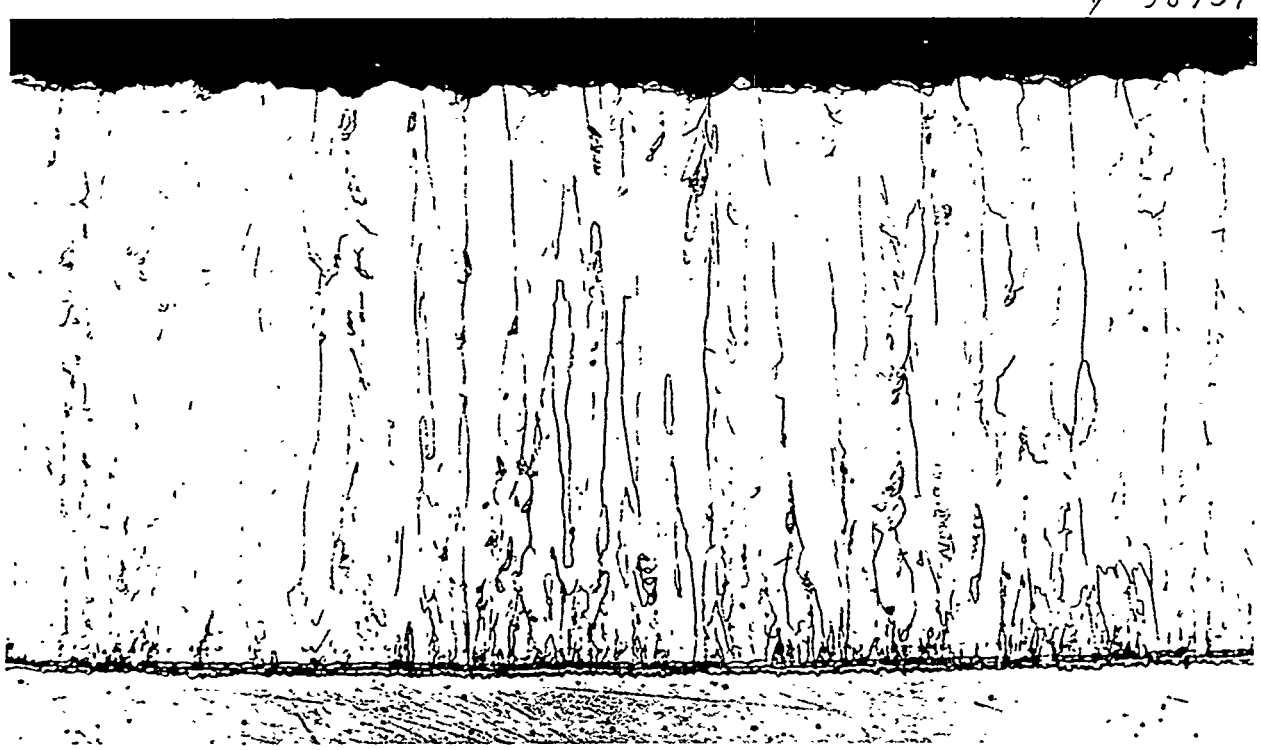

Fig. 6. Microstructure of Vapor-Deposited W–12% Re Alloy. 250×. Reduced 35%.

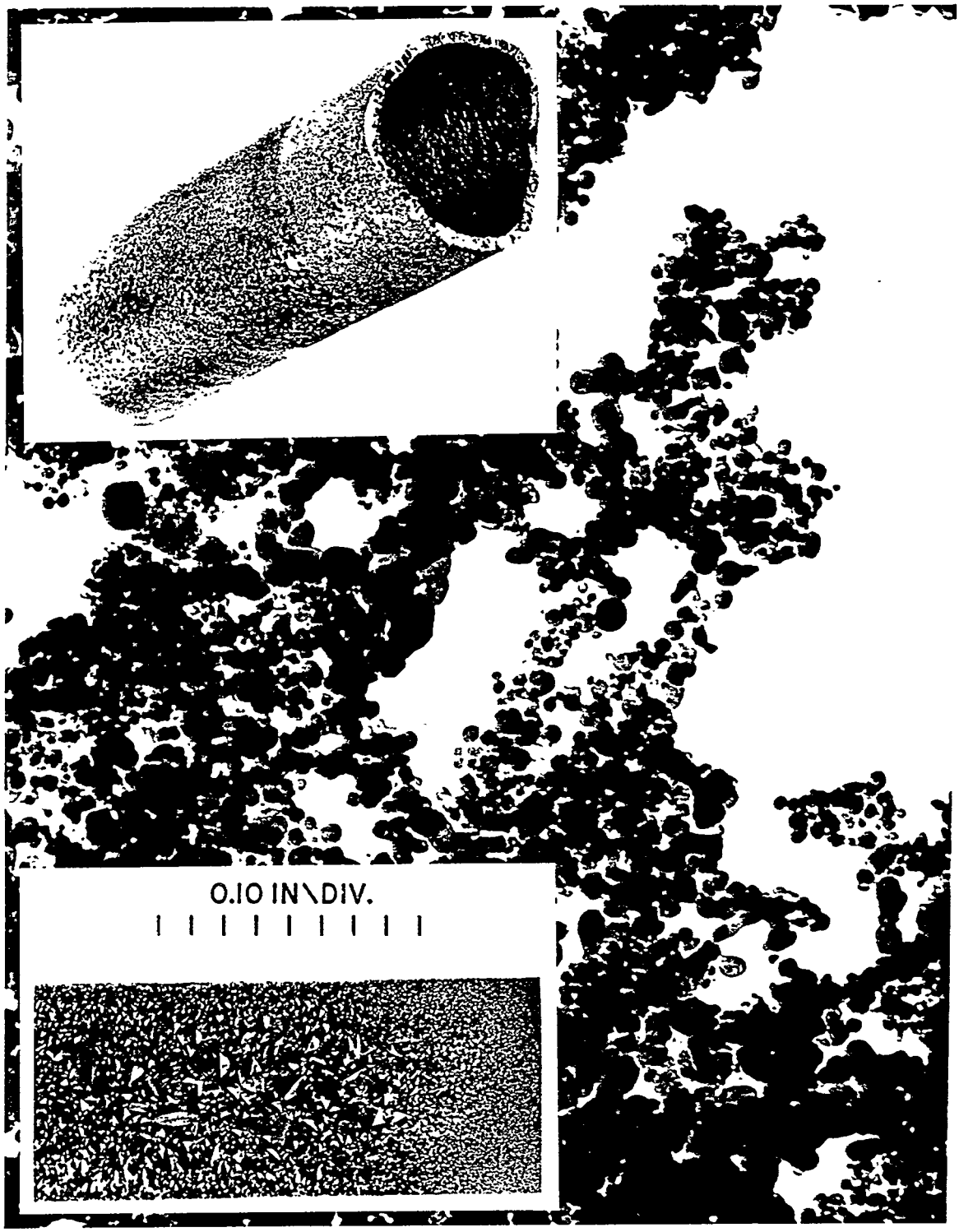

Fig. 7. Samples of Uranium Dioxide Prepared by Vapor Deposition. At the lower left is a dendritic deposit of deep red translucent crystals. At the top is a massive deposit of dense uranium dioxide. The background is an electron micrograph of extremely fine powder, magnification 165,000×. Reduced 16%.

either steam or oxygen at pressures less than 20 torrs and temperatures in the range 900 to 1500°C. In addition, 0.5-mm-diam single crystals of uranium dioxide have been prepared by passage of a gaseous mixture of uranium hexafluoride, carbon dioxide, and hydrogen over a hot platinum filament.

DIFFUSION IN METALS

We have made several recent advances in the subject of diffusion in metals, the process in which material is transported by movement of individual atoms. Diffusion is the controlling mechanism of several important processes, such as annealing, corrosion, and creep.

The effect of heavy-particle bombardment on diffusion was measured directly for the first time. In a silver specimen exposed to alpha particles from a polonium source, the diffusion of lead was increased by an amount that was independent of temperature in the range 360 to 480°C and equal to that expected from the disruption of the metal structure by the alpha particles. In another study, an unusually high concentration gradient resulted when silver specimens containing antimony were subjected to a temperature gradient.

The continuing study of diffusion in body-centered cubic metals has been aided materially by the development of a new and sensitive technique for analyzing thin sections of niobium and tantalum. During a fundamental study of the oxidation of niobium and tantalum, we found that oxide layers formed on these metals by electrolysis were very uniform and easily stripped by plastic tape. This affords a sensitive technique for diffusion measurements. Diffusion is measured by depositing radioactive tracer of the moving element on a surface of the specimen, annealing the specimen for a known time at the desired temperature, removing layers of the specimen parallel to the radioactive surface, and measuring the radioactivity of the successive layers. The new sectioning method permits taking samples only a few hundred angstroms thick, much thinner than possible with the customary mechanical techniques. This has extended the range of measurable diffusion rates and hence the range of temperatures over which rates can be measured. Also, the technique has permitted closer examination of diffusion near the metal surface, leading to discovery of an anomalous near-surface effect and casting doubt on some of the bulk diffusion rates measured by one common simplified method.

ZIRCONIUM METALLURGY

Analysis of Complex Stresses in Zircaloy-2

We have analyzed the behavior of Zircaloy-2 under the complex stresses that occur in pressure tubing. This corrosion-resistant zirconium-base alloy is widely used for fuel cladding in water-cooled power reactors, and its use is being extended to the permanent structure of reactor cores. This extension increases the strength and endurance required of the alloy. Tubing that contains a pressurized fluid is stressed both along its length and along the circumference of a cross section. Strengths are generally measured for one direction. Previously, the results of biaxial stress have been analyzed only for metals with cubic crystal structures, which behave more simply because their properties are isotropic. The analysis has now been extended to anisotropic metals, so the resistance of Zircaloy-2 tubing to deformation can be calculated from tensile data.

Stress-Oriented Precipitation of Hydrides in Zircaloy-2

Hydrogen pickup during corrosion of zirconium alloys in water and steam deters their use as reactor materials, since even modest concentrations of hydrogen can allow precipitation of hydride in alloys cooled from the operating temperature. The decrease in ductility in Zircaloy-2 of low hydrogen content varies from zero when the stress axis is parallel to the hydride platelets to a maximum when the stress axis is perpendicular.

Specimens of Zircaloy-2 having a variety of preferred orientations and hydrogen levels of about 50, 100, and 150 ppm were stressed to 11,000 and 20,000 psi at 400°C, cooled under stress, and studied by a new technique. A three-surface metallographic analysis of the hydride

trace angles relative to selected reference directions, a count of the number of hydride particles per square centimeter of surface area, and a determination of the volume fraction of hydrides present permitted construction of "hydride pole figures," which show the concentration of hydride platelet poles on a conventional pole-figure plot. The results permit us to prescribe fabrication procedures that minimize the damaging effects of subsequent hydriding.

Determination of the (0001) Pole Figures in Zircaloy-2 by Quantitative Metallography

The same three-surface metallographic analysis used in the determination of the hydride pole figures can be used to determine the (0001) pole figure of Zircaloy-2 by the use of a polarized-light metallurgical microscope equipped with a sensitive tint plate. To determine the trace angle of the basal plane relative to the fabrication directions, we rotate the stage of the microscope clockwise and visually observe the stage angle at the purple point as the color of the grain changes from red to blue. These angles for many grains of the matrix are converted to a pole figure by the approximation method used for construction of inverse pole figures from x-ray data. The microtexture of a small volume of a specimen can be readily determined in 1 to 2 hr, compared with several days by conventional techniques. Now one can determine the variations of texture from the center to the surface of tubing having walls as thin as 0.020 in.

Zone-Refined and Single-Crystal Zirconium

Our technique and equipment for purifying and growing single crystals of zirconium and its alloys have been modified to handle large specimens. Bars as large as $\frac{5}{8}$ in. in diameter are routinely zone refined over lengths of 5 to 8 in. As many as ten successive passes of the molten zone have been made without serious distortion of the bar shape. Most of the zone-refined bars are either single or bicrystals of the alpha phase. Seeding with selected alpha-phase single crystals has been demonstrated.

NONDESTRUCTIVE TEST DEVELOPMENT

Use of X-Ray Television to Observe Hidden Motions

We have used an x-ray-sensitive closed-circuit television system to measure the expansion of a specimen that is subjected to temperature fluctuations at the rate of about 1000°F/min. This permits an accelerated test of the ability of materials to survive the rapid temperature changes that occur during reactor startup and shutdown. Since the specimen is hidden, x-ray observation is necessary. During the experiment, measurements of the specimen could be made on the television screen. However, a novel application of delay circuitry permitted us to measure the expansion much more accurately on an oscilloscope triggered by the television signal.

Radiography of Highly Radioactive Materials

Radiography is a very useful method for inspecting materials and components nondestructively. However, radiography of radioactive materials is complicated because the radiations from them fog the film. We have established limiting doses of radiation that the film may receive without losing the desired image and have also devised a film treatment that circumvents these limits. Satisfactory image contrast was maintained on films that had received 1 to 2 r of 50- to 300-kv constant-potential x rays or 32 r of 1.1-Mev gamma rays. These limits could be extended to 16 r of x rays and 380 r of 1.1-Mev gamma rays by application of a photographic reduction technique to the film. In this method the silver in the image reacts with potassium ferricyanide to form silver ferrocyanide, which is then dissolved in hypo. Figure 8 shows the result of this treatment.

Nondestructive Determination of Fuel Assay

Determination of the fuel content of fabricated fuel plates is difficult without destruction of the plate for chemical analysis. Plates that contain enriched uranium may be assayed by measurement

No Number

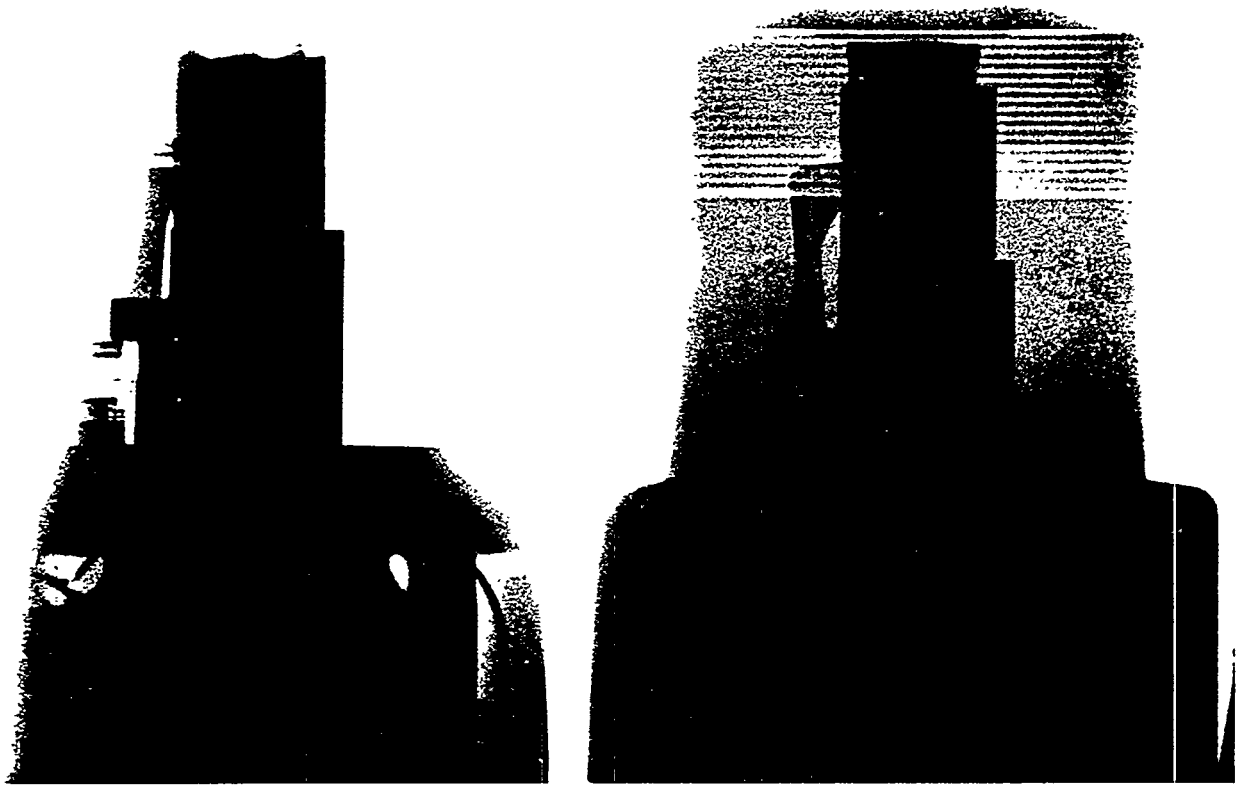

Fig. 8. Radiograph of 5-curie ^{60}Co Source. On the left, the empty housing has been radiographed by ordinary techniques. The oval cobalt source is visible in the radiograph on the right, despite the 12,000-r/hr radiation field of the source. This radiograph would be blank without the treatment to remove the background fogging from the film.

of the gamma radiation from ^{235}U, but the intensity is so low that the method is slow and inaccurate. Recently we have found that rapid and accurate fuel assays can be obtained by an extension of our system for nondestructively measuring inhomogeneity in fuel plates. In this system, variations in fuel concentration are inferred from the attenuation of a collimated x-ray beam as the plate traverses the beam. By calibrating the beam with chemical analyses of scanned plates and developing a method for integrating the point concentrations, we have now extended the method to obtain total uranium concentrations in the plates. Typical plates are scanned in about 8 min, and the total fuel contents found have been accurate to 1%.

Vibrating Eddy-Current Probe

Eddy-current testing is an excellent method for the rapid determination of very small discontinuities in items such as tubing. This is because the use of mechanical systems for moving the tube through or past the eddy-current coil allows electronic discrimination and amplification of the quickly changing signals due to flaws without response to the slower changes due to insignificant variations. However, the more common manual probe systems cannot make this discrimination and thus have low sensitivity to defects and suffer from interpretation difficulties. We have developed a tenfold more sensitive manual eddy-current probe that vibrates rapidly. Thus,

its motion past a small defect produces a quickly changing signal, allowing discrimination and amplification previously possible only with automated mechanical systems.

The eddy-current probe is mounted between two electromagnets. Switching current from one coil to the other pulls the spring-loaded probe back and forth to vibrate it. The signals from the probe are fed to an electronic filter, which is tuned to pass only the high-frequency signals from defects.

RADIATION STABILITY OF STRUCTURAL METALS

We are investigating the damage caused to structural metals by reactor radiations and finding means to minimize this damage. Radiation embrittles metals; that is, it causes pieces to break rather than deform to accommodate the in-service stresses. This effect shortens the useful life of reactor fuel elements. We have irradiated type 6061 aluminum, an alloy that can be strengthened by heat treatment, and found no loss of the added strength in the exposure required of some fuel elements. This alloy is used as fuel cladding in new high-performance test reactors. A larger and continuing effort has been to discover how radiation at elevated temperatures damages stainless steel, how heat treatments can decrease this damage, and the mechanism by which these treatments operate.

When stainless steel is used in a reactor at temperatures high enough that the mobility of the atoms counteracts the displacements that result from collisions by high-energy neutrons, there is still a residual embrittlement caused by thermal neutrons (neutrons that have only the energy of motion of molecules at the prevailing temperature). The damage can be explained by the concentration of boron impurity at the grain boundaries, the production of helium gas by reaction of the boron with neutrons, and the facilitation of crack propagation by the bubbles of helium. Also, we found that starting and propagating such cracks are made difficult by selected combinations of mechanical and thermal treatments to the metal before irradiation. These preirradiation treatments reduce the grain size of the steel and collect the carbon and boron of the steel into deposits on the grain boundaries.

ATOMIC REARRANGEMENTS IN IRRADIATED ALLOYS

The mechanical and physical properties of iron and steel depend strongly on the relative arrangement of the different kinds of atoms in the metal, for example, on whether certain elements such as nitrogen or carbon are precipitated as compounds or are distributed uniformly in solid solution. One measure of the amount of precipitation of nitrogen or carbon in iron is internal friction. We have developed a device that permits low-frequency internal friction to be measured while the sample is in the reactor. The apparatus, shown in Fig. 9, consists of a 0.005-in.-thick sample, $^3/_{16}$ in. wide and 1.5 in. long, that is caused to vibrate in flexure by a voltage applied to a driver electrode. As the specimen vibrates, a vane attached to its end passes between capacitance plates which are connected to electronic equipment located in a room adjacent to the reactor. A signal proportional to the amplitude of motion of the sample is eventually displayed on an oscilloscope screen, and the internal friction is measured by the rate of decay of the signal after the driver voltage is removed. With the use of this apparatus, it has been found that neutron irradiation accelerates the precipitation of nitrogen in iron. The result is significant, for it provides an additional indication that certain alloys, though stable under ordinary conditions, may become unstable when placed in a radiation environment.

Number Unknown

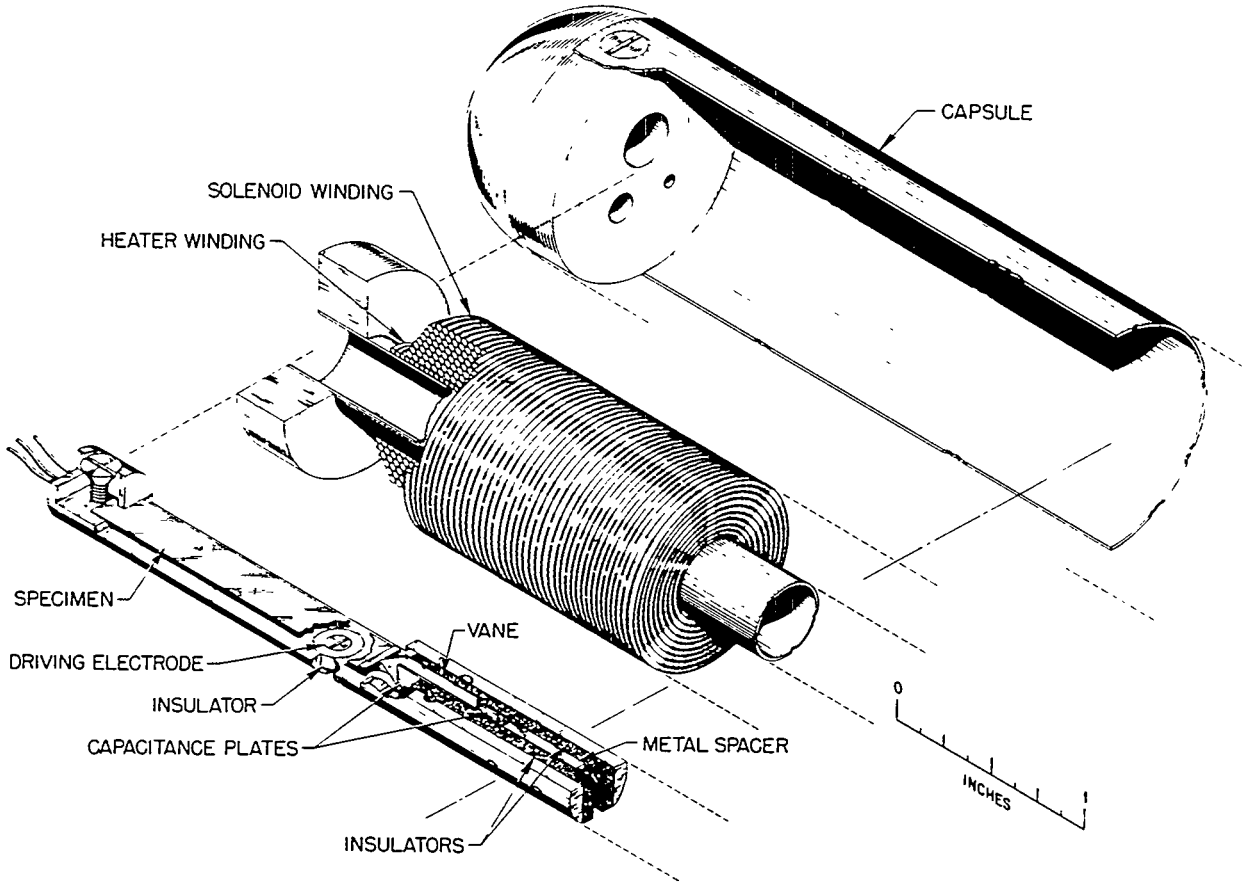

Fig. 9. Flexure Pendulum.

REACTOR COMPONENTS

REACTOR CONTROLS DEVELOPMENT

Measurement of Shutdown Reactivity

To shut down a reactor means to reduce its reactivity below the critical value; the difference – the shutdown reactivity margin – is a measure of the safety of the shutdown reactor against accidental criticality. Unfortunately, additional shutdown reactivity margin can usually be attained only at the expense of core size or life. In power and production reactors, therefore, safety and economics are in direct conflict as regards the shutdown reactivity margin which is provided. Continuous or periodic measurement of subcritical reactivity could provide assurance of adequate margin in such reactors with a smaller economic penalty.

Additional incentives to measure shutdown reactivity are the possibility of monitoring changes in a shutdown core (e.g., the variation in the reactivity effect of boric acid added to the coolant) and the possibility of assaying new or reloaded cores.

We have measured the shutdown reactivity of a reactor from the frequency spectrum of the natural fluctuations in neutron flux in the core. The equipment required was a radioactive neutron source, a neutron detector, and the instrumentation for measuring the frequency spectrum. No perturbation of the reactor or the source is required in this method.

Some spectra measured in the Pool Critical Assembly (PCA) are shown in Fig. 1 for various control-rod configurations with different reactivities. The ordinate is the *power spectral density* divided by the average neutron flux, a quantity which measures the fluctuations as a function of frequency.

The theory of these measurements is based on a stochastic model of neutron fluctuations in a reactor,[1] as well as instrumental considerations. The solid lines in Fig. 1 are theoretical spectra which represent least-squares fits to the experimental data for each control-rod configuration. From these spectra, the reactivity of each configuration was inferred. These results are shown in Table 1, together with independent measurements of the reactivities of the same configurations by R. Perez-Belles *et al.*[2] using pulsed-neutron techniques. It is evident that negative reactivities as large as 10 dollars can be determined in a reproducible way. (A reactivity of 1 dollar is defined to be equal to the effect of the delayed neutrons; in the PCA, 1 dollar corresponds to an excess multiplication factor of 0.008.)

Theoretical and experimental studies are under way to extend this measurement technique to reactors in which there is a high gamma-ray background, such as exists in a core after operation at high power. In this way, we hope to develop the means for monitoring shutdown reactivity whenever a reactor is subcritical and, thus, to avoid the potential hazards at a reasonable cost.

Coincidence Magnet for Reactor Safety Systems

The application of coincidence techniques permits the operation of a safety system to be independent of failure of a single component, since simultaneous action of two subsystems is required to initiate a reactor shutdown. Furthermore, a single subsystem can be tested by simulating a dangerous condition without causing a reactor shutdown. However, the testing and the freedom from false operation cannot involve the element in which the coincidence decision is

---

[1]The theory is based on the work of R. K. Osborn, a Summer Participant at ORNL from the University of Michigan.

[2]R. Perez-Belles *et al.*, *Neutron Phys. Div. Ann. Progr. Rept. Sept. 1, 1960*, ORNL-3016, p. 12.

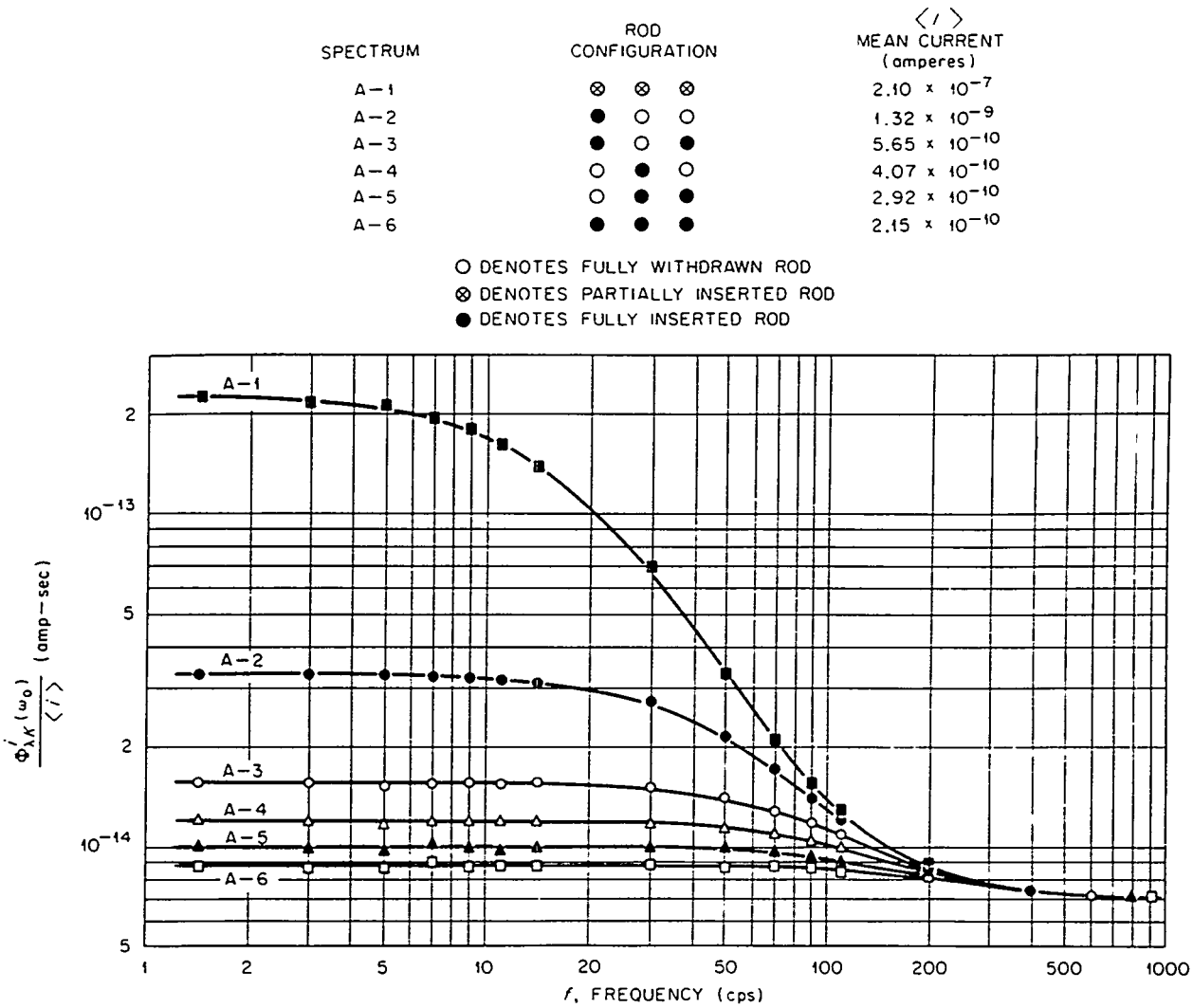

Fig. 1. Measured Frequency Spectra of Neutron Flux Fluctuations in the PCA for Various Rod Configurations.

actually taken, or any components between the coincidence element and the shutdown device. It is therefore advantageous for the coincidence element to be the shutdown device itself, so that the entire remainder of the safety system can benefit from the coincidence arrangement. For these reasons, we have developed a coincidence electromagnet for use in scram latches.

The principle of operation is shown in Fig. 2. A saturating shunt in the magnetic circuit provides the coincidence characteristic. The dimensions and the coil currents are chosen so that when any one coil is energized the magnetic flux will be bypassed through the shunt, with negligible flux in the armature and hence negligible force on the load. As the excitation is increased by turning on the second coil, the shunt becomes saturated and force is developed on the load. Energizing the third coil saturates the yoke or the armature, or both, with little increase in force. Thus the magnet has two-out-of-three logic, producing nearly full force when any two, or all three, coils are energized, and nearly zero force when one or no coil is energized. Each of the three electrically independent coils on each magnet is controlled by one safety subsystem.

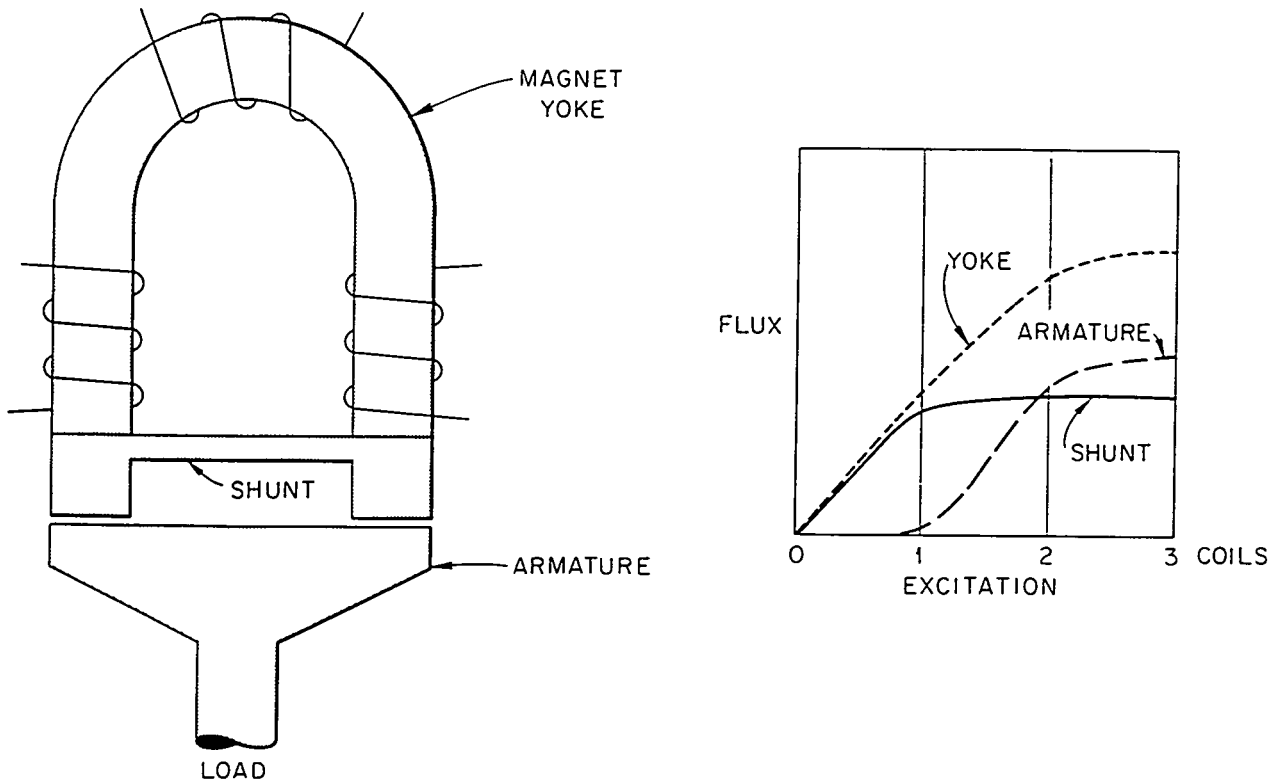

Fig. 2. Arrangement and Principle of Operation of Coincidence Electromagnet.

Table 1. Experimental Results – Negative Reactivities

Rod Configuration[a]	ρ, Reactivity (dollars) (Subcritical Reactor) Spectral Density Measurements	Pulsed-Neutron Measurements[b,c]
● ○ ○	−1.99 ± 0.02	−1.73 ± 0.04
○ ○ ●		
● ○ ●	−4.49 ± 0.06	−5.13 ± 0.18
○ ● ○	−5.97 ± 0.18	−5.52 ± 0.22
○ ● ●	−8.90 ± 0.52	−8.91 ± 0.64
● ● ●	−10.6 ± 0.6	−10.5 ± 0.7

[a]The symbol ● denotes a fully inserted control rod, and ○ denotes a fully withdrawn control rod.

[b]R. Perez-Belles *et al.*, *Neutron Phys. Div. Ann. Progr. Rept. Sept. 1, 1960*, ORNL-3016, p. 12.

[c]Pulsed-neutron measurements corrected for difference in excess reactivity resulting from the effect of chamber location for the spectral density measurements.

Figure 3 shows the operating characteristics of a large coincidence electromagnet embodying this principle which was recently designed, built, and tested for the HFIR. The rated load (force on the armature, applied in this instance by latch springs and pressure) is 880 lb. With this force applied, the release time of the magnet is less than 5 msec when three coils are simultaneously de-energized, and less than 6 msec when two coils are de-energized and the third coil remains energized, simulating failure of a single subsystem.

The use of coincidence magnets makes it possible to keep safety subsystems electrically independent of each other, because the required mixing takes place only in the common magnetic circuit. Testing can be performed during operation by locally perturbing process variables to make each sensor in turn detect an abnormal condition. Observation that the corresponding coil in each magnet is de-energized by the test confirms the operability of the entire subsystem, except for the actual release of the control rod.

65-11744

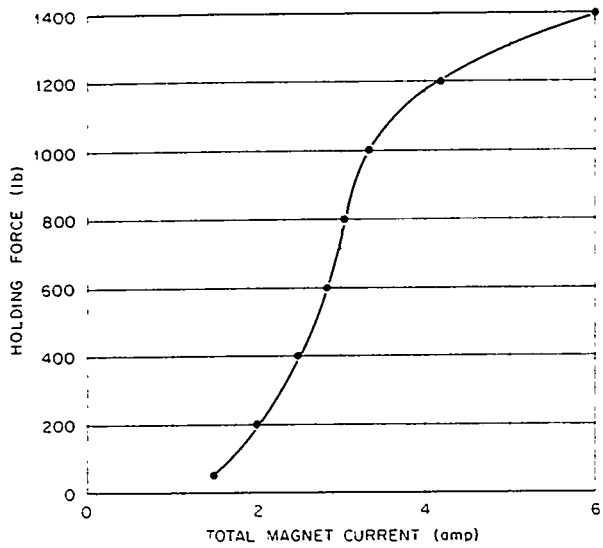

Fig. 3. Force-Excitation Characteristic of Coincidence Electromagnet for HFIR.

ENGINEERING RESEARCH

HEAT TRANSFER AND FLUID MECHANICS

We continued during 1964 our studies in heat transfer and fluid mechanics relating to general reactor technology; the specific areas investigated included (1) boiling phenomena with water and the liquid alkali metals in a variety of experimental circumstances and geometries, (2) the dynamics of vortex-like flows, with emphasis on the effects of high-strength axial magnetic fields in reducing radial turbulent fluctuations, (3) thermal fluctuations at a heated solid-liquid interface arising from the turbulent structure of the flow, (4) a technique for the direct measurement of the Reynolds stresses in a turbulent pipe flow, and (5) the thermophysical properties of the liquid alkali metals, in particular the surface tension. Results obtained in some of these studies are summarized in the paragraphs following.

Data were obtained for the critical heat flux and for the two-phase pressure drop with boiling potassium in forced flow upward through a vertical circular tube. The critical flux values continued to agree closely with predictions made using the correlation for water of Lowdermilk, Lanzo, and Siegel. For fluxes below the critical, the results suggest a lesser dependence on the temperature difference than has been observed with water. Pressure-drop data correlated well with the specific data of Shrock and Grossman for water using the Lockhart-Martinelli method of presentation; the simpler homogeneous model predicted pressure losses which were only one-third of those measured.

The superheat required for bubble nucleation in the liquid alkali metals as a function of surface condition (smooth, porous, or discrete holes) was measured quantitatively over a wide range of pressures (saturation temperatures) in a small natural-circulation loop. We found that on the smooth surface, superheats (at atmospheric pressure) were of the order of 600°F; under similar conditions, the superheat with water is about 40°F. This result was consistent with predictions based on a thermodynamic analysis of liquid-metal boiling. Both the surface with multiple pores and the one with discrete holes effected a substantial reduction in the superheat for boiling. Thus, the superheat with potassium on the surface containing eight 0.006-in.-diam holes was about 10°F at the normal boiling temperature (1400°F).

The magnitude of the critical heat flux was analytically estimated and experimentally measured for the situation of flow blockage at the inlet of a natural-circulation cooled channel immersed in a water pool. We developed two correlations – one, an empirical fit of limited available data; and the other, an adaptation of Wallis' correlation for adiabatic flooding rates in vertical tubes that includes heat effects. The experimental data for tubes of about 0.10 to 0.25 in. inside diameter and 6 to 48 in. heated length fell a factor of 2.2 above the minimum flux predicted by the latter correlation; for tubes of less than 0.10 in. inside diameter, the critical flux was below this correlation, apparently because of the influence of surface tension.

Subcooled swirl-flow boiling was studied for the situation of heat generation within the tape and an adiabatic tube wall over a range of tape-twist ratios, inlet water temperatures, and heat fluxes. We observed the critical flux for a twisted tape to be not markedly greater than for a straight tape (a maximum enhancement of approximately 20% at tape-twist ratios between 7 and 10 at the lowest inlet temperature).

The analysis of the effect of a uniform axial magnetic field on the stability of vortex motion was continued. We derived an exact criterion for the stabilization of both nondissipative pure vortex flow and inviscid pure vortex flow with finite conductivity. For these cases, we found that the magnetic field for marginal stabilization increased linearly with the outer peripheral velocity of the vortex and parabolically with the fluid density but decreased with an increase in radius

ratio of the two concentric cylinders confining the flow.

The experimental investigation of the influence of a uniform axial magnetic film on the stability of an aqueous electrolytic conductor in vortex-like flow was extended to include the effects of injection geometry (slits vs round nozzles). Dye filaments were introduced into the boundary layer along the cylindrical wall of the 1.1-in.-diam vortex tube to visualize the flow. We observed for all injection geometries that the magnetic field suppressed the oscillatory flow instabilities originating at low values of the tangential Reynolds modulus in the boundary layer on the concave wall. Quantitatively, the magnitude of the tangential Reynolds modulus at which the flow changes from laminar to turbulent increased nearly linearly with the square of the Hartmann modulus for geometries with two or four slits or round nozzles; with eight injection slits, the data suggest a more rapid variation. We also found that the Reynolds modulus at the transition increased with increasing numbers of injection slits.

Our measurements on the surface tension of potassium were extended to temperatures near the atmospheric boiling point using the maximum-bubble-pressure techniques. In the temperature span between 70 and 710°C, the surface tension against helium decreased linearly from 111 dynes/cm to 69 dynes/cm; these values fall about 20% above data available in the literature. Similar measurements with lithium yielded values ranging from 409 dynes/cm at 200°C down to 294 dynes/cm at 1000°C and agreed more closely (approximately 5%) with the literature. Data obtained on the densities of both potassium and lithium by varying the depth of capillary immersion during the surface tension experiments were found to agree well with published values.

polarographic characteristics of the $Pb^{2+} \rightleftharpoons Pb^0$ reaction in hydrofluoric acid solutions of concentrations from 1 to 12 *M*.

A study of the chronopotentiometry of plutonium in mineral acid media was completed. Diffusion coefficients of the different species of plutonium were measured, and the possible analytical usefulness of chronopotentiometry for the determination of plutonium was evaluated.

POWER REACTOR FUEL PROCESSING

CHEMICAL ANALYSIS OF ADVANCED REACTOR FUELS

A gas chromatograph was designed for the analysis of corrosive gases such as nitrogen dioxide, dinitrogen trioxide, chlorine, and nitrosyl chloride. The use of tantalum appears to provide the necessary corrosion-resistant material. Gas chromatography was utilized in the analysis of those aliphatic diluents used in solvent extraction processes. The argon-filled beta ionization detector was successfully applied to this problem.

A combined combustion and gas chromatographic procedure for the determination of organic carbon in aqueous and nitric acid solutions was studied further in an effort to increase the recovery of known amounts of carbon.

A sealed-tube dissolution technique has been applied with limited success to a variety of difficultly soluble compounds such as graphite-coated UO_2, carbides, and several organic compounds. In general, the perchloric acid "liquid fire" technique is more successful for the dissolution of fluidized coke or graphite-coated materials.

A horizontal-orifice Teflon dropping mercury electrode (DME) was used to obtain fundamental polarographic data for the $Tl^+ \rightleftharpoons Tl^0$ reaction in 0.1 *M* KCl–1 *mM* HCl and the $Pb^{2+} \rightleftharpoons Pb^0$ reaction in 1 *M* HCl. The data obtained are interchangeable with those taken with glass dropping mercury electrodes. The horizontal-orifice Teflon DME was also used to determine for the first time the

HEAD-END PROCESSES FOR POWER REACTOR FUELS

Fuel Recovery Processes for Graphite-Type Fuels

In high-temperature gas-cooled nuclear reactors, uranium or thorium-uranium carbides or oxides in the form of particles coated with pyrolytic carbon and embedded in a graphite matrix are the most frequently used fuel material. The processing methods being developed at ORNL for these fuels all oxidize the graphite to carbon dioxide, and either dissolve the uranium and thorium in nitric acid for further processing by solvent extraction or remove the uranium (but not thorium) as gaseous uranium hexafluoride by treating the dry fuel ashes with gaseous fluorine.

Two processes have been developed for oxidizing the graphite. The first involves burning the fuel directly in air or oxygen at 800 to 1000°C for 1 to 2 hr or in a fluidized bed of alumina at 700 to 750°C for 5 hr. The second method involves wet combustion of the graphite in a dilute solution (2 *M*) of nitric acid, saturated with air or oxygen, at 200 to 300°C and a pressure of about 1500 psi.

Regarding the first process, burning in a fluidized bed is preferred to open burning, particularly when some of the components of the fuel have low melting points, because temperature control is more easily achieved. The graphite fuel can be crushed or chopped by impact quite readily, and adequate mechanical devices for reducing fuel elements to the desired size for charging to the burner have been tested. The progress of combustion is followed satisfactorily by monitoring the content of CO_2 in the off-gas with either a gas chromatograph or an infrared analyzer.

GL-1576A

After burning, the "ashes" are leached for 5 hr with boiling 4 or 13 *M* nitric acid that is 0.05 *M* in hydrofluoric acid. Recovery of more than 99.7% of both the uranium and thorium is achieved. Alternatively, the ash can be fluorinated at 500°C. Engineering tests of this operation have resulted in the complete conversion of the uranium oxide to volatile uranium hexafluoride, which is then adsorbed on a sodium fluoride bed at 100°C.

The second combustion process was developed from work by others on the low-temperature, high-pressure combustion of powdered coal and sewage sludges in water saturated with air or oxygen. The main advantages of this process include, in addition to the lower temperature and improved heat transfer, uniform and easily controlled rates of reaction, simultaneous burning and leaching of fuel without use of hydrofluoric acid as a catalyst, negligible production of carbon monoxide, and lower volatilization of fission products contained in the fuel. The only objectionable features may be the use of high pressure and the somewhat low reaction rate. The process has been tested with unirradiated fuel both in an autoclave and in a reaction vessel designed for continuous removal of gases and solutions.

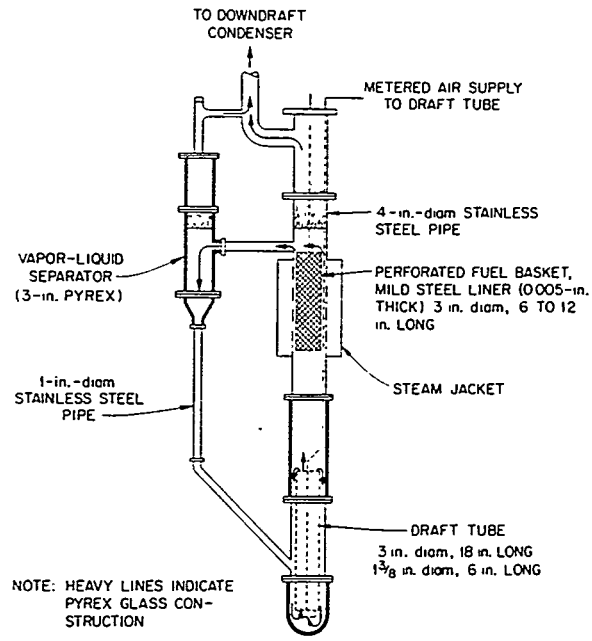

Fig. 1. Recirculating Batch Leacher. Sheared metal-clad uranium oxide and thorium-uranium oxide nuclear reactor fuel is leached from the cladding material by passing nitric acid past a perforated basket which contains the fuel oxides. The nitric acid is recirculated by a thermosiphon generated by a steam jacket. The resulting uranium and thorium nitrates are decontaminated and recovered for reuse by solvent extraction.

Chop-Leach Process for Reactor Fuel Recovery

The chop-leach process is a head-end operation to the use of solvent extraction for decontamination and recovery of nuclear reactor fuel materials contained in metal-clad tubular fuel rods. The process involves the shearing of single or multitubular fuels into short ($\frac{1}{2}$ to 2 in.) lengths to expose the uranium or thorium-uranium oxide, metal, or alloy fuel, followed by leaching of the latter in nitric acid or in nitric acid containing hydrofluoric acid as a catalyst. The chief advantages of this process for these fuels over processes that are all chemical are that it permits the use of well-established technology for subsequent processing and minimizes the problem of storing radioactive waste, since the fuel cladding is stored as waste metal rather than in solution.

The shearing step has been satisfactorily demonstrated on a full engineering scale, using a 250-ton shear, with intact multitubular fuel elements composed of oxide clad with aluminum, stainless steel, or Zircaloy-2, on loose bundles of fuel rods from disassembled fuel elements, and on 3-in.-diam hollow-cylinders of uranium metal clad with Zircaloy-2.

The leaching step has also been demonstrated satisfactorily using a batch leacher in which the dissolver acid is recirculated past the basket by a steam-heated thermosiphon (Fig. 1). Leaching of sheared uranium oxide fuel in boiling 7 *M* nitric acid is 99.9% complete in 2 hr. Equal recoveries were obtained with the more refractory thorium-uranium oxide fuel by using boiling 13 *M* nitric acid catalyzed with 0.05 *M* hydrofluoric acid for 12 to 24 hr.

The chop-leach process development program has now been completed and has been adopted by Nuclear Fuel Services, Inc., as the head-end operation in their private fuel processing plant in New York State.

THORIUM REACTOR FUEL PROCESSING

The extreme radioactivity of short-decayed thorium nuclear-reactor fuel is caused primarily by the presence of protactinium (^{233}Pa, 27.4-day half-life). For fuel that has decayed about one month, 25 to 95% of the total radioactivity arises from this one isotope, which is the precursor of the fissionable uranium isotope ^{233}U, the ultimate valuable product of irradiating thorium fuel. Because of the intense radiation, solvent extraction of short-cooled thorium fuel is very difficult. To alleviate this problem a new adsorption process has been developed to remove the ^{233}Pa before solvent extraction of the uranium and thorium. Another advantage of the new process is that it permits subsequent preparation of very pure ^{233}U from decay of the ^{233}Pa adsorbed.

The new process involves the adsorption of the protactinium from aqueous solution onto unfired Vycor powder. The process has been demonstrated on a laboratory scale with material having a very high activity level. For example, more than 95% of the protactinium was removed from a nitric acid solution of irradiated thorium-uranium oxide fuel (7.5% burnup and 26-day decay). The protactinium was recovered and was contaminated with only 10% fission product zirconium-niobium and less than 0.1% of the other contaminants that were present in the original solution. The ^{233}U from the decay of this protactinium would contain less than 1 ppm of other uranium isotopes.

FLUORIDE VOLATILITY PROCESSING

Work is in progress to develop a fluoride volatility process as an alternative to aqueous methods for recovering irradiated nuclear fuel. This process earlier established a record in the degree of decontamination of zirconium-uranium alloy fuels from fission products. Recently, pilot-plant tests have been extended to enriched aluminum-uranium alloy fuels of the type used in many research reactors. The irradiated fuel used in the final test had a burnup of 39% and a cooling time of only 25 days. Safe operation was demonstrated, and a highly purified uranium product was obtained. This test represented the first successful full-scale demonstration of the feasibility of processing nuclear fuel after such a short cooling period. Fuel recovery after minimum storage is desirable in order to reduce inventories of highly enriched uranium.

The pilot-plant study of the process includes reactions at temperatures above 500°C with anhydrous hydrogen fluoride and finally with fluorine. These reactions take place in a container of molten fluoride salts with no water present. The partially purified (decontaminated) gaseous uranium hexafluoride produced by the reactions is further purified by passing it through beds of sodium fluoride and magnesium fluoride pellets. The pure uranium hexafluoride is then collected in a cold trap.

In the laboratory, the possibility of recovering uranium from the molten fluorides through use of a spray-type fluorinator has been demonstrated. Here, the fluorine contacts falling salt droplets whose diameters range from 50 to 200 μ. This results in rapid volatilization of nearly all the uranium from the salt, again as uranium hexafluoride. The reaction occurs in the 2 or 3 sec required for the droplets to fall about 5 ft in the fluorinator. Spray fluorination may lower the corrosion rate and also permit continuous operation, particularly attractive features in the direct processing of fuel used in the new MSRE.

Other development studies included an investigation of the use of sodium fluoride to absorb uranium hexafluoride, and tests of instruments for continuously determining the concentration of uranium hexafluoride in gas streams. The sorption studies made possible the proper sizing of sodium fluoride beds to be used over a wide range of temperatures, gas-stream velocities, and uranium hexafluoride concentrations. In the instrument tests, uranium hexafluoride concentrations were determined by (1) gas density measurements, (2) ultraviolet and infrared spectroscopy, (3) thermal conductivity, and (4) gas chromatography.

THORIUM UTILIZATION PROGRAM

EXTENSION OF THE SOL-GEL PROCESS TO THE PREPARATION OF MICROSPHERES CONTAINING THORIUM

In the Kilorod Program, the ORNL sol-gel process was successfully demonstrated as a method of preparing mixed oxides of thorium and ^{233}U for loading into fuel tubes by vibratory compaction. An extension of the sol-gel method has been found to provide a very convenient way to prepare beads of thoria containing urania or carbon (Fig. 1). Beads have been prepared in sizes ranging from 10 to 1000 μ in diameter. After calcination, these microspheres have excellent characteristics for use with pyrolytic carbon coatings or in dispersion fuels.

In the preparation of the beads, sol droplets of controlled diameter are produced in a drying solvent either by using a two-fluid nozzle for producing the larger size droplets, or by agitating the solvent as the sol is introduced for producing the smaller sizes. The drops are dispersed and supported in the solvent either as a fluidized bed or by agitation while the water is extracted and the sol becomes a solid gel. Surface-active agents must be present to prevent coalescence or agglomeration of the drops with each other or on the vessel wall. The best drying solvent found was 2-ethyl-1-hexanol, but mixtures of isopropyl alcohol with carbon tetrachloride and other alcohols or alcohol mixtures were also used. After the gel beads form, they are drained free of solvent and are then dried and calcined to give oxide microspheres of near-theoretical density, or porous carbide microspheres when the sol contains carbon. The 2-ethyl-1-hexanol drying solvent is recovered for reuse by a simple distillation to remove water.

A typical preparation, produced by calcining the gel microspheres at 1150°C, yielded 2250 g of 300-μ-diam microspheres of thoria–8% urania having a density higher than 99.8% of the theoretical crystal density of the oxide solid solution.

No Number

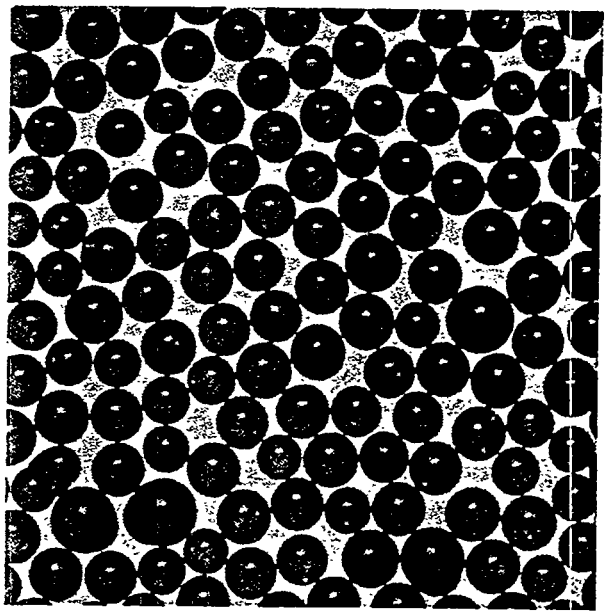

Fig. 1. Microspheres of ThO_2–3% UO_2 Prepared by the Sol-Gel Process. A colloidal dispersion of the mixed oxides is formed into gel microspheres by suspending the sol droplets in an immiscible organic liquid. When the gel microspheres are calcined at 1150°C, the resulting microspheres are very hard and of near-theoretical density.

MOLTEN-SALT REACTOR PROGRAM

INTRODUCTION

In the Molten-Salt Reactor Program we are developing a liquid-fuel reactor that promises to be an efficient thermal breeder and producer of low-cost nuclear power. Fuel for the reactor is uranium-233 tetrafluoride dissolved in a molten carrier salt consisting primarily of lithium (over 99.99% ^{7}Li isotope) and beryllium fluorides. The breeder blanket is a molten mixture of thorium, lithium, and beryllium fluoride salts. Graphite is used as the moderator in the reactor core. Hastelloy N, a new nickel-chromium-molybdenum alloy, is the material of construction for the reactor equipment.

Fuel and blanket salts are pumped through the reactor and heat exchange systems at temperatures above 1100°F but at low pressure. Basically simple chemical and physical processes have been conceived for separating the bred ^{233}U from the blanket salt and the fission products from the fuel salt, and some of them have been demonstrated. High temperature is important to the efficient use of heat to produce electricity. Low pressure implies fewer safety problems. Simple, inexpensive methods of processing the salt are essential to the efficient breeding of fissionable material in a thermal reactor.

In the two previous annual reports[1,2] we described the goals of the program: the Molten-Salt Reactor Experiment – a 10,000-kw reactor for demonstrating the technical feasibility and investigating the special problems of molten-salt reactors – and some of the more important research and development. This year, major construction on the reactor was finished, and a good start was made in the prenuclear operation. Most of the development of the components was completed before they were installed, but their testing continued in the reactor. Fuel and coolant salts and a flush salt for circulating during the prenuclear operation were produced and delivered to the reactor.

An in-pile experiment was completed under conditions proposed for the operation of the MSRE. The results showed that the fuel salt, the graphite, and the Hastelloy N were completely compatible under those conditions.

Equipment for processing the fuel and flush salts with hydrogen fluoride and fluorine gases was installed in a vacant cell in the MSRE building. This plant will provide experience relevant to the processing of the blanket for a large power breeder.

In the laboratory, fuel-salt constituents were separated from fission products by distillation at high temperature under a vacuum. This process shows promise for separating fission products from the fuel in a breeder reactor.

MOLTEN-SALT REACTOR EXPERIMENT

Construction

All the major construction was finished in the first half of 1964. The reactor vessel (Fig. 1) with the graphite core inside was delivered to the reactor building in May. There the reactor vessel, pump, and heat exchanger were set on a jig outside the reactor cell, and the connecting piping and flanges were welded to the equipment in the proper configuration (Fig. 2). Then the pieces of equipment were moved into the reactor cell; the flanges were connected; heater-insulation units were set in place on the piping; and the installation in the reactor cell was essentially completed, as shown in Fig. 3. (The control rod drives were not installed, and a temporary device for sampling was attached to the pump bowl in place of the sampler-enricher, which was still being fabricated. These items were installed early in 1965.)

[1] *Oak Ridge National Laboratory, 1962*, ORNL-3350, p. 40.

[2] *Oak Ridge National Laboratory, 1963*, ORNL-3650, p. 22.

PHOTO 71114

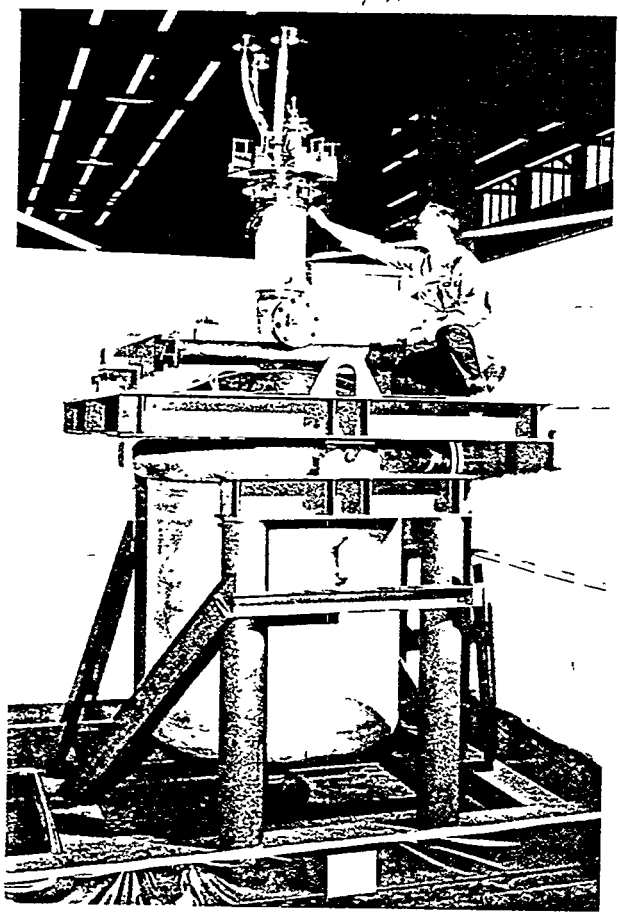

Fig. 1. MSRE Reactor Vessel Ready for Shipment to Reactor Site.

PHOTO 66373

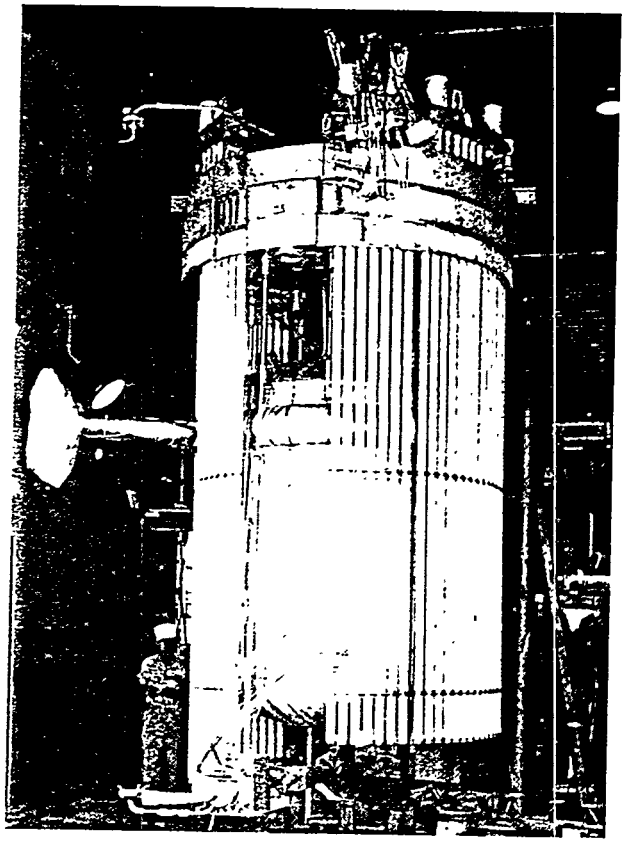

Fig. 2. Reactor Vessel, Piping, and Heater Assembly Just Before Installation.

Operation

Before any new type of reactor can be operated at power, the operators must be thoroughly trained and the equipment must be thoroughly tested. Changes in procedures and some equipment are often required to make the plant perform satisfactorily.

The staff for operating the MSRE assembled early in July and immediately began training. Training sessions were conducted by engineers who had worked on design and development of the reactor for several years. Emphasis was placed on detailed knowledge of flowsheets, control circuits, and procedures for operating the integrated plant. As construction was completed on parts of the plant, operating personnel began checking, calibrating, and testing equipment. By late September this work was proceeding on a 24-hr, 7-day basis.

Preoperational tests of components were completed early in October, the auxiliary systems were in operation, and the fuel and coolant salt systems had been closed and proved leak-tight by testing with helium at 40 psig. The next two months were occupied in purging the salt systems of moisture, heating them to 1200°F for the first time, and charging salt into the coolant drain tank and a fuel drain tank. Salt of the same composition (66 mole % LiF–34 mole % BeF_2) was used in both systems, 5760 lb in the coolant system and 9230 lb in the fuel system.

During the next tests, salt was transferred between the tanks in the drain tank cell to calibrate the weighing devices, check elevations and

No Number

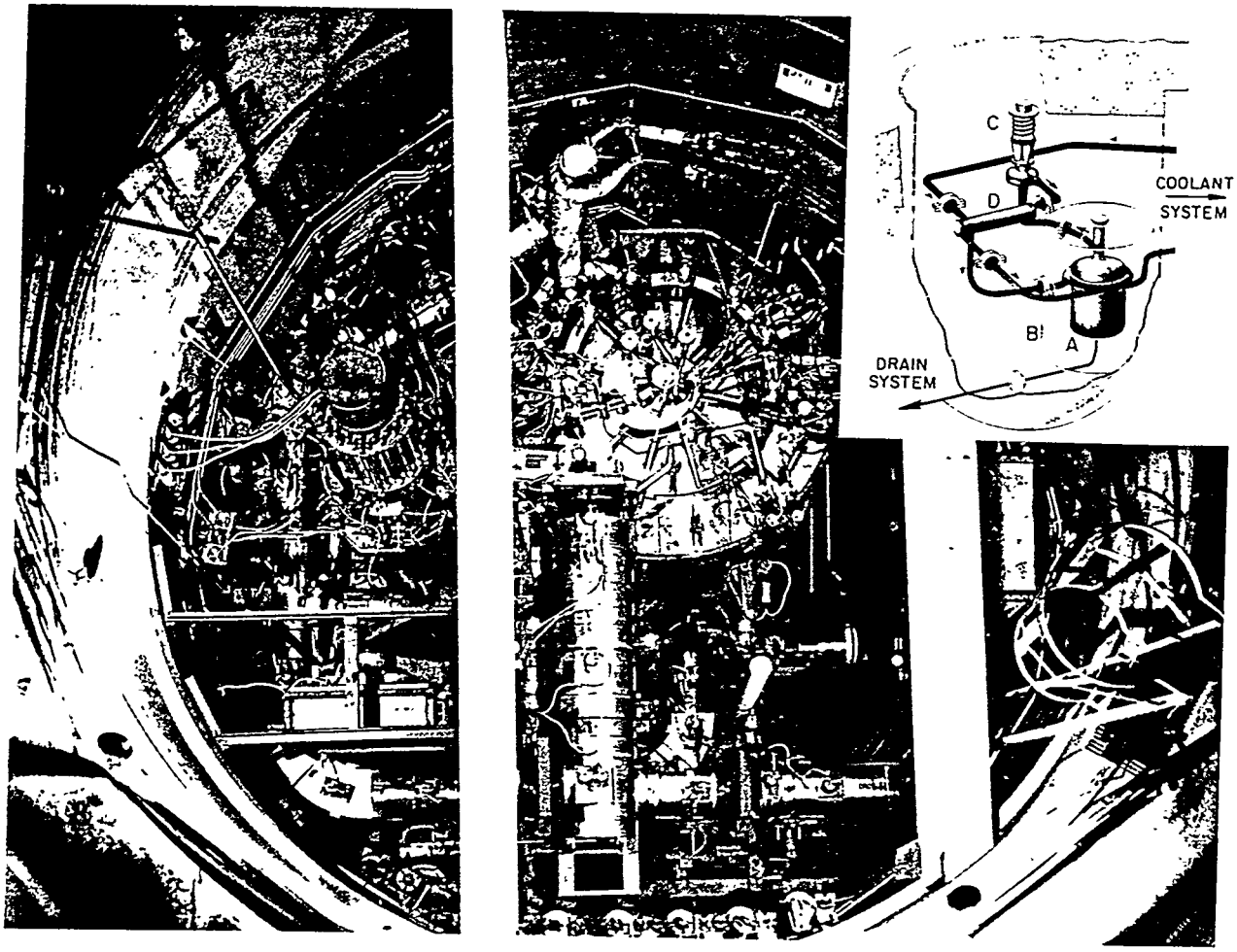

Fig. 3. The Molten-Salt Reactor Assembled in Its Containment Vessel.

volumes, and determine the characteristics of the freeze valves. Meanwhile, the extensive startup check list, which checks all instruments and controls and places all auxiliary systems in service, was completed.

At the end of 1964 the reactor was ready for the last major prenuclear test: operation of all systems, including circulation of salt in fuel and coolant loops.

COMPONENT DEVELOPMENT

Development of the new and special equipment for the MSRE was nearly completed, and most of the equipment was installed in the reactor. Some items with unusual features are described below.

Sampler-Enricher

Samples of the liquid fuel must be taken from the reactor periodically to analyze for chemical changes, and small amounts of fuel must be added to compensate for fuel burned. This sampling and enriching is complicated by the need for maintaining at least two barriers against the escape of large amounts of radioactivity from the circulating fuel into the inhabited areas of the plant. The system developed for the MSRE uses a series of containment areas through which sampling or enriching capsules move into the bowl of the fuel pump, where they are immersed in the fuel salt, and through which they return in being removed from the system. Figure 4 shows the arrangement of equipment. A prototype operated

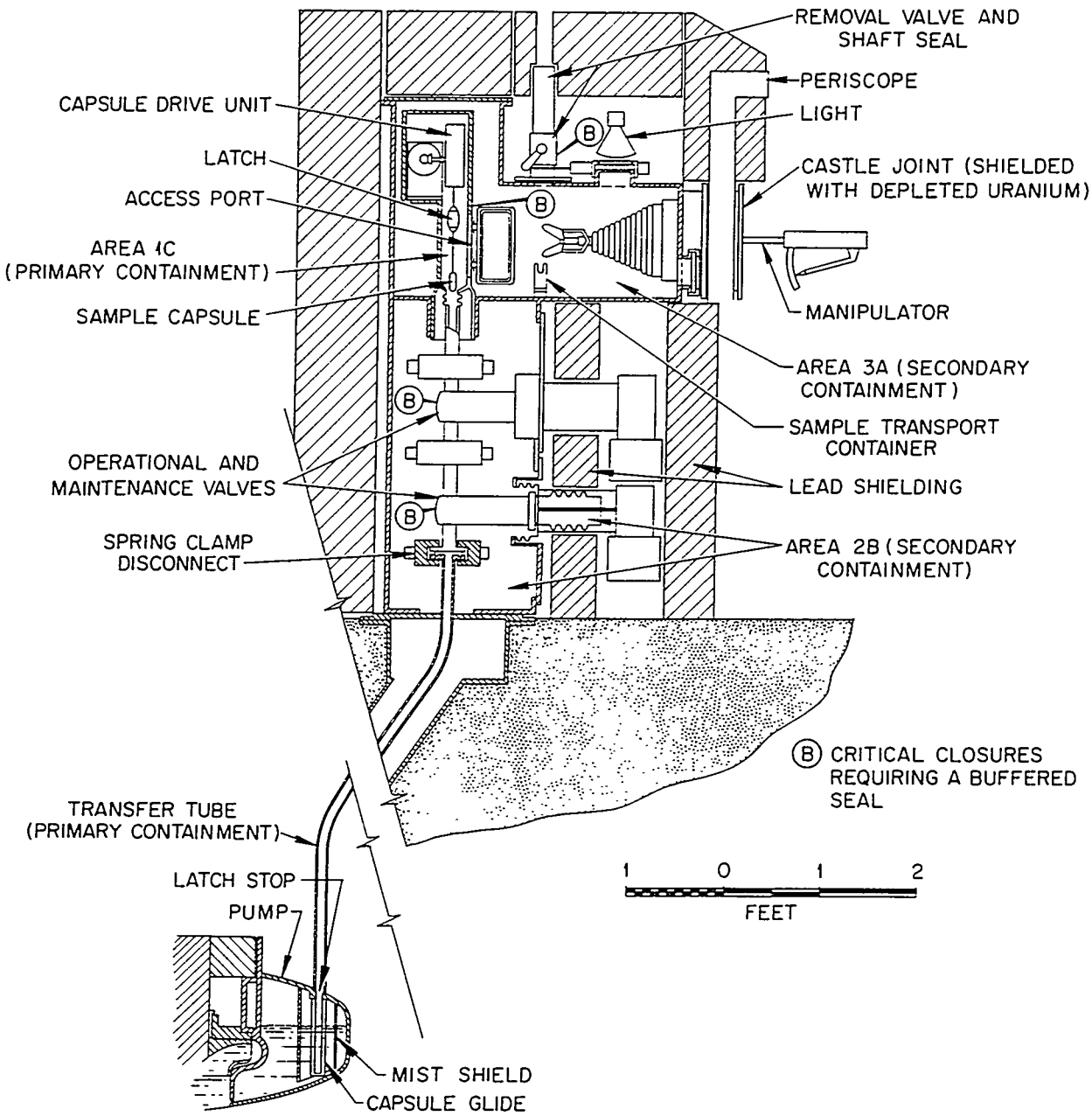

Fig. 4. Component Arrangement for Sampler-Enricher. The apparatus uses a motor-driven cable to lower a small bucket into the liquid in the pump bowl. The cable then raises the bucket into the heavily shielded manipulator area, where it is transferred into a shielded container for transport to the analytical chemistry hot cell. The procedure for enriching is essentially the same as for sampling except that the capsule lowered into the pump bowl is filled with enriching salt. The containment areas are (1) the pump bowl and transfer tube up to the valves – primary containment; (2) the area 1C – primary containment when the valves are open, secondary containment when the valves are closed; (3) area 3A (and 2B) – secondary containment only. Many interlocks are provided to ensure that the operations are conducted safely.

successfully while removing 56 samples and adding 11 enriching capsules to a salt-circulating system.

Oxygen-Removal Unit

Helium is used as a cover gas in the MSRE equipment to prevent moisture and oxygen from contaminating the salt and corroding the hot metal surfaces. Commercial helium can contain traces of these contaminants; so a unit was developed to remove oxygen or moisture in concentrations below 100 ppm from helium in a system operating at medium pressure (250 psig) and at relatively low flow (10 liters/min or less). As is shown in Fig. 5, the unit contains an internal getter tube filled with titanium sponge and surrounded in turn by heaters, insulation, and an outer pressure vessel. The operating temperature of the sponge is 1200°F. With an inlet concentration of 100 ppm of oxygen and a flow rate of 10 liters/min, an outlet oxygen concentration of 1 ppm or less was obtained until 58% of the titanium sponge was consumed. Sufficient titanium sponge was installed in the unit to ensure at least one year of operation before replacement would be necessary.

LR-Dwg. 68585A

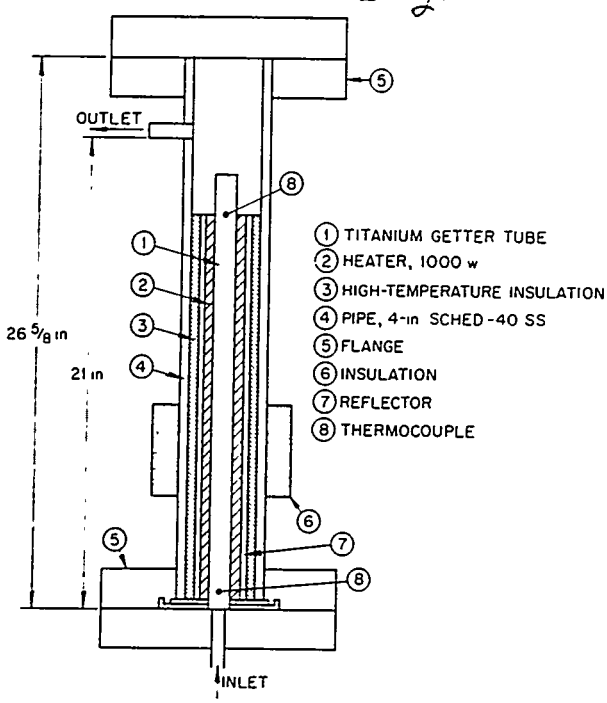

Fig. 5. Oxygen-Removal Unit.

Control Rod

The MSRE has three control rods, which operate in thimbles closely spaced near the center of the core. The rods must be flexible to pass through bends in the thimbles, must be cooled to remove the nuclear heat, and must be provided with a means for indicating when the end of the poison section is near the bottom of the thimble. A mockup of the flexible rod is shown in Fig. 6. The rod is cooled by blowing air down through the center and out through the annulus between the rod and the

Photo 39622A

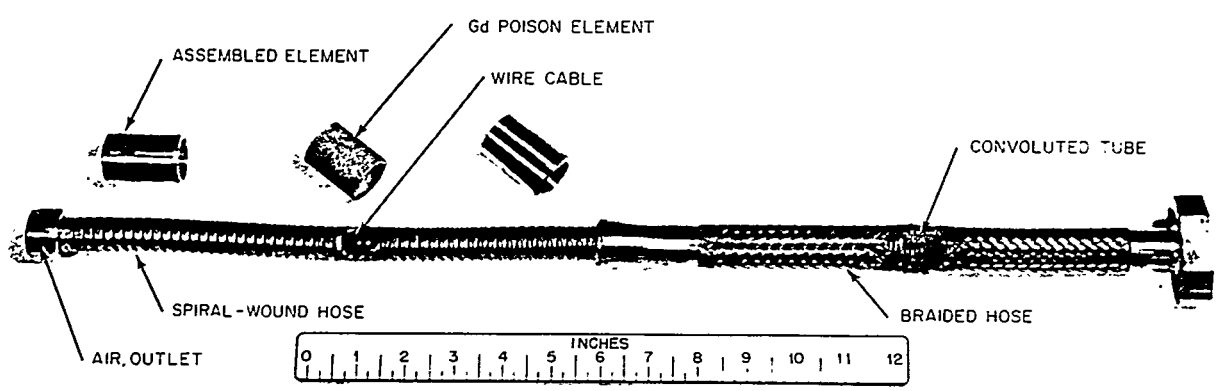

Fig. 6. Structural Mockup of MSRE Control Rod. The poison elements are full size. On the reactor rods the spiral-wound section is about 5 ft long and the braided-hose section is about 7 ft long. The wire cable and braided hose control the stretch of the rod.

thimble. An orifice is installed near the bottom of the thimble. When the air outlet nozzle enters the orifice. the pressure required to maintain the flow increases abruptly, giving a precise indication of the position of the rod. In testing the design, a prototype rod operated without difficulty in a thimble at 1200°F through 38.000 full cycles of 102 in. of travel.

Heaters

The fuel and coolant salts freeze at about 850°F; so the drain tanks and the reactor equipment and piping are heavily insulated. They are also provided with electrical heaters to raise the temperature before the salts are added to the systems and to maintain the temperature when the reactor is not producing heat. The heaters must be rugged to have long life, but they must be removable from above through shielding so they can be replaced if they burn out or removed to obtain access to equipment after the plant has been operated at power and becomes radioactive.

The drain tanks are installed in furnaces. Insulation is permanently mounted in the furnace walls, but the heaters are removable for maintenance. Figure 7 shows a heater unit during assembly. The heater was operated at 1200°F for more than 10,000 hr without incident.

The reactor components are connected by 5-in. pipes. The heaters and insulation for the piping are combined into assemblies of the type shown in Fig. 8. The all-metal reflective insulation was chosen because it is rugged and efficient and reduces the dusting normally encountered in handling refractory insulation. A test assembly has been operated above 1200°F for more than 5000 hr without difficulty or evidence of deterioration.

Fuel and Coolant Pumps

Before the rotary elements for the fuel and coolant pumps (Fig. 9) were delivered to the MSRE, they were thoroughly tested by circulating salt in a test loop at 1200°F for several hundred hours.

The pumps are sump-type pumps that operate in tanks only partly filled with salt. In the fuel pump, some of the circulating salt is sprayed into the helium cover gas in the pump tank to release gaseous fission products from the fuel.

Photo 39334

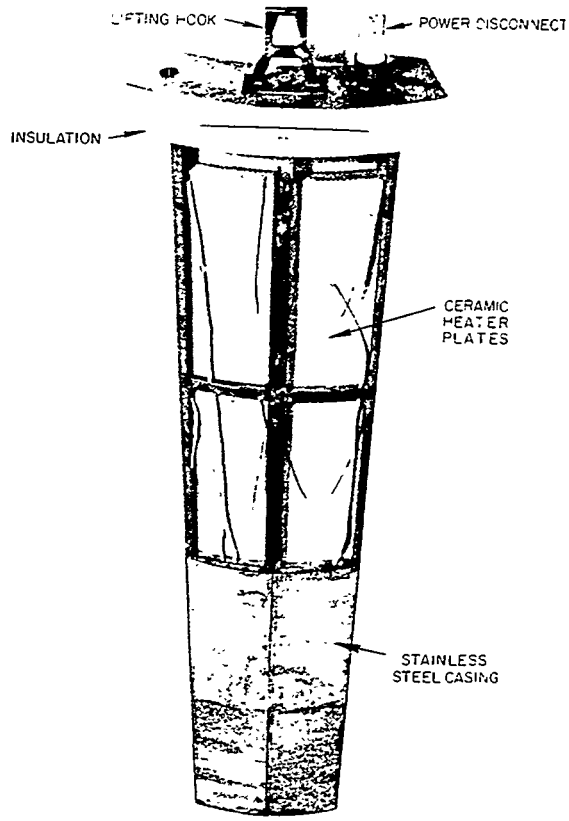

Fig. 7. Drain Tank Heater During Assembly.

Tiny bubbles of helium tend to become entrained in the salt and to be carried into the reactor core. A concentration of several volume per cent of gas in the fuel could adversely affect the behavior of the reactor.

A gamma-ray densitometer was specially developed to measure the amount of gas in the circulating salt. A beam of gamma rays from a strong source is passed through the insulated pipe in the circulating system to a detector. The changes in intensity of the transmitted beam when the circulation is stopped and the bubbles rise out of the salt and when circulation is started and gases gradually reentrain are translated into volume fraction of gas in the salt. The densitometer worked well in measuring gas fractions as low as 0.1 vol % and was able to detect rapid fluctuations in gas concentration. It will be used on the reactor during some of the prenuclear testing and low-power experiments.

Photo 70955A

Fig. 8. Pipe Heaters. The reflective insulation unit consists of a removable section, which surrounds the top and sides of the pipe, and a base, which is permanently attached to the structure below the pipe and supports the top section. There are 11 layers of stainless steel and one 0.002-in.-thick layer of pure silver in the unit. The heater plates are mounted in clips in the top section and are removable with it.

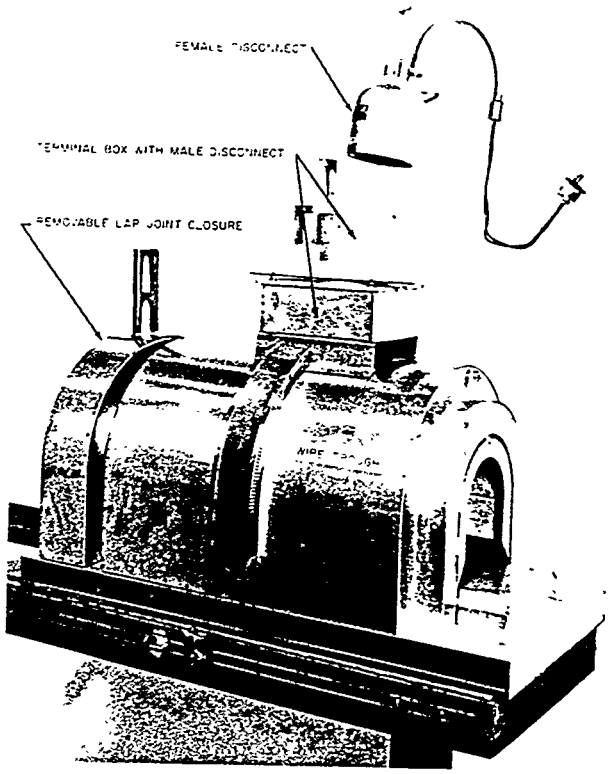

Photo 70901

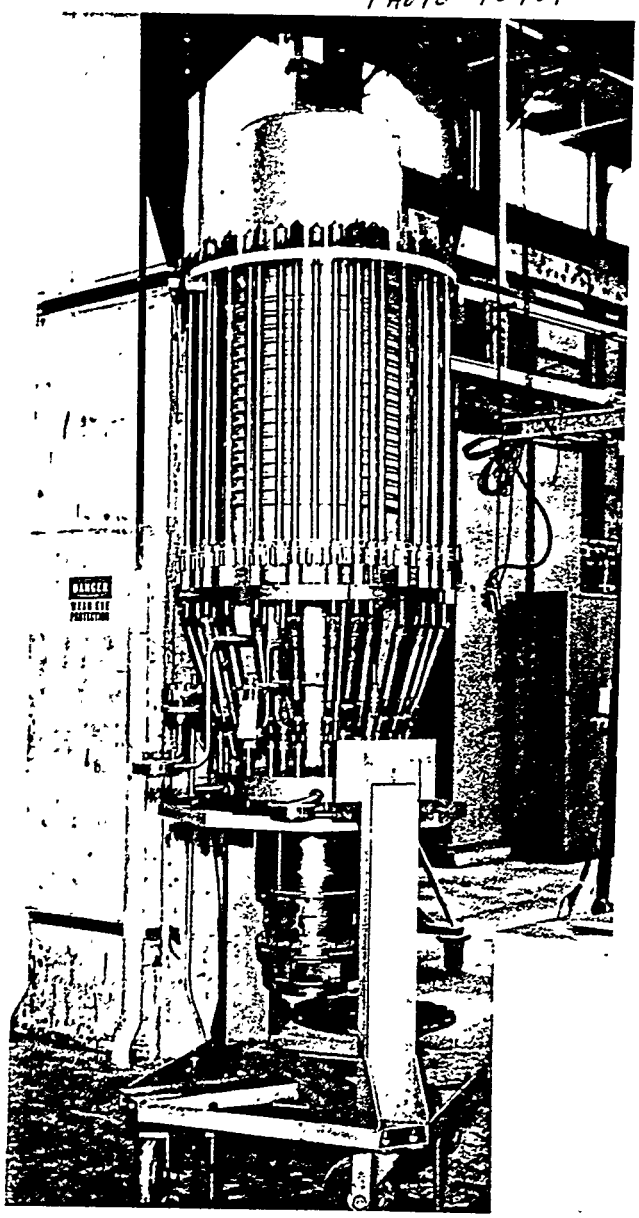

Fig. 9. MSRE Fuel Pump. The rotary element is here shown joined to its electric drive motor. The upper portion (that containing the helical piping) is the drive motor. The middle portion houses the pump bearings and the shaft seals that prevent the lubricating oil from getting into the salt. The lower portion is the shield plug and impeller, which are inserted into the pump tank. The extension rods and universals which surround the motor and bearing housing are used to tighten and remove the bolting associated with the flange couplings by the use of remote tools directly above.

CHEMICAL DEVELOPMENT

Production of Fuel and Coolant Salts

The MSRE requires a total of about 27,000 lb of fluoride salt mixtures for use as fuel and coolant and as a flush salt for prenuclear operation and for cleaning the reactor circuit prior to maintenance operations. The coolant and flush salt mixtures are about two-thirds lithium fluoride and one-third beryllium fluoride and were prepared for direct use in the reactor. The fuel salt was prepared as a solvent mixture of lithium, beryllium, and zirconium fluorides and fuel mixtures of lithium and uranium fluorides. The uranium-containing salt will be added to the solvent mixture in the fuel drain tank at the reactor to obtain the finally desired concentration of uranium. All the lithium fluoride used in the salt mixtures was prepared from lithium enriched to more than 99.99% in the ^{7}Li isotope, which has a low neutron absorption cross section.

Constituents of the mixtures were obtained from commercial suppliers and from AEC sources as the fluoride salts. We mixed them in proper proportions, treated the molten mixtures with hydrogen and hydrogen fluoride gases to remove harmful impurities, filtered the purified melts, and charged them into the drain tanks at the MSRE. Purification of the large quantity of salts was begun in 1963 and completed in 1964 in a pilot plant that had been used to develop production methods and to produce salts for the other research and development programs.

Compatibility of Fuels and Materials

The success of molten-salt reactors is vitally dependent on the fuels and materials being completely compatible in the reactor environment. This compatibility has been the subject of much research in test reactors, but the conditions did not always duplicate those planned for the MSRE, and the results were often unfavorable.

Specifically, we learned that fluorine gas could be generated from fuel salt under irradiation when the salt was frozen and at room temperature. The release of fluorine produced indications of fuel instability in the salt, and the gas chemically attacked the graphite. However, the laboratory and postirradiation findings suggested that no fluorine was generated when the fuel was molten and that none was produced by the radiation from the decay of fission products when the temperature was above 200°C.

These findings were confirmed in an irradiation test that we completed this year in the Materials Testing Reactor. In contrast with previous tests (but in accordance with plans for the MSRE), the fuel in the test capsules was kept molten even when the MTR was shut down and there was only irradiation from the gamma and beta sources present in the reactor and in the accumulated fission products. Under these conditions, no traces of fluorine were detected throughout the entire experiment or the postirradiation examination. The graphite was undamaged, and no uranium deposited on or in the graphite. The surfaces of the Hastelloy N capsule showed no evidence of corrosion. These results indicate strongly that the molten fuel, graphite, and container metal will be compatible under the operating conditions of the MSRE.

FUEL PROCESSING

MSRE Processing Facility

Although special measures are taken to prevent oxygen and moisture from coming in contact with the salts in the MSRE, some contamination is unavoidable. Also, changing the concentration and enrichment of the uranium in the fuel salt is desirable in order to study a range of fuel compositions. The salts are expensive enough that it proved economical to install equipment for processing them in a spare cell in the reactor building (Fig. 10). The molten salts can be treated with hydrogen fluoride gas to convert the oxides back to fluorides and drive off the oxygen as water vapor and with fluorine gas to remove the uranium as the volatile hexafluoride.

The facility will be used infrequently, but it can process full 75-ft^3 charges of fuel or flush salt from the reactor. This is about the capacity required in a plant that would operate continuously to process the blanket of a large power breeder reactor. Because the facility was built for use with molten-salt fuels and to make use of facilities and personnel required for the reactor, the cost was only a small fraction of the cost of a separate processing plant.

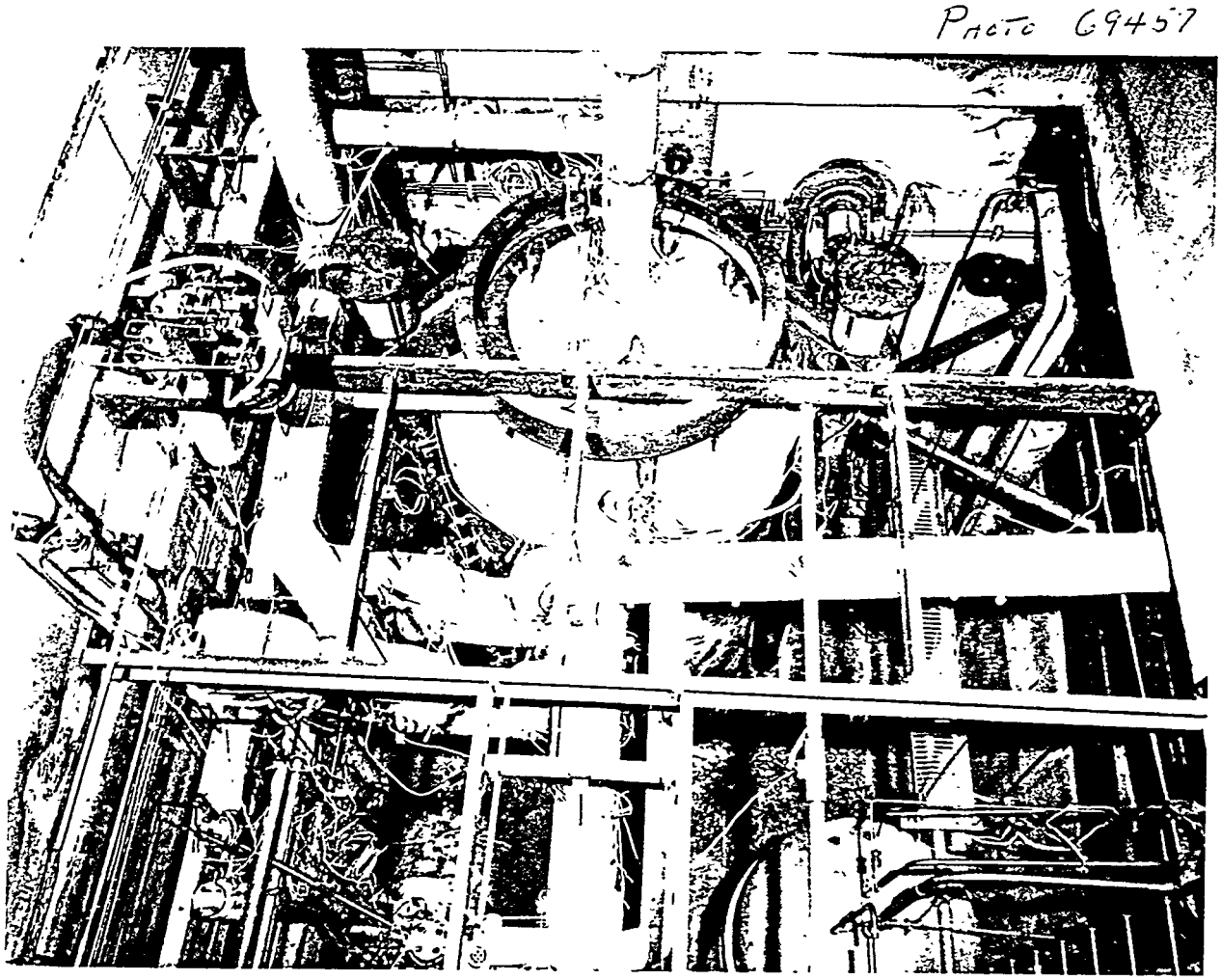

Fig. 10. MSRE Fuel Processing Cell. The cell is about 14 ft square by 20 ft deep. Molten salt is treated with hydrogen fluoride and fluorine gases in the 4-ft-diam × 10-ft-high heated and insulated tank in the top center of the picture. The top of the cell will be covered with shield blocks, and the process will be controlled from a panel located adjacent to the cell at the level of the top of the shielding.

Distillation of Molten Salts

A major potential advantage of a molten-salt reactor as a thermal breeder is the possibility of processing the fuel salt continuously to remove fission products. The rare earths represent a class of fission products for which no very satisfactory method of processing had been advanced. This year we distilled some samples of salt in laboratory apparatus at temperatures near 1000°C and pressures near 1 mm Hg abs and recovered fuel solvent materials essentially free of rare-earth fission products. Removal of uranium prior to the distillation may be desirable, but the Fluoride Volatility Process should be quite suitable for this step. Thus, distillation appears to offer an effective and economic means for minimizing the loss of neutrons to fission products in a molten-salt breeder reactor.

REACTOR EVALUATIONS

REACTOR ANALYSIS

Advanced Converter Reactors

While there is quite general agreement among nuclear engineers that a nuclear-electric power industry must in the future be based on reactors capable of breeding, there is much less agreement on the time when breeders must be introduced and on the stages of development of the industry leading to primary dependence on breeders. Opinions differ, for example, on whether there will be an intermediate period in which advanced converters will hold sway, and, if so, which type of converter will be most attractive for that period. To help define the characteristics of several advanced converters which might be used, we performed a comparative study in 1964 of power costs and fuel utilization in a spectral-shift-control reactor (SSCR), a pressure-tube heavy-water reactor (HWR), a high-temperature gas-cooled reactor (HTGR), and a sodium-graphite reactor (SGR). We included a pressurized water reactor (PWR) in the study as a representative of current power reactors. Our comparative evaluation of these reactors was based on design studies for 1000-Mw (electrical) power plants that had been carried out by several other companies. We received information on the SSCR from Babcock and Wilcox Company, on the HWR from Du Pont, on the HTGR from General Atomic, on the SGR from Atomics International, and on the PWR from Westinghouse. The study included a review and engineering analysis of the reactor and plant designs, a comparative analysis of capital costs, fuel-cycle calculations and determination of fuel costs, and estimation of the quantity of uranium required or committed for each type of reactor as a function of time (up to the year 2020). Sargent and Lundy, Engineers, assisted us in the capital cost studies.

In determining fuel-cycle costs, we postulated an installed electrical capacity of 15,000 Mw for each type of reactor, in turn, and estimated unit fabrication, reprocessing, and shipping costs as a function of the volume of material handled – which is of course related to the reactor fueling rate. These unit-cost estimates were based on detailed flowsheets for the fabrication and reprocessing plants, equipment lists, equipment costs as a function of capacity, and operating requirements such as staff and materials. We assumed that the fuel would be privately owned and that ^{233}U produced in thorium-based reactors would be recycled, but that plutonium produced in slightly enriched uranium reactors would be sold.

The results of the study, in highly condensed form, are presented in Table 1. Details of the study may be found elsewhere.[1]

^{233}U Fuel Value Study

The Private Ownership of Special Nuclear Materials Act (1964) requires the AEC to establish guaranteed purchase prices for uranium enriched in ^{233}U, which shall not exceed the Commission's estimate of the value of the material as fuel in nuclear reactors. To assist the Commission in performing this estimate, values of each isotope were determined, for a 1000-Mw (electrical) SSCR and for a 1000-Mw (electrical) HTGR, which make the fuel costs of each of these reactors (when operating on a thorium cycle) independent of whether the operator sells the ^{233}U-^{235}U mixture discharged from the reactor, and buys fresh ^{235}U at $12 a gram, or recycles the fuel (with makeup ^{235}U as required). Fuel fabrication and reprocessing costs for these reactors were estimated, as in the Advanced Converter Study, with full allowance for the effect of ^{232}U in the recycled uranium. The cost of recycling the thorium was also estimated, as a separate series of cases.

---

[1] M. W. Rosenthal *et al.*, *A Comparative Evaluation of Advanced Converters*, ORNL-3686 (January 1965).

Table 1. Power Costs and Fuel Requirements for Reactors Studied

	PWR	SSCR	HWR-U	HWR-Th	HTGR	SGR
Power costs [mills/kwhr (electrical)]						
Capital cost	2.3	2.1	2.1	2.3	2.0	2.2
Operating cost	0.3	0.3	0.3	0.3	0.3	0.3
Fuel-cycle cost	1.7–1.8	1.6–1.9	1.0–1.2	1.2–1.4	1.3–1.4	1.4–1.5
Heavy-water cost		0.1	0.5	0.6		
Total power cost	4.3–4.4	4.1–4.4	3.9–4.1	4.4–4.6	3.6–3.7	3.9–4.0
30-year net fissile material requirement [kg/Mw (electrical)]	19.5	12.4	23.7	7.4	4.3	17.5

For both reactor types, and over a range of fuel exposures and of fabrication cost penalties for ^{232}U content, the results indicate that the value of discharged fuel may be computed by assigning to ^{233}U a value of about $18 to $20 a gram and to ^{236}U a penalty of about $13 or $14 a gram, with ^{235}U fixed at $12 a gram.

Thorium Breeder Reactor Study

As part of our program of evaluating the prospects and problems of thorium-based fuel cycles, we are again examining the relative performance of several types of reactors deemed capable of a net positive breeding gain. During 1964, results were obtained for two-region molten-salt reactors. The most encouraging aspect of these results is that they indicate that near-minimum fuel costs can be achieved concurrently with short fuel doubling time. The principal departure from previous studies was the inclusion of the recently developed vacuum distillation process, which, in conjunction with fluoride volatility, permits separating lithium and beryllium fluoride, as well as uranium fluoride, from the fission products. We have tried to be quite conservative in estimating the cost of an on-site reprocessing plant, and find the costs low enough to permit very rapid processing of the fuel. As a result, it appears that fuel costs in the range between 0.3 and 0.4 mill/kwhr (electrical) can probably be achieved in conjunction with a breeding ratio of 1.06 and a fuel doubling time of ten years.

Similar studies are in progress for high-temperature graphite reactors, with consideration given to fuels which release some of the high-cross-section fission products, and for heavy-water reactors operating with a thorium fuel cycle.

Other Activities

A number of other studies were made in addition to the major ones described above. These include review of several maritime reactor proposals received by the AEC, an evaluation of a "converter-recycle" seed-blanket reactor concept, and a preliminary study of future ore and separative work requirements of nuclear economies consisting of various combinations of reactors.

Considerable effort was spent in creating and improving computer programs for use in studies and evaluations. A reactor design optimization program, OPTIMERC, that is capable of optimization with respect to as many as 20 parameters simultaneously was developed. This program combines the MERC equilibrium reactor code with an optimization routine that is based on the method of steepest descent. With OPTIMERC a design can be optimized to minimize cost, maximize breeding ratio or fuel yield, or maximize a function in which, for example, cost and breeding ratio are given any desired weighting. Various modifications also were made in the point multigroup depletion program TONG and in the two-dimensional multigroup depletion program ASSAULT, which are our primary tools for fuel-cycle evaluations.

ENGINEERING EVALUATIONS

Advanced Converter Study

Engineering evaluation and capital cost studies were carried out for the six 1000-Mw (electrical) reactor plant concepts compared in the study of advanced converter reactors.[1]

The engineering evaluation studies consisted of (1) an analysis of the thermal and hydraulic characteristics of each reactor core to compare the relative performances and technological limitations of the concepts; (2) a review of plant equipment specifications to compare assumptions used by the designers on performance requirements and manufacturing technology; (3) adjustments in designs to facilitate relative capital cost comparisons; (4) normalization of capital costs to adjusted PWR costs or to construction costs developed in other applicable reference design studies. Sargent and Lundy worked with us on the plant design and capital cost evaluation; the engineering evaluation of core performance was coordinated with appropriate specialized groups of the laboratory.

The six concepts evaluated were:

1. a poison-controlled pressurized water reactor (PWR) – Westinghouse design;
2. a spectral-shift-control reactor (SSCR) – Babcock and Wilcox design;
3. a uranium-fueled heavy-water-cooled and -moderated reactor (HWR-U) – Du Pont design;
4. a thorium-fueled heavy-water-cooled and -moderated reactor (HWR-Th) – Du Pont design;
5. a sodium-cooled graphite-moderated reactor (SGR) – Atomics International design;
6. a high-temperature gas-cooled reactor (HTGR) – General Atomic design.

Some general conclusions reached from the engineering evaluation are as follows:

1. The thermal design of the cores appeared to be adequate, with the reservation that the power peaking factors were not checked by physics calculations and the enthalpy rise factor claimed for the PWR had not been demonstrated. The PWR and SSCR fuel elements appeared to be designed on the basis of current technology; however, the remaining reactors were designed on the basis of extrapolations of fuel element technology well beyond existing data.

2. The plant equipment required for the water-cooled reactors (PWR, SSCR, HWR's) appeared to be within manufacturing capabilities; however, excessive extrapolation would be required to predict the three-year creep and corrosion behavior of the Zr–2.5% Nb pressure tubes used in the heavy-water reactors. The SGR equipment involved a reasonable extrapolation of operating experience, with the exception of the reactor vessel design, which was a departure from previous concepts. The feasibility of the HTGR concept depended largely on successful demonstrations of the prestressed-concrete reactor structure that encloses the entire primary system. A high degree of equipment reliability would be necessary to satisfy the required 0.90 plant availability factor, particularly for the HWR-U, HTGR, and SGR, which have more frequent refueling shutdowns.

3. The construction costs determined (per kilowatt) were as follows: PWR, $133; SSCR, $125; HWR-U, $125; HWR-Th, $134; HTGR, $117; SGR, $130. The HTGR had the largest cost uncertainty, because of lack of experience with the reactor vessel and the equipment of the "all-inside" design.

SPACE REACTOR STUDIES

MEDIUM POWER REACTOR EXPERIMENT

Development of the Boiling Potassium Reactor System

To investigate the stability and control problems of a boiling potassium reactor system such as the MPRE, a test rig was built with an electrically heated boiler and a condenser of a type suitable for operation in space. This direct-condensing radiator was fabricated of 7-ft-long tapered stainless steel tubes to which were brazed axial stainless-steel-clad copper fins. The condensing radiator was operated in the system using a potassium vapor turbine to drive the centrifugal feed pump, which removed the liquid potassium from the condenser and returned it to the boiler.

One of the vital problems in the system has been the vapor flow distribution in the radiator, together with the problem of obtaining uniform scavenging of the condensate. To investigate these problems, it is necessary to obtain a detailed temperature distribution across the entire 144 tubes in the radiator. To have done this with thermocouples would have required at least 7 thermocouples per tube, or about 1000 thermocouples in all, which would have cost around $100,000. An analysis of the problem indicated that an even better insight into temperature distribution could be obtained with infrared film at a very low cost. Figure 1

PHOTO 71954A

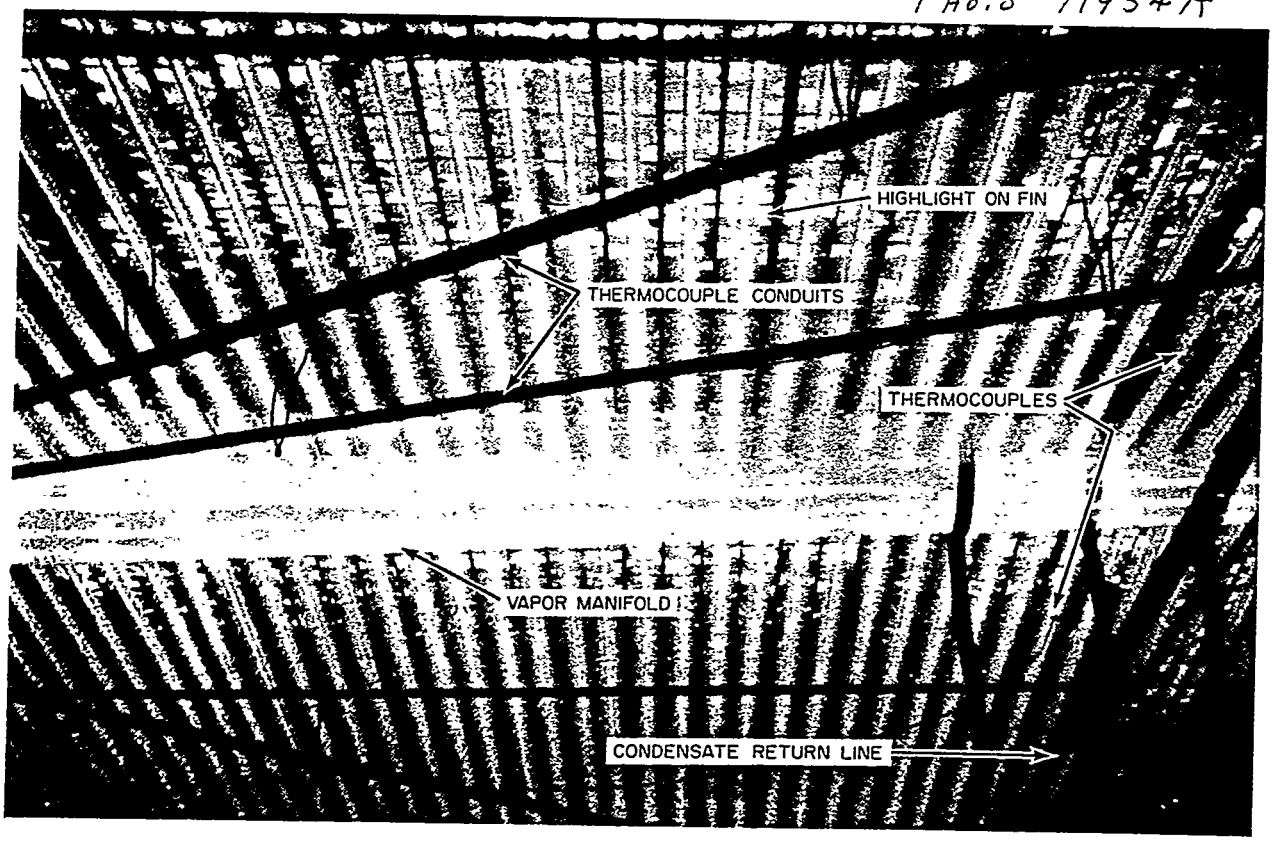

Fig. 1. Radiator of the Intermediate Potassium System. Photograph made with Polaroid infrared film, looking up from below. The radiator was running at about 850°F under cavitating conditions. There was little liquid in the radiator except in the form of films on the tube walls.

shows a picture taken in the course of the temperature distribution investigation with the radiator operating at 800°F (this is more than 200°F below the lowest temperature at which the eye can discern a dull red). The effects of the metal surface temperature on the image in the photograph can be inferred from the 25°F difference in temperature between the roots and tips of the fins. It is possible to deduce local temperatures by comparing the apparent intensity of infrared emission at any given point in the image on the film with the apparent intensity at points where thermocouples are mounted in the field of view (about 36 thermocouples were mounted in this fashion).

Examination of the photograph indicates that the highlights on some of the fins were caused by reflection of infrared light from the central vapor manifold by undulations in the surfaces of the fins, which were warped somewhat in the brazing operation. This and other photographs indicate that the potassium vapor flow distribution in the tube banks was excellent.

MPRE Facility

The MPRE Facility will consist primarily of a spherical containment vessel to house the Medium Power Reactor Experiment power plant. This containment vessel will be located in an underground concrete-lined pit, covered with a steel-frame–metal-sided building to house the auxiliary

PHOTO 71772

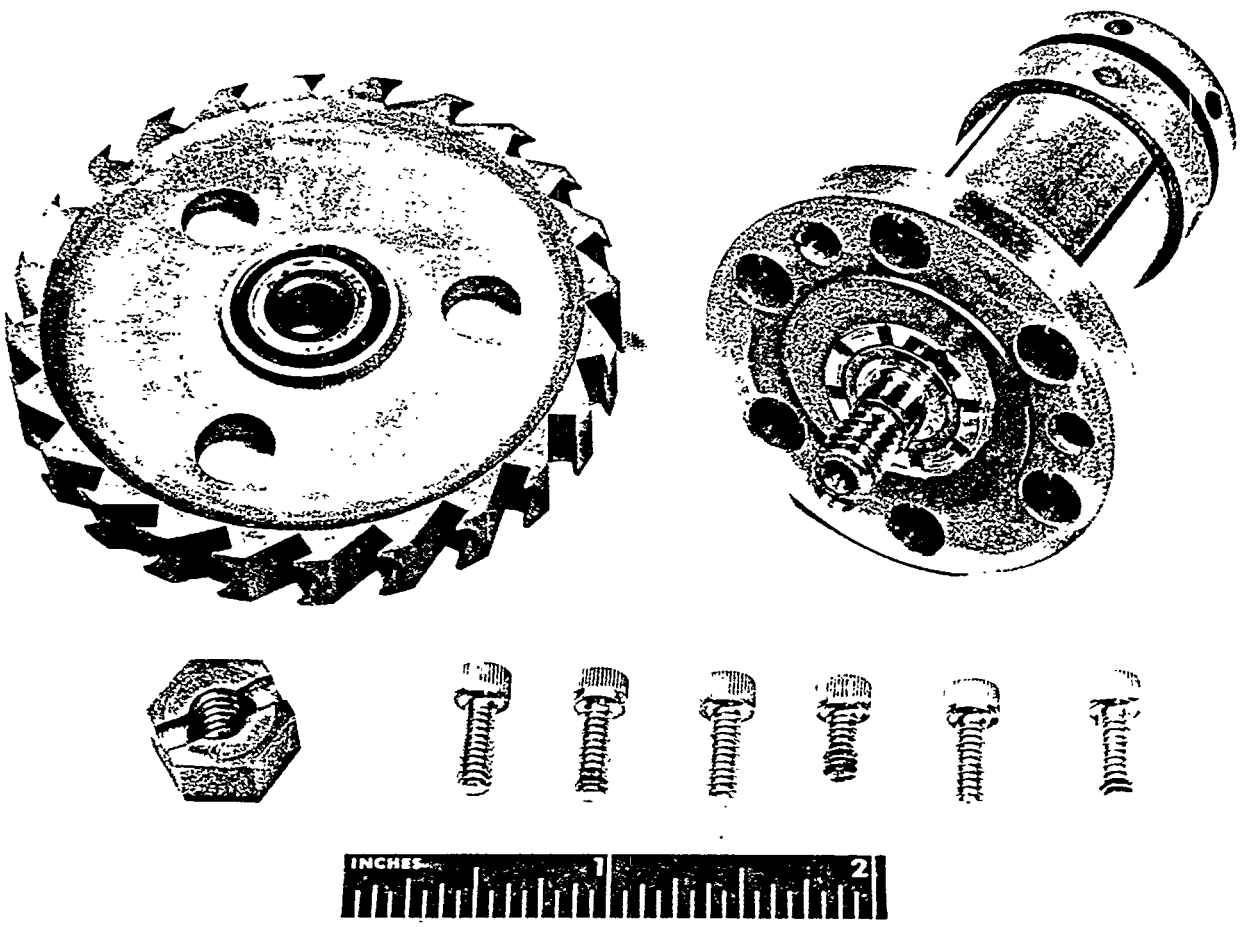

Fig. 2. Turbine-Pump Rotary Assembly. Shown after removal from an experimental system where it operated for 324 hr in potassium and was subjected to 38 starts and stops. Turbine inlet temperature was approximately 1270°F and outlet temperature was 1050°F.

service systems. A separate remote control building will be provided for operating the experiment. A site in Melton Valley is proposed for this installation.

Chicago Bridge and Iron Company was awarded the subcontract for design of the containment vessel and vacuum system. This 40-ft-diam vessel is unique in that it is a carbon steel vessel designed for both pressure (50 psia) and vacuum (10^{-2} torr) service.

Present architect-engineer activity includes the design of the two buildings and their utility services as well as the vacuum, cooling water, waste disposal, heating and ventilating, electrical, and instrumentation and control systems.

Engineering Development

The characteristics of components and systems under development for use in a liquid potassium Rankine-cycle nuclear power plant are under extensive investigation, both analytically and experimentally. Experimental investigations have been accomplished by operating several systems that simulate primary portions of the MPRE reactor, wherein data are collected to reveal thermodynamic and hydrodynamic features. Testing with water as a heat exchanging medium is followed by tests with potassium. The experiments with potassium, in addition, yield information on materials compatibility, corrosion, and possible mass transfer at levels of temperature and pressure that will be experienced within the reactor power plant system.

One small-scale and one intermediate-scale water system have been operated successfully. A seven-heater-rod (small-scale) potassium boiler system has operated without changeout of boiler core for over 1000 hr. During that period a turbine-driven pump unit was run 327 hr before the bearing at the pump end seized (Fig. 2). Various types of nucleation sites have been tested on heater rods to achieve stable potassium boiling, particularly at low power levels. A 91-rod potassium system has been assembled (Fig. 3) and will soon be placed in operation.

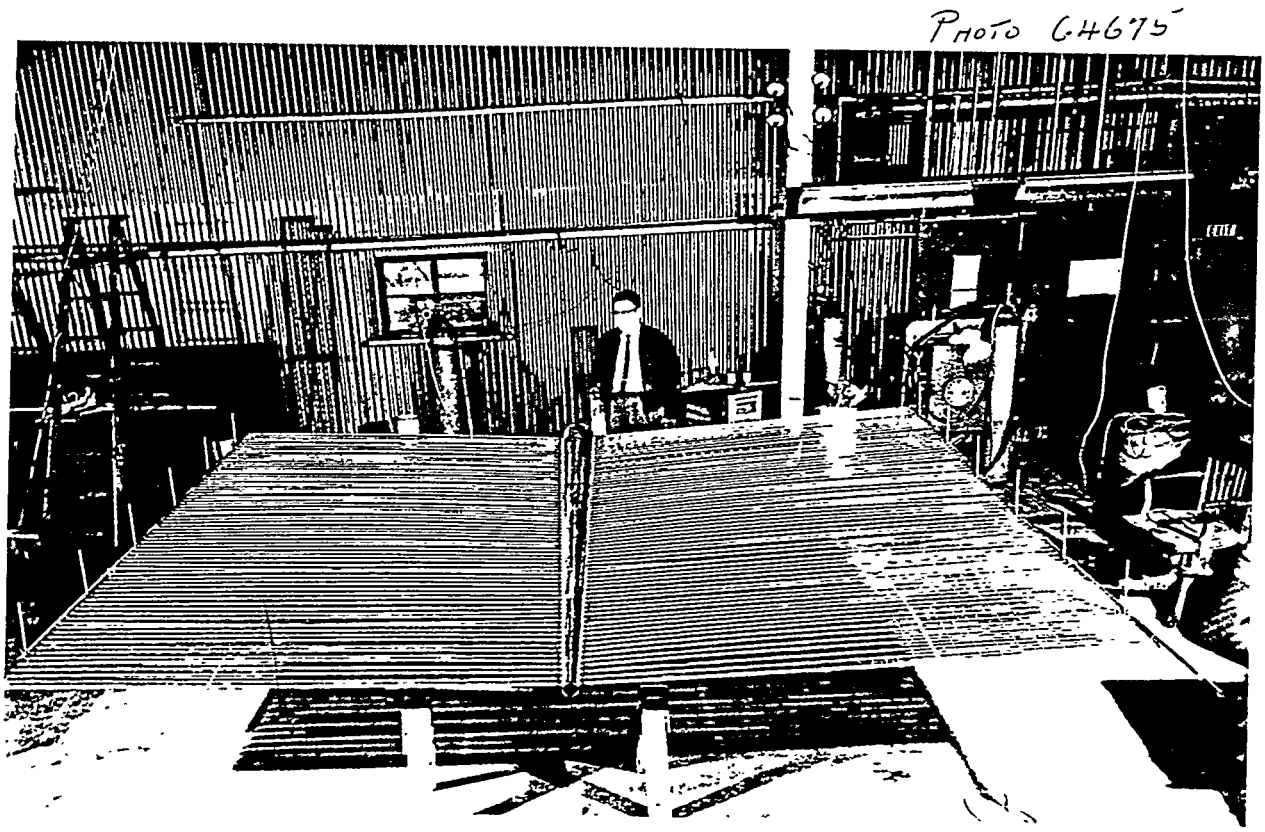

Fig. 3. Core of Tapered-Tube Radiator for the Intermediate Potassium System. Shown during fabrication.

NUCLEAR DESALTING PROGRAM

Design and economic feasibility studies of nuclear heat sources for desalting applications were begun as part of the Laboratory's task assignments in the AEC nuclear desalination program. The reactors investigated fell under two general classifications: (1) dual-purpose reactors, which produce steam for generation of electrical power and for evaporation of saline water to produce freshwater; (2) low-temperature reactors, which produce no electric power or only enough electric power to supply the desalination plant load; the reactor coolant or low-pressure steam generated by the reactor coolant is used to heat brine for distillation.

DUAL-PURPOSE REACTORS

Studies of dual-purpose reactors were limited to comparing prime steam costs of reactors proposed for power applications, except for the ORNL heavy-water-moderated, boiling-light-water-cooled reactor, which had been designed especially for dual-purpose application. Reactors compared were the 1000-Mw (electrical) PWR, SSCR, HWR-U, HTGR, and SGR concepts, which had previously been evaluated in the advanced converter study;[1] the Hanford New Production Reactor; the Du Pont organic-cooled and boiling-D_2O-cooled heavy-water reactors; and the ORNL heavy-water reactor.

[1] M. W. Rosenthal *et al.*, *A Comparative Evaluation of Advanced Converters*, ORNL-3686 (January 1965); see "Reactor Evaluations," this report.

Correlations of capital costs with equipment design parameters developed in the ORNL-3686 study were extended to include the additional reactor concepts, and relative capital cost estimates of the reactors were prepared. New estimates of operating costs were made using a tentative set of desalination ground rules. Prime steam costs were determined for each concept under these ground rules. Information developed in this study has been used as a guide in normalizing prime steam costs reported in other studies to a common set of ground rules, and for parametric studies of capital cost variations as a function of prime steam conditions in lower-temperature nuclear heat supply systems. We are continuing to update the capital cost correlations as additional information becomes available.

SYSTEM STUDIES

Both analytical and computer studies were made of the coupling characteristics between nuclear power plants and evaporators. These studies indicated that over a very wide range of water-to-electricity ratio (w), the cost of water is essentially constant if no subsidy is made from power sales. Practical values of w, with current plant concepts, range from 200,000 to 1,000,000 gal day^{-1} Mw^{-1}. Evaporators in a plant with a high value of w tend to be highly efficient, energized by steam at 260 to 310°F. Those in plants with high electrical output (i.e., low values of w) must operate with low-temperature steam and are less efficient.

LOW-TEMPERATURE REACTORS

Preliminary design studies were undertaken to investigate the economic attractiveness of low-temperature reactors for water-only applications. The more attractive concepts will be recommended for further detailed study. The concepts investigated were a low-temperature sodium-cooled fast reactor using a metallic uranium blanket; a low-temperature pressurized water reactor using metallic uranium fuel; and a low-temperature light-water-cooled, heavy-water-moderated reactor using metallic uranium fuel.

Our evaluations indicate that the heat production cost for a reactor cooled and moderated by ordinary water, fueled with slightly enriched uranium metal, and operated at a lower temperature than conventional pressurized water reactors can be comparable with the cost of heat from heavy-water reactors. The low coolant temperature gives appreciable savings in reactor plant capital costs because of the low pressure required to suppress boiling and the relatively low energy content of the coolant to be contained. Increasing the relative uranium density in the core by use of metal (rather than oxide) fuel and by removal of water greatly increases the fast fission factor, decreases the parasitic captures in water, and increases the conversion ratio.

We also made a preliminary design study of a low-temperature sodium-cooled fast breeder reactor. The reactor consists of an oxide-fueled core and metallic uranium radial blankets operating at a reactor inlet temperature of 500°F and a mean outlet temperature of 800°F. Based on proposed desalination ground rules, this system produces prime steam for less than 9¢ per 10^6 Btu while operating at a breeding ratio of 1.59 and a doubling time of 12 years. Alternatively, it can be operated as a power producer with costs which can be competitive with high-temperature sodium-cooled breeders under some conditions. This latter conclusion from the study suggests that further work is needed to define the appropriate sodium outlet temperature for fast power reactors.

HIGH FLUX ISOTOPE REACTOR

MECHANICAL DESIGN

The design of all major reactor parts is complete. Work is continuing on some remote handling tools, and some parts will be modified as shakedown tests show the need for revisions.

Analytical work on the fuel elements was concentrated on the heat removal aspects. The power-limiting criterion was changed from the conventional one, departure from nucleate boiling, to incipient boiling. This change became necessary because of the paucity of reliable data on departure from nucleate boiling in narrow rectangular channels of a width that approaches the diameter of the steam bubbles formed. The new criterion reduced the permissible short-term steady-state power level. There is still, however, adequate headroom to permit operation at the 100-Mw design power level.

Design of the control rods, guide track and bearing structure, and the control-rod drives was completed. The nominal thicknesses of the control region coolant channels were changed to accommodate various manufacturing tolerances, hydraulic deflections, and thermal deflections of these rods.

A mockup of one quadrant of the control region, capable of operating at high pressures, was constructed and operated at reactor temperatures and pressures. Results from these tests showed that these rods will perform satisfactorily in the reactor. Thermal deflection tests on a stainless steel mockup of the rod indicate that the thermal bowing and stresses of these rods will not present problems.

Satisfactory performance of the control system depends upon close control over manufacturing and assembly tolerances. We have designed jigging tools for assembling the guide tracks to inspect the control rods, and we designed a measuring tool to give a continuous plot of the control-rod contour. A remotely operated gage will enable the operators to determine the radial positions of the rods in the reactor proper.

A detailed study was made of the target to determine the optimum loading of ^{242}Pu and the number of target rods for optimum production of ^{252}Cf in the island region. The existing design of 30 rods with $\frac{3}{8}$-in. diameter and 300 g of target material appears to be close to the optimum.

Temperature conditions in the target tubes were determined for a configuration of close thermal coupling between the pellets and the tube and for one where a finite inert-gas-filled annulus separated the pellets from the external tube. While the maximum central temperature was higher for this latter case, it was still well below the melting point of aluminum, thus permitting the use of a simple assembly method which may result in some gas gap.

The target region in the center of the core is supplied with coolant drawn down through an entrance channel equipped with screens and baffles to reduce the probability of drawing in solid particles which might be introduced into the vessel with the main coolant flow. The weights of the tower, strainer, and associated centering equipment are utilized for clamping the target assembly in the core. The tower is provided with latches which allow simultaneous removal of the target assembly for normal refueling.

Necessary equipment for remote handling of target pins and assembly in both reactor and clean pools is provided. A small recirculating loop in the pool with a spectrum analyzer serves for identifying leaking targets.

A hydraulic rabbit facility is planned as an alternative loading for the central target position. This facility utilizes the three pressure regions occurring in the target system to permit insertion and removal of samples without additional pumps or pressure sources. The sample loading station is in the adjoining clean pool.

Coolant flow distributors, located at each of the reactor vessel inlets, were designed to minimize any possible vibration of the reactor or experimental components due to the coolant entering the vessel.

The flow distributors consist essentially of large perforated plates through which the coolant water enters the upper part of the vessel.

Preliminary hydraulic tests on the primary coolant system, in which the reactor components were simulated by a large orifice in the reactor vessel, were completed. Pressure drops and flow rates for the primary coolant system external to the reactor vessel agreed well with the predicted values. The coastdown times following a power outage to the main pump motors were found to be slightly lower than predicted.

The design of beam tubes and engineering facilities required careful consideration of pressure strain, assembly tolerances, and differential thermal expansion in order to maximize the usefulness of these facilities as experimental tools and still make remote handling possible. The design of the facilities and remote handling tools is now complete.

DEVELOPMENT AND TESTING

Development work and testing of the core components was continued throughout the year. The control-plate pressure equalization test facility was reactivated to obtain additional data on the magnitude and direction of loads on the inner and outer control plates. These additional tests were required as a result of changes in the annular gap width between the control plates and the parts of the reactor structure surrounding the plates.

The corrosion tests for materials used in the fabrication of the reactor components were completed, and a report has been written summarizing the results of these tests.

Tests were conducted in the HFIR mockup to investigate vibrations in a prototype vertical experimental facility tube. These tests indicated that flow diffusers should be installed inside the reactor vessel on the cooling water lines. These diffusers are needed to reduce turbulence inside the reactor vessel and to eliminate impingement of the vessel inlet water stream on the vertical experimental facility tubes. The mockup system was also used to calibrate the control region inlet orifices, which are located in the shroud flange.

The development work necessary for the fabrication of the core structural components, beam tube and experimental facility components, control-rod drive components, and the control-rod guidance components was completed in June 1964. The installation of the reactor core structural components was started in September 1964.

NUCLEAR DESIGN

Analysis of the second HFIR critical experiment was completed during the early part of 1964, and a third experiment (HFIRCE-3) was planned. In comparison with the HFIRCE-2 core, the HFIRCE-3 core fuel loading was increased from 8.0 to 9.4 kg of ^{235}U, the burnable poison (^{10}B) loading was increased from 1.72 to 2.12 g, and the radial distributions of the fuel and poison were changed. Later in the year a set of control rods made of europium oxide, tantalum, and aluminum, similar to those to be used in the HFIR, were fabricated and made available for the experiments.

HFIRCE-3 experiments conducted with the original silver-copper-aluminum rods indicated that the fuel distribution was satisfactory but that the ^{10}B loading should be increased from 2.12 to 3.60 g to accommodate more stringent requirements concerning reactivity tolerances. This ^{10}B loading was specified for the first production core (fabricated by ORNL), which was scheduled for fabrication shortly thereafter.

Subsequent to this time, experiments with the europium oxide–tantalum–aluminum rods indicated that the latter rods were worth significantly more than the silver-copper-aluminum rods; the ^{10}B loading for the second and future production cores was therefore reduced from 3.6 to 2.8 g.

Using reactivity normalizing data from the above critical experiments, fuel cycle calculations were made, incorporating the effects of reactivity variations associated with the plutonium target, with the beryllium reflector poisoning (^{6}Li, ^{3}He), and with tolerances in fuel and burnable poison loadings and distributions. The predicted extreme ranges of the fuel cycles for the first and second production cores at full power were 2 to 16 days and 5 to 16.5 days respectively. It is intended that future fuel loadings will be tailored to provide longer and more nearly uniform fuel cycles.

Transients resulting from reactivity additions were analyzed by analog techniques. By using the

same analog model to calculate SPERT transients it was found that the model was conservative, and thus satisfactory for establishing safe limitations. The results of the analysis indicated that the HFIR can withstand the worst anticipated reactivity addition (optimum void in the flux-trap region) without damage to the core.

SAFETY EXPERIMENTS WITH THE HIGH FLUX ISOTOPE REACTOR FUEL ELEMENT

A series of special experiments was performed with the HFIRCE-3 fuel element in order to assess possible hazards associated with routine handling, storage, and transport. The fissile material in the element was uranium enriched to about 93% in ^{235}U contained, as uranium oxide—aluminum cermet, in aluminum-clad fuel plates curved in the shape of an involute. The fuel plates were mounted in two concentric annuli to form the fuel element, which surrounded a 5-in.-diam target region. The HFIRCE-3 element contained 9.4 kg of ^{235}U, of which 2.6 kg was in the inner annulus and 6.8 kg in the outer.

Under normal conditions, the two annuli will be handled separately but stored as a unit. Spent elements removed from the reactor will be stored under water, to allow fission product decay, on specially constructed spaced racks, each of which has a cadmium-lined annular steel post occupying the target region. However, it is possible that an element might be temporarily located in a corner of the stainless-steel-lined concrete reactor pool rather than on a storage rack. Further, should the annuli become stuck together in the reactor it would be necessary to remove the assembled element, water-moderated and -reflected, from the reactor vessel past a massive steel hatch, which would partially replace the water reflector. Also, a single spent fuel element will be shipped in a stainless-steel-lined lead container with a cadmium-lined spacing annulus in the target region. The multiplication factor of the element was experimentally measured for each of these conditions, and the degree of subcritical reactivity necessary to assure safety was specified.

NUCLEAR SAFETY

The importance of nuclear safety research to the growth of the nuclear power industry arises from two sources. The first of these is the requirement that people be protected from the possibility of exposure to dangerous quantities of radioactive materials that could be released by a reactor accident. This requirement has caused power reactors to be built many miles from the cities where their power is needed and to be enclosed by expensive containment shells. This expense, which retards the growth of nuclear power in an economic sense, provides the second source of motivation for research in the field of nuclear safety. Accurate, objective information may well permit great reductions in cost while preserving the paramount objective of protecting the safety of our people. Early results of the ORNL nuclear safety program showed that it is not reasonable to assume that all the fission products in an overheated reactor fuel material will escape when the fuel melts. The program is currently devoted to determinations of the amounts of fission products that stay airborne long enough to escape from containment shells, study of natural processes that make these materials deposit rapidly, and ways of trapping or removing them quickly from the atmosphere (engineered safeguards).

NUCLEAR SAFETY PILOT PLANT

The Nuclear Safety Pilot Plant was completed early in 1964. Its purpose is to evaluate the transport behavior of fission products or simulated fission products in a containment system of sufficient size to permit extrapolation of fission product behavior observed in laboratory-scale systems up to actual containment systems. It is not intended to simulate the fission product release spectrum of any one postulated accident, but rather to attempt to produce a wide range of fission product types and to observe the behavior of these under various conditions in confined volumes.

The Nuclear Safety Pilot Plant consists of a 1350-ft^3 model containment vessel into which fission product aerosols from melted fuel pins may be released. The fuel specimens are melted by means of a plasma torch in a water-cooled stainless steel furnace, and fission products are released into the 1350-ft^3 stainless steel containment vessel. Various sampling devices make it possible to determine the variation of the quantity and composition of the fission products with time and location in the vessel, and auxiliary facilities permit in-place decontamination of the furnace and vessel. The NSPP was designed for experiments with fuel containing up to 1000 curies of mixed fission product activity, and provision is made for remote loading and unloading of fuel specimens and for remote recovery of all sampling devices.

In the past year, seven runs were carried out in the NSPP, the last five with radioactive ^{131}I. In three of these runs (4, 5, and 6) molecular iodine was released into the containment vessel, and observations were made of the iodine in the vessel. In runs 3 and 7, stainless-steel-clad hollow UO_2 cylinders packed with a mixture of UO_2 and NaI were melted, releasing most of the iodine and some of the UO_2 into the containment vessel, where observations of the aerosol were carried out over periods of 24 to 48 hr. The observations included

1. sampling of the containment vessel atmosphere at intervals using May-pack cluster samplers, paper-tape air samplers, and May-pack—diffusion-channel samplers;
2. collection of fallout over several time intervals during a run;
3. measurement of the concentration of condensation nuclei at intervals during a run;
4. exposure of deposition coupons of various materials during a run and the subsequent purge period.

Iodine material balances were attempted in all runs, and the amount of iodine accounted for ranged from 50 to 80% of that initially present. Purging losses were suspected as one important contributing factor in the low iodine recovery, and provisions to account for these were added.

Significant conversion of the airborne iodine to forms other than I_2 was observed. As much as 40% of the airborne iodine penetrated silver-plated screens, a membrane filter having a 0.5-μ pore diameter, and three layers of charcoal-impregnated glass fiber filter paper and was collected on activated-charcoal beds. Presumably, this material was methyl iodide.

A second compound form was observed that was collected slowly by silver, but more rapidly by rubber, and was quantitatively removed by charcoal-impregnated filter paper. We have not yet identified this form of iodine.

The airborne iodine concentration in the various runs was reduced by factors ranging from 4 to 40. The least reduction occurred in the runs where I_2 was released by melting the Pyrex ampul with the plasma torch, and the greatest reduction occurred in the run in which I_2 was released by breaking the ampul. This suggests that the aerosol produced by the torch may affect the iodine behavior. However, there is no correlation between the iodine release mechanism and particle behavior. At most, 1% of the iodine appears to be associated with particles.

The results of runs 4, 5, and 6, in which pure iodine was used, showed that iodine deposition occurred more slowly than in large-scale experiments previously reported by British workers. This was due, at least in part, to low iodine absorption by the stainless steel wall of the containment vessel. In runs 3 and 7, in which iodine was released by melting a stainless-steel-clad uranium dioxide dummy fuel element containing iodine, iodine deposition occurred more rapidly than when pure iodine was used. It was concluded that vaporized fuel particles did not slow the diffusion of iodine to the tank wall. The uranium dioxide concentration dropped rapidly in the first hour that the vaporized material was in the vessel, but after that time it fell more slowly. The remaining airborne particles were too small to be affected by gravity. A significant fraction of the iodine was converted to compounds that deposit more slowly than pure iodine and are harder to trap. It seems clear that part of the radioactive iodine released by a reactor accident would stay airborne in a dry containment vessel atmosphere for a long time and some of it would escape through leaks in the vessel.

Overall, these runs had the purpose of plant shakedown and equipment evaluation, firming up the sampling techniques, and obtaining some data on the behavior of simulated fission product aerosols in a containment system. The molecular iodine runs had the additional purpose of determining whether the plasma torch produces an aerosol which affects the behavior of iodine. The UO_2 runs had the purpose of producing an aerosol simulating that which might be released by melting of a UO_2 fuel element.

BEHAVIOR OF FISSION PRODUCTS ON IN-PILE DESTRUCTION OF REACTOR FUELS

Miniature stainless-steel-clad uranium dioxide fuel elements have been melted in the ORR with dry helium, moist helium, steam-helium-hydrogen, dry air, moist air, and steam-air atmospheres to study the effects of atmosphere on the behavior of fission products. The absence of shiny droplets of metallic stainless steel from melted or vaporized cladding material was noted when air or steam was in contact with the hot fuel. The extent of oxidation of stainless steel is important, since it has been observed that oxides of the components of stainless steel, particularly iron oxide, may substantially reduce the melting point of uranium dioxide and cause it to form a puddle on the bottom of the reactor vessel. Separate experiments showed that mixtures of this type can melt 2500°F below the melting point of pure uranium dioxide. In experiments in which moist air was used, unusually large amounts of iodine and ruthenium were released from a zone whose minimum temperature was above 1800°F. The ruthenium was retained by high-efficiency filters, showing that it was in the form of particles. The iodine penetrated high-efficiency filters to a greater extent than in other atmospheres, but it was retained by charcoal, indicating that most of the iodine was in the gaseous molecular form (I_2). The nonvolatile fission products strontium, barium, zirconium, and

cerium did not appear to be greatly affected by the composition of the atmosphere, and less than 1% of the amounts of these materials in the fuel was released from the 1800°F zone. This shows that these nonvolatile fission products will deposit on the first cool surface reached by the carrier gas stream. In experiments in which steam was a component of the sweep gas, all fission products investigated except ruthenium appeared to be removed significantly from the gas stream by condensing steam. The retention of fission products by condensed water can therefore be expected to be a significant factor in reducing the danger of reactor accidents where steam is present in the containment system. This condition is likely to exist in accidents with pressurized- or boiling-water reactors, the most common types of power reactors in the United States.

PROPERTIES OF FISSION PRODUCT AEROSOLS PRODUCED BY OVERHEATED REACTOR FUELS

The properties of fission product aerosols produced by overheated reactor fuels are being studied in a Containment Mockup Facility (CMF) located in a concrete-shielded cell to permit working with large quantities of radioactive materials. These studies have revealed that forms of iodine may be produced which penetrate charcoal adsorber beds to a much greater extent than molecular iodine (I_2). The penetrating forms have been identified by other workers as mainly organic iodine compounds, which are presumably formed by reaction of iodine with organic materials present in trace amounts. In one series of experiments, which was done with a steam-air atmosphere in the 7-ft^3 containment shell and with very low iodine concentrations, up to 20% of the iodine was converted to the penetrating form in a few hours. It has also been shown that a greater fraction is converted to penetrating forms if the iodine is present in very small concentrations than when it is present in the higher concentrations that are expected for large reactors. Better trapping systems will be required for organic iodine compounds if further studies confirm the expectation that quantities of these compounds may be formed in reactor accidents. Other ORNL studies have shown that charcoal beds are less effective in retaining methyl iodide, the principal organic iodine compound, when the gas also contains moisture.

NUCLEAR SAFETY INFORMATION CENTER

The Nuclear Safety Information Center (NSIC), established by the Atomic Energy Commission at ORNL, serves the nuclear community by collecting, storing, evaluating, and disseminating nuclear safety information generated throughout the world. The Center's scope now includes seven well-defined subject areas within the broad field of nuclear safety, which involves many disciplines. In each of these areas, an ORNL staff specialist or consultant continually analyzes current information, produces state-of-the-art reports, and is available for consultation. Since its inception, over one year ago, some 4100 documents or other sources of nuclear safety information have been collected, evaluated, and placed in the Center's storage files. The information is readily retrievable for use, by the Center's staff and visitors, on special problems and in the preparation of articles for the quarterly technical progress review *Nuclear Safety* and state-of-the-art reports. The latest accessions will be used each quarter to make up a computer-generated bibliography for extensive distribution. The Center's files are also accessible for use by visitors at any time. As time is available the Center's staff answers specific questions from the nuclear community without charge.

NSIC is expanding the services it can offer by the use of the ORGDP computer facilities. Programs have been prepared to allow NSIC to use the computer for the preparation of an indexed bibliography of its accessions, and the programming will also enable the staff to make retrospective searches of the Center's files.

The data group started keypunching NSIC extracts in September 1964. By the end of 1964, 670 references had been submitted for keypunching. The first issue of the bibliography will include these plus the references cited during the first half of January 1965. An abridged sample of the bibliography was distributed at the San Francisco Atomfair in December 1964.

Planning for a selective dissemination program using the tape storage with another program is currently under way. The program will be initiated

on an experimental basis with about 70 selected individuals at the management level who are actively interested in the subject of nuclear safety. Detailed preparation for and initiation of the program will be undertaken.

During the past year the Center received and answered by letter or telephone 93 specific requests for nuclear safety information, principally from private companies and government agencies. In addition, NSIC staff specialists consulted with 49 visitors. Also during the period, 82 requests were received for addition to the distribution list for all NSIC reports.

TECHNICAL PROGRESS REVIEW "NUCLEAR SAFETY"

Four issues of *Nuclear Safety*, a quarterly technical review prepared by the Oak Ridge National Laboratory for the U.S. Atomic Energy Commission, were issued during 1964. *Nuclear Safety* may be purchased from the Superintendent of Documents, U.S. Government Printing Office, Washington, D.C. 20402, for $2.50 per year for each subscription or for 70¢ per issue.

REACTOR CONTAINMENT HANDBOOK

In 1964, the Reactor Containment Handbook was completed for the AEC, Division of Reactor Development. The purpose of the handbook is to provide detailed information that will be useful in the design, construction, testing, and operation of reactor containment systems. It will be released to an unrestricted distribution as USAEC Report ORNL-NSIC-5, *U.S. Reactor Containment Experience: A Handbook of Current Practice in Analysis, Design, Construction, Tests, and Operation.*

RADIOACTIVE WASTE DISPOSAL

ENVIRONMENTAL STUDIES

Clinch River Study

The final phase of the cooperative interagency Clinch River Study has been to make a mass balance of the input to the river and the output from the river for two years. Analyses of bottom cores from the river have shown that out of the more than 11,000 curies discharged, there is less than 200 curies of radioactive material in the bottom sediments of the Clinch River below the point where ORNL discharges its low-level wastes.

The data from the water-sampling studies have been analyzed and show that the major portion of the radionuclides entering the Clinch River at White Oak Dam flows out of it at the mouth. A limiting maximum value of the amount of activity possibly stored in the biomass has also been computed. The sum of these items shows conclusively that for a clean (i.e., low organic content and low sediment load), fast-flowing stream most of the radioactive material flows through the stream.

The Clinch River safety analyses were based upon the critical-nuclide–critical-pathway approach. Of the critical pathways considered, external exposure from contaminated water and bottom sediments was of less importance as a potential source of radiation exposure than consumption of contaminated water and fish. No population group subjected to the critical exposure pathways received an excessive dose. In 1964, only 2% of the maximum permissible dose was received. However, if the practice of irrigating with river water develops, the long-term effect of crop irrigation with contaminated water would become the most important avenue of exposure. Strontium-90 has been the most important of the critical radionuclides in liquid wastes released to the Clinch River, contributing more than 99% of the dose to the skeleton and total body and 70% to the thyroid.

LOW-LEVEL RADIOACTIVE WASTE DISPOSAL

Processes for removing traces of radioactive elements from large volumes of water are being developed. One process involves the simultaneous precipitation and removal of the calcium and magnesium ions and the radioactive elements. When phosphates and polyphosphates from commercial detergents are present in the waste water, complete precipitation is prevented. Recent work has shown that these phosphates can be removed by adsorption on activated alumina. The water is passed through a column of alumina prior to the precipitation step. After the alumina is saturated, the phosphates can be removed with a caustic solution, thus preparing the alumina for reuse. About 5000 volumes of waste water can be treated by one volume of alumina before regeneration is needed.

INCORPORATION OF INTERMEDIATE-LEVEL RADIOACTIVE WASTE IN ASPHALT

We have shown that incorporation of intermediate-level wastes, containing 1 to 5 curies of radioactivity per gallon, directly in asphalt is a promising method for preparing waste in a solid form suitable for permanent storage. The solid residues are held in the asphalt in a very insoluble condition. Waste solutions are added directly to emulsified asphalt, the water boiled away, and the temperature of the salt-asphalt mixture raised to about 190°C (Fig. 1). The molten asphalt mix is then allowed to harden in a steel barrel, which is used to contain the product for shipment and storage.

Asphalt containing simulated waste was leached with water to determine the dissolution rate of the radioactive elements. Some of the samples were irradiated by gamma rays prior to leaching to simulate the destructive effects of radiations from the radioactive elements. The amounts of radioactive elements leached from the asphalt were acceptably low, being only about $\frac{1}{100}$ of the amounts leached in similar tests with similar wastes contained in concrete. Wastes contained in asphalt were thermally stable up to temperatures of at least 320°C.

65-659.4

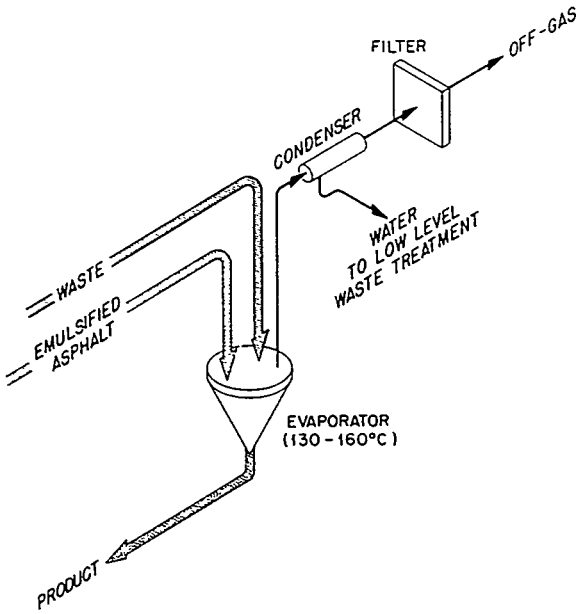

Fig. 1. Incorporation of Waste into Asphalt. In this procedure, intermediate-level wastes are mixed with emulsified asphalt and dried at an elevated temperature. With the radioactive solid residue incorporated in asphalt, little radioactivity is leached out with water, even after extensive irradiation.

HIGH-LEVEL RADIOACTIVE WASTE DISPOSAL

Processes for converting liquid radioactive waste to solids for safe, permanent storage are under development at ORNL. These processes are designed for treating the wastes from plants processing spent reactor fuels that contain high levels of radioactive fission products. Three processes have been developed (see Fig. 2) on an engineering scale. Work on the most advanced of these

64-10944A

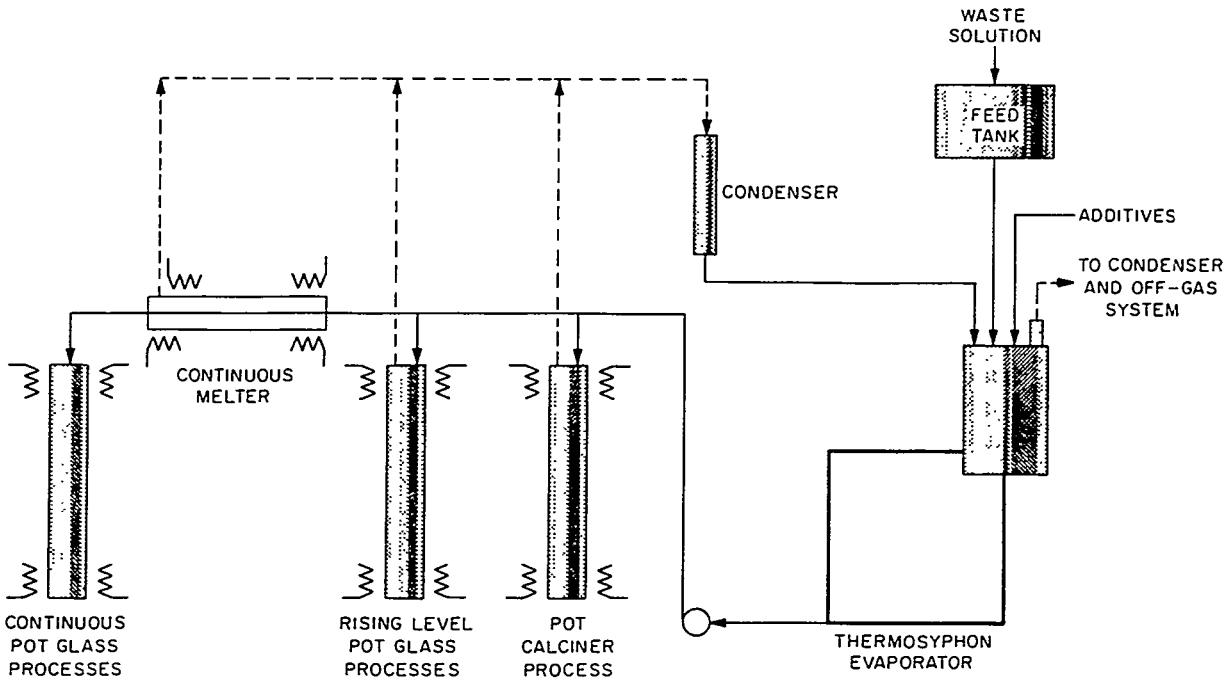

Fig. 2. ORNL Processes for Solidification of High-Level Wastes. All three processes incorporate the radioactive wastes into a solid contained in a pot or tank for permanent storage. They differ only in the nature of the contained solids or in the method of filling the pot. The pot calcination process produces a porous solid, which is soluble in water. The other two processes produce an insoluble glass, which gives added safety. In the rising-level pot glass process, the glass is made in the disposable container. In the continuous pot glass process, the glass is prepared in a separate vessel and poured into the final disposal pot.

processes, pot calcination, has been completed except for pilot planting at Hanford.

The two alternative processes, now under development, fix the radioactive waste in a fused solid "glass." In this form, the radioactive elements are very insoluble in water and will not be leached from the glass if the container is broken in an accident. Elements simulating radioactive fission products resulting from reactor fuel burnups as high as 35,000 Mwd per ton of fuel have been successfully fixed in these glasslike melts.

DISPOSAL IN GEOLOGIC FORMATIONS

Disposal in Natural Salt Formations

The major effort in our studies on the disposal of high-level solid radioactive wastes into underground salt formations is the operation of a field demonstration in a Lyons, Kansas, salt mine. In this demonstration, to be initiated in 1965, 14 Engineering Test Reactor fuel assemblies, contained in seven cans and located in holes in the mine floor, will simulate the heat and radiation anticipated in wastes solidified by the proposed high-level waste treatment processes. The demonstration will last for two years; during this time the fuel assemblies will be exchanged for fresh assemblies three times to increase the radiation dosage to the salt and to perfect handling equipment.

The engineering and scientific objectives are the confirmation of the feasibility and safety of disposal of radioactive wastes in salt mines; demonstration of the waste-handling equipment and techniques; determination of the possible effects of radiation on hole closure, floor uplift, and mine stability in an area where the salt temperatures due to heat from radioactive decay range up to 200°C; determination whether small amounts of chlorine may be released from the salt through the combined effects of heat and radiation; and the measurement of the creep and plastic flow of salt at elevated temperatures. This information will be needed later for the design of an actual disposal facility.

During the past year the mine in Kansas has been completely renovated in the areas which we will use (Fig. 3). A headframe has been built, a new waste charging shaft has been drilled, the experimental area has been mined, and a general upgrading of existing facilities has been carried out. During the past year, a series of laboratory creep tests on model salt pillars (similar to the pillars left to support the roof in actual mining operations) has produced a significant advance in the understanding of creep and plastic flow phenomena in salt mines. For several years we have been making field measurements of the rate of closure of mine openings (rooms) and determining the relationships between vertical and horizontal closure rates. These relationships have been found to be the same in the laboratory models, thus verifying the validity of the models and, at the same time, providing a means for understanding *how* the movements take place. (*Why* the movements take place in the exact manner that they do is not yet understood, but we hope that further model studies will lead to this understanding also.)

Since the salt-pillar models have proved to be valid for predicting the creep and plastic flow behavior in mines at ambient temperature, it is reasonable to assume that they will also be valid demonstrators of behavior at elevated temperatures, such as may be encountered in an actual waste disposal operation (up to above 100°C). Such predictions will be required in the design of a mine layout for waste disposal. The field demonstration, in which one pillar is to be heated, will provide a further check of the validity of elevated-temperature pillar models.

PHOTO 67009

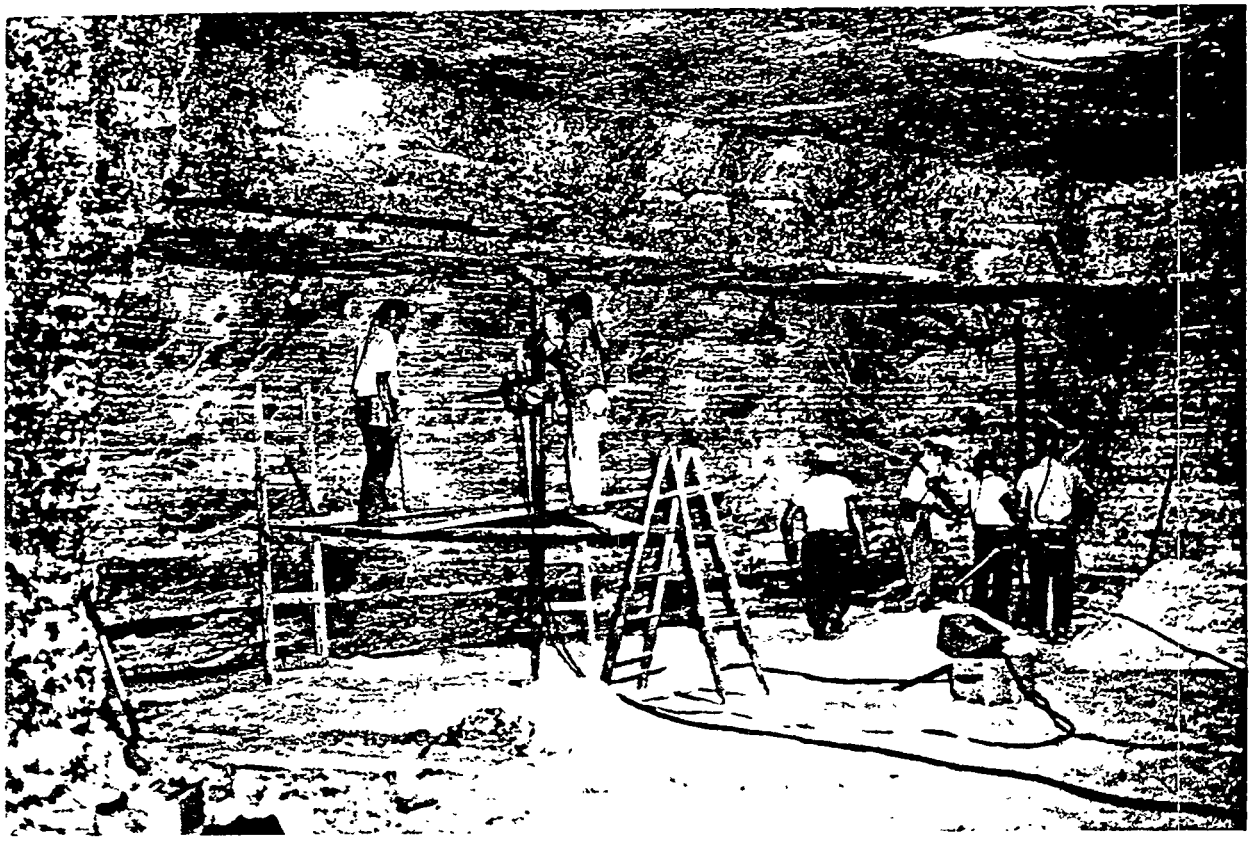

Fig. 3. Salt Mine Demonstration. Personnel of the Carey Salt Company drilling dynamite holes in face of entry to the experimental area of the field demonstration in the Lyons, Kansas, mine. This photograph was taken near the beginning of the mining operation, and only about 15 ft of the entry had been excavated. The completed entry is about 14 ft high, 30 ft wide, and 300 ft long, and has four rooms, each about 60 ft long, leading off to the left. A total of around 16,000 tons of salt was mined. The Carey Salt Company carried out the mining operations under contract with ORNL.

ART WORK - NO NUMBER

PHYSICAL RESEARCH

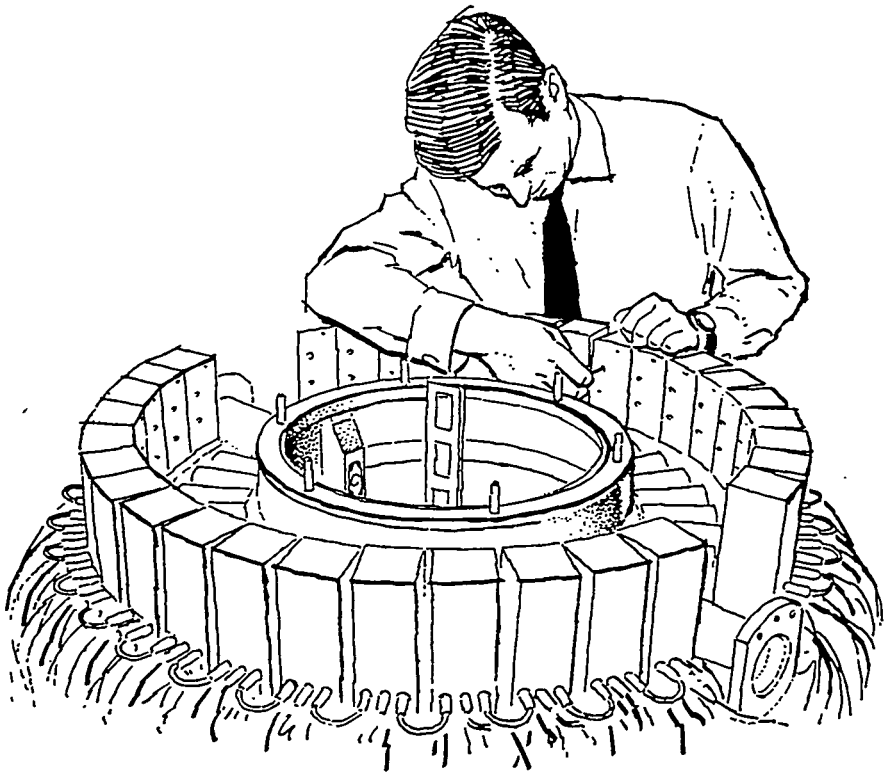

PHYSICS AND MATHEMATICS

SHIELDING AGAINST HIGH-ENERGY RADIATIONS

The joint program to develop and prove methods for computing the effectiveness of shields for space vehicles and high-energy accelerators was continued. Not only must suitable radiation transport methods be originated, but the cross sections at these high energies must also be estimated from available theories or broadly interpolated from sparse experimental data. Thus the program includes both the development and application of calculational tools and the performance of experiments to provide additional bench marks for testing the validity of estimated cross sections.

The analysis of the gamma-ray spectral data obtained in the experiment performed at the Harvard University cyclotron has recently been completed, and Fig. 1 shows the resulting spectrum for a water target bombarded by 160-Mev protons. This spectrum and those obtained for other targets have been compared with spectra estimated by Charles Hill (Second Symposium on Space Shielding, 1964), who used a procedure partially based on the frequency of the various residual nuclei predicted by ORNL cross-section calculations. In general, the experimental and estimated spectra agree within 30%, except for certain gamma-ray lines that seem to be overlooked by the estimation

2-01-058-923

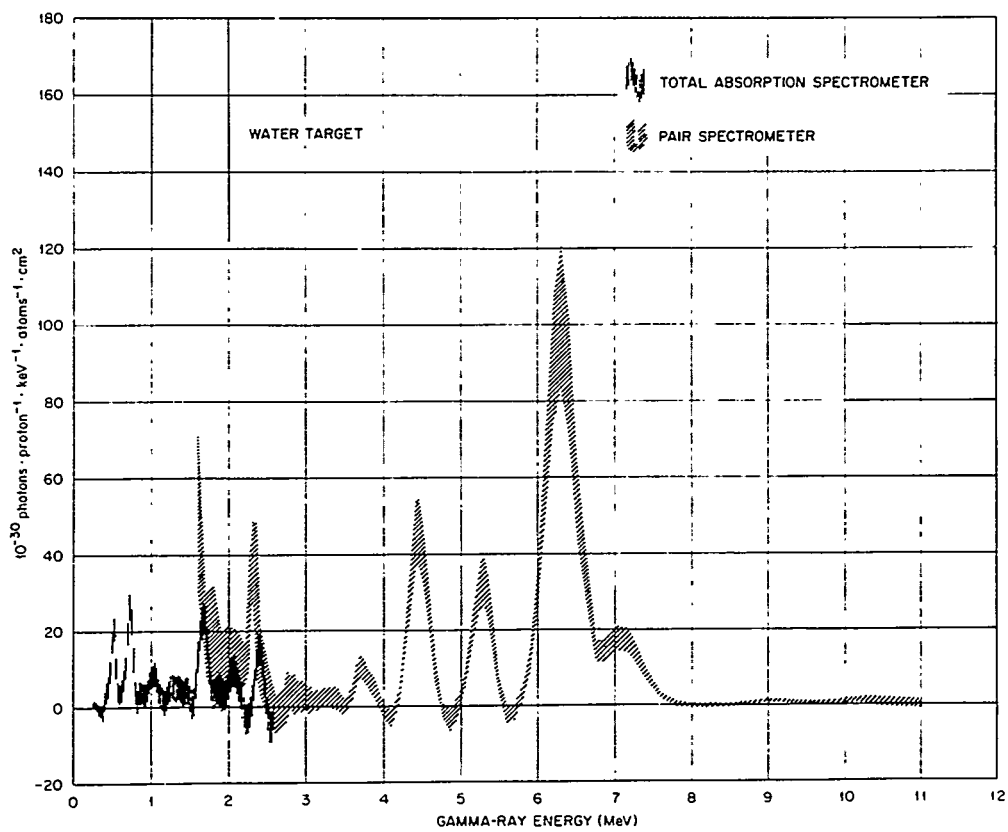

Fig. 1. Absolute Gamma-Ray Yield as a Function of Gamma-Ray Energy Due to the Bombardment by 160-Mev Protons of a 29-Mev-thick Water Target.

procedure. Similar comparisons for gamma-ray spectra from recent experiments at a lower energy (34 Mev) are in progress.

Nearly final experimental secondary nucleon cross sections obtained from the 160-Mev experiment have been checked against predictions made for several nuclei by the Laboratory's intranuclear cascade Monte Carlo program. The agreement is remarkably good, except that for small angles the program seems to predict too hard a proton spectrum, and for angles larger than 90° it predicts far too few secondaries. Experiments have been performed at a higher incident-proton energy (450 Mev) to extend the range of comparison, and the calculations are being similarly extended, but no comparisons have been made yet.

The experimental secondary nucleon data have also been compared with the output of the Monte Carlo nucleon transport code, NTC, for 160-Mev protons incident on thick targets. In this case the agreement is not very good. Comparisons of the transport code with the measurements made at 450 Mev are in progress, and we hope they will give some insight into the reason for the discrepancy at the lower incident energy.

The nucleon transport code has also been used to calculate a variety of results of interest in space-vehicle shielding. For example, it was used to calculate the contribution to the dose in a spacecraft due to secondary particles produced in the shield by solar flare protons. In other calculations it was used to verify that the current-to-dose conversion factors previously obtained with this code are valid and that the straight-ahead approximation, which is used extensively in space shielding calculations, is a good approximation.

Additional calculations have been performed for high energies and deep penetrations using the one-dimensional transport code. In particular, the output of this code has been compared with experimental results on the cascade induced by 10- and 19.2-Bev/c protons in iron and substantial agreement has been found for depths of the order of 1800 g/cm^2.

CHANNELING OF FAST HEAVY IONS BY AN ORDERED CRYSTAL LATTICE

When an energetic particle is injected into an ordered crystal lattice, within a certain range of crystallographic directions, its trajectory may be affected by correlated collisions with rows or planes of atoms which tend to steer the ion away from violent collisions with lattice atoms. This effect, which has been named channeling, was first predicted by the computer calculations at the Solid State Division on the ranges of multikilovolt ions in copper.

In a joint effort of the Physics Division and the Solid State Division, multicomponent beams of bromine and iodine ions with energies up to 80 Mev have been used to study the effect of crystallographic orientation on ion energy losses in thin single crystals of gold. These high-energy beams, which simulate the mass and energy of fission fragments, were produced with the Oak Ridge tandem accelerator (Fig. 2). The artificial fission-fragment beams have the advantage over real fission fragments of being highly uniform in energy, so that small energy changes can be measured with precision. At the same time the accelerator produces many groups of particles, each group having a different energy; thus experiments at different but precisely known energies can be performed simultaneously.

When the beam is passed through nearly perfect gold crystals with thicknesses of only 0.5 μ, it is found that abnormally low energy losses occurred at certain special incidence angles. In contrast to the results of some previous experiments at Brookhaven National Laboratory and at Los Alamos Scientific Laboratory with lighter particles, practically all the bombarding particles are affected. If the gold lattice is mounted with its low-order planes parallel to the incoming beam, then the crystal exhibits these effects at all angles as the mounting is rotated. When rows of atoms come in line with the direction of motion, the penetration of these heavy particles can be very great. It appears that the study of channeling may have a very pronounced effect upon our understanding of the stopping of particles in solids.

STUDY OF THE ELECTRICAL CHARGE DISTRIBUTION IN METALLIC ALLOYS THROUGH THE USE OF THE MÖSSBAUER EFFECT

Through the use of the recently discovered Mössbauer effect, it is now possible to measure gamma-ray energies with extraordinary sensitivity.

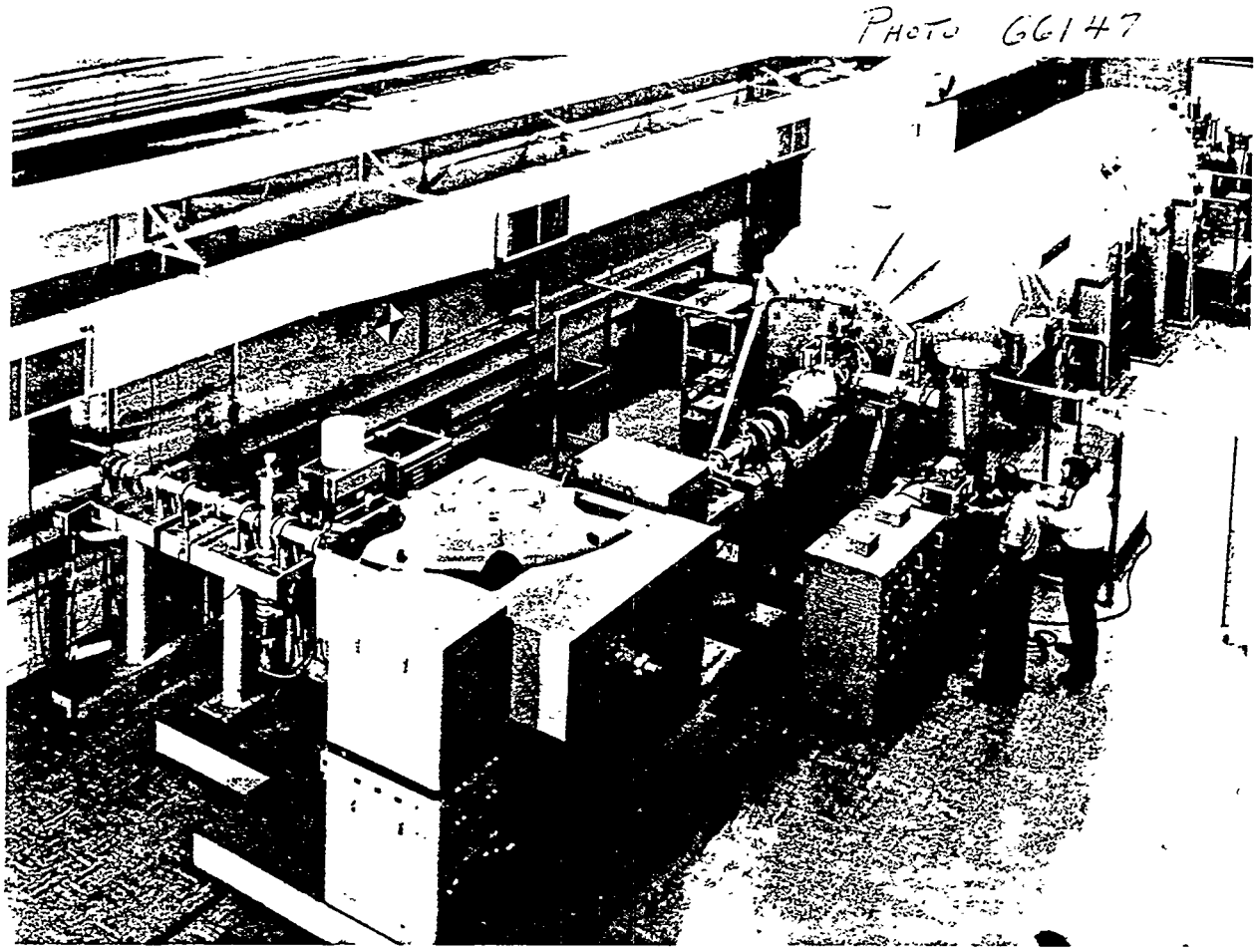

Fig. 2. Tandem Accelerator and Magnetic Analyzer.

This extremely sensitive technique for gamma-ray energy measurement permits the investigation of some properties of solids which could not be measured previously. For example, such properties of metallic alloys as electrical resistivity, magnetism, and hardness depend importantly on the electrical charges that the individual atoms of the alloy assume. Over the years, many basic theoretical studies have been made relative to the effects of this atomic electrical charge on alloy properties, but no way of verifying these theories (i.e., no method of measuring this charge) was available. We have developed a method of investigating this electrical charge. The method combines exceedingly sensitive measurements of gamma-ray energy, using the Mössbauer effect, with measurements of electrical resistivity.

The usefulness of this combination of measurements may be understood quite readily. For example, when an electrically neutral atom of gold is dissolved in silver, it may be expected that the gold atom will assume an electric charge. The gold impurity will impede or resist the flow of an electric current in the silver, and this electrical resistance is closely related to the charge which the gold atom assumes. The electric charge on an atom penetrates the nucleus to a slight extent and thus affects the energy of nuclear processes such as the energy of the gamma rays which a nucleus may emit or absorb. Thus, when an atom of gold is dissolved in silver and becomes electrically charged, the nucleus feels this change of charge and the resonance gamma-ray energy will be minutely different from the value it has when the atom is electrically neutral. The charge on an atom manifests itself then through both the gamma-ray energy and the electrical resistance. The combined study of these quantities gives more detailed information about the charge than would be available from either quantity separately.

These measurements usually must be performed at very low temperatures (e.g., within a few degrees of absolute zero).

Experimental studies have been made for alloys of gold with other noble metals and with transition metals. The results obtained confirm, to a considerable extent, the basic theoretical investigations mentioned above. They also show the way by which a more penetrating understanding of alloys of both scientific and technical importance may be gained through the combined use of the techniques of nuclear and solid-state physics.

NEW TECHNIQUE FOR USE IN NUCLEAR AND SOLID-STATE PHYSICS

An experiment conducted at ORNL has established the feasibility of making Mössbauer measurements using the gamma rays emitted following Coulomb excitation of energy levels in atomic nuclei. This new technique greatly increases the number of nuclei available for Mössbauer studies and should give valuable new information in the fields of nuclear and solid-state physics.

An important aspect of this work is the combining of two well-established techniques used for fundamental physics research: (1) Coulomb excitation is a process that utilizes charged particles of relatively high kinetic energies, which interact through an electromagnetic field with the atomic nuclei of a solid to produce gamma rays. High-energy charged particles are obtained by using some type of accelerator. In this case, the ORNL tandem Van de Graaff accelerator was used to accelerate oxygen ions to an energy of 25 Mev. (2) The Mössbauer effect is a method for measuring minute changes in frequency of a nuclear gamma ray.

The usefulness of the Mössbauer effect stems from the fact that the nucleus is aware of its environment and this awareness is reflected in minute changes in the energy of gamma rays emitted from the nucleus. Gamma rays are similar to radio waves, since they are both electromagnetic in nature, but the gamma rays are of a much higher frequency. The nucleus behaves as if it were a tiny transmitter sending out waves of a certain frequency, and in some cases it may reverse its role and behave as a receiver. The Mössbauer effect makes use of this dual role which a given species of nucleus may play. One piece of material acts as a transmitter, the other as a receiver. But the receiver is sensitive only to the radiation emitted by its own kind and ignores the radiation from all other sources (transmitters).

Nuclei used in Mössbauer experiments are rather particular receivers and ignore the radiation even from transmitters of their own kind if the frequency of the wave is not precisely the value it should be. A frequency difference of one part in 10^{12} is, in some cases, enough to cause the receiver to ignore the signal.

R. Mössbauer discovered how to tune the receiving nuclei and measure these small frequency differences precisely. (For his discovery, Mössbauer won the Nobel Prize in 1961.) It is these small frequency differences which give valuable information about the environment of the nucleus and, therefore, the properties of solid material.

Up to the present, radioactive nuclei have been used as sources of gamma rays used in Mössbauer research. However, our work establishes for the first time the production of the Mössbauer effect by Coulomb excitation. This method greatly increases the number of nuclei which may be used for Mössbauer studies, and consequently the number of different materials which may be investigated is also increased.

Another aspect of this kind of measurement is that it provides a new tool to study material which is being exposed to bombardment by different kinds of particles such as protons, helium atoms, or even heavier atoms such as oxygen. The detailed understanding of the behavior of solids under these conditions derives its importance from the point of view of the technology which must accompany the construction of, for example, reactors and spacecraft.

BINDING ENERGIES OF NUCLEI

The nuclear shell model is an independent-particle model, meaning that each proton and each neutron is considered as being in a state of motion which is not directly influenced by the details of the motions of the other nucleons. Another way of saying this is that the motions of the nucleons are not dynamically correlated. Of course the common potential well in which each nucleon moves in the shell model is, in principle, determined by the nucleons themselves as a collective

property representing the average effect of the interactions between nucleons. The Hartree-Fock equations, originally developed for the electrons in atoms, express the self-consistency conditions relating the potential well and the wave functions of the single-particle states.

Shell-model calculations often successfully obtain the energies of a number of excited states of a nucleus relative to the lowest or "ground" state, but they greatly underestimate the absolute binding energy of the ground state. This deficiency of the model results from the use of assumed weak nucleon-nucleon interactions instead of the realistic strong interactions inferred from proton-proton scattering experiments. At Oak Ridge, a program of calculations which starts from strong interactions is under way. This requires including dynamical correlations between nucleons, but this is being done in the simplest possible way, namely, by taking account only of two-particle correlations. Professor Weisskopf has referred to this extension of the shell model as the independent-pair model. The relative motion of a pair of nucleons is calculated without regard for the details of the motions of all the other particles. The average effect of the other particles is brought in through the collective potential well and through the Pauli exclusion principle, which forbids any two nucleons from being in the same state of motion. The exclusion principle effectively reduces the interaction between two nucleons when they are in a nucleus by forbidding them from scattering into states already occupied by other nucleons.

The independent-pair model was worked out about ten years ago by K. Watson for scattering of a particle by a many-body system and by K. Brueckner for bound states. Extensive tests of Brueckner's theory have been carried out at Los Alamos and elsewhere for the fictitious infinite medium of nucleons referred to as nuclear matter. The effective interactions appropriate for nuclear matter have also been used in calculations for actual finite nuclei. It seems likely, however, that whenever shell effects are important the effective interaction may differ considerably from that appropriate to an infinite medium.

With the availability of fast computers it becomes possible to calculate effective interactions separately for individual nuclei. As a first step, calculations have been made at ORNL for the doubly closed shell nucleus ^{16}O. The binding energy obtained is in good agreement with experiment. Similar calculations are being made for heavier closed-shell nuclei. The matrix elements of the effective interaction will be used also in calculations of excited states.

ANALOG STATES

The investigation of isobaric analog states serves as a method to determine the structure of specific nuclei and to test the hypothesis that nuclear forces are charge independent, that is, that the specifically nuclear forces acting between two protons, between two neutrons, and between a proton-neutron pair are identical. It is convenient to consider protons and neutrons as different charge states of the same particle, which is called a nucleon. One then introduces a new quantum number T, called the isotopic spin, whose Z component T_z is defined as $-\frac{1}{2}$ for the proton and $+\frac{1}{2}$ for the neutron. A nucleus with N neutrons and Z protons has $T_z = (N-Z)/2$. If we assume charge independence, then for each value of T there exist $2T + 1$ values of T_z, which define a group of nuclear states having identical properties with the exception of charge and the energy displacement caused by the different electrostatic interactions. It is thus possible to infer the structure of a given nucleus by investigating the energy levels of its isobaric counterpart.

Nuclear states corresponding to the $2T + 1$ values of T_z are said to form an isotopic spin (or T) multiplet. For example, a triplet associated with $T = 1$ is composed of one nuclear state from each of the isobars ^6He, ^6Li, and ^6Be, whose respective T_z values are 1, 0, and -1. Since the strength of the Coulomb repulsion increases with Z, ^6He ($Z = 2$) is the most stable state of this triplet. For heavier nuclei it is found that the lowest (or ground) state of a nucleus is always that member of a T multiplet for which $T_z = T$. The member of this same multiplet for which $T_z = T - 1$ is an excited state of the isobar having one less neutron and one more proton. This excited state with $T_z = T - 1$ is called the isobaric analog state corresponding to the ground state of the isobar with $T_z = T$. It is also possible to have analogous states neither of which represents the ground state of its nucleus.

An example of analog states is afforded by a reaction which has been investigated at ORNL.

An yttrium target was bombarded by variable-energy protons from the 5.5-Mv Van de Graaff accelerator. The absorption of a proton converts yttrium into zirconium, which decays by neutron emission. The neutrons were observed by using a 5-ft-diam graphite ball detector. The neutron counting rate was measured for various energies of the bombarding protons. A large increase in the counting rate was observed for proton energies of 4.80 and 5.01 Mev. These increased counting rates represent resonance levels in the compound nucleus (^{90}Zr) which are isobaric analogs of the ground and first excited states of ^{90}Y. The lower of the resonances in ^{90}Zr has $T = 6$ and $T_z = 5$. This is the analog of the ^{90}Y ground state, for which $T_z = T = 6$.

These particular states have been investigated further by using time-of-flight methods to determine the energy and angular distribution of the emitted neutrons. Information derived from both experiments can be analyzed to help determine the properties (parity, angular momentum, etc.) of these nuclear states.

EVIDENCE FOR A LAMBDA-NUCLEON RESONANCE

In the last few years a large number of very short-lived elementary particles have been discovered in high-energy physics research. These particles manifest themselves through resonances in the effective mass spectrum of a combination of other particles. Such resonances were first observed in the nucleon-pion system. Lately, resonances in multiple pion systems and in baryon-pion systems have been observed. (Nucleons and elementary particles with mass larger than the mass of nucleons are called baryons.) We have found strong evidence for the existence of a resonance in the baryon-nucleon system. The interaction of Σ^- hyperons with helium was studied. Since the lifetime of the Σ hyperons is only 1.6×10^{-10} sec, they decay or interact within a few centimeters from their point of origin. It was thus necessary to produce these particles inside the helium bubble chamber, which served as a target as well as the analyzing tool. The helium bubble chamber was exposed to a beam of slow K^- mesons created by the Bevatron at the Lawrence Radiation Laboratory. Roughly 12% of the captured K^- mesons yielded Σ^- hyperons. A small fraction of these sigmas interacted with a helium nucleon. The analysis was restricted to events with a π^+ meson and a highly ionizing track at the K^- vertex. This topology can occur only for Σ^- production and permits an unbiased count of Σ^- interactions regardless of their topology. The Σ^- hyperons that interacted with a helium nucleon were found to emit a Λ hyperon, a triton, and a neutron. An accurate measurement of the Λ momentum was obtained from an overdetermined kinematic fitting to the measured momenta and direction of the Λ decay products. The triton stub length yielded a precise momentum measurement from range. The neutron momentum was deduced through kinematic fitting. The momentum spectrum for each of these particles was plotted. The expected momentum spectrum was also calculated theoretically on the assumption that there was no final-state interaction between the emitted particles. The observed distributions and the theoretical calculations were in good agreement for the Λ and neutron spectra but disagreed violently for the triton spectrum. Shown in Fig. 3 is the momentum distribution for the triton. The solid curves give the theoretically expected distribution plotted with and without a cutoff in the triton momentum corresponding to the momentum below which no triton track may be visible in the helium bubble chamber. The disagreement with the observed distribution means that some effect alters the shape of the triton momentum spectrum. Indeed, if one assumes that the Λ and neutron were emitted as a single particle,

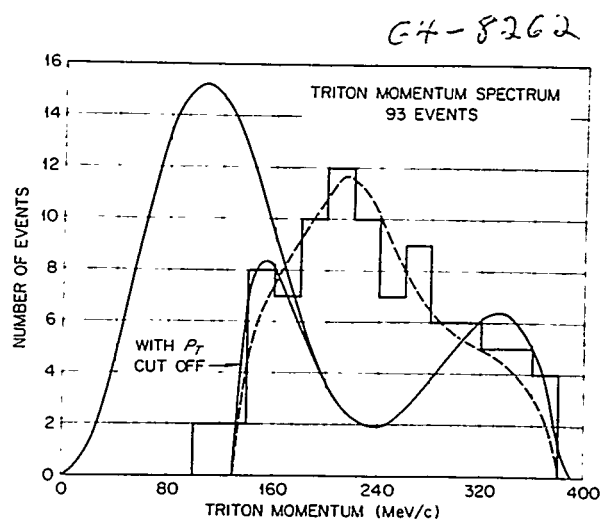

Fig. 3. Triton Momentum Spectrum.

the shape of the triton spectrum is well explained, as is seen from the dashed curve in Fig. 3. The result of this experiment gives strong evidence that a .\-nucleon resonance of mass 2098 Mev/c exists.

FISSION STUDIES, INCLUDING NEW ENERGY DETERMINATIONS BASED ON MEASUREMENTS OF HIGH-ENERGY BROMINE AND IODINE IONS

Techniques for extremely accurate and simultaneous measurement of the velocities and energies of fission fragments have been developed at ORNL. In addition, techniques for the accurate, simultaneous measurement of the energies of the two fragments emitted in fission have been developed. An entire series of experiments employing these techniques in the study of the fission of radium, uranium, plutonium, and californium have been carried out. Results of such measurements have yielded new data of fundamental importance in the understanding of nuclear fission.

In order to understand the mechanism of nuclear fission, it is necessary first to have an accurate and detailed knowledge of the masses and energies of the fission fragments. We must know the distribution of fragment masses and the average energy associated with each fragment. The distribution in total kinetic energy corresponding to each mass pair must be known. We have developed two types of experiments to obtain this information.

The first type of experiment makes use of the simple and well-known equation $E = \frac{1}{2} Mv^2$. (Relativistic corrections are negligible for fission fragments.) From correlated measurements of the energy and velocity of a fission fragment, its mass may be calculated. The velocity of a fragment is determined by measuring the time required for a fragment to traverse a fixed distance, say 1 m. The average time required for a fragment to traverse this distance is about 0.1 μsec; we have developed techniques for the measurement of these times with an accuracy of about 0.6 nsec.

The recent development of semiconductor detectors permits very accurate measurement of nuclear particle energies. Some of our early experiments, however, showed that these detectors behave differently for fission fragments and for lighter nuclear particles such as protons and alpha particles. The matter has now been clarified by our recent, very careful comparison measurements of fission fragments with particles of known mass (^{79}Br, ^{81}Br, and ^{127}I) accelerated to known energies in the ORNL tandem Van de Graaff accelerator. On the basis of these measurements, we have more recently developed a method of absolute energy calibration based only on reference measurements of a ^{252}Cf spontaneous fission fragment pulse-height spectrum, thus making it possible for absolute energy calibrations to be obtained in almost any laboratory.

The second type of experiment which permits acquisition of the mass and energy information discussed above makes use of the principle of momentum conservation. If we allow each of the two fragments to be detected in a semiconductor detector, we may obtain the energy of each fragment, making use of the energy calibration method described above. Then from the principle of momentum conservation, we may also determine the fragment masses. The advantage in this kind of experiment is that the energies of both fragments are measured, thereby permitting the determination of total fragment kinetic energy as a function of fragment mass.

We have carried out an entire series of such experiments in studies of the fission of radium, uranium, plutonium, and californium. The results of these and other experiments exhibit some interesting features which may be attributed to certain known properties of nuclei. For example, in the fission of nuclei heavier than radium, such as uranium and plutonium, the so-called "nuclear shell effects," or "magic numbers," seem to play an important role, and it appears that the properties of the fragments themselves may determine the character of the fission process beyond the saddle point. On the other hand, in the fission of nuclei lighter than radium, such as lead and bismuth, it appears that the character of fission resembles that of a liquid drop as calculated theoretically. Radium-226 presents an interesting anomaly in that both types of fission appear to be present in this case.

The new absolute total fragment kinetic energies resulting from these measurements are several million electron volts higher than those of previous measurements at other laboratories for most fragment mass pairs, and the present results range up to 18 Mev higher in the region of symmetric

fission. The source of the discrepancies has now been found, and some new interpretations of fission, based on these new energies, are expected to follow.

GAMMA-RAY SPECTROSCOPY WITH LITHIUM-DRIFTED GERMANIUM DETECTORS

Nuclei in unstable configurations generally emit gamma rays with discrete energies in proceeding to a condition of stability. The precise measurement of the energies and intensities of these gamma rays is a powerful technique in the study of the structure of the nucleus and can also be used to identify the presence and amount of specific isotopes. Recently, a major advance in this field has been made possible through the development of the lithium-drifted germanium detector. Its importance results from a combination of high resolution (comparable to magnetic and crystal diffraction spectrometers) and reasonable efficiency. Its resolution is about a factor of 10 to 20 better than that obtained with the sodium iodide scintillation spectrometer, which has been the primary tool for gamma-ray studies in the last decade.

Lithium-drifted germanium detectors fabricated by the Instrumentation and Controls Division with active volumes up to 2 cm^3 were employed to determine the energies of gamma rays to within a few hundred electron volts. They include values for the frequently used calibration gamma rays from the radioactive nuclei ^{51}Cr, ^{7}Be, ^{207}Bi, ^{54}Mn, ^{88}Y, ^{65}Zn, and ^{22}Na. The excellent resolution of this detector has made it possible to observe members of very near-lying gamma-ray doublets in ^{102}Rh and ^{106}Rh. Estimates have been made of the relative intensities of the two gamma rays for both nuclides.

Energies of gamma rays from over 50 nuclides which have been Coulomb excited with alpha particles extracted from the 5-Mv Van de Graaff generator were also measured. In this study, previously unobserved gamma rays were found in ^{75}As, ^{77}Se, ^{117}Sn, and ^{119}Sn. To illustrate the contrast between detectors, the spectra of gamma rays from Coulomb-excited ^{75}As as observed with a sodium iodide detector and a germanium detector are shown in Fig. 4 *a* and *b*.

The gamma-ray spectra from thermal and resonance neutron capture in ^{238}U, Bi, Nb, Y, and the isotopes of Zr and Sn have been measured with germanium detectors with active volumes up to 6 cm^3. Neutron capture gamma rays can extend in energy to 12 Mev. In the energy range above 2 Mev, the useful interaction is through the pair process, with subsequent escape of both annihilation quanta. The energy of this double-escape peak is 1022 kev less than the gamma-ray energy, and the amplitude is 3 to 10 times that of the Compton continuum which it overlies. Figure 5 illustrates the data obtained with a 2-cm^3 detector

C4-9538

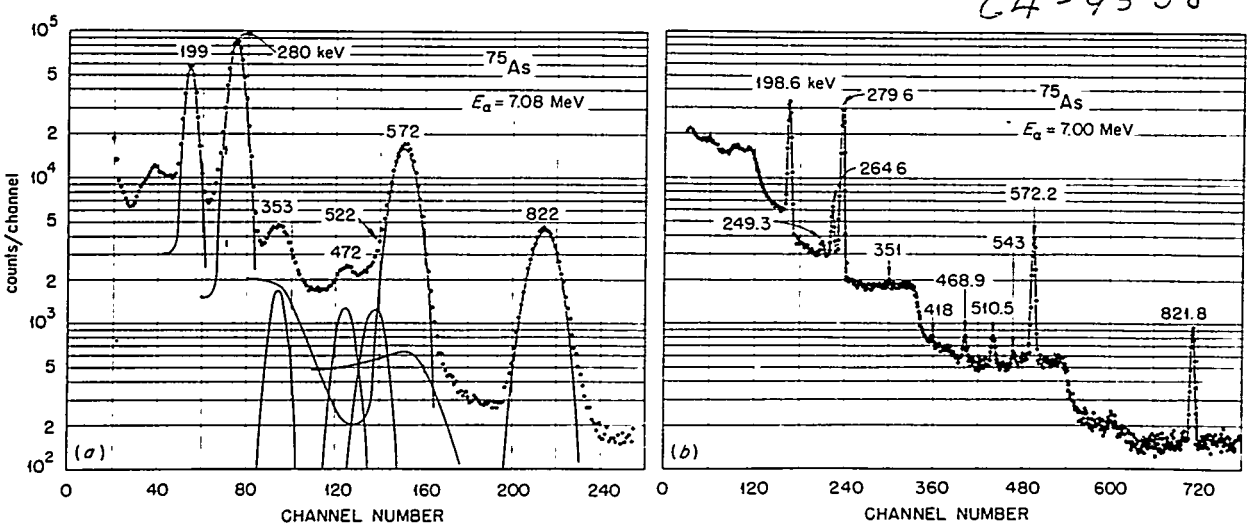

Fig. 4. Spectra of Gamma Rays That Result when Nuclei of ^{75}As Are Bombarded by 7-Mev Alpha Particles. (*a*) Measured with a sodium iodide scintillation spectrometer; (*b*) measured with a lithium-drifted germanium detector.

65-3366

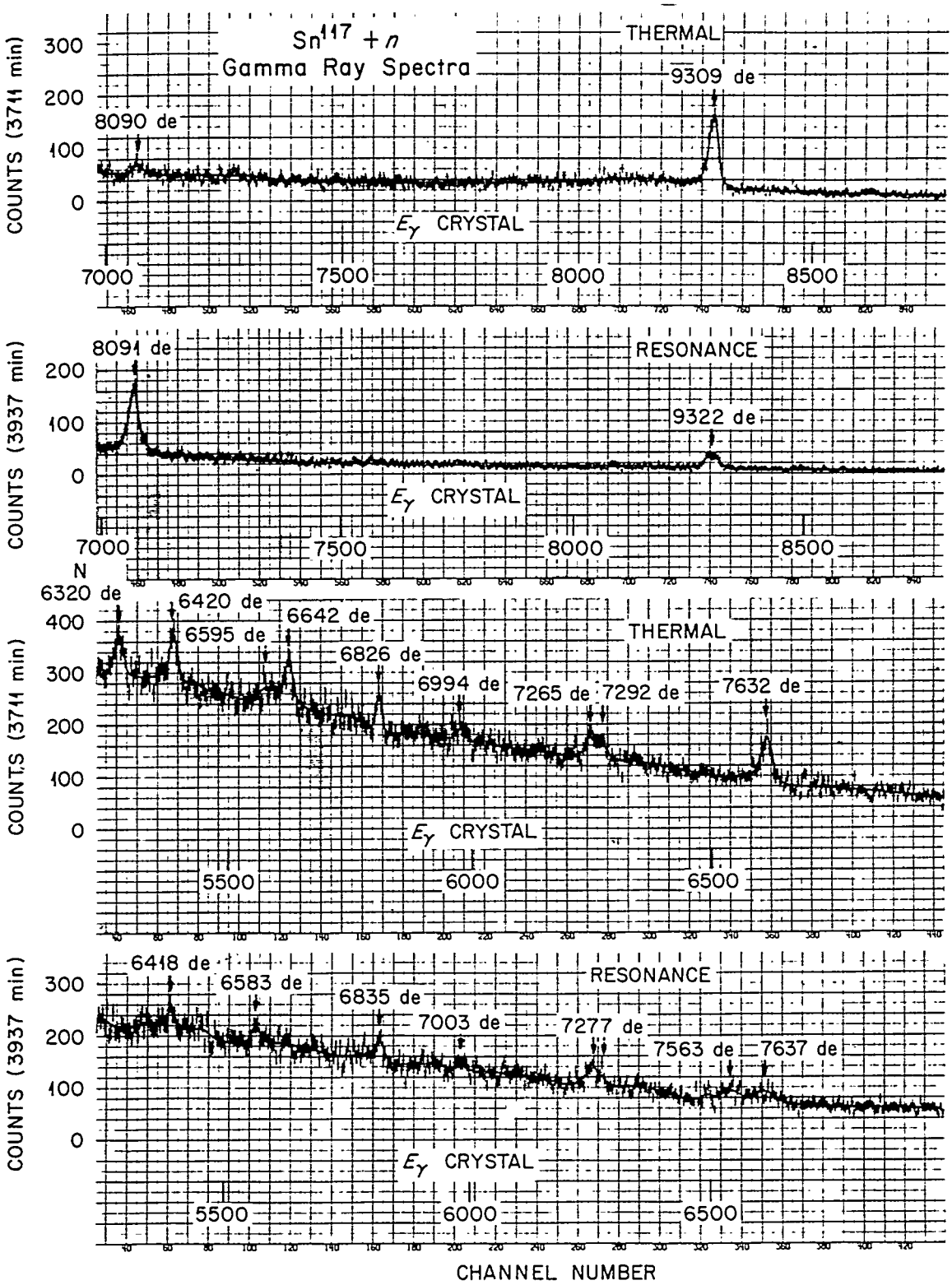

Fig. 5. Data Obtained with a 2-cm^3 Detector from a 35-g Sample of ^{117}Sn for Both Thermal- and Resonance-Energy Neutrons.

from a 35-g sample of ^{117}Sn for both thermal and resonance-energy neutrons. The peaks are all double-escape peaks, but the energies marked on the figure are the energies of the gamma rays. The intensities of gamma rays from resonance neutron capture differ considerably from those from thermal neutron capture. Strong ground-state or near-ground-state transitions were observed from resonance neutron capture in ^{124}Sn, ^{122}Sn, ^{120}Sn, and ^{118}Sn.

A comparison of gamma-ray spectra resulting from thermal neutron capture in Nb with results of the Nb(d,p) reaction shows that 53 gamma rays are found which correspond to either (1) primary transitions from the capturing state (4^+, 5^+ for s-wave neutrons) to levels excited in the (d,p) reaction or (2) transitions from these levels to the ground state (6^+). In 12 cases, both components of a two-component cascade are seen. Some of the strong high-energy gamma transitions, if primary, proceed to levels which are not excited in the (d,p) reaction. Some of these levels may correspond to excited-proton configurations and thus not be populated in the (d,p) reaction.

THE EXPLOSION OF MULTICHARGED MOLECULAR IONS

When an electron of one of the inner shells of a heavy atom is removed, the atom collapses, giving off a large number of extra electrons. For example, if the atom has 56 electrons to start with it will lose on the average 8 or 9 of the electrons, and it has been observed that it may lose up to 20 or more. Extensive ionization as the result of a hole in the inner shell of an atom is common in nature, since such a vacancy can be produced in many phenomena, like the interaction of an x ray with an atom, or in nuclear decay when internal conversion of an electron occurs.

If a heavy atom is attached to a molecule, the result of this extensive ionization is the violent decomposition of the molecule. That such a decomposition occurs has been known for some time, but recently results have been obtained in which the true relative abundances of the different fragment ions and their recoil energies were measured. We now know how really violent this decomposition is! For example, when an x ray interacts with methyl iodide, the molecule explodes into its constituent elements. The data have been compared with calculations, and it would appear that in the most probable case the molecule loses ten electrons, resulting in a doubly charged carbon, three singly charged hydrogens, and iodine with charge 5, and that these positive ions then are repelled from one another with considerable recoil energy.

This evidence for the highly destructive localized damage caused by having a vacancy in one of the inner shells of a heavy atom, coupled with the high cross section that a heavy atom has for x rays, suggests that such molecular explosions play an important role in some biological and chemical systems. That is, if a system is dependent on the action of a heavy atom, even though that atom is present to only a small amount, then the system may be highly sensitive to the nature of the irradiation. This suggestion has been indeed shown to be the case for some organic catalysts containing iron.

POLARIZED PROTON EXPERIMENT

Protons, the nuclei of hydrogen atoms, possess a property called "spin," which is somewhat akin to the angular momentum of larger rotating masses such as the planets. In nuclear reactions produced by protons, any effect of this spin is ordinarily obscured because the spin axes are in random directions. When the protons are polarized, that is, their spin axes are aligned in the same direction, both the direction of their spin and the nature of the target nuclei should affect the way the protons elastically scatter from the target.

At the Oak Ridge Isochronous Cyclotron (ORIC) a beam of 40-Mev protons is specially prepared by bombarding a hydrogen gas target with 80-Mev helium nuclei. The spin axes of about 95% of these protons are aligned in the vertical direction. When such polarized protons are scattered from various target nuclei, the number scattered to the left at any angle is not necessarily equal to the number scattered to the right. By measuring these left-right asymmetries, new information is obtained about nuclear potentials.

The 40-Mev polarized proton beam was used at ORIC to measure the asymmetries in elastic scattering from targets of ^{12}C, ^{40}Ca, ^{58}Ni, ^{90}Zr,

Drawing 3 A=171

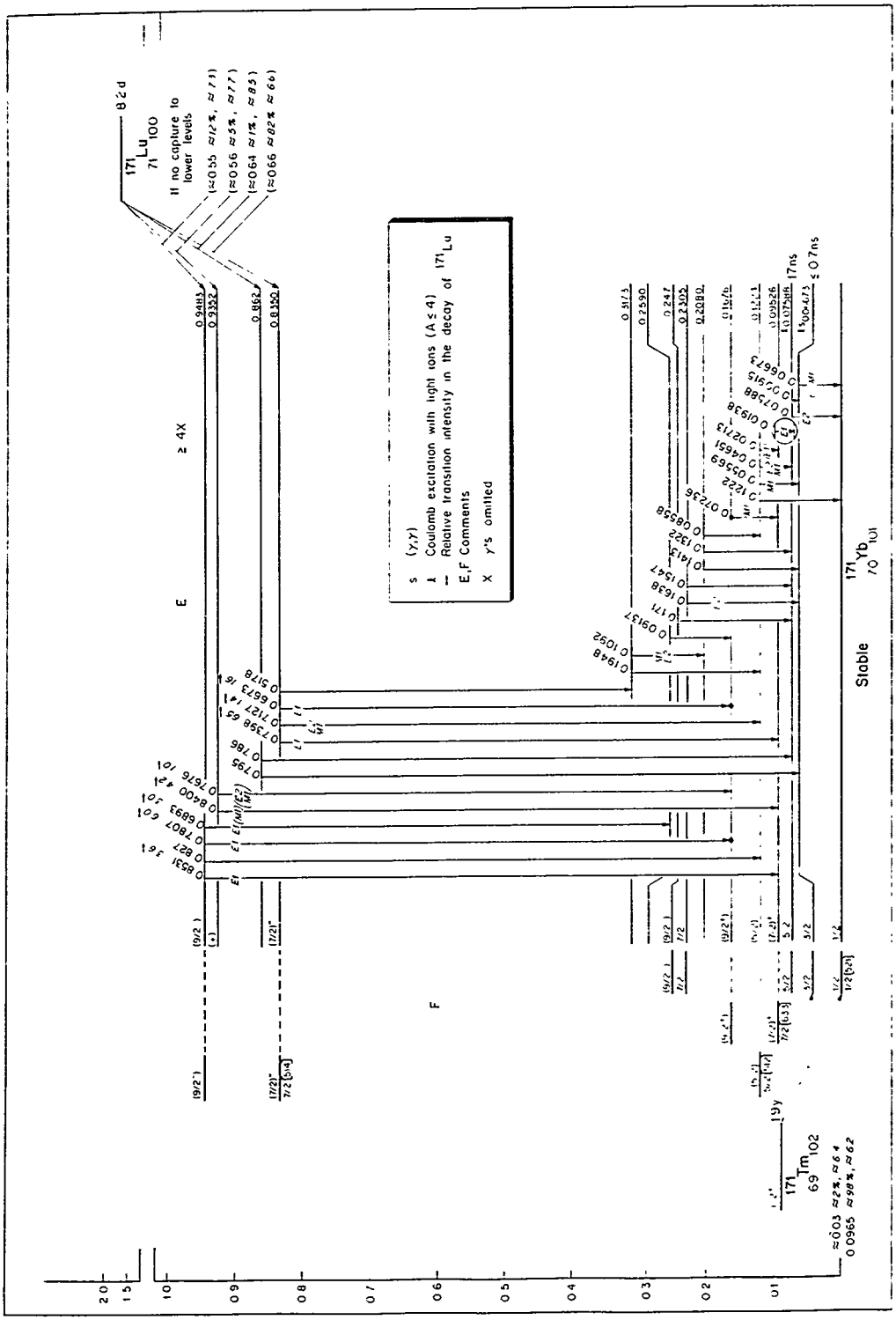

6-4-103 (Dec. 1964)

Fig. 6. Level Scheme of ^{171}Yb. Recently compiled by the Nuclear Data Group.

PHOTO 64106

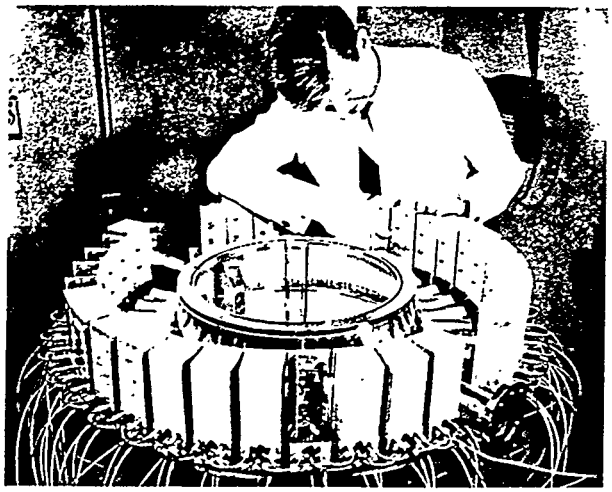

Fig. 7. Apparatus Used in Polarized Proton Experiments. Protons enter through the horizontal beam pipe at the right and pass through thin targets mounted in the frames shown at the center of the scattering chamber. Sixteen sodium iodide scintillation counters are placed 10° apart on each side of the beam line to detect the scattered protons. Precise geometry must be maintained to make the measurements meaningful.

and ^{208}Pb. To gather data efficiently, measurements were made simultaneously at 32 angles in a specially constructed scattering chamber (Fig. 7). The information was processed by a 20,000-channel analyzer, periodically transferred to magnetic tape, and finally analyzed by a digital computer. The same apparatus was used to measure differential elastic scattering cross sections for these elements at angles from 10 to 170°.

NUCLEAR DATA PROCESSED IN 20,000-CHANNEL ANALYZERS

Three of the world's largest multichannel pulse-height analyzers are now in operation at AEC installations. Two are at ORNL, and one is at Yale University. These complex electronic systems, which were built to Oak Ridge–Yale specifications, provide a solution to the problem of handling the vast amount of data required for many nuclear experiments.

In these experiments nuclear particles are usually detected with devices that produce electric pulses, whose amplitudes indicate the energy of the particles. Much of the nuclear-data-taking process is the tallying of these pulses. For example, in a single experiment the physicist may wish to obtain a graph showing the energy and angular distribution of particles arriving at several detectors arranged around one target. Or, he may need to know which of these particles are produced in coincidence, that is, in the same nuclear event. With these complex installations at Oak Ridge and Yale, millions of pulses are electronically evaluated, tallied, and displayed in graphic form. Information accumulated during perhaps hours of operation is available in summary form within seconds.

In its simpler form the pulse-height analyzer is an electronic circuit that measures the amplitude of the pulses from a particle detector and records the pulses in various "channels." By analogy, the experimenter might use pencil and paper to tally the pulses in columns according to their energy, but the analyzer is far faster and more accurate. The analyzer provides, then, a record of the number of particles having the energy range assigned to each of the various channels.

One of these 20,000-channel analyzers (Fig. 8) has become an essential part of the experimental equipment used with the Oak Ridge Isochronous Cyclotron. In a polarized-proton experiment, for measuring the effect of the spin of protons on the way they scatter from various target elements, 32 detectors are positioned around the target and 400 channels are required for each detector. Experiments on pickup reactions require the recording of correlated pulse heights from two detectors to determine the type of particle and its energy. This requires a 50 × 400 channel array, or the full 20,000 channels. In the tallying process the information is recorded in a magnetic-core memory containing 480,000 tiny magnetic rings or "cores." The device can "remember" up to 1,000,000 events in each of the 20,000 channels

At any time during the experiment the information can be displayed graphically on oscilloscopes. At the end of the experiment the information stored in the memory can be transferred to magnetic tape in about 15 sec. The tape can then be analyzed in a high-speed computer. In the case of the experiments on pickup reactions, the computer can, in a mere 25 sec, read the tape and perform the enormous task of sorting through the 20,000 numbers to separate out the pulse-height distributions that belong to the different kinds of particles.

Photo 39905

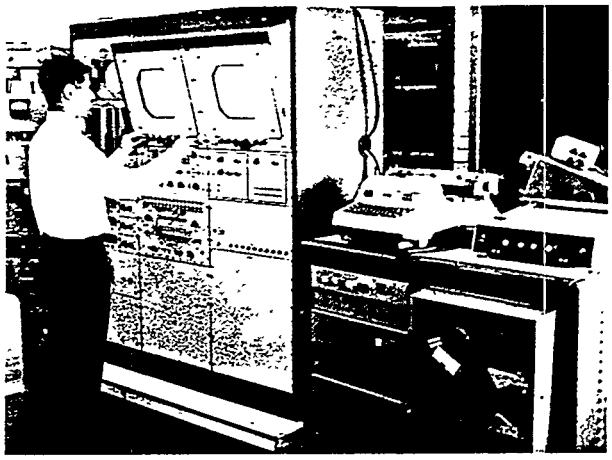

Fig. 8. 20,000-Channel Analyzer. A 20,000-channel pulse-height analyzer is now an integral part of the research facilities of the Oak Ridge Isochronous Cyclotron. The complex electronic circuitry is used for analyzing nuclear events detected with scintillation counters or with solid-state detectors. The electric pulses from several such detectors can be simultaneously evaluated and the information stored in the memory of the 20,000-channel system. With the 480,000 tiny magnetic cores in the memory, up to a million events can be recorded for each of the channels. At any time the contents of the memory can be displayed on the 12-in. cathode-ray tubes shown in the photograph. Or, the entire contents can be transferred to magnetic tape in about 15 sec. This tape is then run through a high-speed computer to provide the desired analysis of the data; typically, this requires less than a minute of computer time.

These electronic systems have enormously increased the speed and accuracy with which data from large experimental installations, such as large accelerators, can be accumulated and analyzed. Experimenters can now undertake investigations that were formerly considered impossible because of the sheer mass of data required for reliable results.

PICKUP REACTIONS

Nuclear reactions in which the bombarding particle picks up one or more particles from the target nucleus can be studied to reveal information about both the target nucleus and the product nucleus. For many such reactions the most suitable energy for the incident particle is in the range from 20 to 50 Mev, but intense beams of particles are needed because the occurrence of nuclear events of this type is rather infrequent. The Oak Ridge Isochronous Cyclotron, with its high intensity and well-controlled beams in this energy range, is an ideal accelerator for these studies.

When a beam of protons from the cyclotron is directed into suitably prepared targets, alpha particles are detected among the products emerging. Experiments at ORNL have demonstrated that some of these alpha particles include the original incident protons which have each combined with, or picked up, a proton and two neutrons from the target nucleus. The pattern of angles and energies with which the alpha particles emerge from the target varies for different target elements. Thus, by analyzing and comparing these patterns, the experimenter can deduce many details about the structure of the various target nuclei involved in the experiment.

Pickup reactions are also obtained by bombarding target elements with a beam of deuterons. For example, it is found that among the particles emerging from the target are some ^{3}He nuclei formed when the incident deuteron picks up a proton from the target nucleus. Again, different scattering patterns are obtained for the various target elements. These two types of pickup reactions are being used to take nuclei apart, bit by bit, to find out how they are put together.

OAK RIDGE ISOCHRONOUS CYCLOTRON

A major improvement in cyclotron performance has been achieved at the Oak Ridge Isochronous Cyclotron (ORIC). More than 50% of the beam circulating within this cyclotron is now routinely extracted for use at external target locations. Previously, 30% extraction efficiency had been considered a high standard of performance. This greater efficiency means that larger output currents can be obtained without inducing unreasonable levels of radioactivity within the cyclotron. Moreover, the beam now available to the experimenter is of exceptionally high quality (small angular divergence and spot size), and the energy is uniform to within 0.5%.

Photo 65025

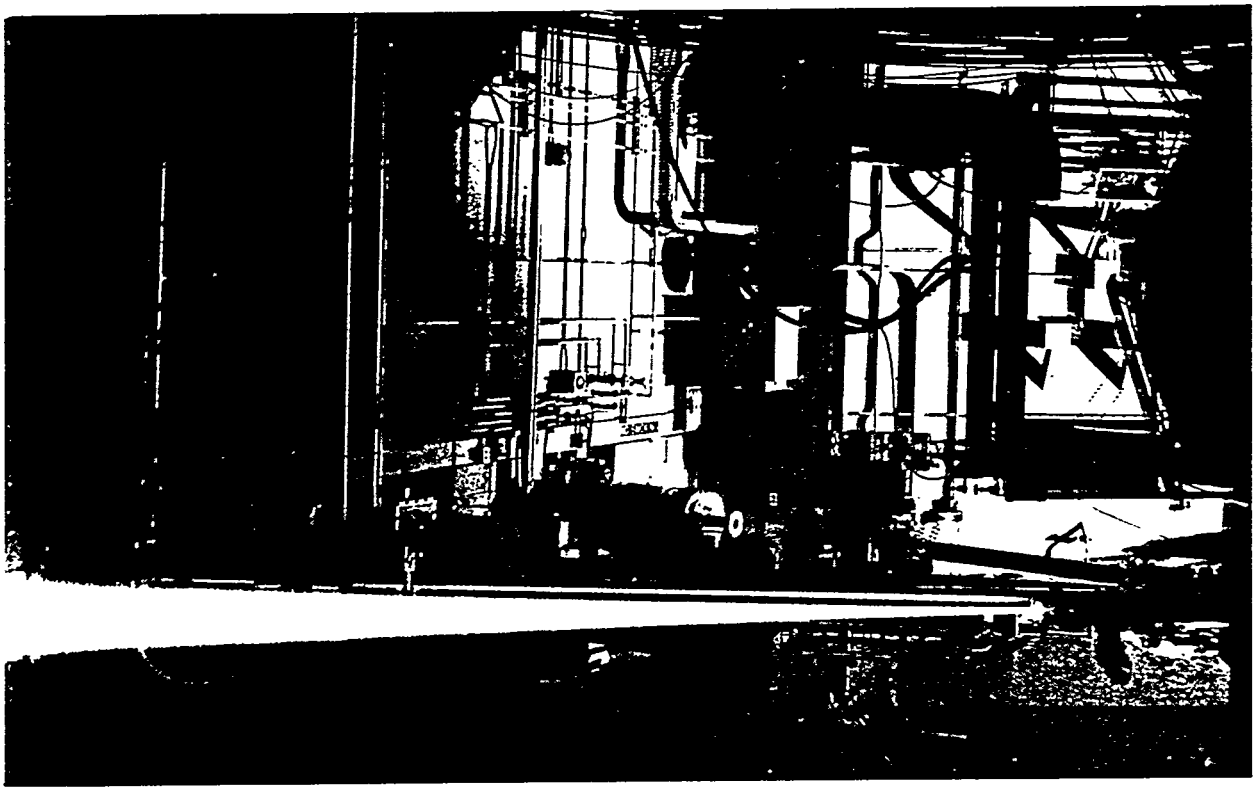

Fig. 9. ORIC Extracted Beam. A 19-ft airglow is produced when an uncollimated 36-Mev deuteron beam from the Oak Ridge Isochronous Cyclotron is temporarily allowed to pass through a 5-mil aluminum foil into the atmosphere. The beam is of excellent quality; the energy spread is less than 200 kev, and the diameter of the beam where it leaves the cyclotron is about 1 in. The total angular divergence is about $\frac{1}{4}°$. The beam pipes in the background transmit the beam from the switching magnet to five target stations in the experiment room beyond the shield wall at the left. After this photograph was made, a 153°, 72-in.-radius inhomogeneous-field ($n = \frac{1}{2}$) magnet was installed to analyze the beam and to direct it back to the right into another heavily shielded room, where additional stations are provided for high-resolution work, including analysis of secondary particles with an Enge-type broad-range spectrograph.

The beam extraction system in ORIC consists of three components, which are readily adjustable during operation. A curved electrostatic deflector, 60° long and with a 70-kv potential across a $\frac{1}{2}$-in. gap, intercepts ions circulating at the outer orbit radius. Still within the cyclotron, these deflected ions pass through two channel magnets designed to reduce the main magnetic field along a narrow path through which the beam of ions can leave the cyclotron. The high efficiency is obtained by carefully shaping and positioning the circulating beam at the outermost orbits so that a very narrow stream of ions enters the deflector, and by precisely positioning the components of the extraction system to minimize any loss of beam along the way.

A novel scheme is used for rather precisely controlling the shape and position of the beam path within the cyclotron. Normally, the beam moves in a very tight spiral path, in which the successive orbits are so closely spaced that a single orbit cannot clear the thin ($\frac{1}{16}$ in.) lip of the deflector. Much of the beam strikes the lip, and a very little spills over into the extraction channel. With the special pole-tip coils in ORIC, a local variation, or "bump," can be introduced into the magnetic field to produce an alternate compaction and spreading of adjacent orbits. By controlling this harmonic motion, or "wobble," in the otherwise closely spaced spiral pattern, it has been found possible to position the circulating beam so that at the moment of widest spacing most of the ions

in a single orbit neatly clear the lip of the deflector. The extractor channel is then adjusted to fit the path of these ions. Since these deflected ions are quite homogeneous in both angular trajectory and energy, the extracted beam is of the exceptionally high quality now so important to the experimenter.

THE SEPARATED-ORBIT CYCLOTRON

Vigorous development work is under way on a new particle accelerator concept, the Separated-Orbit Cyclotron (SOC), which seems ideally suited for the challenging research tasks in the years ahead. There is a growing need to extend the studies of the nucleus of the atom into new frontiers, which can be penetrated only by the use of proton and secondary-particle beams of unprecedented intensity. An intense proton beam with an energy of 800 Mev would be extremely useful for nuclear structure investigations and would also assure the abundant production of mesons. The higher intensity is needed for the study of rare events, for multiparticle correlations, and to achieve improved energy resolution and beam purity. Present considerations are aimed toward a 1- to 5-ma machine. Another possibility, which could prove extremely important, is a superintensity (perhaps 50 ma) accelerator which would generate a high flux of thermal neutrons more intense than is available from any existing or planned reactor. The high-intensity accelerator would also make feasible some otherwise inaccessible experiments, such as scattering of μ mesons, crystal spectroscopy of mesic x rays, and neutrino interactions.

This new accelerator concept incorporates a magnetic guide field of alternating-gradient (AG) magnet elements to confine the accelerating particles to a very narrow spiral path (Fig. 10.) Like a series of lenses, these AG magnets strongly

PHOTO 68148A

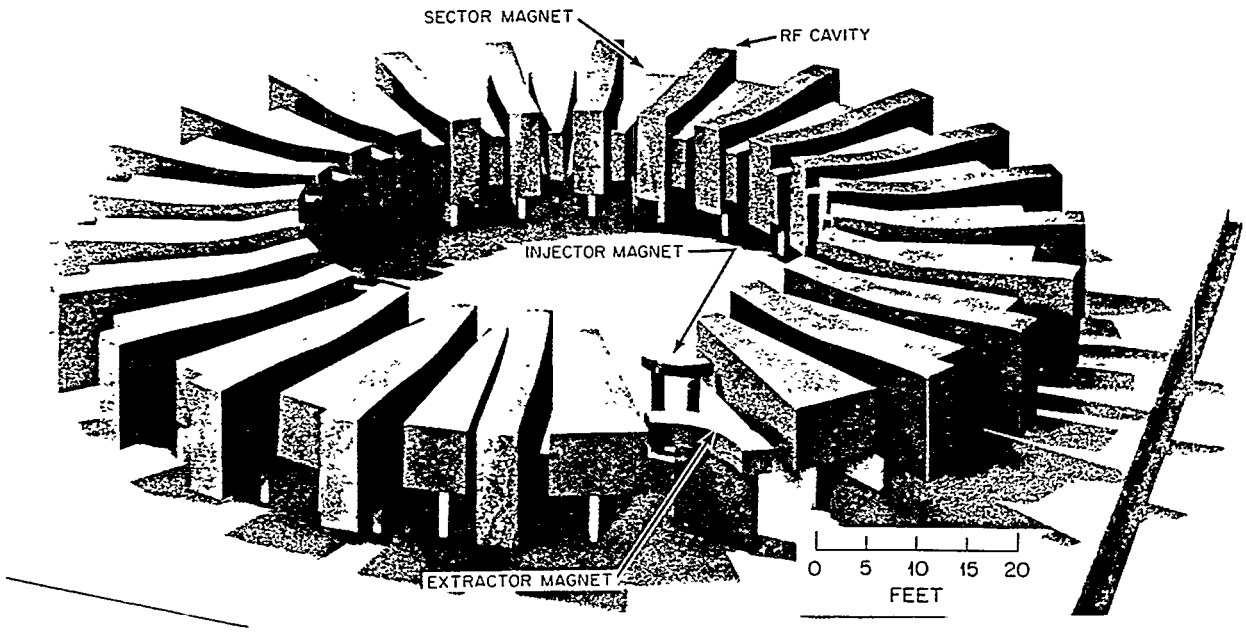

Fig. 10. Conceptual Model of a Proposed 55-ft-radius, 200–800 Mev Separated-Orbit Cyclotron. The 22 wedge-shaped magnets, each with special sets of alternating-gradient pole tips, provide a strong-focusing guide field which defines the path of the proton beam. This very narrow guide field spirals 35 times around, the radius increasing about 5 in. each turn. The large rf cavities placed between the magnets provide the accelerating voltage. They operate at a frequency of 50 Mc, low enough to make use of conventional rf power equipment. A space is left for the insertion of bending magnets for beam injection and extraction. The energy of the extracted beam is varied by intercepting the protons at the appropriate turn with a movable bending magnet. The rf cavities are especially shaped to vary the accelerating voltage with beam radius in such a way as to provide nearly constant turn separation and most efficient use of rf power.

focus the protons so that only a small beam aperture is needed. A large number of rf cavities placed at equal angular intervals between the magnets are driven by an rf source synchronized with the revolution frequency of the particles. From design studies, the protons could gain over 1 Mev of energy every time they circle through each cavity.

The SOC has the advantages of continuous beam, 100% beam extraction, and full-range variable energy. It combines the virtues of the cyclotron (nonpulsed beam, low rf excitation power) and the advantages of the linear accelerator (100% beam extraction, variable energy) while avoiding most of the shortcomings of both.

INSTRUMENTATION AND CONTROLS DEVELOPMENT

The diverse basic and applied programs at the Laboratory require a wide range of increasingly complex, high-performance instrumentation and control systems. A large staff of specialists, of many disciplines, maintains a state-of-the-art capability to provide the needed services at the laboratory and frequently advances the state of the art.

Instrument engineering and design personnel work closely with – often they are members of – research teams, coordinating their specialized knowledge with the experimenter.

National Laboratory Instrument Modules

A significant achievement, in which ORNL played a leading role, was the agreement of the AEC national laboratories to adopt packaging standards for nuclear instruments. Such modules, built to rigid dimensional tolerances and equipped with standardized components and connectors, can be utilized by all participating laboratories in their instrument systems by simply plugging the modules into the instrument racks.

Detailed design and fabrication drawings (designated ORNL series Q-2800) were prepared. A standard bin power supply was designed and one prototype is being tested. Several nuclear research instruments (fast amplifiers, discriminators, etc.), a vacuum-tube amplifier for use with solid-state detectors, and several radiation safety instruments were packaged in conformance with these standards.

Electronic Circuitry

Studies were continued leading to the development of a new generation of nuclear instrumentation that will exploit modern electronic developments and techniques, such as computer techniques, high-speed transistors, tunnel diodes, and integrated circuits. Such instruments will provide increased speed, greater accuracy, better stability, and a highly versatile and interchangeable family of instruments.

Tunnel diodes were used in the design and fabrication of a variety of modular circuitry used in instrumentation for nuclear physics experiments. These modules included fast- and slow-recovery discriminators, fast- and slow-recovery coincidence modules, positive- and negative-output scaler drivers, and a 100-Mc scaler driver. The individual univibrators used in the circuitry and the completed modules were extensively tested to determine the effects of variations in operating temperature, power supply voltages, and input pulse magnitude on resolution, pulse shape, walk, and thresholds.

There has been an increasing need during the last few years for a solid-state electrometer for nuclear instrumentation, since solid-state devices generally require lower operating power, have no heater filaments, are rugged, and are not as sensitive to microphonics as electrometer vacuum tubes.

Three solid-state electrometer current amplifiers were developed: one amplifier has a bipolar transistor in the input stage, the second amplifier has an insulated-gate field-effect transistor in the input stage, and the third is a transistor chopper-type amplifier.

Computer Technology

Without automatic data handling and computation equipment, it would be virtually impossible for scientific investigators to cope with the enormous mass of data generated in modern experiments. At the High Voltage Laboratory a plug-in data center was installed at each of three Van de Graaff

No Number

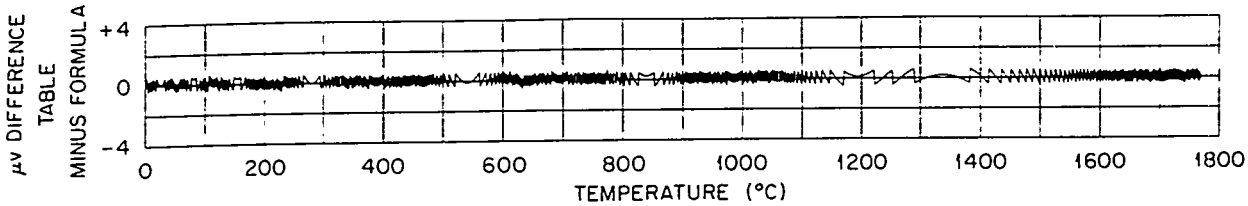

Fig. 11. Comparison of Smoothed Table with NBS Circular 561 Table.

Photo 66223

accelerators to provide a direct link to a CDC 160A computer. Single- and multiparameter pulse-height analyzers will be modified to utilize the computer in experiments. In another experimental program, a computer-controlled x-ray diffractometer system controls the position of the sample and takes and records data by means of internally stored programs, which can be continually updated as the requirements change.

Data Handling Techniques

Data smoothing methods were developed to produce smooth thermocouple emf vs temperature tables which are expressed to a significance of 0.001 μv, and which match the tables in National Bureau of Standards Circular 561 everywhere to within the NBS rounding (1 μv in some cases and 10 μv in others). The results are graphically illustrated in Fig. 11, which compares a smoothed table with the NBS Circular 561 table and shows that the smoothed table splits the rounding pattern of the Circular 561 table almost exactly in two.

Two production-model x-ray scanners for the inspection of HFIR fuel plates were completed. One unit is being used in the production inspection of fuel plates, and the other unit is at ORNL for further studies of fuel plates. In such scanning-type nondestructive test machines, it is desirable to have the test results plotted on a chart in such a manner as to make the chart a map of the object tested, with test results printed in the appropriate places on the map. A multicolor printer (Fig. 12) capable of printing unbroken lines or dots at rates up to 25 per second without making solid contact with the paper was developed. This device is essentially a grouping of air brushes arranged to point at a common spot in space beyond the air exit holes. Each air brush is controlled by a solenoid valve in its air supply line. The printer

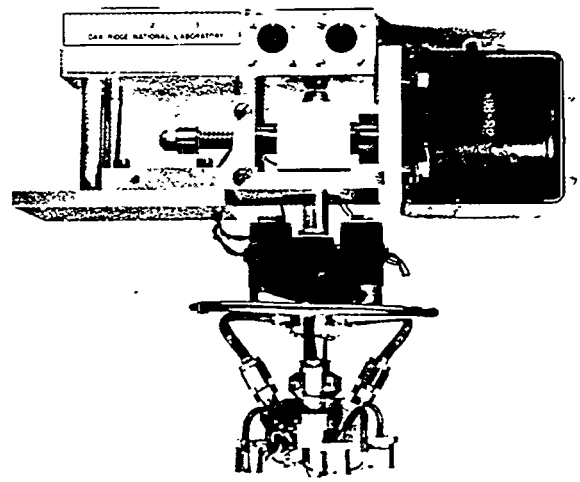

Fig. 12. Four-Color Printer.

and the chart paper are attached to the fixed table of the scanner. The printer scans the paper in the same manner as the detector scans the test piece; the detector output is converted to appropriate signals to control the solenoid valves of the printer.

Temperature Measurement

Thermal emf drift studies on W–5% Re vs W–26% Re and W–3% Re vs W–25% Re thermocouples insulated with high-fired BeO were performed at 1920°C in a tungsten tube furnace using argon gas at slightly above atmospheric pressure. By use of a special constant-power control system, the furnace was held at 1910 to 1920°C throughout two test periods: the first was for 235 hr and the second was for 375 hr. During the total 610-hr period, the temperature indicated by the thermocouples changed less than 1%, as compared with

PHOTO 66034

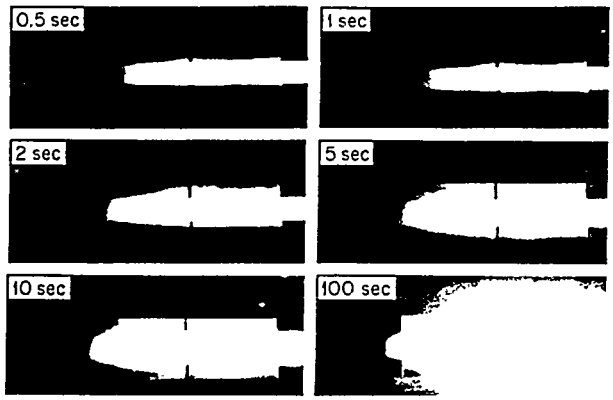

Fig. 13. Infrared Photographs of Internally Heated Radiator Tube, Showing Effect of Exposure.

64-6432

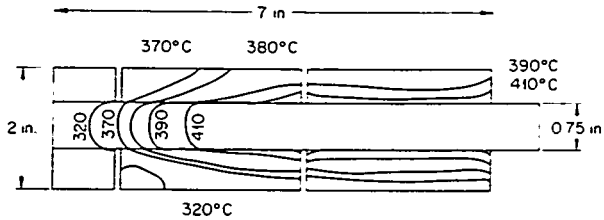

Fig. 14. Isotherms Traced on Radiator Tube Outline with Assigned Temperature Estimated from Contact Thermocouple Readings.

PHOTO 68637

Fig. 15. Infrared Photograph of a Test Rig for the Medium Power Reactor Experiment.

the temperature indicated by an optical pyrometer sighting on a black-body hole.

Platinum resistance-type temperature sensors in approximately ¼-in.-OD stainless steel tubes and ¼-in.-OD sheathed Chromel-P vs Alumel thermocouples were tested for stability at 730°C for a total period of 1800 hr in an air atmosphere. The data indicate that the platinum resistance-type sensor offers no advantage over Chromel-P vs Alumel thermocouples under these conditions.

A resistance-type liquid-metal level element was designed and tested for measuring level changes of up to 48 in. at temperatures to 760°C. Temperature stability of about 1% was demonstrated over the range from 315 to 760°C, using ac excitation for the level element. The thermal emf generated between the level element and the liquid metal was proved to be the limiting factor in the use of simpler dc excitation of the level element. Errors up to 10% were noted with the dc system.

An experimental high-speed infrared film recently developed by the Polaroid Corporation makes possible the rapid qualitative determination of temperature distributions in heat exchangers and other engineering systems at temperatures above approximately 250°C. A method was developed to make use of the new film in determining temperature distributions in an experimental potassium vapor condenser used in a Medium Power Reactor Experiment test rig. Figure 13 shows a series of photographs, taken at various exposures, of a piece of finned condenser tubing which was heated internally by a resistance heating element. Because of the high-contrast character of the film, each photograph shows, effectively, an isotherm corresponding to a temperature in the range present. A series of contact thermocouple measurements was made to assign temperatures to the resulting isotherms. Figure 14 shows the isotherms on an outline drawing of the finned tube. The detail obtainable can be estimated by noting, for example, the slight increase in temperature at the ends of the base of each fin, where there is a reduction in heat conducting area, and the bias toward higher temperatures on the top fin due to convection heating. Figure 15 is an example of an application of the technique to the measurement of temperature distributions in the Medium Power Reactor Experiment test rig. From such

64-6202 A

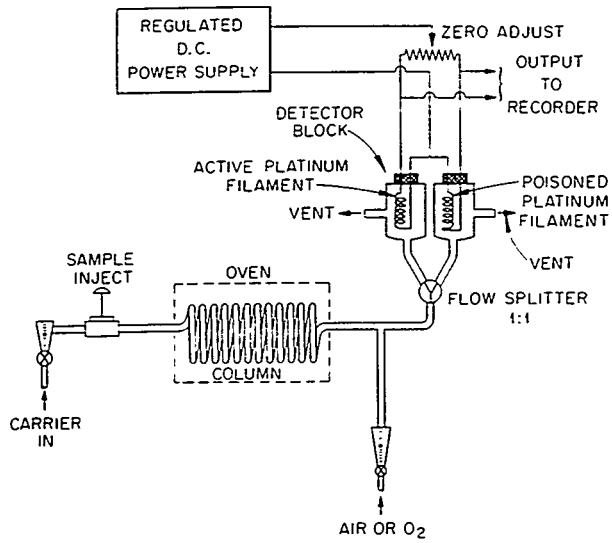

Fig. 16. Compensated Catalytic Detector System.

photographs engineers were able to infer the potassium vapor flow distribution in the tube banks with accuracy greater than could have been attained with 1000 thermocouples.

Gas Chromatography

The widespread use of catalytic combustion detectors for gas chromatography (and general gas analysis) has been seriously limited owing to their sensitivity to extraneous variables. Commonly used catalytic detectors are particularly sensitive to variations in gas thermal conductivity, since they employ an active platinum filament and a reference platinum filament which is sealed in representative samples of the gas to be analyzed. A more desirable method is to expose both filaments to the flowing gas and to poison the reference filament to inhibit catalytic combustion (Fig. 16). Since both filaments are equally affected by gas thermal conductivity, the difference in filament temperature (and resistance) is then only a function of the amount of catalytic combustion occurring on the unpoisoned filament. Many elements and compounds are known to poison platinum, but none in common use has proved to be reliable at temperatures higher than 800°C. Development work in poisoning has shown that a filament poisoned with vanadium pentoxide is stable and reliable at temperatures above 1000°C. Good results have been obtained in measuring the amount of hydrogen in varying amounts of helium and air.

MATHEMATICS AND PROGRAMMING RESEARCH

The Mathematics Division operates and maintains a large computer facility on a custom basis. For this reason, a group within the Division is engaged in making the computer more available to the users, and especially the occasional users, and extending its range of applicability.

A move toward the first goal involves the specification, development, and evaluation of an experimental programming system which would facilitate elementary calculations in a direct-access mode from a remote console. This is designed to give the individual scientist a direct way of solving his medium-sized numerical problems, to give rapid response to needs for computation, and to provide a system that benefits the casual user. This work is in progress.

Among extensions of the range of applicability may be mentioned the use of the computer for library records. A series of computer programs were developed and are in operation for keeping current records of library withdrawal and returns, and a complete book inventory file is on magnetic tape. These computer programs, with only minor modifications, should be effective for many similar uses such as stores, data centers, and the like.

The needs for mathematical research in the Mathematics Division are many and diverse. They are perhaps most obvious in connection with the increasing amounts of numerical computation being done on the computer, where new techniques need to be devised and analyzed and older ones improved. As faster computers are developed, more ambitious computational projects become feasible, but the techniques require critical evaluation with respect to accuracy and overall efficiency. Also, a mathematical approach is proving to be of value in many areas that previously have received only rather crude qualitative treatment.

In the field of numerical analysis, recent results have revealed unexpected power in the so-called "deferred approach to the limit," a method that has already been known for some time and in many guises and is in fact a method of extrapolation. The research staff obtained simple explicit

formulas for a particular application of the deferred approach technique in solving ordinary differential equations. Also, basic results have been obtained that permit the application of a very general type of extrapolation procedure. Other results of a basic nature were obtained in the theory of matrices in numerical analysis.

In planning systems of reactors of several possible types for the production of specified amounts of power over a period of years, it is important to know what mixture of types will be most economical. This leads to a problem in the calculus of variations of a rather unusual form. It was shown that under rather general conditions, at most two distinct types of reactors need to be operated at any one time, and a technique was developed for selecting them.

It has been proposed that the construction of an underground tunnel network may be the most economical and efficient method for providing shelter against nuclear attack in a large city. There are two mathematical problems which arise in the design of such a system. The first involves the placement of the tunnels in the city in such a manner that cost and potential destruction will be minimized. Rectangular grids are studied, since the system must be laid beneath existing streets. The second problem which to date has received the major portion of study is that of dispersing the population to preassigned areas in the shortest time without creation of bottlenecks and other potential forms of traffic delay. A discrete minimization model was studied in which it was assumed that each person moves along a tunnel with uniform speed except for waiting periods at the intersections. Constraints are imposed by requiring that a fixed distance be maintained between moving parties while they are in the tunnel.

CHEMISTRY

ANALYTICAL CHEMISTRY RESEARCH

Analytical Instrumentation

A prototype controlled-potential dc polarograph-voltammeter was designed and constructed in which solid-state instead of vacuum-tube operational amplifiers and power supplies are used. The instrument is to be used with the short-drop-time, vertical-orifice dropping mercury electrodes and with solid working electrodes. The prototype will be used for continued research in polarography and voltammetry and as the basis for the design of several controlled-potential dc polarograph-voltammeters.

To facilitate the evaluation of dc polarographic instrumentation, a number of computer programs have been written, some of which are utilized to solve the Koutecky equation for a value of the diffusion coefficient and provide computer-plotted normalized theoretical curves of a simple, reversible diffusion-controlled process for the regular polarographic wave and for the first-, second-, and third-derivative waves.

Two high-sensitivity coulometric titrators have been fabricated and installed, one in the High-Radiation-Level Analytical Laboratory and the other in the High-Level Alpha Radiation Laboratory. A checkout and test procedure and a troubleshooting guide were prepared for this instrument. About 25 complete sets of engineering drawings for the titrator were sent to interested persons in the United States and abroad.

A safety circuit for an expensive ($600) multiplier phototube of the ORNL model VII flame spectrophotometer was designed and installed. The circuit has already provided automatic shutdown that saved the phototube on two separate occasions.

A study of the significance of the placement of the reference electrode in controlled-potential coulometry was continued with the Bi^{3+}-UO_2^{2+} system. There was no evidence that variation in placement of the reference electrode, even under drastic cell conditions, causes the voltage that drives the electrochemical reaction to exceed the command voltage set into the potentiostat.

X-Ray and Spectrochemical Analyses

The analysis of powdered solids was investigated by the x-ray absorption-edge method with a rotating sample holder. Disposable one-piece polystyrene cells were fabricated for use in the analysis of radioactive solutions by the same method. Computer codes were written for determining the height of an x-ray absorption edge by extrapolation and for analyzing multicomponent alloys by x-ray fluorescence. Ruthenium and selenium were determined at the 0.5-μg/ml level by atomic absorption with an air-hydrogen flame and an end-fed absorption tube. A procedure was also developed for separating traces of barium from the alkali metals, alkaline-earth elements, and other elements by coprecipitation on lead chromate. The barium is subsequently determined by flame photometry.

Mass Spectrometry

A new double-magnetic-deflection mass spectrometer was put into service in a laboratory arranged for the containment of alpha radioactivity (Fig. 1). Ion detection is by secondary electron multiplier, and pulse counting is used instead of current measurement. Only 1 to 2 ng of sample is required; rare isotopes in concentration as low as 1 ppm can be measured.

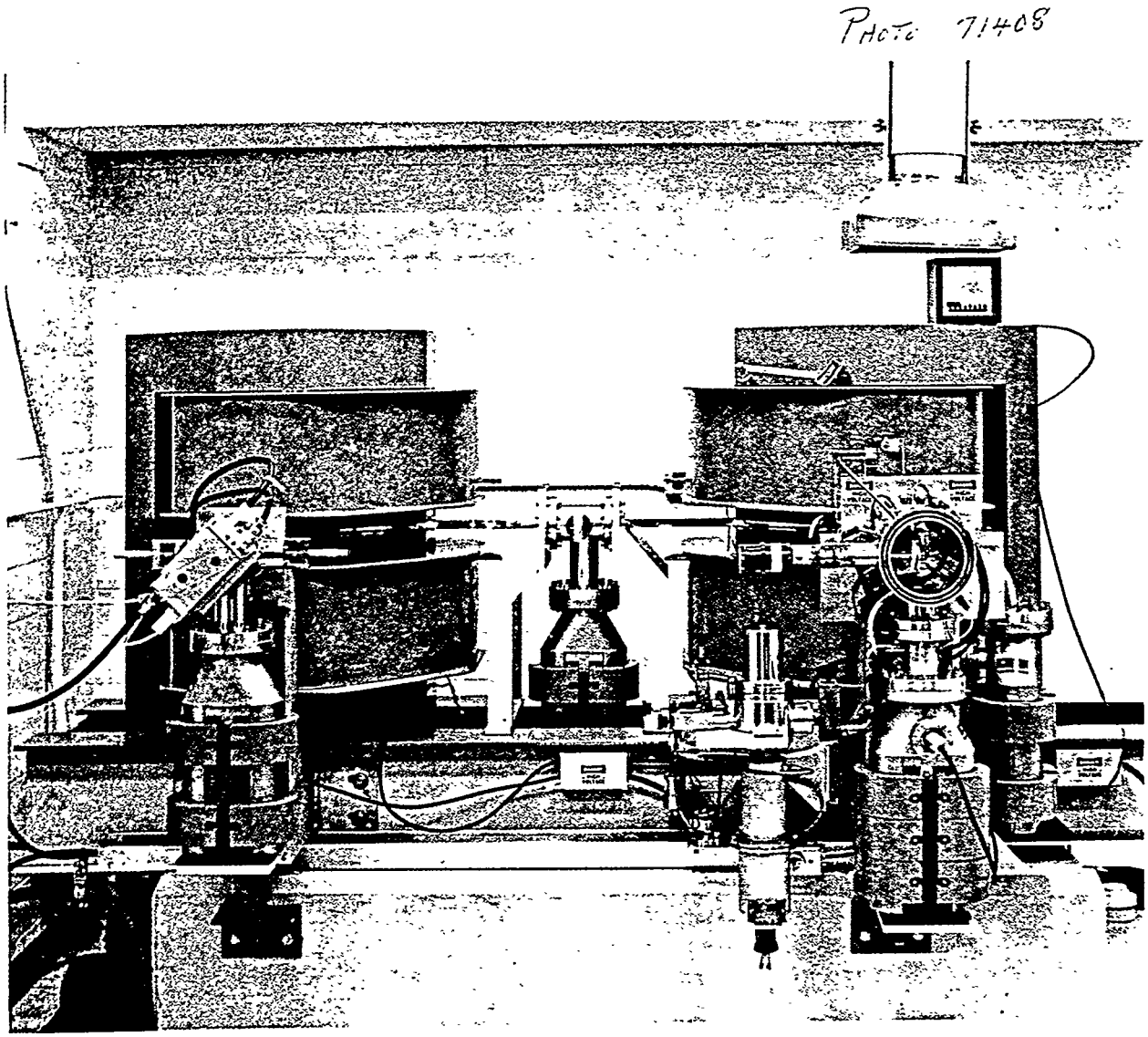

Fig. 1. TRU Mass Spectrometer in Alpha-Containment Laboratory.

Isotopic Composition of Atmospheric Neon

The published results of several mass spectrometric determinations of the isotopic composition of atmospheric neon are not in good agreement. The ready availability of ^{20}Ne and ^{22}Ne of high isotopic and chemical purity and in adequate quantity makes "calibrated" measurement of the isotopic composition possible by correcting for bias in the mass spectrometer. Several standards were carefully prepared from the separated isotopes, and the bias was determined. The results of the analysis for six samples of neon obtained from commercial suppliers agreed with each other. The agreement indicates either that no fractionation occurred in the preparation of the samples or that the same degree of fractionation occurred in different plants. Results obtained thus far indicate

that the isotopic composition (in atomic percent) of atmospheric neon is: ^{20}Ne, 90.514 ± 0.031; ^{21}Ne, 0.266 ± 0.005; ^{22}Ne, 9.220 ± 0.029. The calculated atomic weight is 20.1794 ± 0.0018; this value can be compared with the accepted value of 20.183, a figure that is based on measurements of gas density.

Optical and Electron Microscopy

A new Philips EM 200 electron microscope was installed; resolution of the order of 6 A or better has been achieved with this instrument. In addition, a facility has been placed in operation for the examination of ultramicrostructures of radioactive materials by electron microscopy. An electron microscopical study was made of the effect of cationic surfactants on the structure of thoria sol-gel beads. Vapor-deposited thin metallic films were made for the Physics Division to be used in their semiconductor experiments. In connection with the Nuclear Safety Program, studies have been made of particulates from simulated fallout experiments.

Special Research and Development Problems

Studies with 10 *M* LiCl solutions have revealed that the free-acid concentration of such solutions can be determined in the presence of hydrolyzable cations by direct titration without having to resort to the addition of complexing agents. When several hydrolyzable cations are present, these cations can be differentiated by titration provided there is a sufficient difference in their solubility products. Although not particularly precise, the titration is, nevertheless, useful as a rapid semiquantitative method.

The investigation of solid indicator electrodes made of pyrolytic graphite and "glassy" carbon was continued in order to establish the applicability and limitations of these electrodes. These studies included differential potentiometry, particularly for hot-cell operation, voltammetry, amperometry, and chronopotentiometry.

An apparatus based on the use of flame ionization detection was developed to measure the total concentration of organic contaminants in the atmosphere surrounding reactor fuel burnup test assemblies. Hydrocarbon concentrations equivalent to 5 ppb of methane in air can be detected. An instrument was assembled in a portable cabinet for making measurements at various locations. Subsequent investigations revealed that aerosols generated by a dispersion of oxides of uranium interfered with the hydrocarbon determination.

Modifications were made to the apparatus for the determination of oxygen, carbon, and hydrogen in alkali metals. Some of these modifications are dictated by the necessity for determining the concentration of both oxygen and hydrogen on the same sample.

A microtitration cell that does not require an internal electrode was fabricated of pyrolytic graphite for making potentiometric titrations of highly radioactive solutions. Both redox and acid-base potentiometric titrations can be carried out with a high degree of precision on microliter volumes of solutions with this cell.

Analytical Biochemistry

A new program was initiated to establish a biochemistry group in the Analytical Chemistry Division. Assistance is being provided to the Biology and Chemical Technology Divisions in their project on the recovery and separation of the transfer ribonucleic acids (t-RNA's) from *Escherichia coli* bacteria. Since an inordinately large number of assays are required to determine the efficiency of the solvent-extraction process used to separate the t-RNA's, initial efforts are concerned with modifying the procedures to reduce the overall time required to make an analysis. The precision of alternative methods of rapidly adding reagents by means of various automatic repetitive pipetting techniques is being studied.

EFFECTS OF RADIATION ON ANALYTICAL METHODS

The study of the effect of ^{60}Co gamma radiation on the reaction of nickel with dimethylglyoxime was completed. A postirradiation effect on the nickel-dimethylglyoxime complex was noted in

65-658A

that the color of the complex returns after the sample is removed from the source of radiation. The radiation damage to the colored complex is apparently due to the reduction of the nickel(III) in the complex. A detailed study of the effect of gamma radiation on the determination of uranium(VI) in phosphoric acid solutions of uranium(IV) oxide was completed. Errors due to radiation can be minimized by excluding oxygen from the solutions and by maintaining the uranium concentration as low as possible. Studies of the effect of gamma radiation on hydrochloric, sulfuric, phosphoric, and acetic acid solutions of arsenazo III (a colorimetric reagent) were also completed, while similar studies of 2-thenoyltrifluoroacetone were initiated.

Studies were also initiated on the radiolysis of chloride solutions of high concentration. Free chlorine is not produced at chloride concentrations below 1 *M*, while organic solvents such as methanol are effective in eliminating chlorine produced by radiolysis in high chloride concentrations.

LOW-COST RADIOCHEMICAL ANALYSES BY GAMMA-RAY SPECTRUM RESOLUTION

In many circumstances it is necessary to know how much of each of several radioactive nuclides is contained in a sample of gas, liquid, or solid. Such occasions arise, for example, in connection with safe handling or disposal of radioactive wastes, in determination of the nature of radioactive fallout, and during the performance of many different types of scientific experiments. Since these analyses can be expensive and time consuming, rapid and inexpensive alternative analyses are being sought. The desired speed and cost reduction of these analyses have been achieved for solutions or mixtures of materials containing radioactive isotopes that emit gamma rays.

Each gamma emitter has its characteristic gamma-ray spectrum, whose intensity is proportional to the amount of the element present (Fig. 2). If two or more gamma emitters are present, relatively expensive chemical separations of these radioactive materials from each other might have to be performed before the amount of each can be determined, unless their characteristic spectra are quite different.

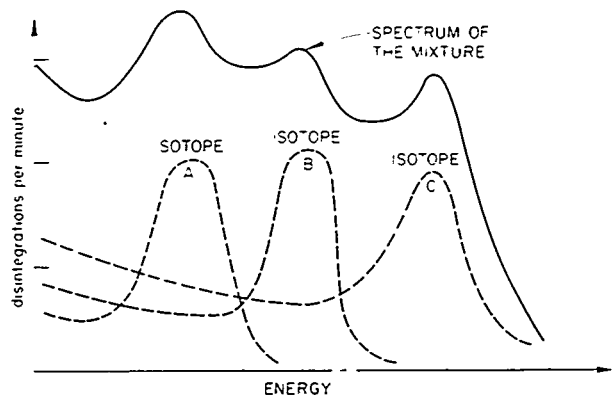

Fig. 2. Gamma-Ray Spectrum of the Individual Components *A*, *B*, and *C* and the Composite Spectrum of the Mixture Whose Proportions Are Unknown.

By combining the modern gamma-ray spectrometer with the modern high-speed computer, the cost of an analysis has been reduced to perhaps 10% of its former value and the time between taking a sample and getting an analysis has been reduced to less than one day. Correspondingly, the capacity of existing equipment has been greatly increased.

To accomplish these savings in time and money, standard samples (i.e., samples containing a known amount of radioactivity) are prepared for each of the isotopes present in the mixture. (These standards actually become part of a reference "library" available for the analysis of all other samples.) The radioactivity of these standards and of the experimental samples is then counted separately with a multichannel gamma-ray spectrometer. All these spectrometer measurements are then put on magnetic tape for processing by a high-speed digital computer.

Data processing involves an "unscrambling" operation whereby the computer calculates the amount of each radioactive material in the test sample by comparison with the standard. This "unscrambling," or computation, is achieved by the method of least squares. The computer (an IBM 7090 or CDC 1604) estimates the probable error in each calculated answer and can perform the whole operation for mixtures of as many as ten isotopes in only a few seconds.

The method has been tested on several thousand samples with excellent results, even when the

amount of an isotope is so small that it meets Federal specifications for direct discharge to the environs (in the range of 10^{-9} curie per gallon of water).

MECHANISM OF RADIATION CORROSION OF ZIRCONIUM ALLOYS

Reactor radiations are known to accelerate the rate of corrosion of zirconium alloys in water or aqueous solutions under oxygen atmospheres at elevated temperatures; these conditions and materials are frequently employed in nuclear reactors. The mechanisms of this radiation corrosion are being explored by comparing the behavior of fast-neutron-irradiated specimens with that of unirradiated controls. Recent studies have confirmed earlier indications that changes produced within the alloy during neutron irradiation lead to acceleration of corrosion. These changes occur only when an appreciable amount of oxygen is dissolved in the metal,[1] and the extent of the effect of irradiation on corrosion increases with increasing amounts of dissolved oxygen. On the other hand, direct neutron irradiation of the oxide film does not affect its protective properties.

Studies of the growth of anodic films on zirconium in oxygenated dilute H_2SO_4 at temperatures from 200 to 284°C have tested the relationship

$$i = 2A \sinh BE ,$$

in which i is the film growth current, B is a field coefficient, and E is the electric field across the oxide film. We found that B increases with temperature, contrary to theory, which predicts $B = qa/kT$, where q is the charge on the mobile ion and a is the activation distance. This discrepancy was explained by applying a local field concept in which the dielectric behavior and dielectric constant, ϵ, of the oxide were included. Use of the Lorentz field, $[(\epsilon + 2)/3](V/X)$, led to more reasonable agreement with theory than use of the simple Maxwell field, V/X. Thus it appears that a field-dependent movement of ions across the oxide film is an important step in the corrosion process.

[1]Oxygen is very soluble in zirconium and some of its alloys, and it is known that oxygen dissolves in the metal during corrosion at elevated temperatures.

CHEMICAL ENGINEERING RESEARCH

Prediction of the Flow Capacity of Pulsed Columns

To obtain a good separation of a mixture of dissolved substances by solvent extraction, it is ordinarily necessary to repeatedly mix and separate the two liquid solutions (usually aqueous and organic) as they flow countercurrent to each other. This is done efficiently in a piece of equipment called a pulsed column (Fig. 3). Pulsed columns have been widely used as equipment for solvent extraction processes for recovery and purification of metals in feed materials plants, for processing of nuclear fuel, and for separation of various other materials such as fission product and transuranium elements. In order to design pulsed columns for a particular process it is necessary to predict the liquid flow capacity. We have collected some 2300 measurements, representing 23 different chemical systems, reported in the literature by about 50 investigators. The data (1100 points) from one type of pulsed column have been correlated using 13 variables which describe column geometry, pulse variation, and physical properties of the chemical systems. The resulting correlation, which is a complex equation, has been successfully used to calculate the flow capacity for other types of column and modes of operation. The correlation makes it possible to design new columns or applications to new processes with a saving in experimental work to prove the design.

Effect of Ionizing Radiation on Coalescence Rates in Liquid-Liquid Systems

The rate of coalescence of a liquid after being dispersed in another liquid with which it is immiscible is often of crucial importance in the design and operation of solvent extraction equipment. We are studying how coalescence is affected by ionizing radiation, which is always present during radiochemical processing. In these tests the organic phases consisted of very pure hydrocarbons, and the aqueous phases were solutions of uranyl nitrate and lithium nitrate. The average time required for single drops of the aqueous phase to coalesce with a plane interface was measured under a variety of conditions, including neutron

65-734A

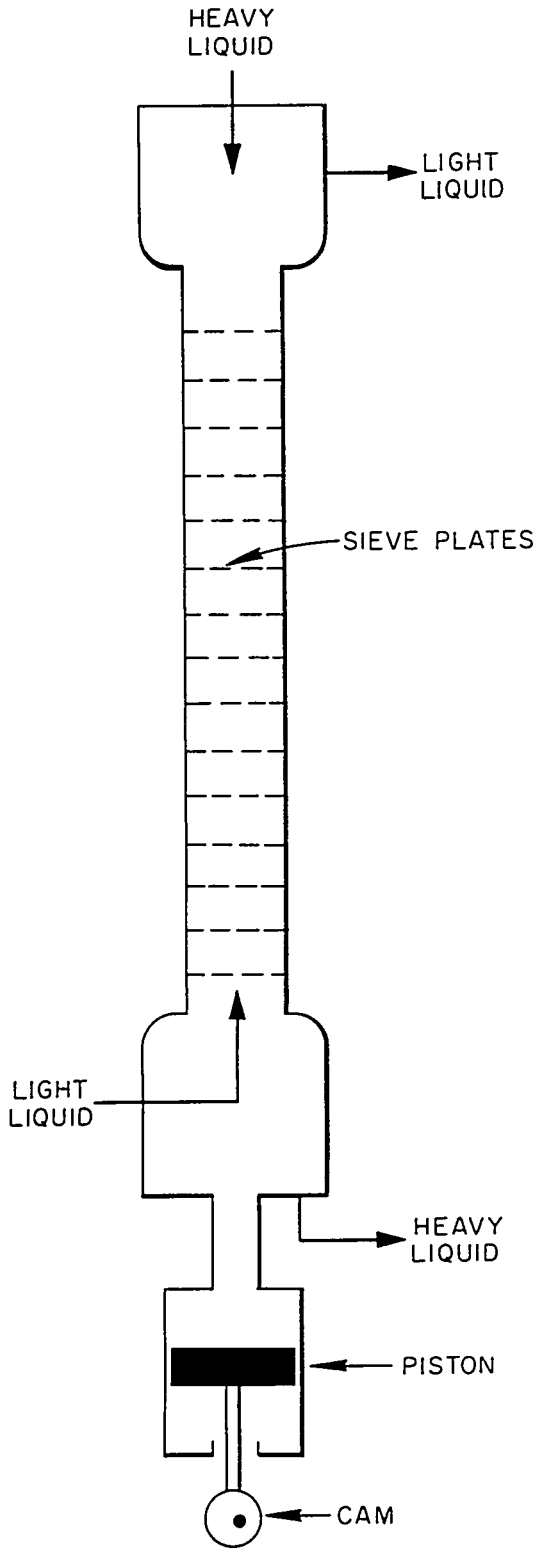

Fig. 3. Pulsed Column for Solvent Extraction. A pulsed column is essentially a piece of pipe mounted in a vertical position. The pipe is usually filled with heavy liquid, which enters at the top and flows out the bottom. The light liquid enters at the bottom, flows countercurrent to the heavy liquid, and overflows at the top. The liquids are mixed in the column by the reciprocating action of the pulser (piston driven by cam), which causes the light liquid to be broken up into small drops as it is forced through small holes in sieve plates spaced throughout the column.

irradiation, which produced either alpha particles (from ^{6}Li) or fission fragments (from ^{235}U) in the solution. In no case were harmful effects observed. Under some conditions, the heavily ionizing alpha particles and fission fragments were found to be beneficial; that is, they increased the rate of coalescence.

The mechanism postulated to explain the beneficial effect is as follows: An ionizing particle traveling in the vicinity of the liquid-liquid interface leaves a track of free radicals among the molecular debris in its wake. Some of these free radicals diffuse to the interface and combine with molecules of the other liquid. The products of this combination are powerful surface-active agents, which reduce the interfacial tension momentarily in the vicinity of the track. This region of reduced interfacial tension acts as a weak spot in the hydrocarbon membrane between the aqueous drop and the plane interface. The membrane can tear at this point, starting the coalescence.

SEPARATIONS PROCESS DEVELOPMENT

New Solvent Extraction Separations

Solvent extraction provides a separation method of great versatility through a virtually unlimited choice of different organic extraction reagents.

Present applications in the atomic energy field include recovery of uranium and thorium from ores, purification of uranium and thorium for use as fuel in reactors, and recovery of uranium, thorium, and plutonium from the used fuels. New applications that have recently been developed at ORNL include (1) integrated extractions to recover and separate fission product strontium and rare earths with a dialkylphosphoric acid and cesium with a substituted phenol; (2) separation of transplutonium actinide elements created in reactors from the accompanying fission product rare earths, either by extraction of the actinides with tertiary alkyl amines, R_3N, or by extraction of the rare earths with dialkylphosphoric acid, leaving the actinides held in aqueous solution by other reagents; (3) recovery of high-purity cesium (and rubidium) from ore leach solutions by extraction with a substituted phenol, to help satisfy the large expected demand for cesium in the 1970's for ion rocket propulsion and power generation systems; (4) recovery of beryllium from leaches of the low-grade domestic beryllium ores by extraction with a primary amine, RNH_2; (5) recovery of sulfuric acid from waste streams (also aiding subsequent disposal of the waste) and purification of crude phosphoric acid by extraction with tertiary amines.

Thorium Recovery from Granitic Rock

Since the long-range production of nuclear power will inevitably require development of very low-grade ores, a continuing interest has been maintained in the supply and cost of uranium and thorium from these sources. Recently, a cooperative survey was made by ORNL and Rice University of the Conway granites in the White Mountains of New Hampshire (Fig. 4). These materials have been found to contain about 55 ppm of thorium and 15 ppm of uranium, as compared with "average" granites in the earth's crust, which contain about 12 and 3 ppm of thorium and uranium respectively. Field and laboratory studies show that the Conway granites contain at least 20,000,000 tons of thorium and 5,000,000 tons of uranium which can be recovered at an average cost of less than $50 per pound of combined thorium-uranium product. A significant portion would be obtainable for less than $35 per pound. This single formation has provided a hundredfold increase in the known resources of moderate-cost thorium within the United States and constitutes an important fuel reserve for a future nuclear power economy.

Separation of Transfer Ribonucleic Acids

According to the present explanation of protein synthesis in living cells, each of the amino acids that make up the protein must first be bound to a specific molecule of transfer ribonucleic acid (t-RNA), which escorts it to the ribosome, the site of protein synthesis. Information coded in the t-RNA, in the form of physical structure, chemical composition, or both, is recognized at the ribosome, resulting in very precise control of the amino acid sequence of the growing protein chain. The details of these steps in protein synthesis are not well known, and further information is essential to provide knowledge of how human cells grow and function. The biochemical and physicochemical investigations have been hampered by the lack of methods for separating and purifying the individual t-RNA's in significant quantity.

In a program designed to fill this need, t-RNA's are being separated by extraction chromatography. Considerable separation has been achieved, and, in particular, several milligrams of the t-RNA for phenylalanine was obtained in a high degree of purity for the first time. Further development of this method is yielding larger quantities of purified t-RNA's, which are being made available for biochemical experiments.

Mixed t-RNA's were recovered from *Escherichia coli* bacteria. The individual t-RNA's were then separated on an extraction chromatography column constructed of a liquid ion exchange solvent, dimethyldilaurylammonium chloride, supported, in the form of a thin film, on inert particles. An aqueous solution flowed down the column, and the t-RNA's were separated as they began to move down the column under the influence of an increasing concentration of sodium chloride in the flowing aqueous phase. Sixteen specific t-RNA's were identified in the aqueous stream leaving the column. The last fraction to leave the column was about 4 mg of at least 60% pure phenylalanine-accepting t-RNA, representing at least 50% of the phenylalanine-accepting t-RNA obtained from the original bacteria.

65-736

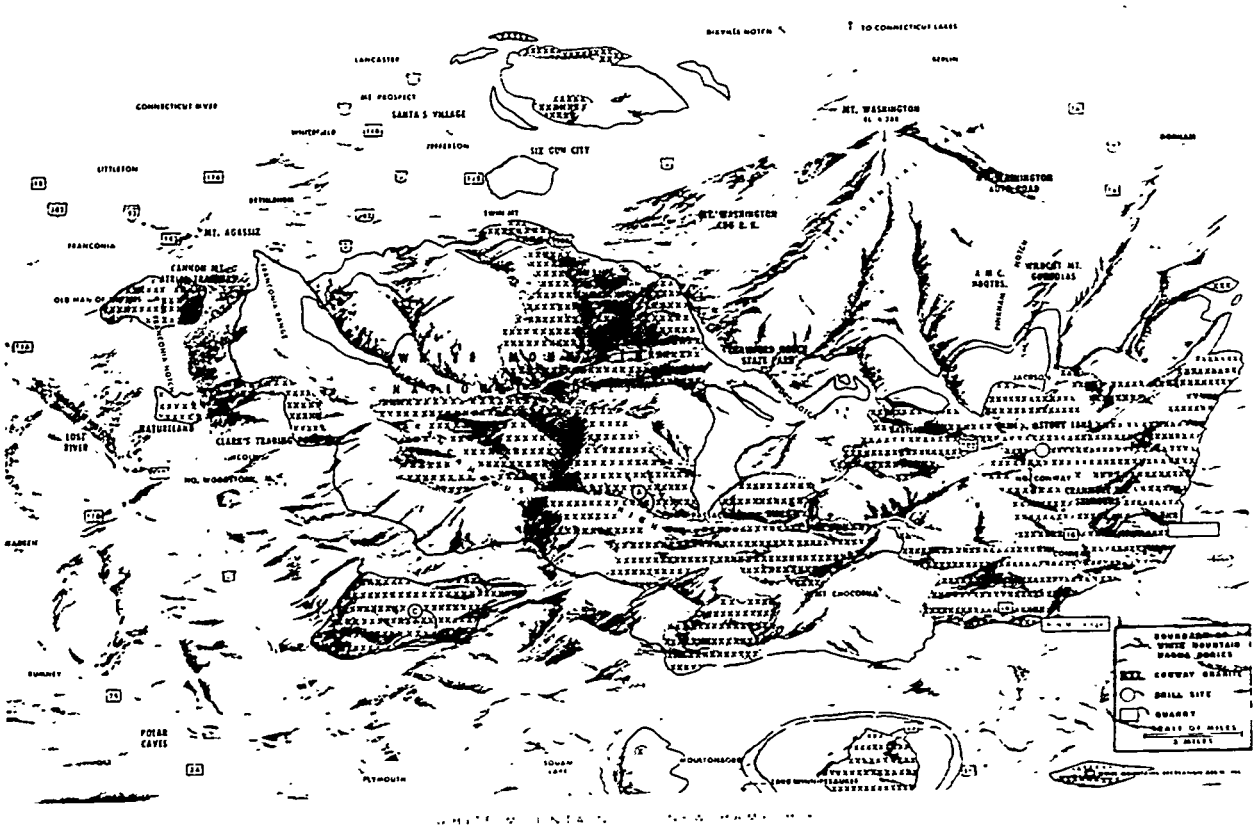

Fig. 4. Conway Granites. The crossed areas outline over 300 square miles of the White Mountains in New Hampshire that are underlain by Conway granite. Hundreds of outcrop samples were obtained throughout this area, and three drill-core samples to 1000 ft depth were obtained at sites labeled *A*, *B*, and *C*. Studies of these samples showed that there are at least 35,000,000 tons of thorium and 8,000,000 tons of uranium in the ground at depths less than 1000 ft, and that about two-thirds of this can be recovered at moderate cost. The tonnages could be increased by going to greater depths.

Waste Streams from Plants Processing Uranium Ores

Mills processing uranium ores produce large volumes of aqueous wastes containing ^{226}Ra in trace amounts but still of sufficient quantity to create a public health hazard if expelled directly to the surrounding environment. The handling of these wastes poses a special problem in areas where sufficient land is either unavailable or too expensive for permanent impoundment of the large volumes. Recent studies have shown, however, that the radium can be removed efficiently from the waste solutions by adsorption on natural minerals such as barytes and clinoptilolite or on synthetic zeolites similar to those used in water-softening plants. The radium from large volumes of solution can be accumulated on a small volume of solids, which can be safely and conveniently stored.

FUNDAMENTAL PRINCIPLES OF SOLVENT EXTRACTION

One important factor in the increasing value of solvent extraction as a separation method is the continuing progress in understanding its mechanisms and in measuring and correlating such quantities as activity coefficients, which are

needed in fundamental calculations. Investigations of this kind improve the usefulness of solvent extraction as a research tool as well as its usefulness for analytical and process separations. Recent advances include the following:

1. Identification of the complex compounds present and their interactions in extraction of sodium and strontium by a dialkylphosphoric acid and in extraction of cesium and rubidium by a substituted phenol.
2. Evaluation of activity coefficients of extraction reagents and of other solutes in the organic solutions.
3. Progress in control of the degradation of extractants that results from their exposure to radiation or to reactive chemicals during use. Usefully stable commercial diluents were identified (e.g., diethylbenzene), and methods were developed to improve other commercial diluents (special kerosenes) by purification before use or by removal of degradation products before recycle. The chemistry of degradation by nitric acid, with and without irradiation, was elucidated, and the principal degradation products from several diluents (both aliphatic and aromatic) were isolated and identified.
4. Use of solvent extraction equilibria to identify complex compounds in aqueous solutions (e.g., sulfate complexes of uranium and thorium) and determine their stability constants, and to determine the activity coefficients of acids in aqueous solutions.
5. Identification of the actual chemical forms in which metal ions are extracted, by measuring rates of transfer of particular substances (uranyl ion and radiotracer-tagged sulfate ion) to and from amine sulfate solutions.
6. Determination of rate constants in an unusually slow extraction (ferric ion extracted by dialkylphosphoric acid) of a type potentially useful for special separations between slow- and fast-transferring ions.

PREPARATION AND PROPERTIES OF ACTINIDE-ELEMENT OXIDES

In the sol-gel process for making strong, dense, large particles of thorium and uranium oxides to be used in reactor fuels, the oxides must first be dispersed to very fine colloidal particles if they are to behave properly in subsequent processing.[2] The size and shape of these fine colloidal particles control many of the handling and flow properties and the ultimate physical properties of the nuclear fuel oxide particles. We have been attempting to ascertain what basic characteristics of the dispersed colloidal particles lead to good nuclear fuel oxide particles. It was shown that undesirable stringy, noncrystalline colloidal particles of thorium oxide, which result from cold precipitation of a soluble thorium salt with alkali, spontaneously convert to the desirable crystalline form if allowed to age for several months at room temperature. It was also shown that colloidal particles of crystalline thorium dioxide, made by heating the oxide no hotter than about 850°C before suspending it in dilute acid, are predominantly single crystals, which are compact and roughly symmetrical. They are neither platelike nor stringy, despite the ability of these suspensions to show exaggerated thixotropy, like that of the no-drip paints. However, these colloidal particles appear capable of sticking together weakly to form agglomerates that are stringy, and it is these very unsymmetrical agglomerates that directly underlie much of the troublesome, complex, and sensitive flow behaviors observed for these suspensions, rather than the fundamental, compact colloidal particle itself (Fig. 5).

The fundamental colloidal particles that result if the thorium oxide is heated much above 850°C are no longer mainly single crystals, however; as the temperature increases, the colloidal particles consist of increasing numbers of crystals stuck together tightly in irregular shapes. These large, tightly bonded multicrystal colloidal particles are undesirable for producing the highest-density nuclear fuel oxide particles at low (about 1150°C) calcining temperatures.

PROTACTINIUM CHEMISTRY

We are studying the chemical behavior of protactinium in aqueous solutions of sulfuric acid and

[2]In this section, the finely dispersed particles in the hydrosol stage of the process are called "colloidal particles," whereas the final product of the sol-gel process after calcination is called "nuclear fuel oxide particles."

No NUMBER

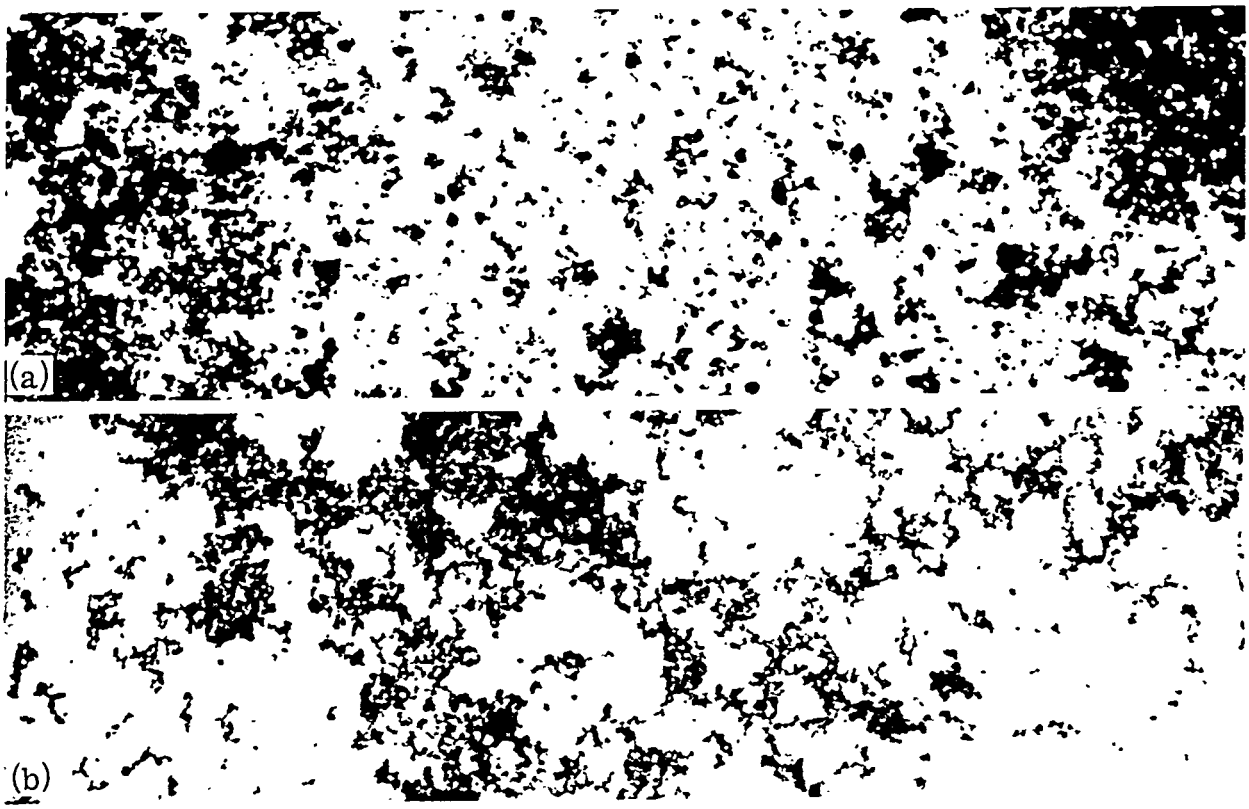

Fig. 5. Colloidal Particles of Thorium Dioxide. (*a*) These colloidal particles are small, nearly uniform in size, and roughly symmetrical. The weak multiparticle agglomerates which are also seen are themselves fairly compact and small. Thorium dioxide sols of these kinds of colloidal particles and agglomerates flow and handle well in processing and will make high-density nuclear fuel oxide particles at the relatively low calcination temperature of 1150°C. (*b*) These colloidal particles are small, nearly uniform in size, and roughly symmetrical. However, the weak multiparticle agglomerates are long and stringy and are capable of causing troublesome flow behavior of the sol, such as getting thick if it is allowed to stand very long in pipes and tanks. Some common causes of this stringy agglomeration are using too little or too much acid to disperse the colloidal particles, or some contaminating surface-active chemicals in the sol. (*c*) These colloidal particles were made from a sample preheated to near the upper limit (850°C) of temperature that will allow making nearly completely dense nuclear fuel oxide particles at a low final calcination temperature. Not only are the fundamental colloidal particles rather large, but a few of the largest of them consist of several crystals stuck together tightly. When such tightly bonded multicrystal colloidal particles begin to predominate in the sol, the nuclear fuel oxide particles will be less strong and less dense unless the final calcination temperature is raised.

hydrochloric acid. Protactinium is an intermediate in the thorium fuel cycle, and an understanding of its chemistry is important in the chemical processing of thorium-base fuels. One of the most troublesome characteristics of protactinium is its reaction with water, forming complex hydrolysis products of uncertain composition, low solubility, and properties that change continually over long periods of time. In addition, limited availability and high levels of alpha radiation have hampered previous studies of protactinium, with the result that the previously existing information was incomplete and often inconsistent.

In concentrated sulfuric acid (18 *M*), the solubility of protactinium is 0.15 g/liter; the solubility increases rapidly as the concentration of sulfuric acid is decreased below 10 *M*. Saturated solutions contain several grams per liter at sulfuric acid concentrations of 2 to 5 *M*. At lower acid concentrations the results are not reproducible, probably because the protactinium is hydrolyzed.

Solvent extraction is being used to study the nature of the complex ions of protactinium that form in sulfuric acid solution. Extraction by amines increases rapidly as the sulfuric acid concentration decreases from 8 to 2 *M*. The concentration of protactinium in solution has an extraordinarily strong influence on its extractability. This has been interpreted to indicate the existence of polymers of protactinium.

IRRADIATION EFFECTS ON GAS-SOLID SYSTEMS

The effects of radiation on matter are of continuing interest, both because a study of such effects sheds light on the basic nature of matter and because such effects are potentially of practical utility. We are investigating the interaction of radiation with systems where gases are adsorbed on the surfaces of solids. In general, the systems involve the chemical reaction of gases in contact with solid catalysts. Irradiation with beta particles was found to affect the catalytic properties of powders of uranium dioxide, zinc oxide, and silica gel, whereas it did not affect the activity of silica-alumina, chromia-alumina, and pure alumina powders. The test reaction used was the decomposition of formic acid (HCOOH), chosen as a model because of the ease with which the decomposition reaction can be followed analytically. Formic acid can decompose to yield either hydrogen and carbon dioxide or carbon monoxide and water. With different catalysts present, the reaction may follow either decomposition mode predominantly. Experimentally, the effect of irradiation was to bring about a temporary increase in the rate of the minor mode of reaction in the cases where irradiation produced a recognizable effect. Apparently not only can the catalytic activity of solids be altered by radiation but also the products of the reaction can be changed. This observation is interesting from the standpoint of increasing our fundamental understanding of catalysts and the effects of radiation on solids. It is also important to the development of possible industrial applications of catalysts under radiation.

Another system studied was the radiation-induced decomposition of water adsorbed on silica gel. The results indicate that there is a transfer of energy from the irradiated gel to the adsorbed water in a way similar to that previously observed with several other systems by workers at Brookhaven National Laboratory. Further study of this system may lead to an explanation of the energy transfer mechanism. Exploitation of such transfers could have application in chemonuclear reactors, where the objective is the direct use of the energy produced by fission in reactor fuels to bring about desired chemical reactions.

SURFACE CHEMISTRY

Thorium oxide is a material of great importance in the development of nuclear reactors, especially those reactors designed to accomplish breeding by means of the thorium cycle. The behavior of thorium oxide in response to environmental factors, such as the humidity of the air, is therefore important fundamental knowledge. Like most ceramic oxides, thorium oxide adsorbs water on its surface by both chemical and physical processes. We are determining how the amount of water adsorbed by each of these processes is influenced by factors such as temperature, the partial pressure of water vapor, the size of the thoria crystals, the size of the thoria particles, the number and sizes of microscopic pores in the particles, and the surface area of the particles.

We are also determining the amount of heat released and the rate of release, as dry thoria surfaces become wetted. Knowledge of the heat energy involved provides additional understanding of the wetting process.

Significant observations to be added to those previously reported are as follows. The surface area of the thoria decreases as water molecules are added to the surface. The surface of thoria from which most of the water has been removed by heating in a high vacuum loses some of its ability to readsorb water. However, it will slowly recover this ability over several months time if it is exposed to moist air. Measurement of the heat released when thoria samples with known amounts of preadsorbed water are immersed in liquid water has disclosed that most samples have a very heterogeneous surface: the amount of heat released per molecule of water adsorbed decreases as more and more water is adsorbed. All of these observations are of vital importance in understanding and predicting the behavior of thoria in nuclear applications.

SOLUBILITY OF MAGNETIC IRON OXIDE IN HIGH-TEMPERATURE WATER

Magnetite (Fe_3O_4) is the stable compound which results from corrosion of metallic iron by water or steam at high temperatures. A precise knowledge of the solubility of this material (long known to be extremely small) in water at various temperatures is needed in order to understand corrosion processes and movement of corrosion products in pressurized-water reactors or, indeed, in any high-temperature system of iron or its alloys in which water is contained and circulated. Our measurements of the solubility of magnetite in superheated water (up to 500°F) indicate that the solubility is in the range of a few parts in a billion parts of water and that it decreases with increasing temperature. The extremely small amounts of iron dissolved in the water (as Fe^{2+}) were detected by use of radioactive ^{59}Fe. This was formed from ^{58}Fe, an isotope present in small amounts in natural iron, by irradiating the magnetite with neutrons in the ORR. A sample of pure ^{58}Fe, produced by a stable-isotope separation process at ORNL, was used to prepare a magnetite containing 300 times as much ^{59}Fe as irradiated magnetite of natural isotopic composition. This gave greater sensitivity in these measurements of extremely low solubility. In addition, this special magnetite was free of interfering radioactive elements which are formed from impurities in natural iron that has been exposed to neutrons.

PHYSICAL CHEMISTRY OF MOLTEN SALTS

Crystal Studies

X-ray diffraction studies on chemical compounds all containing the fluoride anion but having cations as widely different as beryllium and uranium have been made with crystals obtained from various research programs being carried out at the Laboratory on molten salts. The crystal chemistry learned from this work adds to the understanding of much of the physical-chemical behavior of these salts and their mixtures. As examples may be cited the changes that they undergo with increasing temperature, and solid-state phenomena such as diffusion and radiation damage.

The predominant compound in solidified fuel of the MSRE is lithium beryllium fluoride, Li_2BeF_4. We have determined its crystal structure with high precision by x-ray diffraction methods. Figure 6 shows a portion of the crystal as viewed down its hexagonal axis. The shaded balls represent lithium and beryllium atoms and are each connected to four fluorine atoms to form tetrahedra. Down the center of each hexagonal array of atoms is a cylindrical hole of about 2 A radius, suggesting a pathway for rapid diffusion of gaseous atoms out of this material.

Sodium neodymium fluoride, $NaNdF_4$, is the prototype for a number of compounds discovered among the phases existing when rare-earth ions are present as fission products in sodium-containing fuels. Our elucidation of its crystal structure has added to the understanding of the phase transitions that occur among fluorides containing sodium and rare earths. Its structure is shown in Fig. 7. There is possibly a certain amount of exchange of sodium and rare-earth ions in the structure, which produces disorder. As the temperature of this compound is raised, the nature of the disorder changes, causing a phase transition.

C4-8340

C4-6113

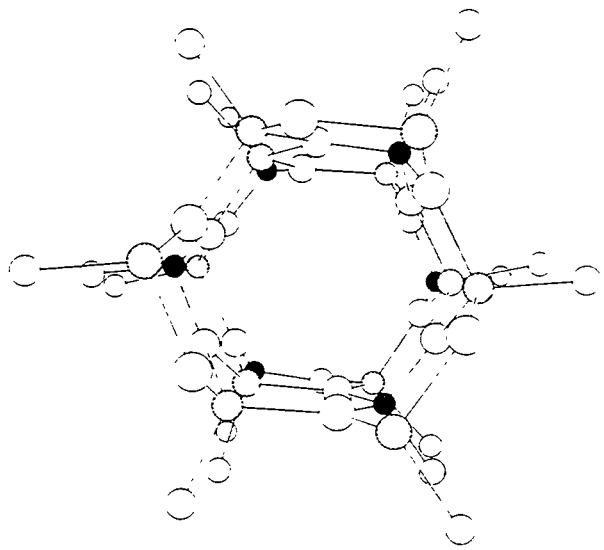

Fig. 6. Crystal Structure of Lithium Beryllium Fluoride, Li_2BeF_4. The solid circles represent beryllium atoms, the shaded circles are lithium atoms, and the open circles are fluorine atoms. The lines between them show how the atoms are bonded together to form tetrahedra. The large open space in the center extends through the entire crystal, providing a diffusion path for atoms.

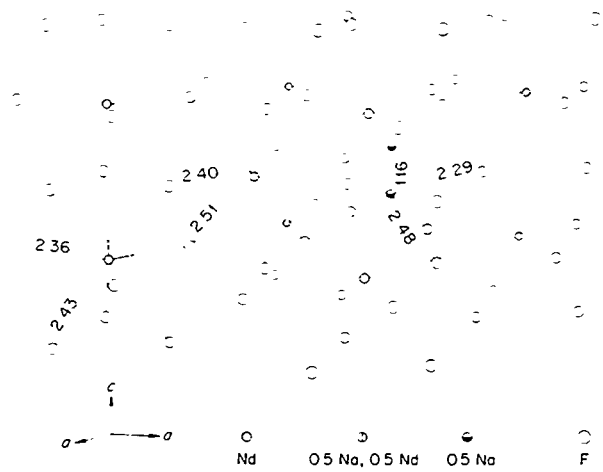

Fig. 7. Crystal Structure of Sodium Neodymium Fluoride, $NaNdF_4$. The split circles indicate sites in the disordered crystal that may be occupied by atoms of either of two kinds.

UF_4-UF_3 Equilibria

Uranium tetrafluoride, a key intermediate in the production of all compounds of enriched uranium, can react with uranium metal at temperatures above red heat to produce uranium trifluoride, UF_3. At higher temperatures, UF_3 becomes unstable in a rather odd way – it reacts with itself to produce UF_4 and uranium metal. By using gaseous hydrogen in place of uranium metal, we have been able to study the equilibrium reaction

$$UF_4 + \tfrac{1}{2}H_2 = UF_3 + HF$$

both with the pure substances and with the uranium compounds dissolved in a molten mixture of lithium fluoride and beryllium fluoride. Equilibrium constants for the reaction were easily determined by measuring the composition of the gas phase, that is, the relative amounts of hydrogen and hydrogen fluoride present, above the mixed solids or the solution. It was found that UF_4 is more stable toward reduction when dissolved in the molten salt mixture than when present in the form of an undissolved solid. The values of the equilibrium quotient increased with increasing temperature over the range 724 to 950°C. Increasing the beryllium-to-lithium ratio in the molten fluoride solvent from 1:2 to about 4:5 also increased the equilibrium quotient, suggesting the presence of important solvent complexing effects. Thermodynamic values of the heat and entropy of the reaction were derived from the experimental measurements. One significant and pleasant implication of the results is that UF_4, now being used as the fissionable ingredient of the fuel for the MSRE, is more stable than had previously been anticipated.

Viscosity of Molten Fluoride Mixtures

The viscosity of a liquid can be measured by determining the torque required to maintain constant velocity of rotation of cylinders immersed in the liquid. We have measured the viscosities of molten mixtures of lithium fluoride and beryllium fluoride in this way; the compositions ranged between pure BeF_2 and a one-to-one mixture of LiF and BeF_2, and the temperature range covered 710 to 1720°F. The viscosity of pure BeF_2 was already known to be extraordinarily high; at

1300°F it was measured to be 1,800,000 centipoises (which compares with a value of 0.9 centipoise for ordinary water at room temperature). When lithium fluoride was added to beryllium fluoride to make an equimolar mixture, the viscosity was decreased by a factor of more than 1,000,000.

The theoretical significance of these results stems from the fact that pure liquid beryllium fluoride is a disordered three-dimensional network in which each fluorine atom is simultaneously bound to two beryllium atoms and each beryllium atom is simultaneously bound to four fluorine atoms; the resulting structure, in which the atoms can move slightly, is like that of a glass, in contrast to the structure of a crystal, where atomic motion is much more limited. In fact, the arrangement of beryllium and fluorine atoms in BeF_2 is analogous to the arrangement of silicon and oxygen atoms in the structure of ordinary glass. When extra fluorine atoms (or ions) are added through the introduction of some lithium fluoride, each such fluorine atom can cause a break in the three-dimensional structure of pure beryllium fluoride; the glassy structure is then converted into smaller units, and the viscosity of the liquid is drastically lowered.

GASEOUS DIFFUSION

The classical model that has been used to describe the migration of gases through porous media regards the porous barrier as a bundle of capillaries which are interconnected in a rather complex manner. While the utility of this model has long been recognized, its limitations, particularly in that range of pressure at which surface effects play a significant role in the gas transport mechanism, are equally well known. Because the pressure range in question is frequently encountered in nuclear reactor technology, for example, in gas-cooled and molten-salt reactors, we have been endeavoring to clarify the effects of surfaces on gas transport in the so-called transition region. This work has led to the development of a "dusty-gas" model, in which the porous septum is mathematically described as an agglomeration of giant, stationary molecules (dust), rather than as a bundle of capillaries. In previous years, the dusty-gas model was successfully applied to the constant-temperature interdiffusion of gases and to the transport of a single gas due to a temperature drop (thermal transpiration). This year we have extended the treatment to include the interdiffusion of a binary gas mixture in the presence of a temperature drop, and have thus predicted several interesting effects, as yet untested experimentally, which had previously been only suspected.

Gaseous diffusion and thermal transpiration are governed to a large extent by the manner with which the gas molecules physically interact with one another; hence studies of the two phenomena can provide a valuable insight into such intermolecular interactions. It is with this purpose in mind that experimental investigations of gaseous diffusion and thermal transpiration are likewise being conducted at ORNL, though the results are also of interest from an applied point of view.

ANALYTICAL STUDIES OF MOLTEN-SALT SYSTEMS

Substantial progress was made in the absorption spectrophotometric studies of various molten-salt systems. The atmosphere of the nickel cell assembly was freed of water, oxygen, and HF by placing chips of titanium sponge in the sample compartment. This procedure has brought about an increase in the stability of the absorption spectrum of U^{4+} in LiF-NaF-KF for periods of 15 hr.

The absorption spectrum of U^{3+} at 500°C in $LiF\text{-}BeF_2\text{-}ZrF_4$ was obtained after the reduction of U^{4+} by either Zr or U metal. The molar absorptivity of the strongest U^{3+} peak at 875 mμ in the near-infrared region was estimated to be 40 liters $mole^{-1}$ cm^{-1}. In the ultraviolet region, at 360 mμ, the molar absorptivity is about 500 liters $mole^{-1}$ cm^{-1}. The spectrum of U^{3+} in $LiF\text{-}BeF_2$ appears to be identical with that observed in $LiF\text{-}BeF_2\text{-}ZrF_4$. The intensity of the 360-mμ peak in these melts provides a sensitive means of observing reactions that generate or consume U^{3+}.

A special holder was devised for very small crystals. With this holder, it was possible to obtain the absorption spectra of crystals whose diameter was about 0.1 mm over the wavelength range from 280 to 750 mμ.

The absorption spectrum of UF_6 was obtained by using a vacuum-tight fluorinated nickel gas cell equipped with crystalline Al_2O_3 windows and

Teflon gaskets. The spectrum is complex in the region 340 to 420 mμ with a maximum at 368 mμ, at which wavelength the molar absorptivity of UF_6 is 5.5 liters $mole^{-1}$ cm^{-1}.

The experimental equipment used to investigate the electroanalytical characteristics of molten-fluoride salt systems was modified to eliminate the possibility of contamination by moisture. With this equipment the decomposition potentials of such metals as Zr, Cr, Fe, Ni, and Mo in molten fluorides were obtained.

Rapid-scan and anodic-stripping methods of voltammetry of nickel in molten LiF-NaF-KF were studied. By means of the latter technique, concentrations of nickel as low as 1 ppm have been measured in the molten salt mixture. Voltammetry was also applied to the analysis of the MSR solvent and fuel salts, wherein the presence of hafnium was indicated by these studies.

Work was continued on the development of a reference electrode that would be compatible with molten-fluoride salts. The platinum quasi-reference electrode is not particularly stable. On the other hand, the Ni-NiO electrode appears to have some utility as a useful reference electrode in the three-electrode controlled-potential circuit, even though it is not satisfactory in the two-electrode circuit because the cell current that flows through the reference electrode seems to produce polarization and subsequent erratic potential measurements.

CHEMICAL RESEARCH RELATED TO THE DESALINATION OF WATER

The basic research program which is carried out at Oak Ridge National Laboratory under an interagency agreement between the Office of Saline Water and the Atomic Energy Commission is designed to develop information pertinent to desalination on equilibrium and transport properties of solutions, phase relationships, equilibrium and transport phenomena at phase boundaries and surfaces, separations methods including hyperfiltration, and corrosion. A large number of theoretical and experimental studies are under way in these fields.

Properties of Solutions and Phase Studies

Our studies were principally in the following areas: thermodynamic properties of aqueous multicomponent salt solutions; model computations of properties of sea salt solutions as a function of temperature and concentration; phase studies and solubility relationships of pertinent salts at high temperatures and as a function of ionic strength; development of emf methods for measurement of activities of salts in solutions; thermodynamics of solutions of electrolytes in water-organic mixtures by emf, solubility, and distribution coefficient methods; salting-in and salting-out properties of electrolytes; measurement of self- and tracer-diffusion coefficients of ions; viscosities of solutions; and dielectric constants. Some of the results are summarized below.

Cation-sensitive glass electrodes were found applicable to measurement of the activity coefficients $\gamma_{\pm}$ of NaCl in aqueous solutions containing a second salt with a common ion. With chloride as the common ion, the other cation was divalent—Mg^{2+}, Ca^{2+}, Sr^{2+}, or Ba^{2+}. Mixtures of NaCl with other sodium salts (nitrate, sulfate, perchlorate) were also measured. With most pairs, measurements were carried out at total ionic strengths of 1, 3, and 6. The present results are in good agreement with unpublished isopiestic measurements of Robinson for the $NaCl$-$BaCl_2$ system and of Scatchard for the $NaCl$-$NaClO_4$ system. Except at very low NaCl concentrations, where the measurements are suspect, log $\gamma_{\pm NaCl}$ at constant ionic strength varied in all cases linearly with ionic strength fraction of NaCl; that is, Harned's rule was applicable. In most cases, the slopes α_{12} of the linear plots were of a smaller magnitude than those of HCl in HCl-salt mixtures.

The studies on solubilities of $CaSO_4$ in NaCl solutions[3] were extended to higher temperatures, and parallel studies were carried out on the solubility of $CaSO_4$ in $NaNO_3$ solutions. The solubilities in this system seem substantially to follow the Debye-Hückel theory, as did the results in chloride solutions; they also provide a satisfactory test of the reliability of presently available solubilities of $CaSO_4$ in water, particularly at the highest temperatures. Judging from current results, the literature values for the solubility of $CaSO_4$ seem to be substantially in error above 200°C.

The solubility of $CaSO_4$ in H_2SO_4 solutions was determined over a wide temperature range. Combination of these data with the solubilities in NaCl

[3] W. L. Marshall, R. Slusher, and E. V. Jones, *J. Chem. Eng. Data* 9, 187 (1964).

solutions now permits determination of the equilibrium constant for the reaction

$$CaSO_4 + H^+ \rightarrow Ca^{2+} - HSO_4^-$$

and of the acid constant of the HSO_4^- ion. The latter was found to vary from about 10^{-2} at 25°C to about 5×10^{-7} at 350°C.

Thermodynamic properties of sea salt solutions were calculated over broad temperature and concentration ranges from known osmotic coefficient data for NaCl solutions and the appropriate formulation of the Debye-Hückel theory. The calculated vapor pressures of sea salt solutions are compared in Fig. 8 with the experimental values of Arons and Kientzler, Forrest and Worthley, and Higashi *et al.* The experimental values scatter widely about the calculated curves, implying that if vapor pressures of sea salt solutions of greater accuracy than the calculated ones are needed, much more accurate experimental measurements must be made.

We also calculated boiling point elevations for sea salt solutions in the range 2 to 28 wt % solids and 25 to 300°C.[4,5] These calculated values lie between those of Clark *et al.*[6] and those of Hickman;[7] at 25°C, where Clark's value is presumably the most reliable, there was good agreement. The minimum energy requirements for recovery of water from seawater were calculated for the range 25 to 200°C. There was good agreement at 25°C with Spiegler's value,[8] but our values are about 10% lower than those of Dodge.[9]

64-6923 B

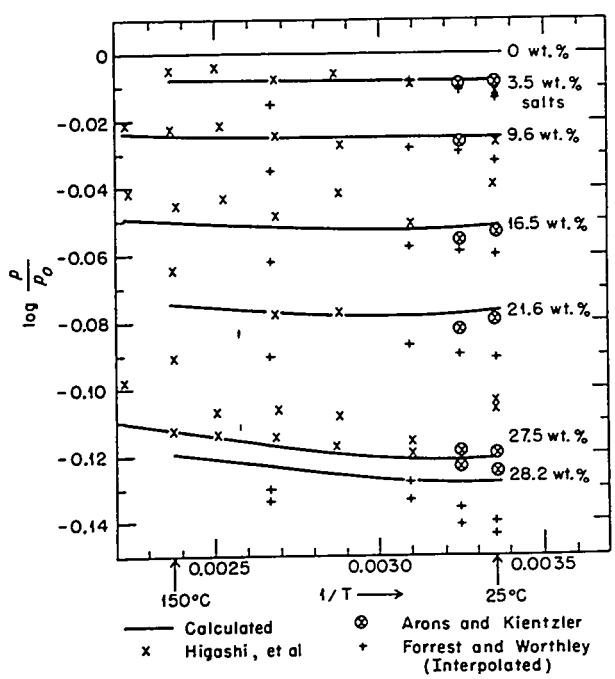

Fig. 8. Deviations of Vapor Pressures of Sea Salt Solutions from That of Water.

Because of great current interest in membranes based on organic substances, considerable emphasis was placed on study of thermodynamic properties of water-organic mixtures which might serve as models for membranes. Activity coefficients of NaCl were determined by emf methods in water-organic systems over broad ranges of concentration and water content. The measurements cover a wide range of dielectric constants. In most systems the activity coefficients varied with concentration essentially as predicted from the Debye-Hückel theory, and extrapolations of activity coefficients to zero salt concentration in the organic-water mixtures could be made with reasonable confidence. A test of the Born equation, which relates these activity coefficients at infinite dilution with dielectric constant and a distance-of-approach parameter, could be made. While for any one water-solvent mixture the Born equation seems reasonably satisfactory, it was found that the distance-of-approach parameter which best describes the data is different for each water-organic system.

A study of activity coefficients $\gamma_{\pm(0)}$ of salts at saturation in glycol, glycerol, and their various acetates was completed.[10] The activity coefficients were found to be principally a function of degree of acetylation of the compounds and of the water content. High values of $\gamma_{\pm(0)}$, which one would need for good salt rejection, were found to

[4] R. W. Stoughton, M. H. Lietzke, and R. J. White, *J. Tenn. Acad. Sci.* 39, 109 (1964).

[5] R. W. Stoughton and M. H. Lietzke, *J. Chem. Eng. Data* 10, 254 (1965).

[6] R. L. Clark, K. J. Nabavian, and L. A. Bromley, *Advan. Chem. Ser.* No. 27, 21 (1960).

[7] K. C. D. Hickman, U.S. Office Saline Water, *Saline Water Conversion Program, Progr. Rept. 12* (November 1956).

[8] K. S. Spiegler, *Salt-Water Purification*, Wiley, New York, 1962.

[9] B. F. Dodge, *Am. Scientist* 48, 476 (1960).

[10] K. A. Kraus, R. J. Raridon, and W. H. Baldwin, *J. Am. Chem. Soc.* 86, 2571 (1964).

require very low water contents. Values of $\gamma_{\pm(0)}$ for NaCl obtained from literature data with cellulose acetate agree reasonably with those measured here, provided comparison is made at the same degree of acetylation and the same water content. The acetate solutions thus seem to be good models for analysis of equilibrium properties of these membranes.

Activity coefficients of NaCl and KCl were determined by a variety of methods for a large number of water-amide systems. As in the acetate studies, $\gamma_{\pm(0)}$ seemed to be less a function of the specific amide selected than of the water content.

Most of the amides, as well as glycerol triacetate (GTA) and glycol diacetate (EGDA), are not miscible with water in all proportions. Addition of NaCl, KCl, and in most cases $MgCl_2$ causes an increase in the miscibility gap. These salting-out effects may be correlated with the activity of water in these systems; the composition of the organic-rich phases is largely determined by a Henry's law type of argument. Examination of the effect of other salts on the miscibility gap in the GTA-water system revealed that most salts proposed by Loeb and Sourirajan as suitable additives in the preparation of their high-transmission membranes cause salting-in and even annihilation of the miscibility gap. A typical set of results is shown in Fig. 9. The insensitivity of the effect to the charge of the cation is striking; this throws serious doubt on claims advanced by some that the important part of the membrane salt which imparts unusual properties to the casting solution is the cation of the salt.

A broad study of tracer- and self-diffusion coefficient measurements for ions in liquids, gels, and membranes has been initiated. For liquids, a

CH-5009

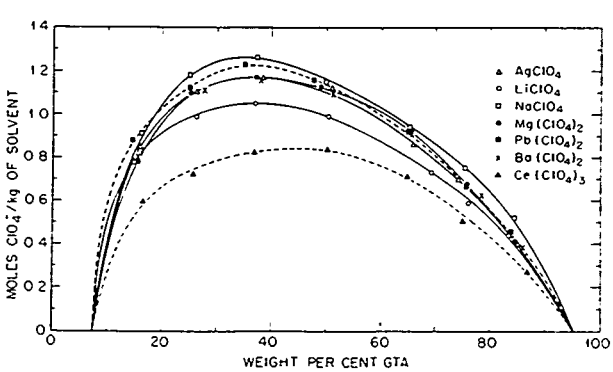

Fig. 9. Moles of Perchlorate Required to Produce Miscibility in the System Glycerol Triacetate–Water.

porous frit method was developed and tested.[11] The method combines reasonable precision with simplicity and rapidity of measurement.

Concentration Polarization at Phase Boundaries

Concentration polarization occurs when transport of one component in a multicomponent mixture is greater at an interface than that of another. This situation arises in essentially all separations processes; we have been principally concerned with those aspects of concentration polarization which are applicable to hyperfiltration (reverse osmosis), where it may impose serious limits on the range of usable transmission rates of membranes.

The studies dealt with (1) theoretical analysis of concentration polarization in flowing systems, (2) development of a concentration polarization method for testing membranes, and (3) boundary layer studies, whose object is development of techniques for increasing mass transfer and decreasing concentration polarization.

In hyperfiltration, the rejected salt tends to concentrate in a more saline layer adjacent to the membrane In an unstirred cell with membranes of finite rejection ability, this salt buildup can be detected through an increase in "filtrate" concentration; this increase will continue until the "filtrate" concentration becomes equal to that of the bulk (feed) solution. At constant flux, the time required for this apparent failure of the membrane to occur will depend on the rejection ability of the membrane, and conversely the rejection-transmission profiles permit evaluation of the rejection characteristics of the membrane. Theoretical curves for such systems have been calculated, simple equipment for testing membranes based on this principle has been constructed, and good agreement was found between calculated break-through profiles and those observed.

In a practical hyperfiltration cell, flow past the membrane is used to keep concentration polarization under reasonable control. We have calculated the extent of concentration polarization for laminar and turbulent flow in channels with salt-rejecting membranes. This work, which parallels similar study at Massachusetts Institute of Technology,

[11] A. E. Marcinkowsky, F. Nelson, and K. A. Kraus, *J. Phys. Chem.* 69, 303 (1965).

G4-10155

has been reported as a combined publication of the two groups.[12]

With laminar flow, there are two essentially different regions of behavior: an asymptotic region, where the concentration profile no longer changes form as one goes down the channel, and an entrance region, in which excess concentration builds up near the wall substantially linearly with distance down the channel. In most practical cases, salt buildup in the entrance region is decisive. Here concentration polarization varies with the cube of the transmission rate and may become very serious with membranes not much more permeable than those now used.

Turbulent flow will suppress concentration polarization more effectively. This will require increased pumping energy consumption and, more importantly, will require design of cells very different from those in current use. While this case is discussed in the reference quoted, Fig. 10 shows a nomogram which expresses, in a rough though informative way, the connection between concentration polarization ($c/c_0 - 1$), transmission rate (v_0), mean channel flow velocity ($\bar{u}$), and work expended per unit product to maintain turbulent flow (W). Note that at a transmission rate of 100 gal day^{-1} ft^{-2}, very large pumping costs are required to hold concentration polarization down to 30%.

Various experimental programs are under way which we hope will deepen understanding of the properties of boundary layers, which often present a limiting resistance for processes, and perhaps will permit development of techniques which may give disproportionate increases in mass (or heat) transfer.

In one of these studies, using air as the working fluid and naphthalene as the material transferred, it was found[13] that the turbulence level of the free stream above a flat plate can have a pronounced effect on mass transfer through the boundary layer when the turbulence level exceeds a certain critical value. In a parallel study[14] it was found that the vortex street eddies shed from multiple cylinders or wires, located one behind the

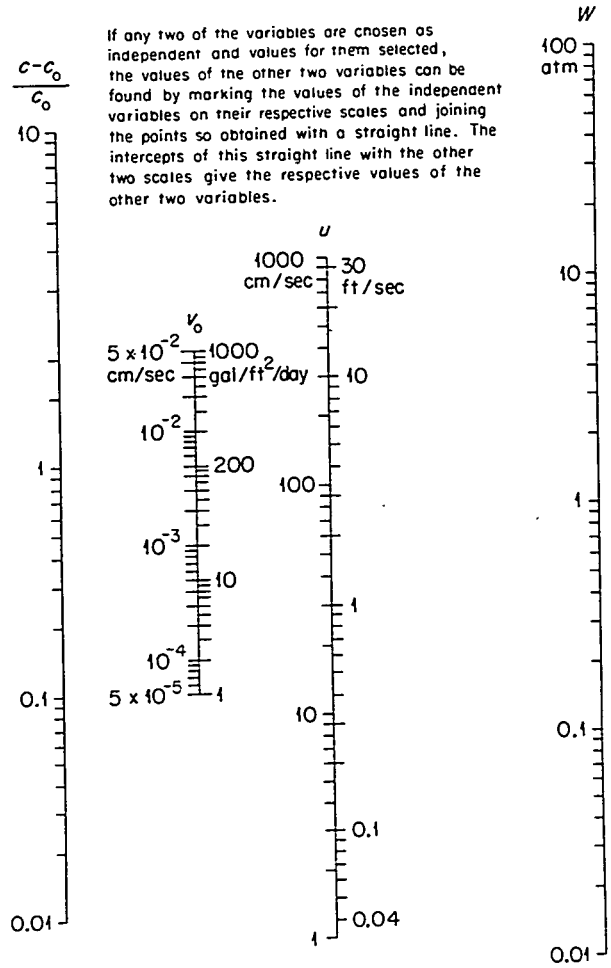

Fig. 10. Concentration Polarization in a System with Turbulent Flow.

other in the plane of flow, interact in a very complex manner, even considerable distances downstream from the cylinders. Expansion, contraction, coalescence, and even complete cancellation of vortices were observed, the effect depending critically on the distance between wires. Typical interaction patterns are shown in Fig. 11; they differ only in the distance of separation between the two wires. Most notable is the last pattern, in which there was substantial cancellation of the vortex street.

Periodic Phenomena in Flowing Suspensions

Some of our studies have been oriented toward understanding problems encountered in flow of dilute suspensions, such as one might have (intentionally or unintentionally) in water treatment

[12] T. K. Sherwood *et al.*, *Ind. Eng. Chem., Fundamentals* 4, 113 (1965).

[13] D. G. Thomas, *A.I.Ch.E. (Am. Inst. Chem. Engrs.) J.* 11, 520 (1965).

[14] D. G. Thomas and K. A. Kraus, *J. Appl. Phys.* 35, 3458 (1964).

PHOTO 71864

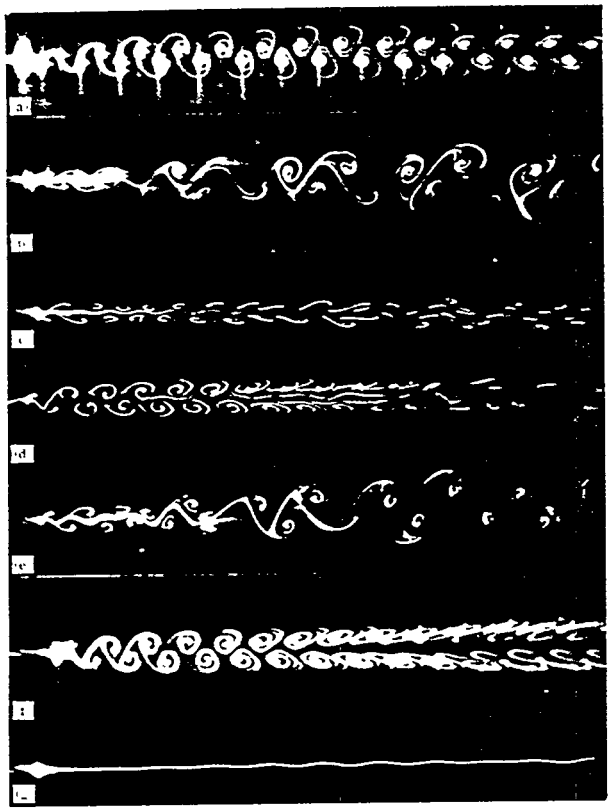

Fig. 11. Interaction of Vortex Streets Shed from Two Cylinders Located One Behind the Other in the Plane of Flow. Reynolds number, 62; cylinder diameter, 0.24 cm. (*a*) Single cylinder; (*b*)–(*g*) two cylinders with center-to-center spacings of 16, 10.4, 8.5, 8.5, 6.6, and 3.6 cylinder diameters.

processes. Periodic deposition phenomena were observed; under appropriate conditions, the particles of the suspension arranged themselves in periodic waves or dunes along the pipes. These dunes had characteristic wavelengths and moved along the pipes substantially more slowly than the bulk stream.[15,16]

Reactions and Transport Phenomena at Surfaces

Aside from corrosion studies, which are discussed below, our studies in this field dealt primarily with properties of porous electrodes and interaction of metal surfaces with ions in solution and with precipitating solids such as one would find during the formation of scales.

The distribution of current and potential in porous electrodes is a problem of considerable interest to desalination and water treatment, as well as other technological processes. Because of their large surface-to-volume ratio, porous electrodes may have applicability to redox processes, adsorption reactions of ionic and nonionic species, separations, and reactions in flowing streams. Solutions in closed form were derived for the distribution of current and potential in idealized, one-dimensional porous electrodes for simple oxidation-reduction reactions under pure activation control.[17]

Double-layer capacity measurements also provide an important means for studying electrode systems; they can reflect the presence of specifically adsorbed substances at the interface. For this reason capacity measurements are being used for study of adsorption processes in porous electrodes. A theory of potentiostatic and galvanostatic transients which occur during the charging of the double layer in porous electrodes was developed and was verified on porous carbon electrodes in sodium chloride solutions at 25°C. The curves of capacity vs electrode potential compared favorably with similar capacity curves observed with pyrolytic graphite electrodes of known area in the same solutions. The effect of iodide ions on differential capacity curves in 1 *M* NaCl was determined. Iodine species could be adsorbed at positive potentials and removed from solutions flowing through porous carbon electrodes by proper control of electrode potential. Even at the concentration levels existing in seawater, iodine species could be removed effectively by adsorption at controlled potential.

A variety of studies are oriented toward elucidation of the mechanism of adhesion of salts to metal surfaces. The principal emphasis was on the behavior of potassium sulfate as it precipitates under a temperature gradient in the presence of a zirconium alloy; however, interaction of other salts with other metal surfaces was also examined. Zirconium was chosen as substrate because prior ion exchange studies with hydrous zirconium oxide had been particularly extensive and because it was

[15] D. G. Thomas, *A.I.Ch.E. (Am. Inst. Chem. Engrs.) J.* 10, 303 (1964).

[16] D. G. Thomas, *Science* 144, 534 (1964).

[17] F. A. Posey, *J. Electrochem. Soc.* 111, 1173 (1964)

GH-4933

anticipated that there would be a close relationship between certain properties of bulk oxides and the surfaces of the metals. Striking effects were found correlating solution composition and adhesion of salts. Thus change of pH caused a large variation in adhesion on zirconium and on stainless steel. With zirconium, a striking influence of the phosphate concentration of the medium on adhesion was also demonstrated. In particular, under some circumstances, adhesion was not a monotonic function of phosphate concentration, but instead tended to go through a minimum at a critical phosphate concentration. Correlation of these results with phosphate ion adsorption studies on the metal surfaces and on high-fired oxides is now in progress.

Corrosion Studies

Our program on corrosion dealt principally with aluminum. It consisted of dynamic studies at high temperatures in titanium loops and electrochemical studies at lower temperatures (70°C); a program of electrochemical studies in flowing systems at high temperatures has also been initiated. During the loop studies, cases of catastrophic corrosion of titanium were observed; exploratory studies regarding the cause of this corrosion are under way. Typical results of the program follow.

Aluminum Corrosion. – The titanium-loop studies in NaCl solutions have shown the 5454 alloy (0.7% Mn, 2.7% Mg, 0.10% Cr) to be the most resistant to corrosion among the 11 commercially available alloys tested (EC, 1100, 3003, 3004, 4032, 5050, 5052, 5154, 5454, 6061, and X8001). Thus, in a short-term comparative test (211 hr, pH 6.5, 150°C, 1 *M* NaCl) the 5454 alloy corroded at a rate of less than 1 mil/year, as compared with a rate of 8 mils/year for the generally recommended 6061 alloy. The 5454 alloy was also more resistant to pitting attack.

The data have been correlated graphically in terms of temperature (100 and 150°C), pH (5.5 to 9), flow velocity (7 to 37.5 fps), and new aluminum area initially present. The correlation may be used to evaluate the important factors in the longer-term corrosion behavior of aluminum alloys and the effect of added seawater constituents or pollutants.

A small titanium loop was equipped for electrochemical corrosion studies under dynamic conditions. A suitable reference electrode assembly

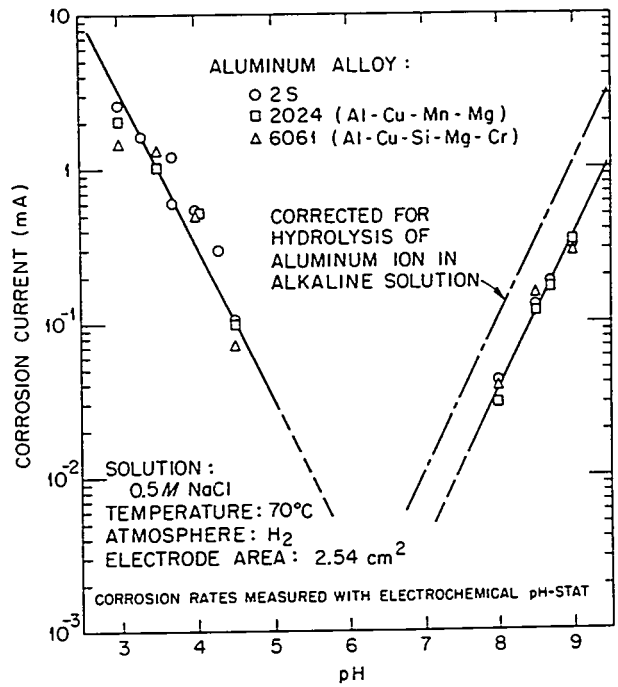

Fig. 12. Corrosion Rate of Aluminum Alloys as a Function of pH in 0.5 *M* NaCl at 70°C.

was installed, and provision was made for three electrodes, which are electrically isolated from the loop itself. Equipment was assembled for measuring and recording electrode potentials and polarizing currents for both potentiostatic and galvanostatic modes of operation. Initial experiments with aluminum in NaCl solutions at 150°C showed that polarization measurements are feasible with this experimental configuration and that the variation of corrosion rate with time calculated from polarization measurements is consistent with measurements by other methods.

The electrochemical pH-stat[18] was used to measure the corrosion behavior of aluminum alloys in NaCl solutions as a function of pH. The data of Fig. 12 show that a sharp minimum in corrosion rate exists in the vicinity of pH 6 and that the corrosion rate is relatively independent of the nature of the alloy. In the alkaline region (pH 8 or above), aluminum ions released during the corrosion process are hydrolyzed to form aluminate ions, and hydroxide ions are consumed by the overall corrosion reaction. The current from the

[18] F. A. Posey, T. Morozumi, and E. J. Kelly, *J. Electrochem. Soc.* 110, 1183 (1963).

pH-stat can be corrected for the influence of the hydrolysis reaction in this region. In the region from pH 5 to pH 8, measurement of corrosion rate by use of the pH-stat is insensitive because there the overall corrosion process does not cause a significant pH change.

Titanium Crevice Corrosion. – Significant corrosion of titanium in saline waters was encountered in connection with the aluminum alloy studies. A typical example of attack is shown in Fig. 13, a photograph of a clamping band used in assembling a specimen holder, which was exposed to 1 *M* NaCl for 96 hr at 150°C. The 8-mil-thick strip was practically severed. A photomicrograph showing the type of attack is given in Fig. 14. The following factors seem significant, based on observations thus far:

1. A tight crevice is a necessary but not entirely sufficient condition, since the attack is quite inconsistent.
2. The attack is more likely at higher temperatures, having been observed only once at 100°C, but with increasing frequency as the temperature is raised to 200°C.
3. The attack appears to be somewhat favored by low pH, though it has been observed over the pH range 5.5 to 10.3 at 150°C.
4. The bulk of the observations have been under deaerated conditions, but attack also was found with aerated solutions.

PHOTO 67202

Fig. 13. Corroded Titanium Clamping Strip. 1 *M* NaCl, 150°C, 96 hr.

PHOTO 67194

Fig. 14. Titanium Crevice Corrosion.

These observations raise a significant question about the validity of the generally held belief that titanium is immune to corrosion attack by salt water; such areas as the rolled-in ends of heat exchanger tubes may be particularly susceptible.

Hyperfiltration (Reverse Osmosis) and Membrane Studies

Our studies in this field dealt principally with (1) development of equipment and methods for study of transport of water and salts across membranes under pressure (see also the section "Concentration Polarization at Phase Boundaries"), (2) experimental and theoretical studies with uncharged membranes to gain insight into the fundamental processes involved, (3) development of new hyperfiltration membranes with particular emphasis on ion exchange membranes, (4) evaluation of possible use of inorganic membranes, and (5) theoretical studies of salt filtration with microporous ion exchange active bodies. Some of the results are discussed below.

While many membranes were prepared and tested, particular attention was paid to two ion exchange membranes. A cation exchange membrane was prepared by grafting polyacrylic acid onto cellophane. It rejected salt appreciably (35% in 0.5 *M* NaCl and 80% in 0.01 *M* NaCl at 2500 psi) and had a much higher permeation rate than standard electrodialysis membranes with comparable rejection.[19] An anion exchange membrane having similar properties was prepared by amination of polyvinyl chloride film. Neither of these membranes has permeation rates as high as the best cellulose acetate membranes developed so far. But, if they can be prepared with active layer thicknesses of the order of a micron, then permeation rates with these (and similar) ion exchange membranes would be substantially greater than with Loeb-Sourirajan-type cellulose acetate membranes, and they might find application in desalination of some brackish waters.

In an attempt to better understand the effect of various factors involved in hyperfiltration, we have carried out an analysis of transport of salt and water through membranes under pressure. The factors considered are distribution coefficient, D^* (ratio of moles of salt per kilogram of H_2O in the membrane to molality of feed); diffusion coefficient, $\mathcal{D}_2^*$, of salt, in appropriate units; rate of water permeation, J_1; degree of coupling of water and salt flow, β; and membrane thickness, l. With D^*, $\mathcal{D}_2^*$, β, and activity coefficients taken as constant, salt concentration profiles were computed for the limiting cases of complete coupling, $\beta = 1$, and of independent transport of salt and water, $\beta = 0$. For a given value of D^*, the profiles and salt rejection were found to depend on a dimensionless variable $\sigma = J_1 l/\mathcal{D}_2^*$; concentration profiles are given for various values of σ with $D^* = 0.1$ and $\beta = 1$ in Fig. 15 and rejection for different distribution coefficients ($\beta = 1$) as a function of σ in Fig. 16. Subscripts α and ω indicate feed and product interfaces.

Although the assumptions made are somewhat arbitrary, and some approximations are made in the computations, the model should be realistic enough to be instructive. If no pressure is applied (equilibrium), J_1 and σ are zero and the solute concentration is the same on both sides. Application of pressure starts permeation, which causes a concentration decrease at the effluent interface and an effluent concentration lower than that of the feed. As pressure is further raised, rejection, for $\beta = 1$, approaches $(1-D^*)$ as an asymptote. With uncoupled flow ($\beta = 0$), rejection approaches unity asymptotically, but rejection at a given value of σ is generally greater for smaller values of D^*. In both cases, if J_1 is linear with pressure and

64-9700

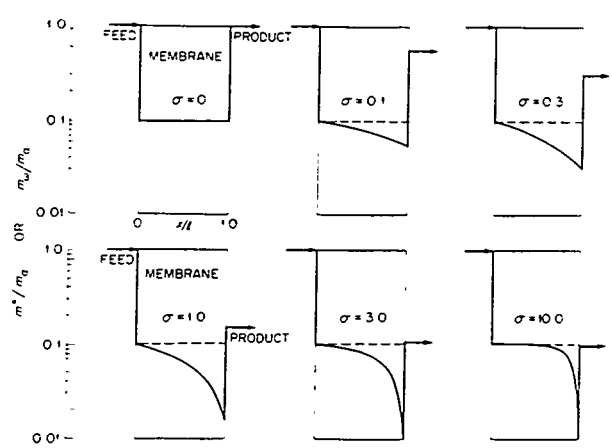

Fig. 15. Concentration Profiles in Hyperfiltration with Coupled Flow. $\beta = 1$, $D^* = 0.1$, $\sigma = J_1 l/\mathcal{D}_2^*$.

[19] W. H. Baldwin, D. L. Holcomb, and J. S. Johnson, Jr., *J. Polymer Sci.*, Pt. A 3, 833 (1965).

64-5329A

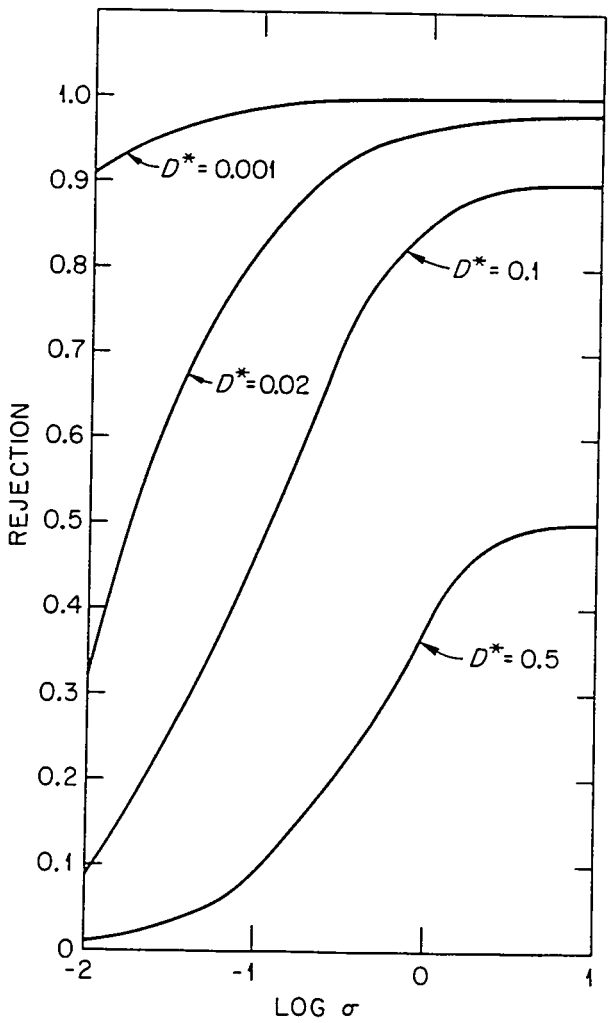

Fig. 16. Rejection of Membranes with Coupled Flow of Solvent and Solute. $\beta = 1$.

inversely proportional to l, rejection at a given pressure is not affected by decreasing membrane thickness.

The variational method developed for solving the Poisson-Boltzmann equation for charged microcapillaries immersed in electrolyte solutions[20] has been used in an attempt to calculate distribution coefficients of a salt between a solution and the liquid in the microcapillary. The results for the larger capillaries, however, showed a need for revision; the trial function used was apparently insufficiently accurate for these extreme cases. Use of a more accurate trial function unfortunately involves very formidable computational difficulties. Recent calculations in which the variational results were compared with other approximate methods of calculating distribution coefficients (based on the method of Dresner and Kraus[21] and the method of Schofield and Quenouille[22]) indicate that for smaller capillaries the simple trial function gives fairly accurate results. Thus, although its use must be restricted to relatively small capillaries, the variational principle with the simple trial function previously used can still be used to study the thermodynamic equilibria of charged microcapillaries.

PARAMAGNETIC RESONANCE STUDIES OF SHORT-LIVED FREE RADICALS IN LIQUIDS

The paramagnetic resonance method is often used to identify free radicals and to elucidate their properties. Frequently such radicals are formed as short-lived intermediates in chemical reactions; their role in radiation processes is particularly important whether these processes be of technological importance to nuclear energy, of biological importance, or of fundamental interest in chemistry. Much emphasis has been placed on studies of solids at low temperatures, where the radical lifetimes are long, but more recently various techniques have been devised for working with liquids at higher temperatures. Because of the shorter lifetimes in liquids the radicals are usually generated while they are being examined. At the Laboratory an intense source of ultraviolet light has been combined with a highly sensitive paramagnetic resonance spectrometer. In this way liquids may be irradiated, and short-lived radical products studied as they are formed, even at room temperature.

In recent work of R. Livingston and H. Zeldes small amounts of hydrogen peroxide were added to simple alcohols, and the products of irradiation were studied. The hydroxyl radical (OH) is first formed from the peroxide, and this radical in turn abstracts hydrogen from the alcohol, giving the radical that is observed. Many of the radicals

[20] L. Dresner, *J. Phys. Chem.* 67, 2333 (1963).

[21] L. Dresner and K. A. Kraus, *J. Phys. Chem.* 67, 990 (1963).

[22] R. K. Schofield, *Nature* 160, 408 (1947).

made in this way have been unambiguously identified, and some of their properties have been studied. The main aid to identification is the hyperfine interaction of the unpaired electron of the radical with magnetic nuclei (usually hydrogen) contained in the radical. An interesting and unusual case has been the radical formed by abstraction of hydrogen (in the position alpha to the OH group) from allyl alcohol. This free radical exists in two forms that differ only in geometric configuration. Both forms have been observed, and hyperfine effects have been accurately measured for all five of the hydrogens in each form. There are small but easily measurable shifts in the hyperfine couplings, depending upon the geometric form. The relative abundances of the two forms depend upon the temperature of the allyl alcohol at the time of the irradiation. Another unusual case has been the radical formed by abstraction of an alpha hydrogen from benzyl alcohol. A spectrum of 109 lines has been observed at room temperature, and its analysis gave precise values for the hyperfine parameters for all seven of the hydrogens in the radical. The pair of ortho hydrogens and also the pair of meta hydrogens were inequivalent, which demonstrated that the substituent on the aromatic ring could not be freely rotating.

STRIPPING PROCESSES IN CHEMICALLY REACTIVE COLLISIONS

We have discovered that some chemical reactions occur so rapidly that the nonreacting part of an attacked molecule is unaware that its neighboring atom has been removed. This effect, dubbed "stripping" from its similarity to the nuclear reaction mechanism of that name, occurs even when the attacked molecule consists of only two atoms.

These findings are the result of studies using the method of crossed molecular beams. In this method, which was originally developed at ORNL, two molecular beams containing potentially reactive molecules intersect each other. If a molecular collision in the crossing zone leads to a chemical reaction, the product molecules are scattered at some angle with respect to the initial directions of the beams. An analysis of the amount of product formed and the angular distributions of the products can lead to a detailed picture of the collision which led to the reaction. Thus, for example, the angular position of the product can be related to the molecular orientation at the time of collision, and the angular spreading is related to the amount of energy with which the reaction products recoil from each other.

The stripping effect was observed in a series of experiments on the reactions of alkali-metal atoms (K, Rb, and Cs) with simple halogen molecules such as bromine and iodine. The experiments demonstrated that these reactions occur at very large intermolecular distances (more than 5 A). Moreover, it was found that almost all of the heat of reaction appears as vibrational excitation of the alkali halide product molecule. Subsequent experiments have shown that there is a high probability for transferring this energy to electronic excitation of alkali atoms. Both of these latter effects may find application in the construction of new types of chemical lasers.

STEREOSCOPIC CRYSTAL-STRUCTURE ILLUSTRATIONS PLOTTED BY COMPUTER PROGRAM

With the widespread availability of large computers, crystallographers are able to solve increasingly complex crystal structures and to fit more elaborate mathematical models to x-ray, neutron, or electron diffraction data. The results of a crystal-structure analysis are three dimensional in nature, yet they must be communicated on the two-dimensional printed page to the biologist, chemist, or physicist interested in the stereochemistry of a structure. The graphic illustrations needed to convey the three-dimensional character of the results obtained by modern crystallography require time-consuming and diligent draftsmanship. C. K. Johnson has devised a computer program, OR TEP, for drawing crystal-structure illustrations automatically with a computer and a digital *x-y* plotter. The equipment needed for this technique is already available at several AEC and university computational centers. Stereoscopic pairs of drawings for three-dimensional viewing are produced by this automated technique in a small fraction of the time normally required for an ordinary two-dimensional manually drawn illustration.

65-695

The use of computer-drawn stereoscopic illustrations shows promise of alleviating a bottleneck in the presentation of crystal-structure information. The stereo figures can be viewed in stereo directly from a bound journal with the aid of an inexpensive hand stereoscope (cost from 35¢ to $10). Two examples are shown here (Figs. 17 and 18). In one example (Fig. 17) the stereo mates are printed close together so that a stereoscope is not necessary.

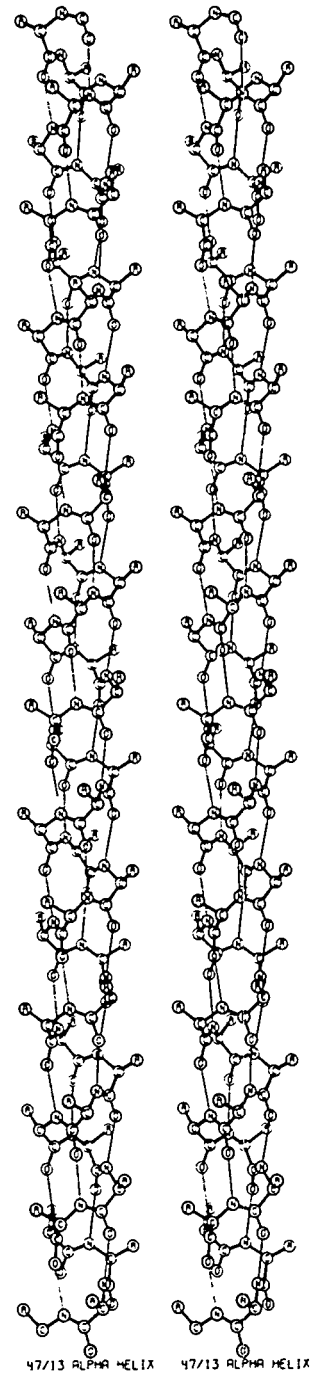

Fig. 17. The Pauling and Corey α-Helix Model for Protein Structure. One of the most significant structural models in molecular biology, this configuration is a major structural component in both fibrous proteins, such as muscle, and globular proteins, such as hemoglobin. For clarity, the hydrogen atoms have been omitted. The symbols R represent amino acid side chains. Stereoscopic viewing of this figure is facilitated by placing a sheet of cardboard between the helices. When correctly visualized, the helix appears right handed.

64-6522A

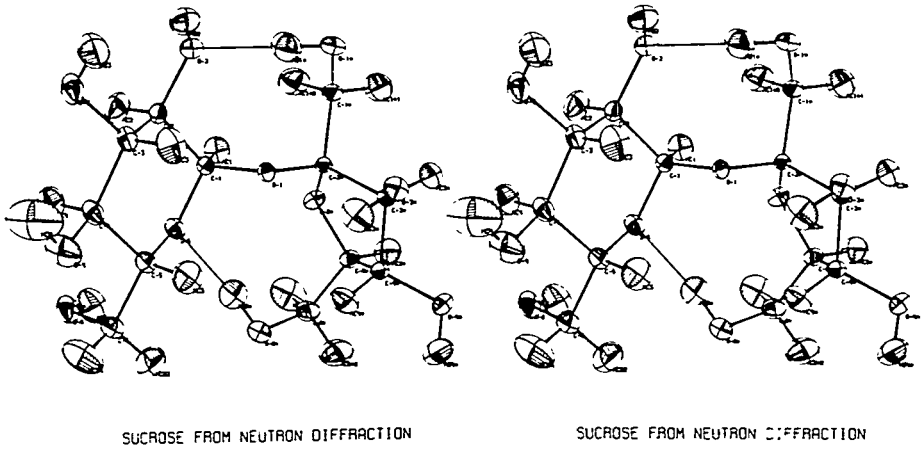

Fig. 18. Crystal Structure of Sucrose. From a neutron diffraction structure analysis by G. M. Brown and H. A. Levy. The ellipsoids situated on the atomic centers portray the three-dimensional thermal motion derived during the mathematical refinement of the crystal structure. Thermal motion patterns are relatively easy to recognize with this type of figure, since the orientations, relative sizes, and positions of the entire set of ellipsoids can be visualized simultaneously. Stereoscopic viewing of this computer-drawn figure is facilitated with a hand stereoscope but can often be realized without optical accessories.

64-11537A

SOLUTIONS OF METALS IN MOLTEN SALTS

The measurement of equilibrium cell potentials has long been an important means of determining thermodynamic properties of systems. In addition, equilibrium emf measurements can yield information as to the species present and the number of electrons involved in the potential-determining process. The application of this fundamental measurement to a unique group of solutions, namely, the alkaline-earth metals dissolved in their molten halides and the rare-earth metals in their respective molten halides, has not been possible because of their extreme corrosiveness to all known ceramic insulator materials.

H. R. Bronstein has evolved an *all-metal* cell technique, which represents a considerable advance both in concept and technology, for the measurement of equilibrium potentials. The new technique is applicable not only to molten metal–metal-halide solutions corrosive to ceramic materials but in general to all systems.

The method may be illustrated by two examples with the convention adopted to represent an emf cell contained in an *all-metal* system. An aqueous system:

$$\underline{Ta}\ \underline{\begin{matrix}Hg^0, Hg_2SO_4\text{(solid)}\\ \text{Saturated solution}\\ H_2O\end{matrix}}\ \vdots\ 1\ N\ H_2SO_4\ \vdots\ \underline{\begin{matrix}Ag^0, Ag_2SO_4\text{(solid)}\\ \text{Saturated solution}\\ H_2O\end{matrix}}\ \underline{Ta} \qquad (1)$$

A molten metal–metal-halide system:

$$\underline{Ta}\ \underline{\begin{matrix}Cd^0, CdCl_2\\ \text{saturated}\end{matrix}}\ \vdots\ LiCl, KCl\ \text{eutectic}\ \vdots\ \underline{\begin{matrix}\text{Unsaturated solution}\\ \text{of Cd in } CdCl_2\end{matrix}}\ \underline{Ta} \qquad (2)$$

The solid line represents a metal tube containing the respective solution, and the dotted line a porous metal plug welded into the side of the tube (Fig. 19). The symbol of the metal of construction is placed as shown, and the electrode tubes are separated by the bridging liquid. It is implicit in the convention that the bridging liquid is held in a container of the same metal as the electrode tubes. As in the normal convention, the electrode on the left of the bridging liquid is the anode, at which oxidation occurs, and the tantalum metal tube assumes the corresponding potential. Similarly, the right-hand tantalum tube assumes the potential of an electrode (cathode) at which reduction occurs. Effective electrical communication of the solution in each tube with the bridging

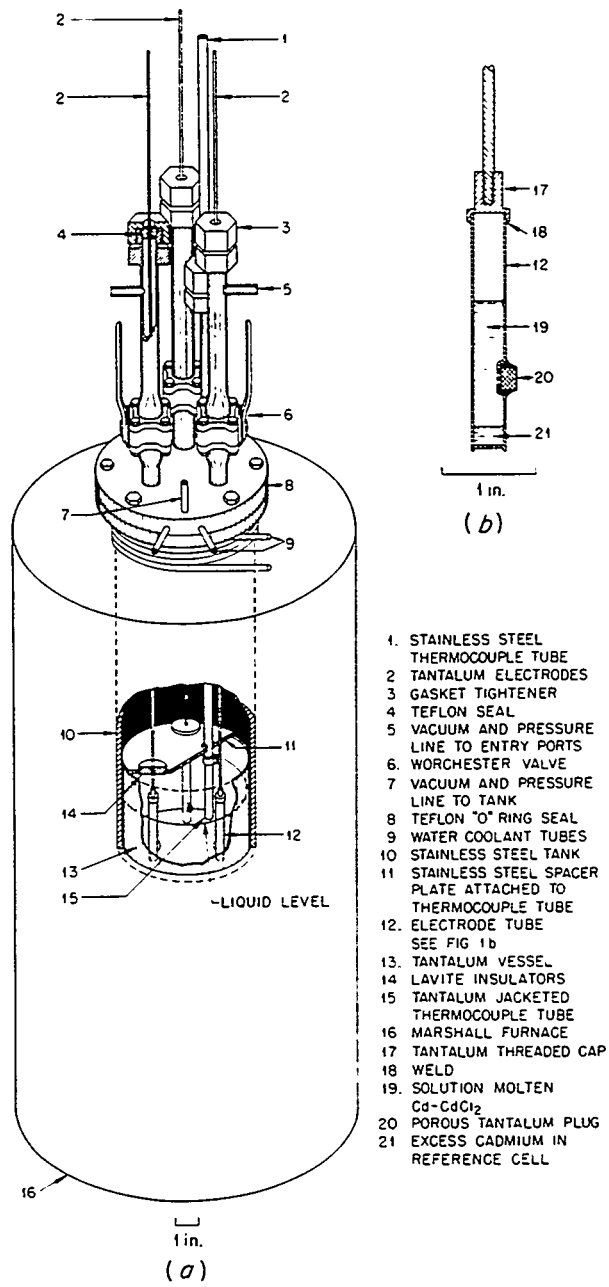

Fig. 19. All-Metal Cell for Measurement of Equilibrium Potentials. (a) Assembly; (b) detail of electrode tube.

solution is provided by means of the sintered porous tantalum plug. An important aspect of this new technique arises from the consideration that if there were no such communication, a current would not be expected to flow on connecting the two electrode tubes by an external wire unless the potential difference between them was greater

than the decomposition potential of the bridging liquid or than that of any other possible redox process which may be present. However, since the decomposition potentials of the bridging liquids in cells (1) and (2) are not exceeded by their half-cells in combination, no current can flow. For the aqueous cell, No. (1), the theoretical emf and the emf measured experimentally in a conventional cell made of insulating material are +42.3 and +42.0 ± 0.5 mv, respectively, at 25°C, which is well below the potential difference necessary for the decomposition of the sulfuric acid (namely, the decomposition potential of water) and also below that of the anodic dissolution of tantalum metal. In the molten system of cell No. (2), the decomposition potential of the constituents of the molten eutectic mixture, 3.00 v, is greater than any potential that can be developed in this system, 10 to 100 mv. With these requirements met, and with the porous metal plug providing an ion path for transport of current, the potential between these all-metal cells should be the same as that measured in the conventional glass-insulator apparatus. The experimentally determined potentials of cells (1) and (2) completely verified this expectation.

It will now be possible to measure the equilibrium potentials of molten metal—metal-halide solutions corrosive to ceramic material. With the proper choice of bridging solutions, the method is applicable in general to any system.

TRANSURANIUM-ELEMENT PROCESSING

The Transuranium Program, which is a part of the national heavy-element program, has the objective of producing sizable research quantities of americium, curium, berkelium, californium, einsteinium, and fermium. Recently the first material, 20 g of curium (predominantly ^{244}Cm) and 20 g of ^{243}Am, was recovered, separated from the associated fission products, and purified. This material, as well as the heavier elements to be produced in coming years, is to be made available to research workers in laboratories throughout the country for studies of the chemical, physical, and nuclear properties of these elements and for related research work.

This production program is a combined effort of ORNL and the Savannah River Laboratory.

PHOTO 68241

Fig. 20. Transuranium Processing Plant. Construction is essentially completed; process equipment will be installed and tested in 1965, and the facility will be ready for full-scale operation early in 1966.

The initial irradiation and processing was done at SRL. New facilities, including the High Flux Isotope Reactor (HFIR) and the Transuranium Processing Plant (TRU), are under construction at ORNL to continue the irradiations in a very high flux reactor and to provide a facility in which targets irradiated in the HFIR may be processed and the man-made elements recovered and purified (Fig. 20).

Initially 10 kg of ^{239}Pu was bombarded with neutrons in an SRL production reactor. In the reactor the plutonium atoms capture neutrons and increase in weight by one mass unit for each neutron captured. By a series of captures, accomplished by irradiation over a period of several years, a small portion of the ^{239}Pu will be converted to elements as much as 12 to 14 mass units heavier than the starting material. Unfortunately the major fraction of the material is lost by fissioning during the reactor irradiations, since the isotopes ^{239}Pu, ^{241}Pu, and ^{245}Cm have high fission cross sections. Thus the heavy elements as initially produced are highly contaminated with fission products, which must be removed before meaningful research is done with the elements. To date, the starting material (^{239}Pu) has been converted to one intermediate product containing about 1000 g of ^{242}Pu (separated and purified from the fission products) and a second product containing about 250 g each of ^{243}Am and ^{244}Cm. Two-thirds of this plutonium has been returned to Savannah River for further irradiation. The other

third will be fabricated into target elements for irradiation in the HFIR, scheduled to begin operation in 1965. In the HFIR the irradiation pace will step up considerably because of the higher neutron fluxes available.

Included in the continuing irradiation at SRL are 18 target rods, containing 10 g each of ^{242}Pu, which are identical to the target elements to be irradiated in the HFIR. In addition, six similar rods were included which had been irradiated for six months previously as part of the development program to ascertain that the rods possessed the heat dissipation and other characteristics required for use in the HFIR. From these six rods, about 300 μg of berkelium and more than 1 mg of californium will be recovered next year. This is several times the amount of these elements presently in existence.

DEVELOPMENT OF SEPARATION PROCESSES

The man-made heavy elements are separated from the fission products by processes somewhat similar to those used to recover uranium and plutonium from reactor fuels. The heavy elements are preferentially extracted from a strong water solution of lithium chloride by an organic solvent, in this case a tertiary amine. Fission products remain in the chloride solution, and the transplutonium elements are removed from the organic solvent with strong hydrochloric acid. These steps are performed continuously in a device called a mixer-settler, in which the immiscible solutions are alternately mixed thoroughly by agitation and allowed to separate into two distinct layers.

PHOTO 62704 A

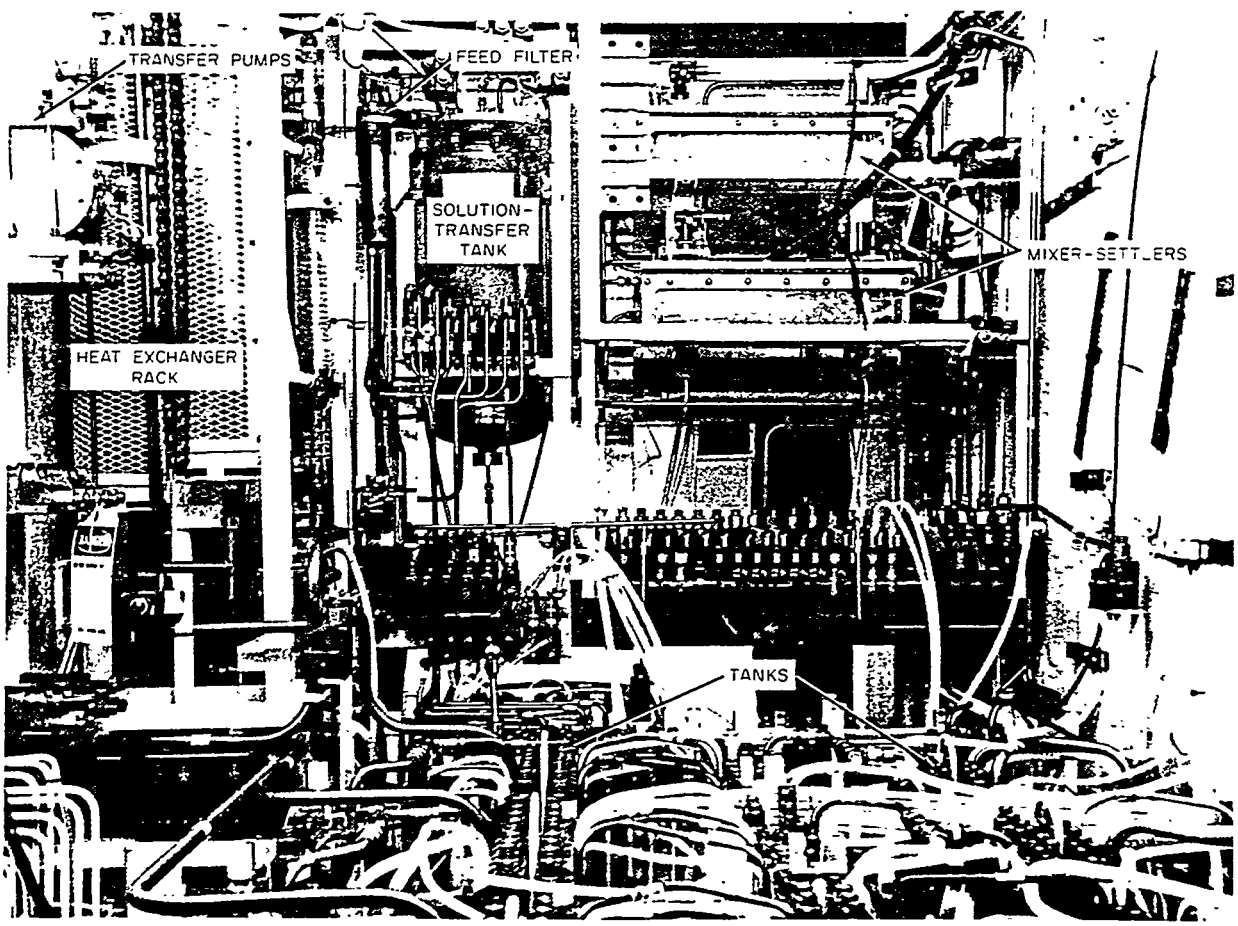

Fig. 21. Curium Recovery Facility. Pictured through the 4-ft-thick lead glass viewing window is the chemical processing equipment used to develop processes to recover the transplutonium elements.

In the initial runs in which this process was tested with actual materials from the production irradiations, 20 g of ^{243}Am and 20 g of ^{244}Cm were recovered. This processing was done in the Curium Recovery Facility, a shielded hot-cell facility in which the chemistry of the transplutonium elements is being studied (Fig. 21). The facility will also be used to produce curium for potential use as a heat source for thermoelectric generators in space applications.

These chemical separations are complicated by the very corrosive nature of the solutions and by the effects of radiolysis. In addition to beta and gamma radiation from fission products, energetic alpha particles from the heavy elements contribute to the breakdown of solution components. Methods of stabilizing acid concentrations in spite of this radiolysis have been found, and the use of very special materials of construction, such as tantalum and zirconium, has minimized corrosion problems.

A continuing program of chemical research has brought improvements in this process for separating the transplutonium elements from the fission products and solved many problems encountered in its application. This research has also provided a potentially attractive alternative process for purifying the elements. In this latter process, the fission products are extracted in preference to the trivalent actinides by a different solvent, di(2-ethylhexyl)phosphoric acid, from aqueous solutions containing lactic acid and diethylenetriaminepentaacetic acid. This method avoids the use of high and closely controlled concentrations of corrosive chlorides and permits processing in containers made of more common and cheaper materials.

METALLURGY AND MATERIALS

TECHNICAL ACCOMPLISHMENTS OF THE PURE MATERIALS PROGRAM

The Pure Materials Program is concerned with developing the necessary techniques for the growth of ultrahigh-purity and controlled-impurity research specimens of both immediate and long-range interest to ORNL, other AEC installations, and other AEC contractors. Our materials technology of tomorrow is dependent upon an improved understanding of presently known materials and upon insights into new and novel materials. The use of single crystals is required for the unambiguous characterization of many physical phenomena. Inasmuch as suitable crystals are frequently difficult to obtain, we are conducting a continuing program both to provide crystals needed in research and to devise and improve methods for producing superior materials. The following are listed as some of the significant accomplishments that have occurred as a consequence of this program during the past year.

Single-crystal tungsten of high quality and perfection has been produced and used to demonstrate an anomalous penetration as a consequence of bombardment by heavy ions of kev energies. The effect of crystallographic orientation on this anomalous penetration and channeling has been shown to be larger for this type of body-centered cubic crystal than for such face-centered cubic crystals as aluminum and copper.

Large (200-g) single crystals of potassium chloride have been grown under carefully controlled conditions that ensure a higher reproducibility of quality and as high a purity as has previously been attained. Possession of such ultrapure crystals has permitted a careful investigation of the influence of impurity type and concentration upon the radiolytic decomposition of alkali halides when exposed to nuclear radiation, by using crystals into which known quantities of chosen impurities had been deliberately introduced. In addition, the availability of materials of such high purity has made possible quantitative experiments on doping that have led to ultrasensitive analytical techniques. In the case of lead impurity, optical absorption studies have demonstrated a linear relation between the intensity of a characteristic absorption band and the lead concentration. This technique of analysis is sensitive to an impurity concentration of 50 ppb or even lower, and is far less time consuming and expensive than the conventional methods of atomic absorption spectroscopy.

Isotopically enriched single crystals of lithium fluoride weighing 300 g have been produced with a divalent cation impurity content of less than 30 ppb. The low-temperature thermal conductivity of these crystals is such that one can critically examine the isotopic scattering relaxation time. Measurements of the thermal conductivity of selected crystals that have been grown by the Czochralski process from these isotopic materials have opened up the possibility of studying the details of both phonon-phonon and phonon-boundary scattering processes in a solid conductor for the first time.

Highly purified beryllium hydroxide has been prepared by solvent extraction techniques, and the end product is equivalent to beryllium oxide of 99.998% purity. Prior attempts to ascertain the material transport properties of beryllium oxide have shown that the ionic conductivity and beryllium diffusion were controlled by the impurity-induced cation vacancy concentration; hence, the intrinsic properties could not be evaluated. It is anticipated that possession of such highly purified materials will permit investigation of the intrinsic transport behavior in this important material.

More than 20 refractory inorganic compounds have been synthesized in single-crystal form by traveling-solvent techniques, from supercritical aqueous systems, or by flame fusion. These crystals have been utilized in x-ray analysis of

neutron damage and in magnetic, electron spin resonance, and optical investigations. Good-quality crystals of thorium oxide, both pure and doped with rare-earth ions, have been prepared and have permitted a study of the electronic character of the rare-earth ion by electron spin resonance and by optical absorption methods. These electron spin resonance studies employing the thorium oxide host crystal are being extended to the transplutonium elements.

Single crystals of uranium dioxide in the form of elongated grains up to 25 mm in length and 3 to 5 mm in diameter have been grown from sintered polycrystalline rods by passing a molten zone through the center of each rod. X-ray photographs have verified the existence of single crystals and indicate that the crystal perfection is good. An initial examination of the crystals, which were grown in a nitrogen atmosphere, shows no inclusion of uranium metal, and the oxygen-to-uranium ratio is 2.003. Spectrochemical analyses indicated that a single pass of the molten zone reduced the metallic impurity content (initially 10 to 50 ppm) by about half.

Perhaps the most important accomplishment of the Pure Materials Program has been that of promoting an enhanced cooperation between analytical chemists, neutron activation specialists, mass spectrographers, crystal growers, and crystal property researchers. Any improvement in the techniques of one group is therefore reflected in the subsequent data and analyses of the other groups. Analytical techniques have been changed in certain instances from that of routine analysis to that of a continuing program of basic research on a specific material. The presence of unexpected impurities, or the pronounced effect of certain impurities, has sometimes been revealed only by using a wide variety of analytical and crystal-growth procedures.

CRYSTAL STRUCTURE OF CALCIUM BERYLLATE

The atomic arrangement of a very unusual compound of calcium and beryllium oxides has been determined by x-ray diffraction. The compound, $Ca_{12}Be_{17}O_{29}$, is obtained by rapid cooling of a melt of the component oxides. Its high symmetry and open structure suggest that it should resist radiation damage; this, along with its high beryllium content, suggests its use as a moderator or as a fuel diluent for high-temperature reactors. The crystal is made of repeating cubic units, each containing 48 calcium atoms, 68 beryllium atoms, and 116 oxygen atoms. Many features of the geometric arrangement of the atoms are unique to this compound, which appears to be near the border line between crystalline and glassy materials.

GROWTH OF URANIUM DIOXIDE SINGLE CRYSTALS

We have succeeded in growing single crystals of uranium dioxide up to 50 mm long by 5 to 8 mm across. Figure 1 shows a section of a typical specimen. Uranium dioxide rods that had been prepared by isostatic pressing and sintering were heated by induction in a nitrogen atmosphere, and the crystals were produced by passing a molten zone along the length of the rods. The crystals contained no inclusions of metallic uranium and had an oxygen-to-uranium ratio of 2.003. Spectrochemical analyses indicated that a single pass of the molten zone reduced the metallic impurity content, which was initially 10 to 50 ppm, by about half. Study and measurement of the properties of these crystals will provide a better understanding of the factors governing radiation damage and other characteristics without the complications due to grain boundaries.

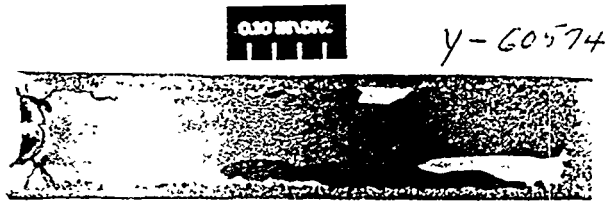

Fig. 1. Large Crystal Grown in a Uranium Dioxide Rod. The rod was traversed slowly with an induction coil. A molten zone swept through the rod, consuming small grains in its path and depositing the large crystal in its wake.

STRUCTURE OF THIN FILMS

An improved understanding of the distortions in the structure of metal oxides formed as thin films on the metals has been obtained recently. Careful measurement of the x-ray diffraction patterns of cuprous oxide films on copper, combined with refined theoretical interpretation, has revealed two new features in the film structure related to the forces operating in corrosion. When x rays are reflected by crystalline materials, the possible angles of reflection measure the spacings between planes of atoms in the crystal. Strain in the crystalline oxide film, caused by forces between it and the metal upon which it grows, shifts the angles of reflection. In the recent work, comparison of these shifts for two angles has revealed which of two possible kinds of planes is the first to form on the metal surface. Because the film is thin, the beam is not reflected through an exact angle but is spread somewhat. An analysis of this spread has now shown that the film is not uniform in thickness.

CORROSION OF ALUMINUM-BASE ALLOYS

Aluminum alloys would be good fuel cladding for some power reactors if they could be used at higher temperatures without excessive corrosion; the cladding materials used at present are more difficult to fabricate and to reprocess. We are investigating the corrosion behavior of aluminum alloys in pressurized water at 200°C. Alloys with various yttrium and zinc contents behaved similarly to aluminum alloys containing iron and nickel. Aluminum alloyed with 2 to 10% yttrium or with 20% zinc showed a substantial reduction in corrosion rate, and the severe intergranular penetration typical of pure aluminum was avoided. Each alloy contained a second phase. The yttrium-rich phase is probably anodic with respect to aluminum and acts as a sacrificial anode, whereas the zinc-rich phase is cathodic. Phenomenologically the corrosion behavior of these alloys is similar to that observed elsewhere in aluminum-nickel-iron alloys, whose improved corrosion resistance has been explained by the second phase preventing solution of excessive hydrogen in the matrix. Further understanding of the corrosion mechanism should guide future development of more satisfactory alloys.

OXIDATION OF REFRACTORY METALS

A characteristic feature of several technologically important refractory metals is their tendency to dissolve substantial quantities of oxygen at elevated temperatures. The large stresses that are thereby produced in the surface layers of the metal may lead to a dramatic acceleration of the oxidation rates through the physical rupturing of otherwise protective oxide films. We have discovered that anodically formed oxide films on tantalum and niobium are permeable to oxygen. We used specimens bearing such films to study stress generation due to oxygen solution in these metals without the complications produced by the simultaneous formation of additional surface oxide. The results were consistent with our previously proposed model, in which the stress gradient in the specimen was related to a corresponding oxygen gradient in the surface layers of the metal.

METALLURGICAL APPLICATION OF THE MÖSSBAUER EFFECT

We have applied the Mössbauer effect to study the effect of metallurgical treatments on the structure of alloys. In this effect, changes in the way an atom is bound to its surroundings affect the intensity and the energy of gamma rays emitted without recoil or absorbed in resonance by the nucleus of the atom. We have used Mössbauer spectroscopy to follow the state of very low concentrations of cobalt in aluminum after various heat treatments. Cobalt dissolved in the lattice, cobalt segregated at defects (possibly as Co_2Al_9), and an intermediate state have been observed.

DIRECT OBSERVATION OF LATTICE DEFECTS

We are using electron microscopy to study the deformation of metals. Metals are useful largely because they can deform plastically; this permits

No NUMBER

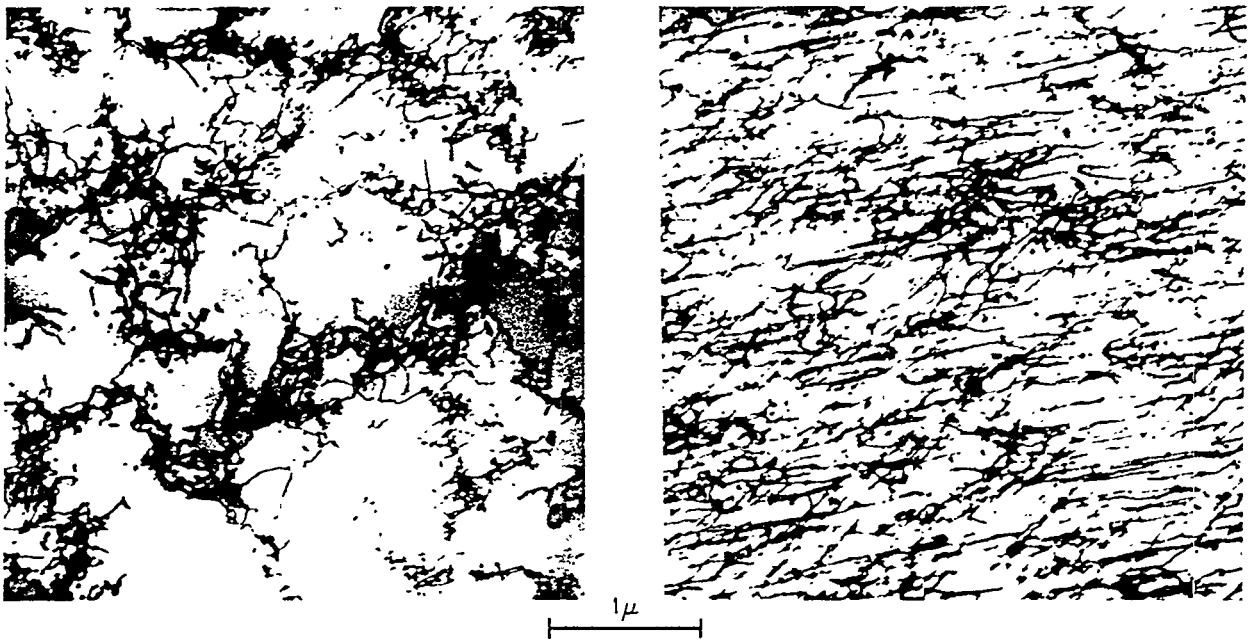

Fig. 2. Dislocations in Metals. These electron micrographs illustrate the way in which alloying additions strain the lattice to restrict dislocation motion and thereby strengthen metals. The motion of dislocations permits planes of atoms in a metal to move past each other and thus permits the metal to deform plastically under the applied stress. The dislocations, which appear as black lines in the micrograph, are very mobile in pure niobium (left) and tangle together. In the stronger niobium–7.5 at. % tungsten alloy (right), mobility is decreased and the dislocations occur as isolated straight segments. Studying alloying additions that strain the lattice in different ways should lead to discovery of the most effective strengthening addition.

both ready fabrication and accommodation of in-service stresses. Plastic deformation occurs through the creation and motion of dislocations, which are structural defects that extend for appreciable distances along lines in the crystal. When a dislocation glides along a plane of atoms, atoms above the plane move relative to those below the plane. Dislocations may be observed directly with the electron microscope; the changes in their appearance and arrangements as deformation conditions are changed show why and how metals are strengthened. To find the basic principles by which alloying strengthens metals, we have been studying body-centered cubic metals and their alloys, which have many high-temperature applications. The type of dislocation substructure and the type of dislocation motion have been related to the effects of temperature, strain rate, alloying, and impurities in these materials, and a model was proposed to explain the behavior in terms of the effective stress acting on moving dislocation segments. For the first time, all these factors can be interrelated. After some initial flow, whether further deformation or fracture occurs depends on the nature of the grain-boundary region. These studies suggest ways to produce refractory body-centered cubic alloys that are relatively ductile at low temperatures.

PREDICTION OF THERMAL CONDUCTIVITY

While developing diverse and accurate methods of measuring thermal conductivity and other physical properties, we have found correlations that should in some cases permit estimation of thermal conductivity without tedious measurement. This property is needed for estimation of the rate at which heat can be removed from nuclear fuel elements. However, its measurement at high temperatures requires elaborate apparatus and

specimens larger than those normally available for materials under development. The thermal conductivity of a material is the sum of contributions from the motions of electrons and atoms; the electronic contribution is readily calculated from the electrical conductivity, which can be measured easily. Figure 3 shows our data for iron, which is commonly used as a standard for checking thermal-conductivity apparatus. Only the electronic part is affected by the purity; so the thermal conductivity of any reasonably pure iron can be found from a simple electrical measurement. We have also found that for some materials the atomic part varies with temperature in a very simple manner; so high-temperature thermal conductivities can be estimated from thermal conductivities measured at relatively low temperatures, together with electrical measurements. We are now seeking a way to predict for which materials this method of estimation is valid.

64-5875 R

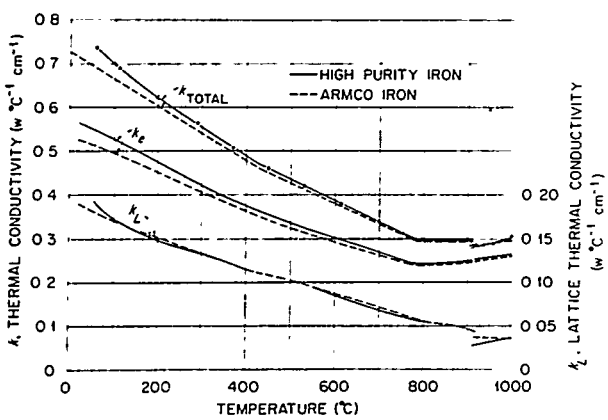

Fig. 3. Thermal Conductivity vs Temperature. Measurements on a high-purity iron (99.95%) pure) and an Armco iron (99.5% pure) by a radial heat flow method to within ±1.5%. The thermal conductivity is the sum of an electronic portion, which can be calculated from the easily measured electrical resistivity, and a lattice portion. The figure shows that impurities reduce the thermal conductivity by lowering the electronic portion, leaving the lattice portion unchanged. These results allow the thermal conductivity of any reasonably pure iron to be predicted by adding the lattice portion to an electronic portion calculated from the electrical resistivity.

EFFECT OF FABRICATION METHOD ON METAL STRUCTURE

We have found that the orientation of the individual crystals in a metal is affected by the method of fabrication. The mechanical properties of fabricated pieces are influenced by this orientation. There has been a widely held belief that the orientation after fabrication depends only on the direction in which the metal flows during working. However, markedly different patterns of crystal alignment were found when an aluminum rod was reduced in diameter by drawing, swaging, and extrusion. These orientation differences were great enough to cause a 75% variation in the stress required for plastic deformation of the metal. These observations should help a fabricator select the best manufacturing method for metal products.

FUNDAMENTAL INVESTIGATION OF RADIATION DAMAGE IN SOLIDS

Semiconductor Research

It has been well established that exposure of many semiconductors, such as germanium, silicon, and compounds formed from elements of groups III and V of the periodic table (e.g., gallium arsenide, which has become important as a laser material), to nuclear radiation profoundly alters their electrical behavior. The technological importance of this radiation sensitivity becomes immediately apparent when it is remembered that electronic devices fashioned from these semiconductors are even more sensitive to energetic radiation than the bulk specimens. Degeneration of device performance because of damage by space radiation is an important problem in our space satellite program.

We have extended our investigations of radiation damage in semiconductors to include the compounds formed from elements in groups II and VI of the periodic table. Typical examples are the well-known photoconductors cadmium sulfide, cadmium telluride, and zinc sulfide, all of which show potential for device application. During the past year these studies have led to several important results. Primarily by using different radiation energies it is possible to create elementary

defects (interstitials and vacancies) in either the sublattice of the metallic constituent or that of the nonmetallic constituent. This effect is associated with the mass difference between the component elements; the energy of incident radiation capable of ejecting light atoms from their normal positions in the crystal lies below the threshold required for the displacement of the heavier atoms. On the other hand, because of its larger nuclear charge, the heavy atom presents a larger cross section to the high-energy radiation for displacement than the lighter component does. Experimentally it is observed that exposure of *n*-type cadmium sulfide to 0.67-Mev gamma rays, which are able to displace only sulfur atoms, causes a decrease in electrical conductivity. On the other hand, 1.25-Mev gamma rays, which preferentially displace cadmium atoms, cause an increase in conductivity. Similar results were obtained for cadmium telluride. Not only will this important development open new avenues for investigating the nature of radiation damage in these binary compounds, but it may be useful technologically as a means of tailoring the electrical properties to desired values.

Effect of Ionizing Radiation on Ionic Crystals

A matter of considerable interest to the nuclear energy program is the decomposition of solids by high-energy nuclear radiation (radiolysis). This is caused by the ionization accompanying the absorption of the radiation and is quite different from the radiation damage caused by the "billiard ball" interaction between fast particles and lattice atoms. A convenient series of compounds in which to study radiolysis is the alkali halides, an example being sodium chloride. The decomposition products created in alkali halide crystals by gamma rays, beta rays, etc., are usually atomic-scale defects in the crystal structure and are manifested by their characteristic absorption spectrum, hence the term "color centers." The concentrations of various color centers, many of whose structures have been determined, produced by a given radiation exposure are exceedingly sensitive to crystal purity, radiation intensity, and temperature. Each of these variables is being investigated in an attempt to determine the mechanism of radiodecomposition of these solids. The influence of purity has been evaluated, and it has been shown that as little as 1 ppm of certain contaminants such as lead markedly affects the rate of color-center introduction in potassium chloride at room temperature. At temperatures below 100°K the impurity effect is much reduced but still apparent. However, the defects introduced in these two temperature ranges differ in stability, since the coloration induced at 77°K can be completely removed at room temperature by exposure to visible light, whereas coloration induced at room temperature cannot be completely removed by visible light.

These observations indicate that both ionization and the thermal motion of lattice imperfections are important in the production of stable color centers in alkali halides. Such studies should be of assistance in choosing materials for prolonged service in a nuclear-radiation environment.

Light Absorption and Emission by Alkali Halide Crystals

The absorption and emission of light by pure alkali halide crystals, such as sodium chloride and potassium iodide, are related to changes in their electronic structure. The electronic states associated with these optical processes can be divided into two general classes. On absorbing light of a certain wavelength, an electron may be placed in a *conduction band state* in which it is free to move throughout the crystal. Light of somewhat longer wavelengths will cause the electron to go into an excited state of lower energy, in which it is still bound to the atom with which it was associated at the instant of excitation. These states are called excitons or *exciton states*. The exciton states are largely responsible for the characteristic optical properties of alkali halide crystals.

We have carried out detailed theoretical calculations on the electronic structure of exciton states. The calculations are extremely complex and can be done only with the aid of a large electronic computer. Perhaps the most important new feature of the work is that it takes into account the distortions of the lattice in the neighborhood of the excitons. The calculations have resulted in several fundamentally new ideas about the optical and electrical properties of pure alkali halide crystals. For example, it now seems clear that an exciton state can actually

move up into the conduction band as a result of lattice distortions. This means that the onset of photoconductivity does not necessarily imply the beginning of excitations to conduction band states, as has been generally assumed heretofore.

The results of the calculations also appear to have led to a clarification of the relationship between the states from which light is emitted in the pure crystals and those from which it is emitted in crystals which have been subjected to bombardment by electrons, gamma rays, and x rays.

Neutron Spectrometer Facility

A triple-axis neutron spectrometer facility has been constructed at the ORR and is now in operation. This facility has been designed to permit maximum flexibility in using an intense neutron beam from the ORR for solid-state research. In addition to conventional neutron diffraction, experiments will be performed in which the neutrons are scattered inelastically, because such experiments provide the only method of obtaining direct information on certain dynamical properties of solids. Investigations will be made on magnetic and nonmagnetic materials to determine magnon and phonon interactions in both metals and compounds. Preliminary results have already been obtained for the phonon spectrum of copper.

Channeling of Energetic Atoms in Solids

With the aid of a high-speed computer, we have carried out theoretical studies of the slowing-down in crystalline solids of ions having energies from 1 to 100 kev. The computer is programmed to simulate the motion of the moving ion as it slows down through binary elastic collisions with the target atoms, which have been correctly located on their lattice sites. It was found that ions entering the crystal along high-symmetry directions penetrated for much greater distances than those entering along arbitrary directions. A detailed analysis of these long trajectories showed the moving ion to be traveling in channels bounded by close-packed atomic rows of the crystal. Expressed differently, the moving ion experiences a sequence of correlated glancing collisions with the atoms in the close-packed atomic rows, which act to steer the ion between and along the rows. These glancing collisions involve small energy loss and therefore lead to large penetration depths. This "steering" ability of the crystal lattice is called "channeling" and has led to the prediction that the penetration of ions in single crystals should depend on the orientation, an effect which has since been experimentally confirmed, both at Chalk River and in the High Voltage Laboratory at ORNL. The hitherto unsuspected importance of the crystal structure to the slowing-down process at these relatively high energies has provided a basis for understanding sputtering yields in single crystals, as well as stimulating researchers to make penetration measurements in single crystals. The data from these measurements, in turn, are providing information that should lead to a better understanding of the interatomic potential, which is crucial for constructing a sound theory of radiation damage in solids.

Neutron Diffraction

The neutron diffraction technique is capable of providing direct information concerning the microscopic magnetic properties of solids. Such measurements can lead, particularly when they are carried out in conjunction with classical magnetic and thermal studies, to an understanding of the fundamental processes responsible for magnetism in solids.

Our single-crystal neutron diffraction studies of the heavy rare-earth metals terbium, dysprosium, holmium, erbium, and thulium have led to the discovery of a number of novel magnetic structure types, and these results, coupled with those obtained at the Ames Laboratory, often on the same specimens, on thermal, magnetic, and electrical properties, have provided a source of information from which considerable progress in the understanding of the magnetism of these materials has been made.

The results of the neutron diffraction studies are summarized in Fig. 4. Each of the five metals undergoes a magnetic ordering transition from the paramagnetic to an antiferromagnetic state at a temperature T_N ranging from 228°K in terbium to 56°K in thulium. The antiferromagnetic structure adopted at this temperature is either the helical arrangement *a*, as illustrated in Fig. 4*a*, or the static linear oscillator structure *d*. In each of these

64-8919

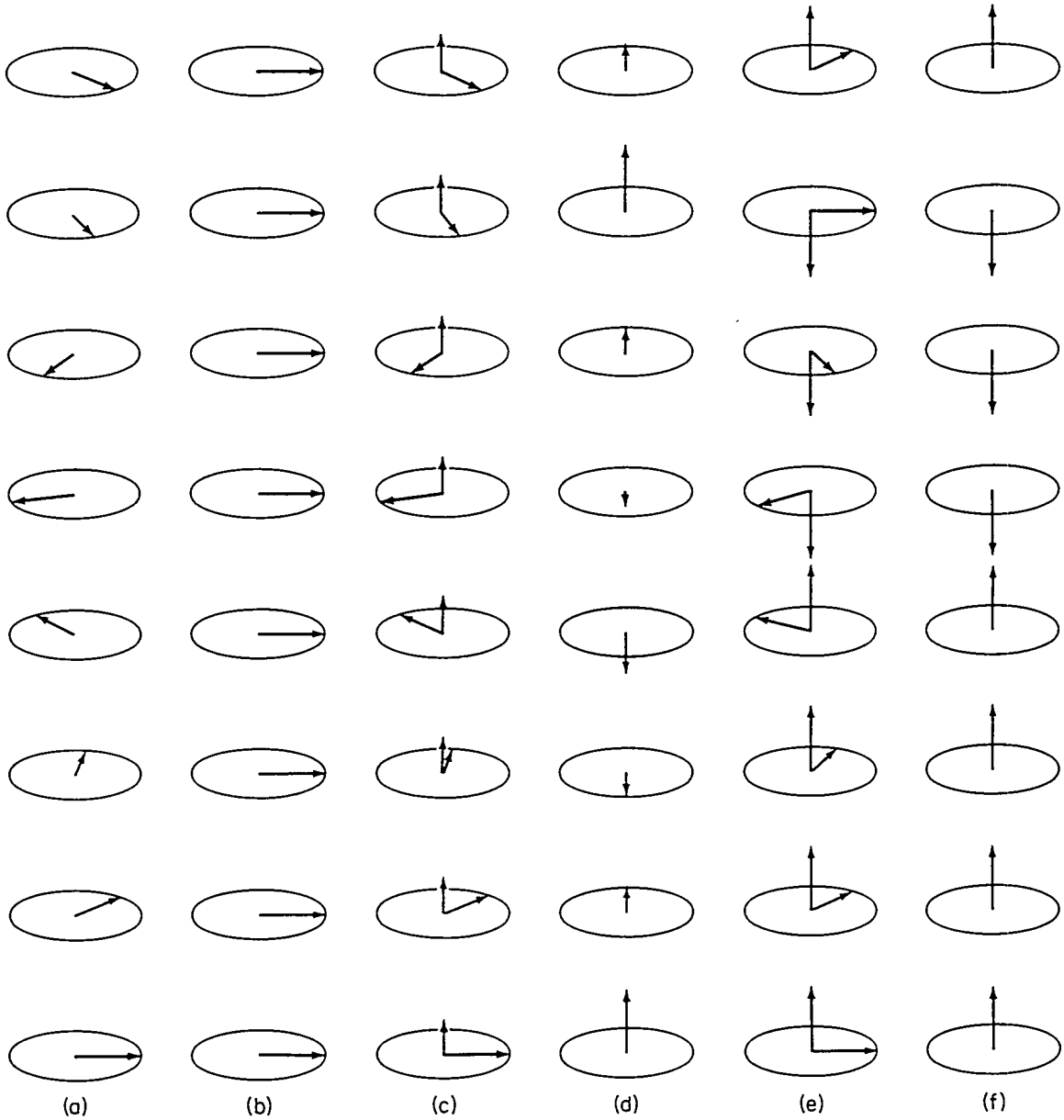

Tb	$228° \geq T \geq 218°$	$T < 218°$				
Dy	$179° \geq T \geq 87°$	$T < 87°$				
Ho	$133° \geq T \geq 20°$		$T < 20°$			
Er			$T < 20°$	$80° \geq T \geq 53°$	$53° \geq T \geq 20°$	
Tm				$T \lesssim 56°$		$T \sim 4°$

Fig. 4. Schematic Representation of Magnetic Structures of the Rare-Earth Metals. (*a*) Simple helix, (*b*) classical ferromagnet, (*c*) ferromagnetic spiral or conical configuration, (*d*) linear oscillator, and (*e*) and (*f*) antiphase domain type structures. The temperature ranges of stability are indicated in the lower part of the diagram.

arrangements the moments within a given hexagonal layer of the simple hexagonal close-packed structure are parallel, but the magnetic structure undergoes a sinusoidal modulation either parallel to or perpendicular to the c axis of the crystal, with displacement along the c axis.

At lower temperatures there are observed, as shown in the lower part of the figure, further order-order transformations to classical ferromagnetic (terbium and dysprosium), conical (holmium and erbium), or antiphase domain type (erbium and thulium) configurations.

The oscillatory nature of the magnetic structures can be understood if the interaction between rare-earth ion moments is long range and oscillatory; the different directions of magnetic order and the transformations between configurations are well explained if the several orders (four) of anisotropy energy are properly taken into account.

The long-range exchange interaction has usually been assumed to be of the Ruderman-Kittel-Kasuya-Yosida type, and indeed this interaction has been successfully invoked to explain a number of observations on the pure metals and alloys. A number of details of the experimental results have not, as yet, yielded to interpretation, and it appears that the simple RKKY theory is not a wholly adequate framework in which to discuss the rare-earth metals.

X-Ray Observations of Defects in Nearly Perfect Copper Crystals

The intensity of x rays transmitted through a given thickness of a crystal when it is set at the proper angle for diffraction can be greatly enhanced if the crystal is perfect or nearly so. This so-called anomalous transmission comes about because the incident x-ray beam and the diffracted beam interact to form a wave field which is propagated along the crystal planes. The interaction between the wave field and the atoms is minimized for atoms exactly in this plane; hence this effect is only observed in nearly perfect crystals. Previously applied to nearly perfect crystals of germanium and silicon, this effect has been utilized to make x-ray pictures of nearly perfect crystals of copper, the defects in these crystals appearing as local deviations of intensity. This technique allows the observation of dislocations and clusters of point defects in thick specimens of nearly perfect crystals. In addition, the behavior of dislocations so widely spaced as to be nearly independent of each other can be investigated.

The x-ray photograph (Fig. 5) is an example of dislocations in a copper crystal; copper crystals with from 50 to 5000 dislocations/cm^2 have been investigated. Since such photographs are also the result of a diffraction phenomenon, the techniques developed for the utilization of electron micrography can generally be applied. The Burgers vectors, types, and spatial arrangement of

No Number

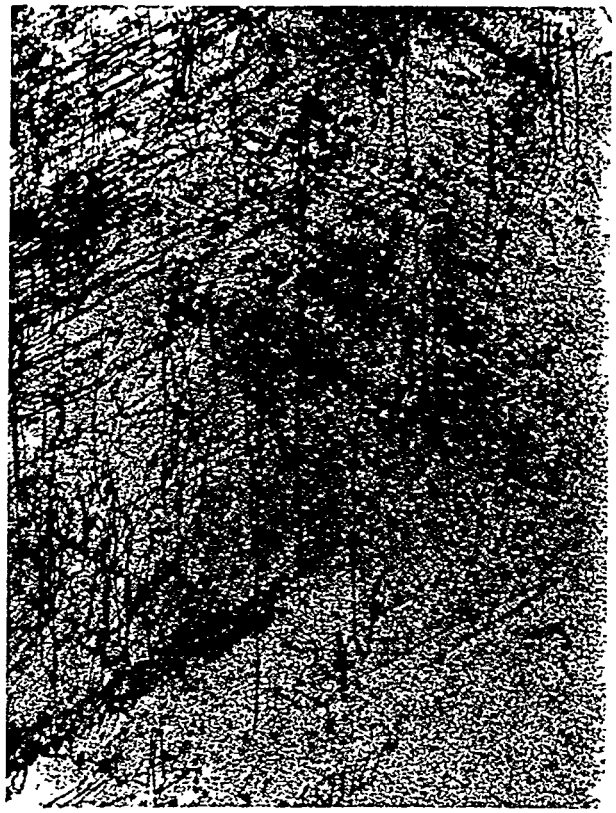

Fig. 5. X-Ray Photograph Showing Some of the Dislocations Introduced by an Extremely Small Strain in a 0.5-mm-thick Copper Crystal. The long lines are individual screw dislocations lying approximately parallel to the surface. A group of dislocations in a slip plane which lies at an angle of 70° to the surface is seen at lower left. 40X. Reduced 58%.

the dislocations existing in annealed copper crystals have been investigated. Clusters of vacancies, which are caused by the agglomeration during cooling of those vacancies formed by thermal excitation at high temperatures in these perfect crystals, have also been observed. Such experimental observations are possible only with this technique.

In related experiments, the intensities of the beams anomalously transmitted through such nearly perfect copper crystals have been measured and thereby the corresponding x-ray constants determined. A preliminary investigation has indicated that the transmitted intensities are only slightly affected by previously subjecting the copper crystals to neutron irradiation.

CONTROLLED THERMONUCLEAR RESEARCH

INJECTION-ACCUMULATION PROGRAM

General

There are several experiments in various countries seeking to accumulate a controlled fusion plasma by injecting high-speed atomic particles into a magnetic trap and holding some of them there. ORNL was the pioneer in this attack, the DCX-1 experiment having been started years ago on the basis of molecular ion injection (the experiments use H_2^+ at 600 kev) and dissociation upon a vacuum carbon arc. In DCX-1, the H_2^+ ions make a single loop within the magnetic trap, and then most of them emerge from the magnetic field to strike a target. In DCX-2, the H_2^+ ions are injected deeply into the magnetic field, they make many passes (perhaps 100) through a lithium vacuum arc, and most of them are dissociated into trapped H^+ ions.

In Russia, the OGRA I is a large experiment that works in an arrangement roughly similar to DCX-2. In France, MMII uses injection from an annular ion source that extends all around the magnetic field, in the equatorial plane between magnetic mirror coils. There are now three or four experiments that use injection of hot neutral atoms (H^0) that are ionized, and therefore trapped by one means or another within the region of magnetic field. PHOENIX in England, ALICE at the Lawrence Radiation Laboratory at Livermore and the Aerojet-General experiment in the United States, and OGRA II and VGL II in Russia all use this attack. It is of interest to compare the performance of these various devices, insofar as they have matured sufficiently to yield results.

Such a comparison has been drawn up by P. R. Bell, and it is presented diagrammatically in Fig. 1. In this diagram, the hot-ion density achieved is plotted as the ordinate. The abscissa is a quantity that depends upon what might be called the specific particle input, that is, the trapping current I divided by the plasma volume V, and upon a particle containment time τ that is supposed to be determined only by the composition and amount of residual gas in the vacuum system, and which in fact is calculated from these two data.

Now the total number of trapped ions in the plasma volume is $n_i V$, and since this population must be replaced by a trapping current I acting over a mean time τ, we must have $n_i V = I\tau$, if indeed the only loss is due to interactions with the background gas. This relationship is plotted as the straight line marked "charge-exchange limitation" in the figure.

We observe next that, except at low densities, all reported injection-accumulation experiments give performance curves that droop below the straight line. This means that above densities of about 10^8 fast ions/cm^3, losses stemming from origins other than the background gas are coming into play. The game that is being played all over the world is to increase the specific particle input, I/V, so as to force one's way toward the right in this diagram. Then if a loss due to instabilities occurs, the density achieved falls below the straight line. Curing the instability raises the density until the performance point again falls upon the line, and then a better vacuum enables the performance to move upward along the line to higher densities.

The chart shows three things:

1. All injection-accumulation experiments are showing severe losses at densities that are too low for use in a fusion reactor by factors of 1000 to 10,000.
2. Various applied factors have had beneficial effects.
3. Oak Ridge is doing as well as anybody else.

64-11383R

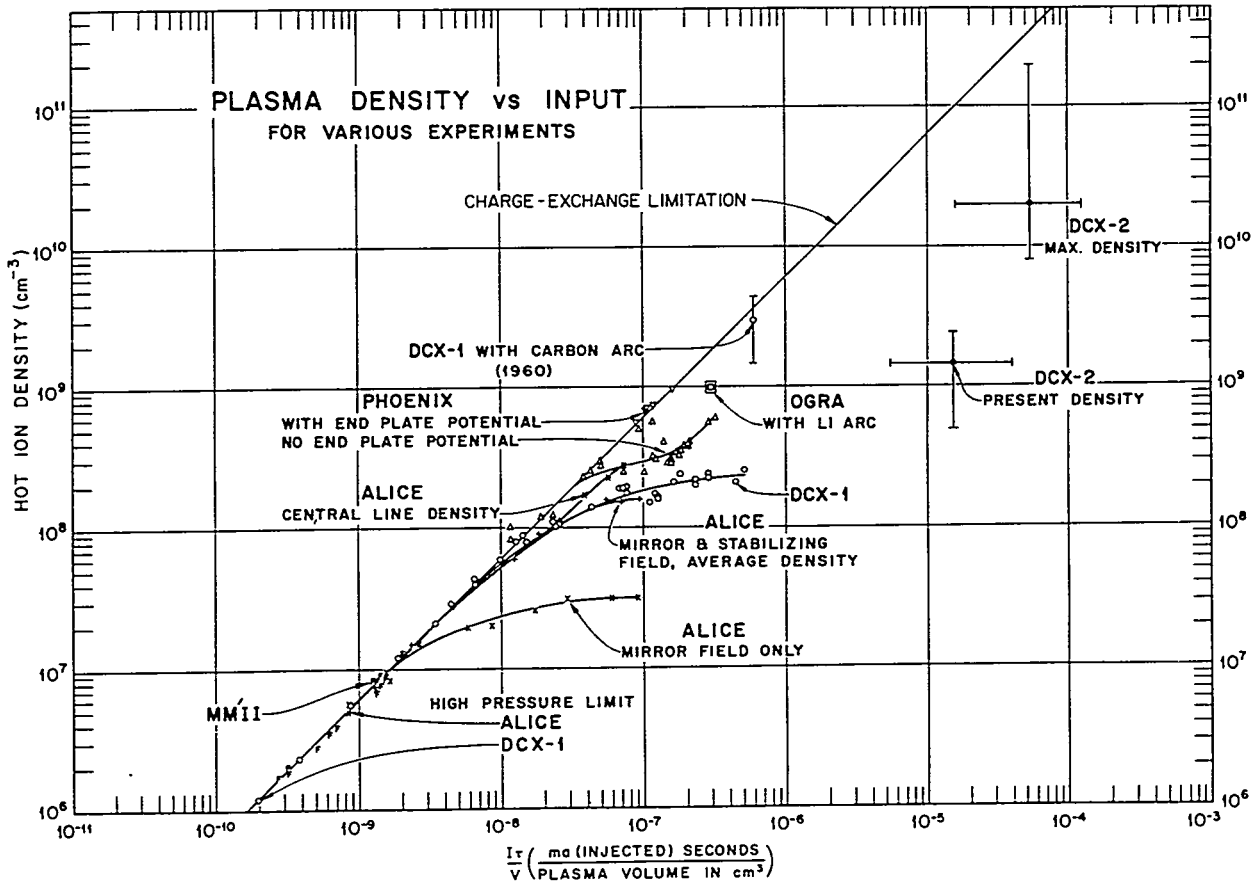

Fig. 1. Plasma Density vs Input. A diagram which serves for intercomparison of the world's injection-accumulation experiments in controlled fusion research. The hot-ion densities are plotted as ordinates, and the abscissa is a parameter that expresses the excellence of the vacuum and the number of ions that are forced into the trap per unit volume per second. A discussion is given in the text.

The DCX-1 Experiment

During 1964, we have reached a good understanding of the instability losses that are limiting the plasma density in DCX-1, even though sufficient trapping current is available to force the density almost ten times as high. The losses are due to a class of instabilities called "microinstabilities." Microinstabilities are accompanied by internal electric fields that develop in the plasma, leading to clustering and nonuniform density distribution, and manifesting themselves by emission of radio-frequency signals at the ion gyrofrequency (in this case, 14 Mc) and its harmonics. These signals are readily observable upon an antenna or probe inserted into the vacuum vessel close to the plasma. In DCX-1, loss of trapped protons has been experimentally associated with the presence of these radio-frequency signals. The presence of the microinstabilities is the result of too much order in the motions of the trapped particles; the cure lies in introducing disorder.

There is a variety of ways of introducing disorder into the ion motions in DCX-1, and a trial of several of these has started. Already we have seen that the onset of the microinstabilities depends sensitively upon the amount of disorder,

so the initial response may pay off rather handsomely. However, to do a thorough job of disordering will require major modifications, particularly in the means of injection.

DCX-2

The performance of the plasma in DCX-2 is complex, and we do not yet have a complete and coherent description of it. It is structured, consisting of at least three components. First, there is a cold component, mainly generated from the lithium arc. Second, there is a fast component that is "tilted" in the sense that it preserves the longitudinal drift that is imparted by the slant angle of injection (about 83° to the horizontal magnetic axis). Third, there is a remarkable, fast component that shows essentially no longitudinal drift, the ion motions being azimuthal. This third component appears most strongly when the magnetic field is made *very* slightly weaker at the midplane than in regions somewhat nearer the ends. This component results from purely plasma interactions that are as yet incompletely understood; it can contain most of the fast-ion population that is trapped, and it shows the astonishing energy spread that can make its mean energy be as high as 800 kev, as opposed to the trapping energy of 300 kev from the original beam. The second or tilted component, on the other hand, preserves its trapping energy fairly closely, not departing much from 300 kev.

Representative and compatible performance figures for DCX-2 are: a fast ion density of 8×10^9 cm^{-3} and a mean energy of 800 kev, this being the result of injecting about 40 ma of H_2^+ ions at 600 kev. After stop of injection, the decay curve of the trapped ions has been found not to be a simple exponential, because the disappearance of the trapped ions depends upon encounters with neutrals and cold ions in the vacuum system, and these themselves vary in density and location with time. Furthermore, energy changes continue to take place, and these shift the loss rates. A kind of "average" decay time, however, would be about 0.1 sec.

Microinstabilities are present in DCX-2, as evidenced by the energy spread and by radio-frequency emission. The latter is remarkable in that harmonics of the ion gyrofrequency up to about the 100th have been observed. However, no particle losses have yet been detected as directly associated with the microinstabilities.

INJECTION INTO A HOT-ELECTRON PLASMA

Although fairly dense (5×10^{11} cm^{-3}) hot-electron plasmas have been produced by electron cyclotron heating, as in the apparatus called EPA, such plasmas by themselves are not of fusion interest because the ions are cold. One method of introducing hot ions is to shoot the particles in as neutrals (H^0 or D^0). The hot-electron plasma then serves as an ionizing target (or, more precisely, its cold-ion component serves as the target), and the incoming neutrals are trapped in the magnetic field by collisional ionization.

Experiments of this kind have been started in EPA. The apparatus is shown in Fig. 2. Starting with an ion source, H^+ and H_2^+ ions are accelerated to 40 kev, and then passed through gas in a long injection tube. Here they are converted to neutral hydrogen (40- and 20-kev H^0), and, preserving the directionality of the original beam, they are sent across the magnetic field into the electron cyclotron plasma. A current of neutrals equivalent to about 20 ma is used.

The atoms that are ionized in the plasma are caught in the magnetic field, and circulate as stored H^+ ions until they encounter a background gas molecule and reneutralize themselves. They then fly out of the magnetic field and can be detected by instruments so located as to be well clear of the primary injected beam. Thus a decay time for the fast trapped ions can be measured, if the injected beam is cut off, while leaving the hot-electron plasma present.

Even without the hot-electron plasma, a few of the injected neutrals will be ionized and trapped. Thus it becomes possible to compare the decay times for the trapped ions in the presence, and in the absence, of the hot-electron plasma.

The preliminary result of the experiment is that under comparable pressure conditions, the hot, stored ions last 15 times as long when the electron cyclotron plasma is present as they do when it is absent.

64-4366

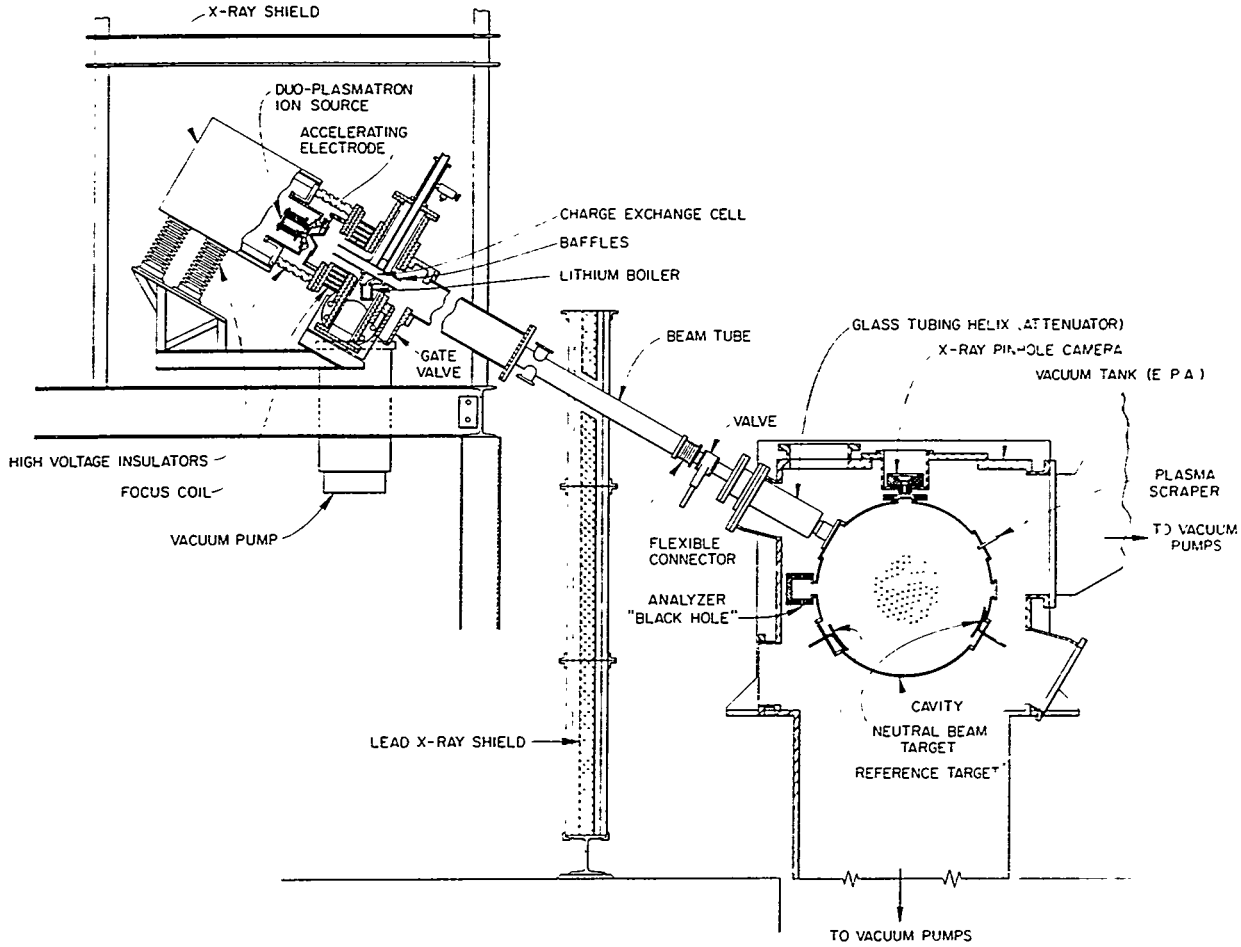

Fig. 2. Diagram of Neutral Injection Experiment, Using Plasma as a Target. The ion source is at the left, and it, with the sloping tube, constitutes the gun which shoots 20-kev H^0 atoms into the plasma. The plasma is created by electron cyclotron heating between magnetic mirror coils that are not shown, inside a cylindrical microwave cavity that is shown end on. The beam tube is about 10 ft long.

ION HEATING BY BEAM-PLASMA INTERACTION

In research toward controlled fusion, ions in a deuterium plasma have to be heated to the neighborhood of 200,000,000°, or 20,000 ev. We have discovered and studied an unexpected steady-state heating mechanism. It is based upon the interaction of an electron beam with the self-generated plasma that it creates when it is shot through a gas in a magnetic field, and typifies some of the peculiar properties of plasmas.

In Fig. 3*a*, a hot filament at one end emits electrons that move from left to right, along the direction of the magnetic field. An accelerating voltage of about 5000 v is applied, and when gas is admitted into the vacuum system, the beam generates a sharp-edged luminescent plasma column, as the photo shows. Now if the beam power is increased, or if the gas pressure is decreased, the plasma column can abruptly change to the fuzzy appearance of Fig. 3*b*. This is the mode of operation that generates the hot ions.

If the magnetic field is changed so that it is weaker at the center than at the ends of the electron beam (i.e., if the beam runs between so-called magnetic mirrors), the hot ions congregate in rotary motion, around and through the electron beam, in

the central, weak-field region. Figure 4 shows a sketch of the arrangement in cross section; both the beam and the magnetic field are now normal to the paper. To measure the ion energy, a detector and a curved deflection channel were introduced, as shown. When a given voltage is applied to the deflection plate, ions of only one energy can reach the detector. The measurements showed that in a deuterium plasma, deuterons of 20,000 ev are indeed produced in good quantity, although unfortunately not all of the deuterons get this hot. The plasma action transforms longitudinal energy of electrons at 5000 ev to rotary energy of ions at 20,000 ev.

R-120

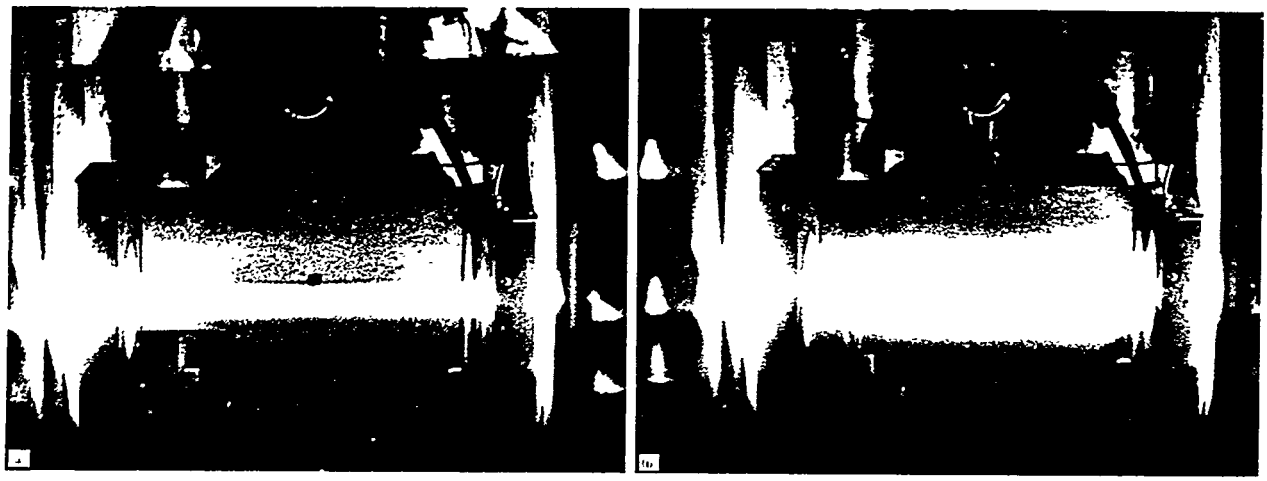

Fig. 3. Beam-Plasma Interaction. (a) Normal, quiescent plasma. The axial magnetic field runs left to right; in these pictures there is a plasma source at each end of the plasma column. (b) Ion-emitting plasma. Note the broad band of light which is due to energetic ions ejected across the magnetic field.

64-11762 R

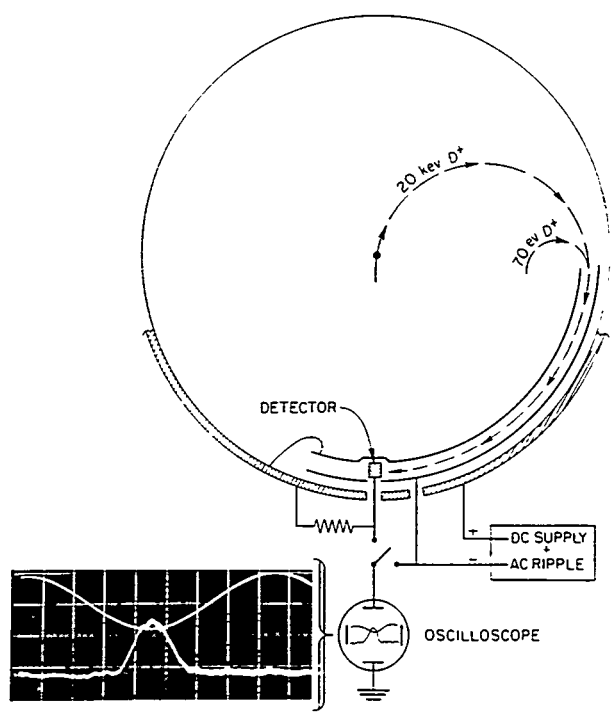

Fig. 4. Measurement of the Energy of Ions Heated by Beam-Plasma Interaction. When a given voltage is applied between the two plates that make the curved channel in the lower right quadrant, ions of only one energy can reach the detector. The use of an alternating-current ripple and oscilloscope is a physicist's neat way of recording the measurement.

65-796 A

FLUTE SUPPRESSION ON THE HYDROGEN ARC

The confinement of hot plasma in magnetic fields is a central problem in controlled thermonuclear research. One dangerous way by which plasma can escape is by the formation of flutes on the plasma surface, which curl outward and permit some of the plasma quickly to escape from the magnetic trap. In cross section, the flutes may look qualitatively as illustrated in the sketch (Fig. 5); they extend along the length of the plasma in the direction of the magnetic field and may be several feet long.

At Oak Ridge, the flutes have been studied using a locally developed vacuum arc, fed with deuterium gas, the arc running steadily down the magnetic field between electrodes in a vacuum environment. When a conventional magnetic trap is used (Fig. 6*a*), the flutes are observed, and they have been fully characterized as to size and as to radial and angular velocity as they move outward.

Recently it has been observed that if the arc is shifted so that it runs through only one coil (Fig. 6*b*), the flutes are dramatically suppressed. The finding is interpreted in terms of the curvature of the magnetic lines of force; when they are convex

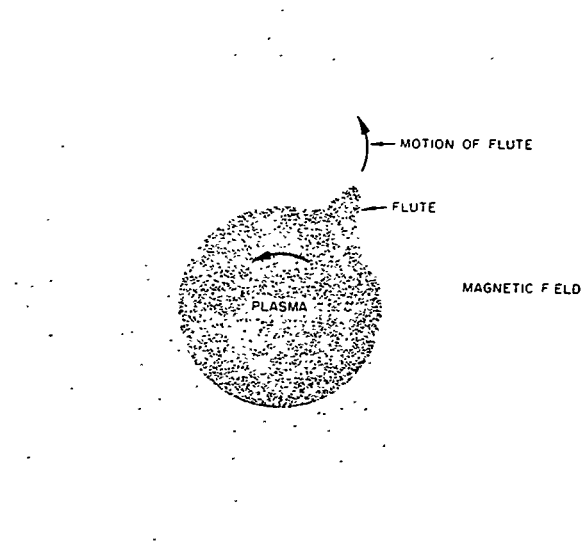

Fig. 5. Flute Formation. Cross section of plasma in a magnetic field normal to the paper, showing schematically the formation of a surface flute and the plasma loss that results when the flute swings outward.

65-797

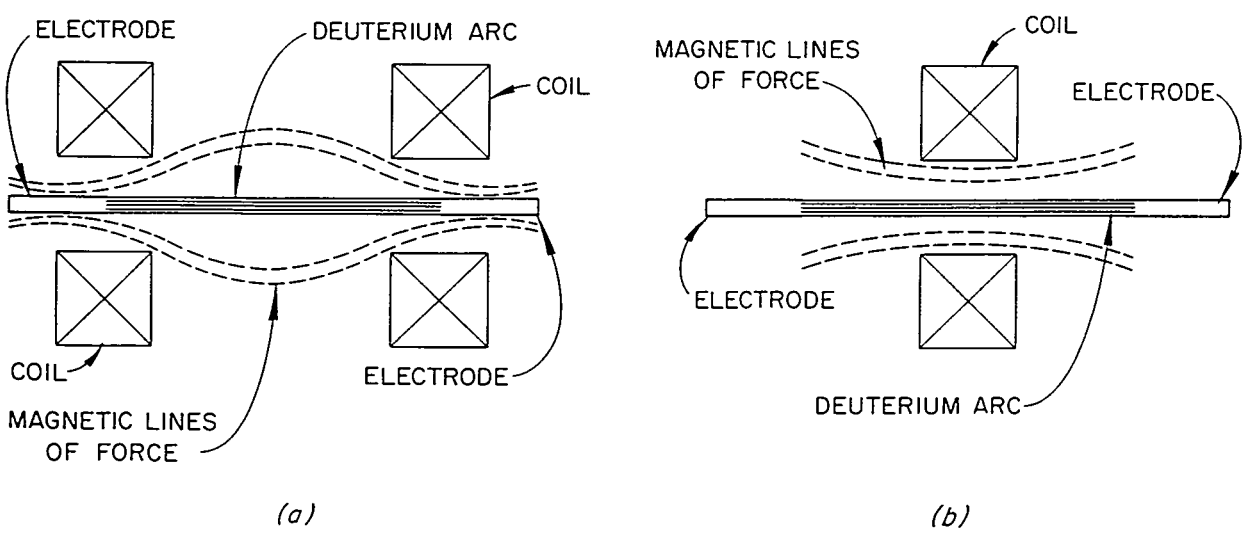

Fig. 6. Flute Stabilization. (a) Arrangement of deuterium arc running between electrodes in a conventional magnetic trap. The lines of magnetic force are concave toward the arc over much of their length, and the arc is flute-unstable. (b) A shift of the electrodes makes the arc run through one coil only. The magnetic lines of force are convex toward the arc, and the plasma in the arc is flute-stable.

PHOTO 68464

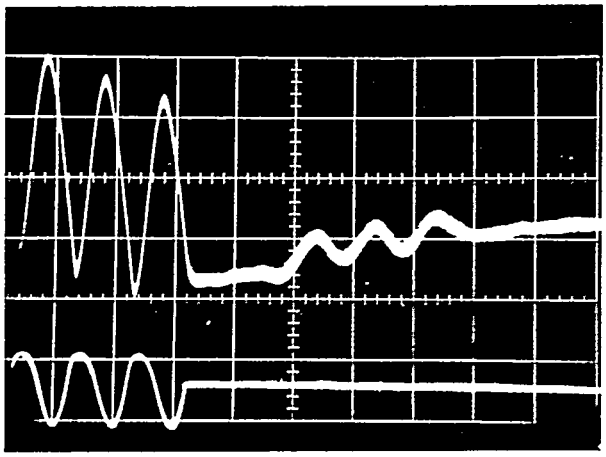

Fig. 7. Velocity of Ion Sound Waves by Time-of-Flight. The lower trace shows three sine-wave voltage pulses as applied on the transmitting plate in the ion-sound-wave experiment described in the text. The upper trace, reproduced with greater amplification, shows the signal registered by the receiving plate. Direct capacitive coupling gives the larger oscillations that are simultaneous with the oscillations on the transmitter. Ion sound waves produced the smaller wiggles, delayed by the propagation time from transmitter to receiver. The time scale is 10 μsec per division.

toward the arc (as in Fig. 6*b*), the flutes do not develop. Unfortunately this configuration is not itself a trap useful for controlled fusion; so intermediate cases are now under study in which the magnetic curvature is partly "good" and partly "bad." If some regions of "bad" curvature can be tolerated, the engineering difficulty and expense of constructing an effective trap may be relieved.

ION SOUND WAVES: VELOCITY MEASUREMENTS BY TIME-OF-FLIGHT

A glass bulb about a foot in diameter contains gas at low pressure. At one end, an anode-cathode arrangement creates plasma, which fills the rest of the bulb. From two opposite sides, flat plate-like electrodes are mounted, facing one another a few inches apart. One of these plates acts as a transmitter, and the other is used as a receiver.

A few pulses of alternating voltage are applied to the transmitting plate, and then it is kept quiet. An oscilloscope connected to the receiving plate now sees two signals. The first signal is a reproduction of the pulses that were applied to the transmitter, as a result of direct capacitive coupling between the two plates. Some time later, the second signal appears. It is due to the ion sound waves that were generated by the application of voltage to the transmitter, which take a finite time (about 50 μsec) to pass from transmitter to receiver. Figure 7 shows the instantaneous and the delayed signals as registered on the receiver. A measurement of the time delay from the oscilloscope trace and a knowledge of the distance between the plates permit a direct and simple evaluation of the ion sound wave velocity.

THE MAGNET LABORATORY

The availability of abundant dc power and large cooling facilities has led to the establishment of a Magnet Laboratory in the Thermonuclear Experimental Building. The Magnet Laboratory contains at present two high-field dc solenoids, and two more are planned. The existing solenoids are (1) a 3.5-Mw solenoid that gives 60 kilogauss in a volume 6½ in. in diameter and about 4 in. long, and (2) a 7-Mw solenoid that gives an 85-kilogauss field 6½ in. in diameter and about 6 in. long. The third solenoid is under construction now; it will be a large-bore device (13 in.) with a 65-kilogauss field that will be unique in the world in that it will be homogeneous to the eighth order over an amply large experimental volume. The fourth solenoid is now being planned as a Helmholz pair; it will be the only facility with an equatorial gap.

These powerful direct-current, steady-state magnets make our Magnet Laboratory the equal of any other large-volume facility in the world. The solenoids are being used for tests of superconducting coils, for other magnet development, and for instrument testing, and they have been used also for magnetohydrodynamic fluid-flow experiments in the Reactor Division. They are available for other experimental work within the ORNL research divisions. The director of the Magnet Laboratory is W. F. Gauster.

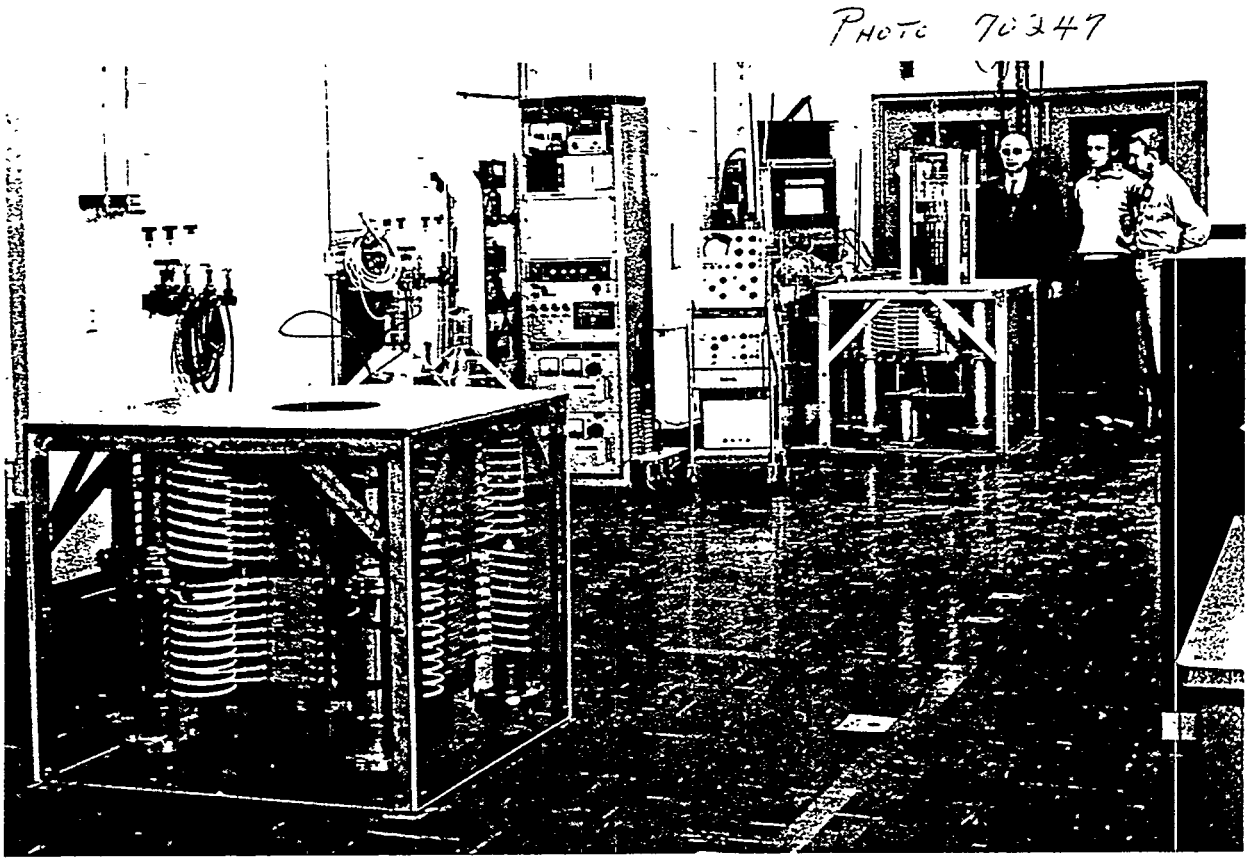

Fig. 8. Magnet Laboratory. Two of the planned complement of four solenoids are shown. In the foreground is the 7-Mw solenoid, and in the background is the 3.5-Mw solenoid, with a liquid-helium Dewar in place for an experiment on superconductivity. Both solenoids were locally designed and manufactured.

THE ATOMIC AND MOLECULAR PROCESSES INFORMATION CENTER

The year 1964 saw the formal organization at ORNL of an information center concerned with the collection, review, and dissemination of experimental and theoretical information relating to certain kinds of atomic and simple molecular collision processes. The sections of this enormous field that have been selected for specialization are ion-ion and ion-neutral collisions, excitation and ionization by external fields, and energy losses during passage through matter.

This activity is an outgrowth of more than a decade of experimental research by C. F. Barnett on the measurement of atomic collision cross sections. Barnett had, in the course of his work, assembled a compilation of cross-section data that he issued in a volume called "σ-CTR," which is shorthand for "cross sections of interest to workers in the field of controlled thermonuclear reactions." In 1964, a second, enlarged edition of this work was issued; both editions received wide professional acceptance.

Last autumn, the National Bureau of Standards recognized this information center as a unit of the National Reference Data System. Barnett will act as the director, and he plans to preserve a close relationship between the activities of the information center and the continuing activities of the research group.

ART WORK – No NUMBER

BIOLOGY AND MEDICINE

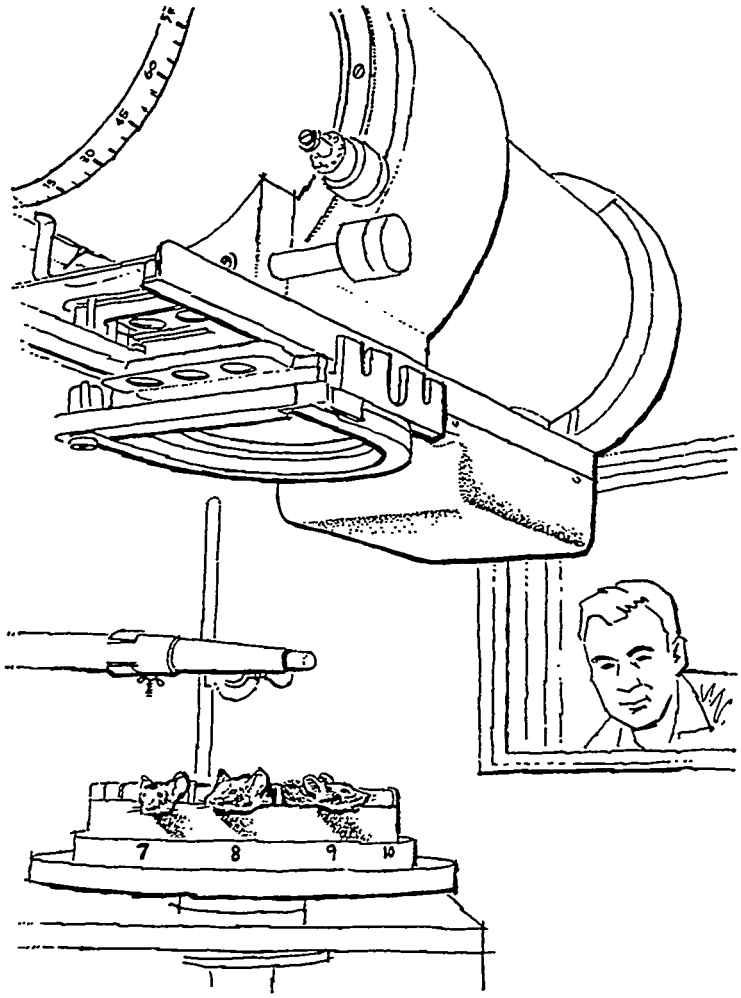

SOMATIC EFFECTS OF RADIATION

STATISTICAL SERVICES AND RESEARCH

A staff of statisticians and supporting personnel in the Mathematics Division is actively engaged in basic research in statistics and biomathematics and is also providing consultative services in the design and analysis of experiments. In recent years this group has demonstrated applications of the theories of Markov chains and spectral analysis to numerous problems in the biological and physical sciences. Among the more interesting applications of statistics to a problem in biology was a study of the human karyotype. Data on the length of chromosome arms were collected in an effort to estimate the errors of measurement attributable to various sources. Mean lengths of the long and short chromosome arms were computed, and simultaneous confidence regions were placed on the means for each chromosome in a cell. These regions take the form of ellipses in the plane of the long-arm and short-arm means. One ellipse was plotted for each chromosome, with the center at the point specified by the mean lengths of the long and short arms. When all ellipses had been plotted on the same graph, the overlap gave some indication of the inability (using present techniques) to tell one chromosome from another solely on the basis of length measurements.

A series of experimental designs of the factorial type, but modified along the lines of response-surface designs, were developed and recommended for use by biologists working on mammalian recovery. The excellence of the results obtained is directly attributable to the use of the recommended experimental designs.

Similarly, a design recommended for studying the uptake of strontium by small marine animals resulted in a rather complete description of strontium uptake as a function of the concentration of strontium and calcium in the animal's habitat.

A study of methods of approximating the quantiles of probability density functions was begun. A simple formula was discovered which approximates certain quantiles of Student's t distribution with a maximum error of one unit in the fourth decimal place.

Further study was made of the method of maximum likelihood as a means of estimating parameters of a structural relations model. This resulted in a complete solution to the problem as it was formulated with respect to experiments in the fractionation of radionuclides.

PATHOLOGY AND PHYSIOLOGY

Radiation-Induced Myeloid Leukemia

Leukemia Virus. – Attempts to isolate the virus responsible for transmission of radiation-induced myeloid leukemia in mice have been carried out with the ultracentrifuge and electron microscope. Cell-free extracts of leukemic tissue, which transmit the disease, have been found to contain numerous tailed particles similar in many respects to other mouse leukemia viruses. The presence of such particles in uninoculated mice developing leukemia after irradiation, and their rarer occurrence in normal controls, is compatible with the hypothesis that they represent a latent leukemogenic virus which is activated by irradiation.

This interpretation is supported by the observation that bacteriologically sterile mice reared and maintained in a sterile environment (Fig. 1) develop as high an incidence of leukemia after whole-body x irradiation as their conventionally reared counterparts do. Such mice, furthermore, show virus particles in their leukemic tissues similar to those mentioned above. These results suggest that the leukemia virus may be acquired via the fertilized egg or placenta and not necessarily through environmental contact.

Chromosome Aberrations. – Although it is not known how the leukemia is caused by the virus, mice with the disease have consistently shown chromosomal changes in their bone marrow cells. It is tentatively postulated, therefore, that the leukemia virus, once activated by irradiation, may cause the leukemia by direct injury to the chromosome.

These chromosome changes set this leukemia apart from the other animal leukemias that have been studied to date and suggest that it may afford a model system in which to investigate the cause and significance of the similarly characteristic chromosome abnormalities in chronic myelogenous leukemia of man.

PHOTO 39208

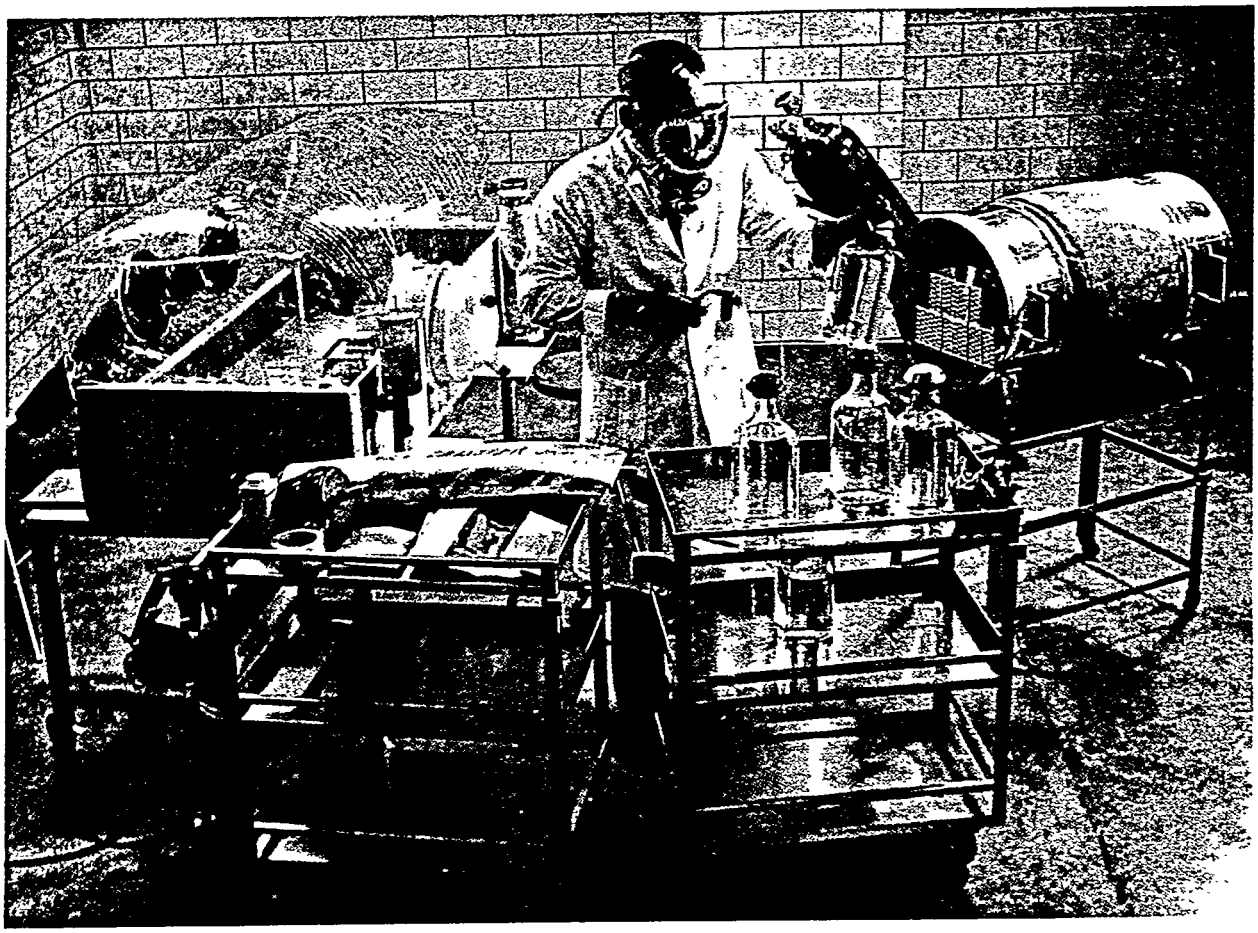

Fig. 1. Leukemia Studies. One of the many steps in preparing a germ-free environment for mice. Here a technician sprays water bottles. Shown at right is a stainless steel cylinder that contains food and bedding; at left, an isolator equipped with rubber gloves for manipulating environment from outside. Food and water are transferred into the isolator in a careful procedure designed to keep pathogenic organisms to a minimum. Germ-free mice are being used in research on viruses involved in human leukemia, and serve as "base-line animals" for comparison with mice raised and maintained normally. Such studies suggest that myeloid leukemia virus may be acquired via the fertilized egg or placenta and not necessarily through environmental contact.

RADIATION GENETICS

CYTOLOGY AND GENETICS

Studies on Reparable Premutational Lesions with Alkylating Agents

Earlier work has shown that a large part of the mutations induced in *Paramecium aurelia* by x rays, alpha particles, and ultraviolet light are initiated as reparable, premutational lesions that become fixed as final mutation at the first postirradiation chromosome duplication. Evidence has now been obtained that the same thing is true for mutations induced by the alkylating agents nitrogen mustard and triethylenemelamine (TEM). The same kinds of evidence – reduction in mutational yield by posttreatments given after exposure to the alkylating agent but before synthesis of deoxyribonucleic acid (DNA); a decrease in mutation as the time between exposure and DNA synthesis is increased – were obtained as for radiation. TEM is quite suitable for such studies, since it has little if any effect on the cell cycle at exposures that yield large numbers of mutations, but nitrogen mustard has large effects on the cell cycle at such exposures. The fact that repair occurs after such a variety of mutagens suggests that the repairing enzymes can act on a wide range of different initial lesions in the DNA.

Repair of Damage Induced in DNA by Ultraviolet Radiation

When cells are exposed to ultraviolet radiation, their deoxyribonucleic acid (DNA) is altered. Since DNA is the repository for cellular information, any changes that radiation induces in DNA can have profound effects on the ability of cells to survive or mutate.

We have discovered that some cells possess the ability to repair damage to their DNA that is caused by ultraviolet light (uv). This discovery has great importance for the study of mutagenesis and dose-rate effects, since it indicates that to a large extent the sensitivity of cells to radiation of any kind is determined by how well they repair damage caused by the radiation.

Error-Correcting Mechanism. – In many cases, uv damage to DNA molecules consists of a rearrangement of thymine groups. Thymine is one of four pyrimidine groups whose arrangement along the twisted DNA molecule constitutes the hereditary code. Normally, thymine groups are not linked to one another, but uv produces such links, or dimers. These links are "errors" in the extremely long DNA chains and are apparently recognized by certain enzymes and cut out of the chain. The censored sections are then replaced by the correct sequence. How this is done is still uncertain, but it seems to be related to the double structure of DNA, which consists of two matching strands twisted around one another like a twined rope. If one strand is damaged, the other still has clues to the correct sequence.

In commenting on these findings, Dr. Renato Dulbecco of the Salk Institute for Biological Studies in San Diego, a leading authority in the field, has observed that this discovery may constitute the first clue to a complex system of error correction by enzymes. If so, all present theories regarding genetic changes and, perhaps, the origin of cancer "will have to be changed."

The discovery of such enzymatic repair has pointed out important difficulties in studying the molecular bases of mutagenesis. Between the mutations which are formed at first in DNA and those finally detected there exists a series of screens – error correction, degeneracy of the code, and variable influence of different amino acid substitutions on protein function. Other factors, however, *promote* mutagenesis. It has been found, for example, that the acridine dyes interfere with the excision of thymine dimers; thus, by suppressing error correction, they may cause mutagenesis.

We are currently investigating several aspects of the enzymatic recovery mechanism by chromatography and gel filtration.

Repair Enzyme. – Since recovery from injury is accomplished by repair enzymes, it is important to determine the nature of these enzymes and what parts of the damaged molecules in the cell they affect. Other investigators in the Biology Division have achieved a purification of one repair enzyme, the photoreactivating enzyme from yeast, approximately 4000-fold over the crude extract. The crude extract contains a large number of proteins, most of which do not have this repair function. This is the first time any repair enzyme has been purified to such a degree. The result of this purification suggests that the photoreactivating enzyme is similar to some enzymes that are used in cellular respiration, and that it could have evolved as a mechanism of adaptation in the evolution of the cellular respiration system.

Biologically active purified DNA irradiated with uv loses activity, which can be partially restored with preparations of yeast extract administered in the light; this process is called photoreactivation. When irradiated with uv, synthetic polynucleotides of known composition and simpler than DNA may form photoproducts similar to those of uv-irradiated DNA. The photoproducts in the polynucleotides may interfere with photoreactivation of DNA by competing for the yeast enzyme.

By measuring the amount of uv photoproducts in the synthetic compounds, as well as their ability to compete for enzyme with DNA, it is possible to find which uv-induced damages in DNA are repaired by the yeast enzyme, and whether they are important in the restoration of biological activity. With this method the specific uv-induced changes in irradiated DNA which are concerned with photoreactivation have been determined. These changes are concerned with linkages between pyrimidine units, which, like thymine, absorb ultraviolet light.

Are Sister Chromatid Exchanges Sister Strand Crossovers or Radiation-Induced Exchanges?

When chromosomes are labeled with tritiated thymidine, it is found that at the second metaphase following labeling, sister chromatid exchanges are visible. Taylor, who first observed this phenomenon, reasoned, from the ratio of such exchanges that affect both homologous chromosomes (twin) to those affecting only one member of a homologous pair (single), that the strands within a chromatid are polarized. If the strands were not polarized, a ratio of at least 10 singles to 1 twin would be observed. The actual ratio found was 1 single to 2 twins.

The above ratios are based on the hypothesis that the exchanges are caused by spontaneous sister strand crossing-over that is equally probable in either of the two cell cycles that occur between labeling and the metaphase at which the observations are made. The expected ratio of singles to twins when the strands are polarized is 2 to 1 and not the 1 to 2 observed.

Because (1) there is this discrepancy in the ratios, (2) sister strand crossing-over has been very difficult (or impossible) to observe genetically, and (3) incorporated tritiated thymidine can induce chromosome aberrations, we decided to analyze the possible results if the sister strand exchanges were radiation-induced and not spontaneous sister strand crossovers.

If the strands within the chromatids are polarized, then any exchange that occurred in the first cell cycle would appear as a twin at the second division, whereas an exchange that occurred in the second cycle would be a single. At the first cell cycle, both chromatids are labeled. The dose of radiation from incorporated isotope then will be proportional to 2, and the yield of radiation-induced exchanges, which increase as the square of the dose, will be proportional to 4. At the second cell cycle, only one chromatid per chromosome is labeled. The dose of radiation will thus be proportional to 1, as will the yield per diploid genome. There are, however, twice as many chromosomes present, so the yield of singles will be proportional to 2. The expected ratio of 2 twins to 1 single is exactly the ratio observed in the experiments.

We conclude that sister strand exchanges are more likely radiation-induced exchanges than spontaneous sister strand crossovers.

X-Ray-Induced Forward Mutation Rates for Mutants in the *ad-3* Region of *Neurospora*

A heterokaryon of *Neurospora* that permits the recovery and analysis of both $ad\text{-}3^{R}$ mutants (reparable on adenine-supplemented medium) and $ad\text{-}3^{IR}$ mutants (irreparable both on adenine-supplemented minimal medium and "complete" medium) has been

used to study the kinetics and mechanism of mutation induction by 250-kv x rays. Samples of mutants recovered after exposures of 1, 2, 5, 10, 20, and 40 kr have now been characterized with respect to reparability and genotype. Although the frequency of all *ad-3* mutants increases as the 1.3 power of the dose, the analysis has shown that *ad-3*^{R} mutants increase in direct proportion to the dose, while *ad-3*^{IR} mutants increase as the square of the dose. This leads to the interpretation that *ad-3*^{R} mutants result each from single hits inside the *ad-3A* or *ad-3B* locus, while *ad-3*^{IR} mutants each result predominantly from two hits located in the regions immediately adjacent to or between the *ad-3* loci. If the latter lead to interstitial deletion, in *ad-3*^{IR} mutations one or both of the *ad-3* loci would be inactivated in addition to other loci in the immediately adjacent regions.

The mutation rate for *ad-3*^{R} mutants is merely the proportionality constant between the dose (x) and the mutant yield (y). The parameter for all *ad-3*^{R} mutants is 6.6×10^{-6} mutant kr^{-1} survivor^{-1} (2.2×10^{-6} for *ad-3A*^{R} mutants and 4.4×10^{-6} for *ad-3B*^{R} mutants). The *ad-3B* locus, therefore, appears to be twice as sensitive (maybe twice as long) as the *ad-3A* locus. For *ad-3*^{IR} mutants the relationship between mutant yield and dose is $y = a^2x^2$, where a represents the average rate of production and recovery of hits which can interact in pairs to cause *ad-3*^{IR} mutants. This parameter has a value of about 5×10^{-4} hit kr^{-1} survivor^{-1}. There is evidence to suggest that this parameter underestimates the true incidence of these events in the *ad-3* region. Two such events which do not include one or both *ad-3* loci should also cause irreparable damage, but would not be recovered as an *ad-3*^{IR} mutant. It appears that two such events either will not interact to cause a mutation or will not be recovered if they are too far apart. One might have expected that the *nic-2* locus located 2 to 3 map units to the right would have also been inactivated in many *ad-3B*^{IR} or (*ad-3A ad-3B*)^{IR} mutations; however, few (*ad-3A ad-3B nic-2*)^{IR} mutants or (*ad-3B nic-2*)^{IR} mutants were found among the *ad-3*^{IR} mutants analyzed genetically. With a heterokaryon it has been possible to obtain a class of x-ray-induced mutants in forward-mutation experiments which previous techniques have not detected in *Neurospora* and to show that they result from events at least 70 times as frequent as the events that lead to the reparable biochemical mutants.

Mammalian Cytology and Cytogenetic Effects of Radiation

This research program is primarily concerned with the cytogenetic effects of radiation and other mutagens on mammalian cells, both in vitro and in vivo. These studies have included the formal aspects of mammalian cytogenetics (including human), chromosome cytology of mammals, and induction of cellular changes by radiation.

The effects of radiations and chemicals can be measured by a variety of cytogenetic criteria including chromosome aberrations, mitotic inhibition, gene mutation, and capacity for reproduction and survival. We are currently attempting to correlate these phenomena with the concomitant modifications in synthetic and metabolic processes in the treated cells. The cell cycle and stage radiosensitivity, the architecture and the mode of replication of chromosomes, and the mechanism of chromosome breakage and rejoining are being investigated. One area of special interest is the comparison of the radiosensitivity in terms of induced chromosome aberrations between human, mouse, and other mammalian cells in vitro. This comparison will provide a base line for extension to in vivo studies on laboratory animals, and will be useful in making estimates of the genetic hazards of radiation and other mutagens to humans.

Since neoplastic transformation involves certain permanent hereditary changes of the cells, it is of interest to characterize such changes and to find the underlying mechanisms. Experiments are in progress to correlate the mutagenesis and carcinogenesis in mammalian cells. It is through expansion of basic knowledge of normal living matter that one can understand abnormal changes, whether one is dealing with the effects of radiation or with atypical growth.

It has previously been shown that the effectiveness of inducing chromosome aberrations with ultraviolet light (uv) at different wavelengths approximately parallels the uv absorption spectrum of nucleic acids. Cells with thymidine substituted by its analogs are significantly more sensitive to uv. The wavelength dependence for chromosome aberrations in analog-substituted cells is similar to the uv absorption spectra of these analogs. These results strongly suggest that the initial damages to deoxyribonucleic acid (DNA) account for the majority of uv-induced chromosome breakages.

Chemical analysis of chromosomal DNA from irradiated mammalian cells showed that thymine dimers are formed by uv. Evidence was obtained that neither splitting of dimers by photoreactivation nor cutting out of dimers by the dark repair process recently found for bacteria occurs in mammalian cells. Photoreactivation was not observed for chromosome aberrations. The relation between thymine dimers and chromosome breakage is yet unclear.

Cell stage sensitivity to uv or x rays in terms of chromosome aberrations has been studied, both with random cell populations and with chemically synchronized populations. Results from both types of experiments indicate that the frequency of the x-ray-induced chromatid aberrations reached a peak after DNA synthesis (stage G_2), whereas that of the uv-induced aberrations was the highest during DNA synthesis (stage S), particularly at early S. Although chromosome aberrations can be induced by uv in all stages of the cell cycle, this result probably indicates that chromosomes are more vulnerable to uv irradiation during replication. Since the various stages of the mitotic cycle respond differently to the same dose of one type of radiation, and respond differently to different types of radiations, these measurements are essential for estimation of dose-effect relationships and radiation hazards to man. These measurements of stage sensitivities are also being used in the search for the biochemical mechanisms of chromosome breakage and rejoining and other cellular damage following radiation exposure.

Attempts have been made to study the nature of radiation resistance in human cells. In studies with x-ray-resistant clonal derivatives of human amnion cells grown in vitro, we are attempting to find if the resistant cells lose less DNA or if they can repair the damage after irradiation, and to discover if and how radiosensitivity of cells can be manifested at the enzymatic level. This investigation is being carried out with electrophoretic techniques. Cytological examinations of possible chromosome changes are being made.

Studies on the incorporation of radioactive isotopes into chromosomal DNA can reveal the time sequence of replication in different regions of chromosomes. This asynchronous nature of DNA synthesis along chromosomes has been shown to occur in cells of a number of organisms; we have studied the pattern of DNA synthesis in normal chromosomes and in X-autosome translocations in the mouse. The results reveal small but discrete differences in the timing of DNA synthesis between the two X chromosomes in female mice, and should permit cytologic identification of the X chromosome and autosome involved in the translocation. At least part of the translocated autosomal segment retains its autonomous timing of replication. Genetic evidence indicates a limited influence from X to autosome with respect to gene inactivation. The present cytological evidence establishes the independence of gene replication in the distal autosomal part of an X-autosome translocation, corroborating the genetic finding of limited spread of inactivation.

DROSOPHILA CYTOLOGY AND GENETICS

Distributive Pairing and Aneuploidy in Man

The simultaneous occurrence of various kinds of rare chromosome abnormalities within single human families has led a number of authors to suggest that these events are not fortuitous. The coincidence of similar kinds of events has been observed in the female of the fruit fly, *Drosophila melanogaster*, where the principles underlying chromosome behavior during meiosis have been elucidated and incorporated into the "distributive pairing" theory of meiosis. According to this theory, which was developed from studies on *Drosophila* at ORNL, two types of pairing, rather than just one, occur during meiotic division of germ cells. Homologous pairing (i.e., highly specific pairing necessary for exchange) occurs first and is followed by a second type of pairing, termed distributive pairing, which determines segregation. Chromosomes that have undergone exchange, and are presumably physically joined, disjoin regularly and have no opportunity to join with a nonhomolog. Chromosomes that have not undergone exchange make up a pool whose members may pair homologously or nonhomologously or not at all, depending on the composition of the pool.

By applying this theory of meiotic division to man, we have provided an explanation for a number of puzzling cases described in the cytogenetic literature, including (1) aneuploidy for an autosome in one individual and a translocation involving two

different autosomes in a related individual, (2) aneuploidy for a sex chromosome in one individual and a translocation between two autosomes in a related individual, and (3) aneuploidy for a sex chromosome in one individual and aneuploidy for an autosome in a related individual.

Medically the coincident occurrences of such karyotypic abnormalities are recognizable by the syndromes they produce – so that both mongolism and retarded mutism, or mongolism and sex mosaicism, or mongolism and Turner's or Kleinfelter's syndrome are observed in different members of single families. The incidence of each type of abnormality is so low that the premise of their independent origin is practically ruled out.

The distributive pairing hypothesis has been carefully tested in the fruit fly. Its application to human gametogenesis, while still speculative, provides a reasonable genetic explanation for hitherto anomalous events. Further research should reveal whether the interpretation is correct.

MAMMALIAN GENETICS

Induction of Mutations by Neutrons

For several years there have been urgent requests from national and international bodies to obtain data on the induction of gene mutations by neutrons in mice. Estimates of genetic hazards of neutron irradiation in man had to be based on theory or extensive extrapolation from limited information. The only neutron information on gene mutation in mammals was that obtained at ORNL from the small numbers of animals that had been placed in a cyclotron beam or enclosed in lead chambers exposed to a nuclear detonation. The recent construction of the Health Physics Research Reactor, however, has now made possible more extensive mouse mutation experiments. The reactor core, which is suspended beneath the reactor framework, can be positioned remotely in the center of a large rack of mouse cages. One great advantage of this reactor is that it can be used to test a wide range of dose rates. Ever since the discovery of a dose-rate effect of x and gamma radiation on mutation, it has been of vital importance, both from the hazard point of view and for an understanding of the fundamental nature of the dose-rate effect, to know whether or not a similar effect occurs with neutron irradiation.

In experiments with mouse spermatogonia, it has been found that at high doses and high dose rates the mutation frequency drops below that obtained at lower doses. This phenomenon parallels that reported for acute x irradiation and can be attributed to the same cause, which is believed to be selective elimination, at high doses, of the more mutagenically sensitive stages in the spermatogonial cells. This introduces a complexity into the calculation of relative biological effectiveness (RBE) and into the estimation of dose-rate effects. The difficulty can be avoided, however, by limiting comparisons to doses below the level at which the drop in mutation frequency is noticeable. At this dose, it has been found that dose rate does not significantly affect mutation frequency in spermatogonia – a finding in contrast to the marked dose-rate effects observed with x- and gamma-ray-induced mutations.

In spermatogonial experiments on the RBE of neutrons, a weighted mean dose of 60 rads resulted in 35 mutations in the 51,993 offspring examined; 300 r of x rays at 90 r/min resulted in 40 mutations in 65,548 offspring. The RBE of fission neutrons with respect to x rays as calculated from these two sets of results, with allowances for the gamma component in the reactor exposures and with conversion of the x-ray doses to rads, is 5.8; the estimate is not significantly different (5.1) when the comparison is limited to the high-dose-rate portion of the neutron data.

Since there is, so far, no evidence of a dose-rate effect for neutron irradiation of spermatogonia, it is clear that the RBE of neutrons with respect to x or gamma rays will be much higher at low dose rates. The ratio of mutation frequency per rad of x rays at 90 r/min to all gamma-ray exposures at 0.009 r/min and below is 3.3. The RBE of fission neutrons with respect to gamma rays for mutations induced in mouse spermatogonia at low dose rates can, therefore, be estimated as $5.8 \times 3.3 = 19.1$.

This estimate of RBE for low-dose-rate irradiation has been confirmed by an entirely independent set of neutron and gamma-ray data. In this neutron experiment a total dose of 101 rads delivered in 12.1 hr produced 20 mutations in 19,506 offspring. In the gamma-ray experiment, a dose of 576 rads delivered in 12.6 hr gave 10 mutations in 28,059 offspring. The gamma-ray data, although limited,

are supported by the fact that they are in exact agreement with the average mutation frequency obtained at all lower dose rates. The RBE calculated from this particular low-dose-rate neutron-gamma comparison is 18.1. This is in close agreement with the above independently obtained value of 19.1.

COOPERATIVE NIH-AEC CO-CARCINOGENESIS PROGRAM

Association Between the Complementation Type and the Reversibility of the Nitrous Acid–Induced *ad-3B* Mutants of *Neurospora crassa*. – During the last years the basic chemical reactions leading to genetic alterations have been identified in viruses and bacteria. In these organisms the nucleic acid is organized in a relatively simpler way than in higher organisms, where the nucleic acid is a part of chromosomes of complex structural organization. The association between the genetic alterations at the molecular level and the effect of these alterations on the enzyme structure and organization in the cell are important problems to be studied in higher organisms. The genetic alterations can be identified by measuring the reversibility of the mutants by specific mutagens, and the extent of the influence of the genetic damage at the protein level is likely to be reflected in the complementation patterns of the mutants. An attempt to correlate these two fields of study may be expected to provide information about the gene-enzyme relationship in higher organisms.

The use of nitrous acid (NA), ethyl methanesulfonate (EMS), and ICR-170 (a monofunctional acridine mustard) should permit one to distinguish the following three classes of genetic alterations: (1) single base-pair substitutions (revertible by NA and EMS), (2) single base-pair insertion and deletion (revertible by ICR-170 and possibly by EMS), and (3) other unidentified genetic alterations.

Among the nitrous acid–induced *ad-3B* mutants, three different classes of complementation patterns were found: nonpolarized, polarized, and noncomplementing. A priori one would expect mutants with nonpolarized patterns to be base-pair substitutions, and indeed 60 out of 67 appear to have this genetic alteration, whereas only 18 out of 28 of the polarity-type mutants and 19 out of 36 noncomplementing mutants apparently were base-pair substitutions. The mutants which revert only with ICR-170 (base-pair insertion and deletion type) are not found among those with nonpolarized patterns, but occur with the same frequency among those with polarized patterns and the noncomplementing class (4 out of 28 and 7 out of 36 respectively). Mutants which do not revert at all (no reversions found among 3×10^8 conidia) do not occur among those with nonpolarized patterns, but are divided equally among the polarized and the noncomplementing classes. We can therefore conclude that mutants with nonpolarized complementation patterns arose predominantly from base-pair substitutions, whereas other kinds of genetic alterations give rise to noncomplementing mutants and polarity-type mutants.

That the three different classes of genetic alterations mentioned above can be distinguished in *Neurospora crassa* implies many other possibilities, for example, the selection of a tester set of mutants resulting from various types of base-pair substitutions, insertions, and deletions. With such a tester set, many mutagens can be screened for their predominantly mutagenic action, and it would be particularly interesting to use compounds known to be antineoplastic with such a tester set.

COMBATING DETRIMENTAL EFFECTS OF RADIATION

MAMMALIAN RECOVERY

Effect of AET on Acute Lethality from Dimethylnitrosamine

In earlier work it was shown that some amelioration of damage to bone marrow, spleen, and thymus after administration of 9,10-dimethylbenzanthracene was provided by bone marrow transplantation. We are now engaged in a program to determine the value of radiation protection and recovery agents in preventing acute lethality from representative members of the different classes of chemical carcinogens. S,2-Aminoethylisothiourea (AET) administered before carcinogenic hydrocarbons and butter yellow failed to reduce acute lethality from these compounds. The present report shows that some protection against the acute toxicity of the highly carcinogenic substance dimethylnitrosamine (DMN) could be achieved with AET. Results were obtained for 19-week-old male and female $BC3F_1$ mice given AET orally before DMN was administered intraperitoneally. Three-tenths of a milligram of DMN killed 51% of the mice in these experiments, whereas only 15% were killed when AET was given a few minutes before the DMN. At lower doses of DMN the mortality was so low that an AET protection could not be demonstrated. With 0.4 mg of DMN, all mice died regardless of the AET protection. These results indicate that in a very restricted dose range of DMN, some prevention of acute lethality with AET could be achieved.

RADIATION IMMUNOLOGY

Aging and the Immune Mechanism

Although the immune mechanism of an individual is presumed to play an essential role in aging, very few systematic data have been available on the ability of an individual to respond to an antigen as a function of age. We have determined the antibody-forming potential of mice of varying age groups and of the spleens of donor mice from varying age groups. The purpose of the latter type of study was to establish whether the change in the immune system of an individual with age is due to a change in the functional lymphoid tissue or other factors. This study, which was carried out over a period of five years, confirms and extends earlier findings at the Laboratory.

Spleen cells of 1- to 126-week-old mice were cultured together with test antigen in heavily x-irradiated isologous 12-week-old mice. The results showed that the maximum growth rate of the primary antibody-forming potential of the spleen occurred during the first month after birth. The highest antibody-forming activity was obtained with cells of 40-week-old mice. The primary antibody-forming potential of the spleen increased 600-fold between 1 and 40 weeks of age. In contrast, the body weight increased only eightfold and the spleen weight fourfold. After 40 weeks of age the primary antibody-forming potential of the spleen decreased gradually with age. Evidence was obtained to show that the change in the primary antibody-forming potential of the spleen with age is due mainly to change in the number of potential antibody-forming cells rather than to change in the efficiency of antibody-forming cells or change in the number of antibody-forming cells arising from potential antibody-forming cells.

The pattern of change in the primary antibody-forming potential in spleen cells was comparable with that of intact mice, indicating that the change in the number of potential antibody-forming cells

in the spleen with age is not due to the immigration-emigration phenomenon of these cells but accurately reflects the immune potential of an individual.

Although these data show that growth and senescence of the primary antibody-forming potential of mice are reflections mainly of the number of potential antibody-forming cells, they do not indicate *why* this number changes with age. Nevertheless, the data suggest that one fruitful approach to understanding growth and senescence in other proliferating somatic tissues is to put greater emphasis on the undifferentiated stem cells capable of transforming into functional cells, rather than on the differentiated functional cells, as is commonly done.

AEC-NASA SPACE BIOLOGY PROGRAM

Dosimetry of Beta-Ray Irradiation Device for Radiation–Space-Flight Interaction Experiment

Dosimetric studies with the irradiation device for the radiation–space-flight interaction experiment to be performed in the Gemini III flight were completed. The principal dosimetric feature for irradiation of blood cells in the Gemini III vehicle is that blood samples in 3-mm-deep plastic containers are sandwiched between pairs of ^{32}P plaques of known activity. The plaques consist of thin ^{32}P layers deposited on platinum disks, 40 mm in diameter and 0.076 mm thick, backed by 0.76-mm-thick aluminum plates.

The total thickness of beta-ray shielding materials is no less than 0.7 g/cm^2; hence no more than 0.002 of the beta particles escape from the irradiation box. The efficiency of production of x-ray photons by beta particles absorbed in a target material is usually a few percent. We estimate that the ratio of beta particles to x-ray photons outside the irradiation box is no more than 0.03.

Calculation based on Loevinger's empirical formulas leads to about 500 rads/hr for a pair of 2.5-mc ^{32}P plaques, if backscattering effects of platinum disks and edge effects of ^{32}P plaques are neglected. The dose rate in the sample holders at standby position was about 10 rads/day.

Gemini III Experiment

The progress in this experiment up to December 1964 has been reported in the annual report, *Synergistic Effect of Zero-G and Radiation on White Blood Cells. An Experiment for the Gemini III Manned Space Flight,* ORNL-TM-940 (January 1965). The report contains a complete coverage of development and testing of the actual package to be used.

The Gemini III flight took place on March 23, 1965; the ORNL biological experiment was entirely successful and is reported in *GT-3 Final Mission Report.*

MOLECULAR- AND CELLULAR-LEVEL STUDIES

CYTOCHEMISTRY AND CELL REPRODUCTION

Mutagenic Action During Meiosis and Antimutagenic Action During Mitosis by 5-Aminoacridine in Yeast

Mutations induced by the acridines in the dark in bacteriophage have been attributed to base losses or base insertions, which shift the reading frame of the gene. Mutation induction by acridines in the dark has not been demonstrated in other organisms, although an antimutagenic effect has been reported in bacteria. In yeast, during vegetative growth (mitosis), it was possible to show that when the cells were grown in the presence of 10 μg/ml of 5-aminoacridine, the forward mutation frequency from canavanine sensitive to canavanine resistant decreased from 3.7×10^{-8} to 1.2×10^{-9}. For a presumed reading-frame mutant, hi_{1-1}, the reversion frequency decreased from 2.9×10^{-9} to 5.2×10^{-10}. During meiosis, when cells were pretreated and sporulated with 4 μg/ml of 5-aminoacridine, the forward mutation frequency ($CAN^s \rightarrow can^r$) increased from the spontaneous frequency of 4.5×10^{-7} to 1.1×10^{-5}. For hi_{1-1}, treated with 2 μg/ml of 5-aminoacridine, the reversion frequency changed from 3.8×10^{-9} to 1.8×10^{-8}. Thus the mutagenic and antimutagenic effects of acridine appear to be associated with stages of the life cycle where the amounts of genetic recombination differ.

CELL GROWTH AND DIFFERENTIATION

Epigenetic Control of Genes

Recent developments in genetics and biochemistry have clarified the physical nature of genes and the basic mechanism of the gene-controlled synthesis of specific proteins. Since the life of cells is controlled by proteins, this has been a great step toward understanding cellular life. However, these genetic principles are not sufficient for this understanding, because in the reality of cellular life particular genes are selected to function according to factors coming from outside the nucleus (where the genes are found), either from the cell's own cytoplasm or from the cellular environment. In higher organisms, unlike microorganisms, this selection is highly elaborated and often very stable. The mechanism of such "epigenetic" control of genes should be basic for understanding and control of growth and many pathological phenomena including cancer, malformation, and nervous disorders.

We are engaged in the study of epigenetic control of cellular specificity in vertebrate animals, utilizing autoradiography, immunochemistry, tissue culture, and electron microscopy. For this purpose a phenomenon called Wolffian lens regeneration has been selected, in which iris cells are transformed into lens cells when the normal lens is removed from the eye of a newt. We have used autoradiographic studies with isotopically labeled compounds and have found that when the lens of the newt is removed an increased synthesis of ribonucleic acid (RNA) and protein takes place in the iris cells. Following this increase in RNA and protein synthesis, the iris steps up its production of deoxyribonucleic acid (DNA). A period of proliferation follows. After cessation of DNA synthesis, the cells begin to synthesize lens-specific antigens and to differentiate into primary lens fibers. With immunofluorescent techniques it was possible to demonstrate that one group of lens-specific antigens, called γ-crystallins, are characteristic for lens fiber cells. These γ-crystallins are always synthesized when cells enter the fiber-differentiation stage, but never at any other time. Some of the data obtained indicate that during transformation the cells go through a condition similar to embryonic development (Fig. 1).

No Number

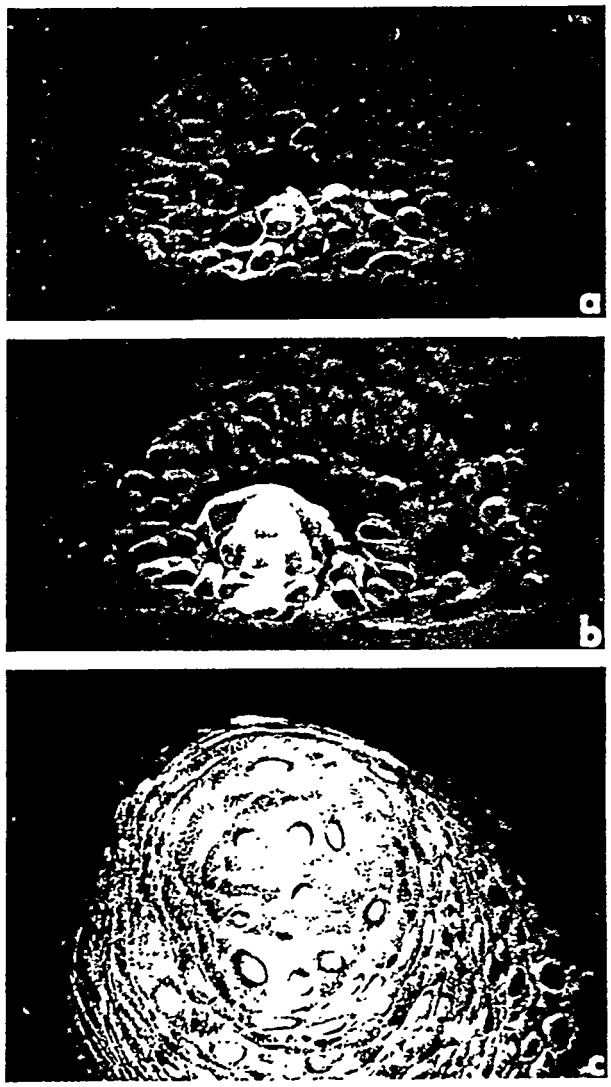

Fig. 1. Regenerating Lens. Pictured above are three stages in the development of a new lens in the eye of a lentectomized newt. Bright areas indicate the presence of γ-crystallins, which are always synthesized when cells enter the fiber-differentiation stage, but never at any other time. (*a*) Early stages of regeneration; only a small part of the cell population indicates a positive reaction. (*b*) The number of positive cells is increasing. The cytoplasm is intensely positive, while the nuclei show a weak reaction. (*c*) A small lens has formed; the main part of the lens (lens-fiber area) shows strong reaction for γ-crystallins. Cells tend to migrate downward around the central cavity, and as they move they begin to synthesize γ-crystallins. Combining the immunofluorescent technique with autoradiography, we demonstrated that γ-crystallin synthesis does not begin until DNA synthesis has ceased.

Since finding with the use of autoradiographs that lentectomy first induces an increase in nuclear RNA synthesis, we have also initiated an investigation into the role which RNA synthesis plays in morphogenesis. One approach to this problem was to apply actinomycin, which is known to suppress RNA synthesis dependent on DNA, to the regenerating cells during different stages in tissue transformation. We found that in the early phase of differentiation, when cells are still dividing, they are very sensitive to actinomycin, and development stops; when they are beginning to synthesize lens-specific protein, however, they become increasingly resistant to actinomycin. This result seems to indicate that RNA produced by the nuclei of iris cells after lentectomy is necessary for specific protein synthesis.

When x rays were substituted for actinomycin, results were obtained which have much in common with those obtained with actinomycin treatment. When the lens fibers begin to form they become relatively resistant to x rays. As the cells finish proliferation and enter the differentiation phase, the cytoplasm becomes independent of the nucleus.

This work represents a preliminary step in the understanding of the implications of the processes involved in tissue transformation as related to the control mechanism of normal and abnormal growth.

RADIATION MICROBIOLOGY

Postirradiation Growth, Division, and Recovery in Bacteria

Microscopic studies of the growth and division of irradiated bacteria on rich nutrient media have led us to postulate that ionizing radiation produces cell inactivation (loss of colony-forming ability) by affecting either processes leading to cell growth or processes leading to cell division. For any particular bacterial strain, one of these routes usually predominates. For example, cells of several strains of *Escherichia coli* produce long filaments after exposure to ionizing radiation. In these filaments, growth is initially normal, but the cell division mechanism has been damaged.

These filaments do not produce macroscopically visible colonies. Other strains of bacteria do not form filaments after exposure to radiation but simply fail to grow appreciably. It can be assumed that in these strains, processes leading to growth have been damaged.

Twenty strains of bacteria representing several genera have been examined after exposure to ionizing radiation and placed into two classes: (I) division inhibited and (II) growth inhibited. It was predicted that recovery of colony-forming ability would be observed if organisms of class I were exposed to agents known to stimulate cell division; likewise, it was predicted that recovery of organisms in class II would be favored by agents known to stimulate cell growth. These predictions have been verified. In this way we are bringing some order to what has previously been a bewildering array of recovery conditions applied to irradiated bacteria.

CELL PHYSIOLOGY

Freezing of Multicellular Systems

Although most cryobiologists believe that the formation of large ice crystals within a cell is invariably lethal, there have been recent reports that this is not so in some tissues. If verified, such findings would have important implications to theories of low-temperature injury. Knowledge of the physical events occurring in multicellular systems below 0°C should also be helpful in solving a current problem, namely, the freezing and thawing of whole organs with the full retention of function.

Whether or not ice formation occurs in single cells has been shown to depend on whether water is able to leave the cells during cooling rapidly enough to prevent its becoming supercooled. A differential equation describing the kinetics of water loss has been derived. Solutions to this equation for yeast, red blood cells, and sea urchin eggs agree reasonably well with experiment. The equation has now been extended to a model multicellular system, namely, a sphere composed of three concentric layers of cells and surrounded by ice. The kinetics of water loss are described by seven differential equations. Four of these give the vapor pressure of water in each layer and in ice as a function of temperature. The other three give the rate at which water moves from one cell layer to the next and finally out of the cell in response to the differences in vapor pressure between the layers. A computer program for the simultaneous solution of the seven equations has been developed, and solutions have been obtained for models having the dimensions and permeability characteristics of mammalian cells. One interesting conclusion to emerge to date is that even when the system is cooled at 1°C/min, a rate generally thought to be optimal, it is possible for the cells in the innermost layer to freeze intracellularly while the cells in the outer layers are dehydrating without freezing.

SUBCELLULAR AND VIRAL PHYSIOLOGY

Isolation of Rat Macroglobulin in the Zonal Centrifuge

High-molecular-weight antibodies and macroglobulin are widely distributed and of considerable immunological importance. Although good separations of small quantities of material have been obtained by rate zonal centrifugation in swinging-bucket rotors, the separation and purification of macroglobulin in quantity is difficult. We have applied the zonal centrifuge for the purification of rat macroglobulin and have carried out physical and chemical studies on the highly purified product.

The macroglobulin from 60 ml of pooled rat serum, partially purified by two precipitations in 40% ammonium sulfate and exhaustive dialysis against tap water, was separated in the B-IV zonal rotor on a 1-liter 10 to 20% sucrose gradient containing phosphate buffer (pH = 7.5, μ = 0.1) by centrifugation to $4 \times 10^{11}\ \omega^2 t$ (approximately $6\frac{1}{2}$ hr at 40,000 rpm). Each run yielded 200 to 300 mg of macroglobulin. The preparation was ultracentrifugally and immunoelectrophoretically pure. Electrophoresis at pH's from 3.5 to 8.5 gave a single peak. The isoelectric point was 4.38; the carbohydrate content was 10%; the partial specific volume calculated from the amino acid analysis was 0.743. A molecular weight of

859,000 was calculated from diffusion and sedimentation data ($S_{20,w} = 20.0$, $D_{20,w} = 2.22 \times 10^{-7}$ cm^2/sec). Treatment with 0.1 *M* mercaptoethanol dissociated the macroglobulin into smaller units (approximately 7S).

The usefulness of the zonal centrifuge for the preparation of large quantities of rat macroglobulin has been demonstrated. The quantities obtained are adequate for physical, chemical, and immunological studies. Preliminary studies demonstrate that the technique is applicable to other proteins in the 20S class.

NUCLEIC ACID ENZYMOLOGY

Mechanism of Breakage and Rejoining of Bacteriophage T2 DNA

Studies are continuing on the biochemical events associated with the phenomenon of breakage and reunion of parental bacteriophage DNA during the infection process.

In the transfer of parental DNA to progeny DNA, there is a 10 to 20% reduction in the contribution of parental hydroxymethyldeoxycytidylic acid (HMCP) relative to the contribution of the other three parental deoxynucleotides. Base labeling, as well as phosphorus labeling, indicates that the entire nucleotide is involved. Experiments involving labeling of very early phage progeny show an elevated labeling in HMC residues. This result suggests that breakage of T2 DNA occurs at HMC-enriched residues, and repair of these residues is an early function in rejoining of DNA. "Second generation" experiments indicate some specificity in the removal and repair of certain HMC residues. Current experiments are designed to confirm the specificity of the process and to locate the areas involved. For this purpose a mild acid hydrolysis (the diphenylamine–formic acid hydrolysis of Peterson and Burton) of DNA is carried out to produce the original pyrimidine sequences. Preliminary results of these studies with T2 DNA whose pyrimidines are tritium labeled reveal that the "deletion" of HMC residues occurs significantly in the residue purine-$(HMC)_3$-purine, less in the residue purine-$(HMC)_2$-purine, and not at all in the residue purine-(HMC)-purine. These analyses are presently quite incomplete.

ENZYMOLOGY

Protein Synthesis

We are studying the fundamental control mechanisms involved in normal growth and differentiation of cells through experiments on the enzymic mechanism in protein biosynthesis and how this process is controlled by hormones.

Cell-Free System. – The problem of how amino acids are condensed into the large macromolecular proteins is being investigated at the molecular level in a number of cell-free systems. One such system has been developed to the point where it is possible to observe the expression of a gene under experimental conditions. In this system synthesis of the enzyme β-galactosidase can be induced by a cell-free preparation from certain intestinal bacteria (*Escherichia coli*). Synthesis of this enzyme requires the continual presence of the DNA carrying the gene that determines the amino acid sequence in the enzyme protein. Studies are being conducted to determine the sequence of events occurring between the free amino acids and the fully formed protein, and to determine the manner by which information on the sequence of amino acid in the gene is transmitted to the protein-synthesizing machinery. Preliminary experiments indicate that the genetic information is translated to a special kind of RNA, called "messenger" RNA, and that the latter associates itself with ribosomes, thus becoming the specific template for synthesis of this enzyme. One interesting observation is that the inducer of the enzyme must be present during the transcription of the genetic information from DNA to RNA. In the absence of inducer, although new RNA is made, such RNA does not contain information for the synthesis of this enzyme. This phenomenon is being pursued because an understanding of the function of the inducer may help us to understand how different genes in various cells are turned on and off at different stages of growth and metabolism.

It has been extremely difficult, however, to prepare this cell-free system on a reproducible basis using a French pressure cell for cell disruption. Gentler methods of disruption are currently being investigated in order to obtain a more stable particle fraction that may be used as a component of a cell-free system for β-galactosidase synthesis.

Mechanism of Protein Synthesis. – The use of amino-acid-incorporating systems has led to the discovery that during protein synthesis aminoacyl synthetases and transfer RNA (t-RNA) interact in a highly specific manner. Such specificity is unique and highly unprecedented in enzyme reactions. In some way an enzyme protein (polypeptide sequence) is able to specifically recognize a nucleotide sequence in RNA and acylate this RNA with 1 to 20 amino acids. We are examining this phenomenon by the isolation and purification both of the synthetases and of their substrates, the t-RNA's. Once these goals have been accomplished, a concerted study of the mechanism of their interaction can be initiated.

Hormonal Control. – We are currently studying three systems in which steroid hormones play a regulatory role in protein synthesis.

Analyzing changes in the metabolism of RNA that accompany the induction of hepatic enzymes by hydrocortisone in live rats by pulse-labeling techniques, we have found a marked increase in the rate of synthesis of nuclear RNA. This increase begins shortly after hydrocortisone administration and precedes the increased enzyme synthesis that results in induction. Synthesis of cytoplasmic RNA is unchanged.

Estrogen effects on protein synthesis in the rat uterus have been studied with an amino-acid-incorporating system prepared from this tissue. Shortly after ovariectomy, the capacity of ribosomes for leucine-^{14}C incorporation is impaired, but this capacity is raised to the normal level within a few days after surgery. Ribosomes prepared from ovariectomized animals, while equivalent to normal with respect to leucine incorporation, are much more responsive to added messenger (polyuridylic acid) than are ribosomes from normal animals or estrogen-treated castrates. These results are interpreted as indicating that the diminished population of ribosomes in the castrate uterus carry out a synthesis that is essentially independent of renewal of messenger RNA, that is, utilizing stable templates.

Androgen effects on RNA synthesis in the seminal vesicle of the rat have been investigated, and it was found that synthesis of all types of RNA is stimulated by the hormone.

In these studies we hope to learn the mechanism by which steroid hormones act to regulate growth and differentiation at the molecular level, in the belief that knowledge of these mechanisms is essential to understanding the phenomenon of uncontrolled growth (cancer) and to the development of satisfactory means of reproductive control.

PLANT PHYSIOLOGY AND PHOTOSYNTHESIS

Studies of Normal and Abnormal Development in Histologically Simple Structures During Growth Without Cell Division

In grass embryos the coleorhiza is the sheath enclosing the embryonic roots, and the epiblast is a projection off the coleorhiza. Although these structures are largely insignificant from a practical point of view, we have found that in germinating wheat they are very favorable for certain developmental studies. The coleorhiza and epiblast can be considered most extraordinarily determinate; all the cells finally present at cessation of their growth are already present in the embryo of the mature grain. Moreover, they are histologically simple, consisting only of parenchyma surrounded by an epidermis. They are also the first structures to grow during germination. In addition, the epiblast is an appendicular structure that, except for its contiguity with the coleorhiza, is isolated from the rest of the plant. Thus, its behavior is little constrained by contact with other parts of the embryo or seedling. Studies of normal epiblast growth at different temperatures have indicated, contrary to the usual interpretations of determinate growth, that in this simple and highly determinate structure the final extent of growth is not biologically determined by the rate and duration of growth.

In certain regions of plants in which growth normally has already ceased, high concentrations of indoleacetic acid or other auxins are known to induce in parenchyma tissues "auxin tumors," which are excessive, disorganized growths with much cell division. When treated with various auxins, the coleorhiza and epiblast also grow in an excessive, disorganized manner and resemble "auxin tumors" except for the absence of any cell divisions. Anatomic examination of this histologically simple tissue indicates that the site of action appears to be the parenchyma rather than the epidermis. Another similarity to "auxin tumors" is that these disorganized hypertrophic

growths can be "induced" by auxin treatment of coleorhizae that have already stopped normal growth. These results suggest that cell divisions, although necessary for sustained growth in a typical "auxin tumor," are not necessary for the "induction" of the initial disorganization which precedes their development.

Photosynthesis

For many years, our work has been aimed at understanding the energy conversion steps of photosynthesis. Over the last three years we have been engaged in an intensive study of the details of the delayed light emission of living plants, because this dim glow affords a means of studying electron transitions over a wide time range within the functioning photosynthetic apparatus. We have now studied this emission over eight orders of magnitude in time, from 5×10^{-5} to 6×10^{3} sec. Although the physical mechanism of delayed light emission remains as unclear as the mechanism of photosynthetic energy conversion, there is ample evidence that the delayed light is closely associated with the mechanism of photosynthesis. Both processes have the same action spectrum. Both processes have an absorption cross section equal to 300–400 chlorophyll molecules, implying the existence of groups of chlorophyll molecules which act together as units. Both processes are heat inactivated at the same temperature, and poisons of photosynthetic energy conversion invariably have a drastic effect on the kinetics of delayed light emission. The turnover time for a photosynthetic unit is reflected in the effects of temperature on the delayed-light decay. Both processes show a complex interaction between two pigment systems. It thus seems clear that an understanding of the delayed light would give deep insight into the physical basis of photosynthetic energy conversion.

BIOPHYSICS

UV Photoproducts Produced in Bacterial Spores

Recent studies have implicated thymine dimers produced in the DNA of the bacterial genome as a major lesion in the death of bacteria irradiated with ultraviolet (uv). Since thymine dimers cannot be formed in dry DNA, it appeared possible that the resistance of bacterial spores to uv irradiation might be caused by the lack of production of dimers in their DNA.

Bacterial spores produced in medium containing ^{3}H-thymidine were irradiated at a wavelength of 2650 A and analyzed by standard methods for ^{3}H-containing photoproducts. The resulting chromatograms contained no radioactivity in the region normally occupied by thymine dimers. At a slightly higher R_F value, however, 28% of the radioactivity was involved in an unknown photoproduct. At a similar dose, vegetative cells of the same organisms would contain about 7% of the activity in thymine dimers. The unknown product is not split in solution by light of 2637 A, as pyrimidine dimers are.

Re-Pairing of Long-Lived Free Radicals

The decay rates in air at temperatures from 4 to 150°C of long-lived free radicals produced by x-ray and 14-Mev-neutron irradiation of glycine, alanine, glutamic acid, leucine, and glycylglycine have been studied by electron spin resonance techniques. The radicals in leucine decay most rapidly, largely by interactions with oxygen, we believe, and glycylglycine decays slowest. Except for leucine, identical results are obtained in air or in vacuo below the sublimation temperature. Preliminary results indicate that decay following neutron irradiation is very similar to that following x rays. Present analysis of the data is based on the model that irradiation generally produces several radical species. For a brief period, very rapid decay occurs, perhaps by the diffusion model of Summermeyer, until the more mobile radicals are re-paired. Thereafter, long-term decay, we assume, follows essentially some kind of second-order kinetics of pairing relatively stable radicals. From Arrhenius plots of the rate coefficients at different temperatures, energy barriers between the free-radical states and their decay products are estimated to be (in kilocalories per mole): glycine ($^{0}NH_2$ radical), 19; glycine ($^{+}H_3N \cdot {}^{0}CH \cdot CO_2^{-}$ radical), 16; alanine, 24; glutamic acid, 18 plus a stable component; and glycylglycine, 8.

Mechanism of DNA Transfer in Bacterial Mating

There are two main theories for the transfer of DNA from Hfr to F^- in bacterial mating: one, proposed by Jacob and Brenner, according to which a replication of the chromosome occurs simultaneously with mating, a newly replicated copy being transferred; the other, proposed by Bouck and Adelberg, involving the transfer of a finished chromosome with the condition that a round of DNA replication must be completed before transfer can start. Since there is no overwhelming evidence in favor of either model, we attempted to test some of the predictions they allow.

Crosses were made between Hfr CR34 (λ) (thy^- L^- Str^S) and F^- C-416 (ade^- arg^- try^- met^- λ^R Str^R). The DNA synthesized in the Hfr was labeled with thymine-^{3}H. DNA synthesis was prevented in the F^- by adenine starvation before and during the cross. The analysis of the amount of DNA transferred was made by quantitative autoradiography after separation, by shaking, of the couples. The distinction between F^- and Hfr was by morphology (the F^- is spherical, the Hfr rod-shaped) and by differential thymine uptake (DNA synthesis continues normally in the Hfr and is much higher than DNA transfer to the F^-).

(1) Kinetics of DNA Transfer. – The Hfr is labeled for seven generations, thymine-^{3}H being also present during mating. Regardless of the model, DNA transferred will be labeled on both strands. In this system, transfer is initiated rapidly and remains linear up to 50 min. The rate of transfer thus determined is 9.8 μ/min, that is, 112 min for a chromosome 1100 μ long. This is in good agreement with genetic data (100 to 110 min).

(2) Chaser During Transfer. – If, in the same type of experiment as in (1), a chaser of cold thymine is introduced 20 min after contact, the subsequent transfer of label is decreased by half. Analysis of grain counts shows that the same proportion of F^- cells is labeled at 20 and 50 min (last time used). The rate of transfer of lambda is the same with and without chaser. It seems, therefore, that half of the DNA transferred is newly replicated. If unlabeled Hfr's are mated to F^- and a pulse of thymine-^{3}H is introduced at 20 min, when transfer is taking place in a large majority of the cells, label occurs in the F^-, increasing linearly with time. A chaser introduced at 30 min stops further passage of label. Here again, newly replicated DNA is introduced in the F^-

These experiments rule out the possibility that finished chromosomes only are transferred. They agree with the hypothesis that a special type of DNA replication is involved in bacterial mating, so that the F^- receives one branch of a newly replicated chromosome. Further experiments, along the same lines, to determine the origin of normal replication in the bacterial chromosome are planned.

NIH-AEC DEVELOPMENT OF AN ULTRACENTRIFUGE

Continuous-Flow Separation of Virus Particles. – High-speed continuous-flow rotors suitable for use with small infectious virus particles have not been previously available. Theoretical studies on the sedimentation of small particles in narrow annular spaces have led to the design of a continuous-flow rotor (B-V) suitable for operation up to 40,000 rpm. This rotor is suitable for use with virus particles which can withstand pelleting. Studies with T3 bacteriophage, adenovirus 2, Echo 28, and live polio virus indicate slightly better performance than predicted by theory.

Since a number of viruses are known which cannot withstand pelleting, methods for combining continuous-flow centrifugation with isopycnic banding[1] have been examined, using a series of rotors designed for this purpose (B-VI, -VII, -VIII, and -IX). The problems associated with the design and operation of rotors of this type are many, since a density gradient must be set up in the rotor, kept in position while large volumes of virus-laden culture fluid flow centripetal to it, and then recovered without mixing at the end of the experiment. This has now been successfully done with adenovirus 2 and T3 phage.

[1] N. G. Anderson, *Nature* 199, 1166 (1963).

PHYSICS OF TISSUE DAMAGE

Tracer Studies of Vacuum Pump Oil Deposition

The adverse effects of the deposition of diffusion pump oil on samples in a vacuum are well known. Thus a method was developed to ascertain the effect of this factor on our optical experiments. A radioactive tracer technique was used as a quick, simple nondestructive method for measuring the deposition of diffusion pump oil within a vacuum system. A simple bell-jar vacuum system was assembled consisting of an oil diffusion pump, multicoolant baffle, gate valve, and bell jar with associated gages. Dow Corning 704 silicone fluid was irradiated in the Low Intensity Test Reactor at ORNL, where the ^{30}Si, constituting 0.54% by weight of the oil, became activated to ^{31}Si. The results indicate the presence of an initial backstreaming surge when the oil is first heated and also show the relative effectiveness of air-, water-, and liquid-nitrogen-cooled baffles. Deposition rates of a few angstroms per hour were measured. The technique is also a valuable method of evaluating the operational effectiveness of various vacuum system components. This method has proved so sensitive and useful that at least one pump oil manufacturer is considering tagging diffusion pump oil with tritium for similar studies.

Optical Studies of Graphite

Optical experiments on graphite using unpolarized light have been completed. The optical properties of hot-pressed pyrolytic graphite were studied in the wavelength region from 1100 to 3000 A. The real and the imaginary part of the complex index of refraction were obtained from the reflectances measured at 20 and 70° incidence. The complex dielectric constant and the energy-loss function were determined from these values. The energy-loss function was found to exhibit a maximum at a wavelength of 1800 A, corresponding to an energy of 6.9 ev. This peak corresponds to a 7.5-ev loss in electron energy-loss experiments, where it has been attributed to the excitation of the conduction-electron plasma.

Mean Free Paths of Low-Energy Electrons in Solids

A study of experimental work on electron interactions in solids reveals a lack of information for interactions which occur when electron energies are between those normally associated with solid-state physics (below 3 ev) and those of x-ray physics (above 10 kev). This energy region is of considerable importance in radiobiology, radiation chemistry, and radiation dosimetry because it includes the very high electron flux found in electron slowing-down investigations and the region of collective electronic interactions found uniquely in condensed media. Electron transmission minima for metallic films of aluminum about 200 atoms thick were found at 10 and 40 ev and attributed to surface and volume plasmon production. Transmission decreased above 120 ev because of *L*-shell ionization. A Monte Carlo calculation has been initiated to see if the transmission data on this and other metals are consistent with theoretical estimates of electron-plasma and inner-shell cross sections.

TERRESTRIAL AND FRESHWATER ECOLOGY

In the Radiation Ecology program a number of promising new developments were achieved during the year. In plant ecology the new program in radiation botany completed experiments on the interaction between ionizing radiation and light in inducing responses by higher plants. Preliminary results showed that the timing of radiation insult in relation to photoinduction significantly affected the number of flowers produced. Since day length is a seasonal variable in the natural environment, sublethal ionizing radiation could modify photosensitive mechanisms, the "life history" response of plants to photoperiod, and species capabilities for regenerating by seed and competing in a radioactive environment.

In our ^{137}Cs forest project an important finding was that the concentration of roots in the surface decimeter of the soil plays a major role in the turnover of cesium in the cesium cycle. More broadly this finding is of importance because we have little information on the relation between the quantity of roots and the turnover of nutrient elements – a matter of long-term agricultural importance. Rain leaching from the canopy still seemed to be the major pathway of contamination from tagged trees to untagged trees and ground vegetation.

In our aquatic program a number of new developments occurred during the year. Our studies of chemical relationships between organisms and their environment, particularly strontium interactions between mollusks and water, suggested that the long-term cycle of strontium in the environment has been altered through the imposition of an agricultural economy on a formerly forested landscape. Laboratory experiments indicated that strontium and calcium uptake could be modified by changing the environmental concentrations of other elements such as magnesium, sodium, or potassium. Reflooding of part of White Oak Lake afforded the opportunity to use the contamination by ^{137}Cs to estimate the feeding rate and determine the basal metabolism of White Oak Lake carp. New studies on Melton Hill Lake using ^{85}Sr were concerned with assimilation of this isotope by planktonic algae populations. The first results suggest that assimilation of ^{85}Sr was correlated with oxygen production, which gives rise to the possibility of using this radioisotope to estimate aquatic biomass production.

The new program in systems ecology emphasized the development of mathematical models using the compartment model approach. Using this technique a model was developed for ^{137}Cs behavior in carp which showed that uptake cannot be explained by simple diffusion between compartments. Active transport is required for accumulations in flesh and bone. Four blood-processing organs (heart, liver, kidney, and gills) obtain direct input of activity from the gastrointestinal tract (presumably via lymphatics). In a theoretical study of two-compartment exchange systems it was found that specific activities are not necessarily equal under conditions of total-element equilibrium. A model of cesium behavior in the soil-litter compartments of a forest ecosystem showed that the rate of leaching of radiocesium from deciduous litter is not altered by presence of soil, but increases when microflora are present. Cesium activity in soil and microflora is nonleachable. Application of digital (high speed) computer techniques to a variety of ecological problems and to data processing was gotten under way, and a number of programs are in various stages of completion.

RADIOLOGICAL PHYSICS, HEALTH PHYSICS, AND RADIATION INSTRUMENTATION

RADIATION PHYSICS

Atomic and Molecular Radiation Physics

This activity is an integral part of a radiation physics program in which a fundamental study of the interaction of ionizing radiation with matter of various types (gases, metals, plasmas, and particularly molecules of direct biological importance, e.g., water, oxygen, proteins, and amino acids) is made. The Atomic and Molecular Radiation Physics program emphasizes studies dealing with the effects of radiation on individual atoms and molecules. Efforts are made to study the phenomena (e.g., excitation and ionization of gases, electron transport in gases, negative ion formation) involved in sufficient detail that they have direct application to the understanding of radiation chemistry and radiation biology. The most important examples of new work developed under this activity during the past year are as follows:

1. **Ionization and Excitation of Argon with Alpha Particles.** – Experimental data on alpha-particle ionization of binary mixtures of gases involving argon suggest that two states of electronic excitation persist long enough after the passage of the charged particle to allow collisions of the type $Ar^* + X \rightarrow Ar + X^+ + e^-$ to occur. One of these states is near the metastable levels in argon, approximately 11.6 ev, and the other is at approximately 14 ev. Examination of electron energy loss data and spectroscopic data leads to a tentative identification of these states as resonance levels; thus, their lifetimes are due to the trapping of photons in the apparatus. Ionization yield data were fitted to a kinetic model representing the above suggested mechanism with good agreement between the model and the experimental data. Other evidence for the existence of excited states of long lifetimes was derived from light emission experiments with argon in which continuous emission spectra suggest Franck-Condon transitions in excited argon molecules.

2. **Energy Partition in Gaseous Mixtures.** – Ion-yield measurements in gaseous mixtures, when interpreted along lines previously suggested,[1] indicated that the concept of energy partition in irradiated solutions may be defined with a precision hitherto unsuspected. A scale of molecular parameters has been established in this manner for 18 gases, permitting the evaluation of dose partition in any of their mixtures.

3. **The Determination of Electron Capture Cross Sections with Swarm-Beam Techniques.** – A method was developed which combines electron swarm and electron beam techniques to obtain absolute electron capture cross sections as a function of electron energy. Data on Cl^- from *o*-chlorotoluene obtained at electron energies near 1 ev and on O^- from oxygen at electron energies of about 7 ev were treated, employing this method.

4. **Interactions of Low-Energy Electrons with Polyatomic Molecules.** – The different ways by which low-energy electrons (2 ev or less) interact with polyatomic molecules in the gas phase were investigated. For the halogenated benzene derivatives for which the electron affinity of the halogen atom exceeds the energy for dissociation of a halogen atom from the molecule, a dissociative electron capture occurs at about 0.7 ev, which is always accompanied by a second dissociative process at thermal electron energies. Energy-integrated cross sections were determined for the process occurring at about 1 ev, and the different possible mechanisms for this interaction were studied.

---

[1] C. E. Klots, *J. Chem. Phys.* 39, 1571 (1963).

5. **Time-of-Flight Studies of Electron Transport in Gases.** – It had been shown[2] that electron swarm experiments may be arranged to satisfy the boundary conditions applicable to a one-dimensional, time-dependent transport equation. Under such conditions it may be shown that the distribution of the times of arrival of individual electrons may be interpreted in terms of the diffusion coefficient and the drift velocity. The integrals of the distribution functions, that is, the total numbers of electrons arriving, before and after the addition of an attaching gas, are directly related to the attachment coefficient. Since, in such experiments, time is a more accessible independent variable than length, it is not surprising that much more information on the basic character of electron transport in gases is obtained than can be obtained from a Townsend experiment.

The original apparatus[2] was improved by providing a direct experimental means for measuring the instrument fluctuation arising from such sources as variation in time of electron release from the photoelectric surface and the variation in electron detection time. Correcting for these fluctuations led to improved accuracy for the measurement of the diffusion coefficient. New results were (1) better values of the diffusion coefficient in ethylene as a function of the ratio of the electric field to the gas pressure, (2) values for the diffusion coefficient in mixtures of ethylene and water vapor, and (3) the ratio of the momentum transfer cross section in water vapor to the momentum transfer cross section in ethylene.

The first of these methods used a gas-discharge single-electron detector and hence is limited in application to counting gases. A new method was developed which employs a surface-type electron multiplier separated from the reaction chamber by differential pumps; hence the restriction to counting gases is removed.

Polarization Studies in the Vacuum Ultraviolet

Recent studies of optical properties of solids have demonstrated the need for good polarizers. Theoretical studies revealed that, contrary to popular opinion, reflection-type polarizers are indeed useful in the vacuum ultraviolet region. A method was found, well suited to the vacuum ultraviolet region, for determining the degree of polarization produced by a polarizer at a given wavelength and for determining the polarization introduced by a grating monochromator. An evaluation was made of the degree of polarization necessary in a polarizer for use in optical studies to determine, for example, the reflectance of a surface for light of parallel or perpendicular polarization. Data were obtained in the spectral region between 500 and 1300 A for experimental gold and silver reflection-type polarizers and for a grating used in the Seya geometry.

Transition Radiation and Low-Energy Bremsstrahlung

A theoretical determination was made of the number distribution of photons emitted from a semiinfinite dielectric slab irradiated with electrons at an arbitrary angle of incidence. It is found that this quantity contains contributions from radiation generated by the induced electric polarization of the dielectric medium (transition radiation), by multiple small-angle scattering of the electron on scattering centers assumed to be randomly distributed in the dielectric medium (bremsstrahlung), and by interference effects between these two types of radiations.

Theoretical spectra were found for plane copper, silver, and gold foils irradiated by electrons at normal incidence and were compared with available experimental data. Good agreement is found at the higher electron energies (100 kev), but the agreement is not as good at low electron energies (25 kev). This is felt to be partly due to uncertainties in the theoretical expression used for the mean-square scattering angle and partly due to the fact that the foils used in obtaining the experimental results are too thick to satisfy the assumptions of the present theory.

Numerical theoretical results corresponding to the electron irradiation of plane silver foils at various angles of electron incidence were also obtained. An intense "peaking" of the emitted radiation around the wavelength $\lambda = 3260$ A is noted as the electron approaches grazing incidence. The inverse energy dependence of this radiation identifies it as bremsstrahlung. Comparison of these results with recent experimental data shows fair agreement, but further work is necessary before conclusive interpretations can be made.

[2] G. S. Hurst *et al.*, *J. Chem. Phys.* 39, 1341 (1963).

INTERNAL DOSE ESTIMATION

The Internal Dose Estimation program is directed toward estimating the dose to various body tissues resulting from the deposition of radioactive material in the body. Estimates of internal exposure depend upon a model for the metabolism of the material by the human body. In the case of radionuclides of long radioactive half-life, this model must include data on the retention of the nuclide in the body over many years. During the past year considerable progress has been made in assembling data to revise and to extend the concept of Standard Man. Standard Man was defined originally as a typical occupational worker whose bodily characteristics are the basis for most evaluations of internal exposure of radiation workers. Until now no similar basis has been developed for other categories of the population. To provide a basis for estimation of exposure of the population the weights and dimensions of some 36 organs and tissues are given as functions of the age of the individual. The elemental composition of these tissues is specified, and in most cases major organic components such as blood, fat, and protein are given for these tissues.

Data also are given on the composition of a typical diet and on the excreta of the individual. In addition to the variation of these data with age, a measure of individual variation has been included whenever possible. The data selected are, for the most part, from American or European sources so that the individual so defined may be considered as typical of these populations. The study is expected to be completed within a year and represents the joint efforts of an international Task Group on Standard Man which was constituted by the International Commission on Radiation Protection. Three members of the five constituting the Task Group are involved in the program of the ORNL Internal Dose Estimation Section. When completed, the report will offer the first comprehensive compilation of data needed to determine what population groups might receive the greatest dose in a specific exposure situation, to estimate the mean dose in the most exposed group, and to provide an indication of the range of individual variation about this mean dose.

HEALTH PHYSICS TECHNOLOGY

Studies of the redispersion of contaminating dusts from surfaces have been carried out under conditions approximating an average clean working environment. Nonradioactive particles of zinc sulfide and of copper oxide having count median diameters of about 2 μ were allowed to settle in the test chamber. Then the air in the chamber was sampled while working activities were being simulated, and the resuspended particles were determined by fluorescence in the case of zinc sulfide and by neutron activation analysis in the case of copper oxide. The average resuspension factors that were found indicate that for every 500 particles per square foot of surface about one particle may be inhaled per hour of light to medium work. A new contamination sampling technique has been developed which provides a sample related to the likelihood of particles being redispersed into the air, and a prototype of a portable air redispersion sampler has been built and tested. Further work is concerned with the effect of surface treatment on resuspension factors. For example, whereas the above resuspension was observed in the case of waxed floor tile, when a light film of oil was applied to the surface, the resuspension of freshly deposited particles was effectively zero. Similar studies are being done with concrete and other standard surface materials. Basic studies on the forces of adhesion between particles and surfaces are aimed at improvement of surface treatment materials and of decontamination techniques.

The effect of radiation and radioactivity on the transport, deposition, and adhesion of particles to surfaces is studied by taking advantage of local sources of high-level radiation, for example, the Health Physics Research Reactor. For intermediate radioactivity levels, on the order of 0.1 to 1 mc/m^3, the major effect on airborne conductive particles is to reduce any asymmetry of electrical charge that may have been induced on the particles during their formation. Irradiation of dielectric surfaces with doses of about 10,000 rads has been observed to produce locally intense electrical polarization, which enhances deposition and adhesion of particles on the surface.

HPRR OPERATIONS AND SPECIAL PROJECTS

The Health Physics Research Reactor has been utilized for over 300 operations with experiments pertaining to neutron and gamma-ray dosimetry, radiobiology, and physics research. Users have included ORNL and Y-12 Health Physics Divisions, the ORNL Biology Division, the UT-AEC Agricultural Research Laboratory, ORINS, U.S. Public Health Service, Savannah River Project, Japanese National Institute of Radiological Sciences, Pacific Northwest Laboratory, and several colleges and universities. The most advanced dosimetry systems and techniques are utilized to give all researchers the best values of "dose," spectrum, and depth-dose distribution that is possible. The steady-state mode was utilized more than 50% of the time, although an increasing percentage of the operations utilize the burst mode. Although only about 30% of the operations were primarily for animal irradiations, about 65% of the total number of kilowatt-hours was accumulated during such exposures.

BASIC INSTRUMENTATION

Lithium-Drifted Germanium Detectors

Since the gamma rays produced by radionuclides most frequently have energies in the range of one-tenth to several million electron volts, there is a need for semiconductor gamma detectors of improved energy resolution with useful detection efficiencies at these energies. Although limited portions of this energy spectrum are accessible to existing silicon detectors, improved response results from the use of germanium.

For gamma-ray spectrometry, detectors made of germanium have a decided advantage over silicon devices, because the nuclear charge Z of germanium is more than twice that of silicon and the linear photoelectric absorption cross section of an element varies approximately as Z^5. The higher Z of germanium represents about a factor of 40 in increased photoelectric efficiency. While silicon detectors are limited to gamma energies below about 200 kev, germanium devices operate very effectively in the Mev range.

The spectrum of ^{60}Co (Fig. 1) illustrates the excellent energy resolution obtained at 1.33 Mev with a germanium detector; the photopeaks have an energy resolution of 0.3% or 4.2 kev full width at half maximum (fwhm). Sodium iodide scintillation detectors are often used in this energy range, but the energy resolution for ^{60}Co is only about 6%. To illustrate the resolution of the two detectors, two spectra of ^{57}Co are shown (Fig. 2). One spectrum was measured with a germanium detector and the other with a sodium iodide (3 × 3 in.) scintillation detector. The germanium detector has clearly resolved the 122- and 136-kev gamma transitions, whereas the sodium iodide detector has not.

Simplified techniques were developed for compensating germanium by lithium drifting so as to permit 7- to 8-mm-deep junctions to be made uniformly without the attention of the operator during drifting. A method was devised to stabilize the junctions after drifting so that the encapsulated devices can be given long (months) leveling or cleanup drifts without loss of junction properties.

C4-9477R

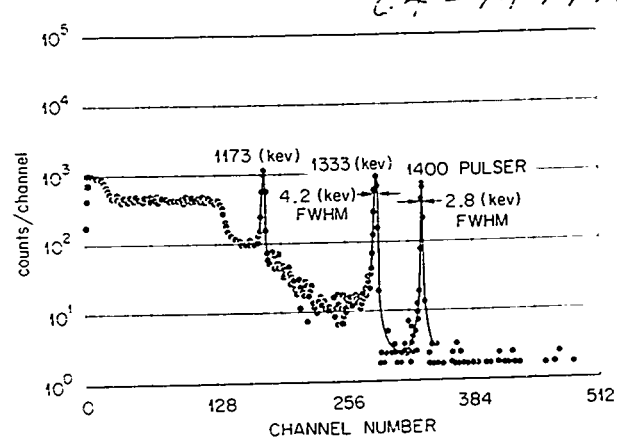

Fig. 1. Spectrum of Gamma Rays from ^{60}Co. Precise energy determination of high-energy gamma rays is readily accomplished by the use of lithium-drifted germanium *p-i-n* junction gamma detectors. This is a ^{60}Co spectrum obtained with lithium-drifted germanium detector No. 20, 150 v reverse bias, 77°K, and 1.4-Mev pulser.

65-753

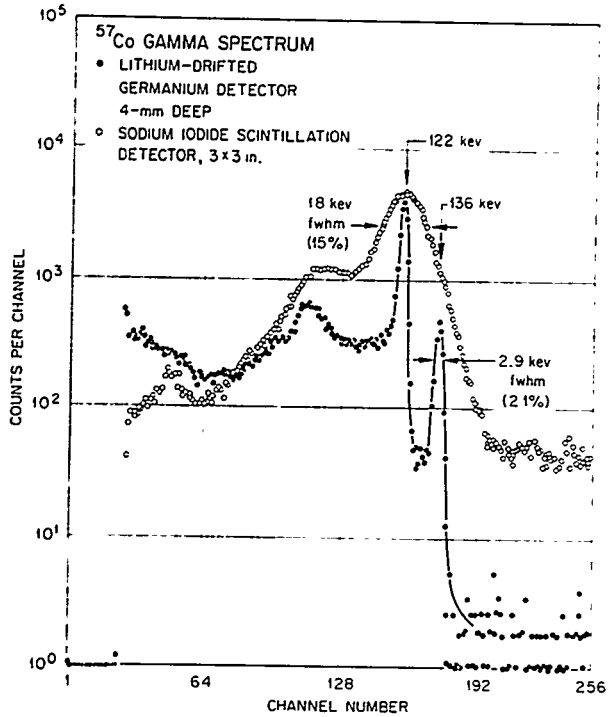

Fig. 2. Spectra of Gamma Rays from ^{57}Co. Gamma detectors fabricated of lithium-drifted germanium have shown substantially better energy resolution than scintillation detectors. This is demonstrated in these ^{57}Co comparison spectra.

Further, the stabilizing treatment minimizes the deterioration that normally occurs if the detector is accidentally left without proper cooling during use. Final encapsulation of the drifted, stabilized junctions by cold welding is performed entirely in a cryogenic vacuum to minimize the concentration of condensable vapors within the capsule and to avoid the necessity of a pump-out tubulation.

Encapsulated detectors have demonstrated excellent reliability in field use. The following performance is typical. The energy resolution of a 2.5-cm^3, 9-mm-deep detector was 3 kev fwhm for ^{57}Co (136 kev). A smaller detector, 1.8 cm^3 volume and 7 mm deep, showed an energy resolution of 6.1 kev fwhm for ThC″ (2.6 Mev).

The simplest method of cooling the detector for use is direct immersion in liquid nitrogen. The detector is attached to a suitable length of a specially constructed, low-capacitance coax and inserted into a liquid-nitrogen-filled Dewar.

Preliminary studies of the problems involved in the vertical float-zone refining of promising high-atomic-number semiconductor materials have been made. The principal advantage of vertical float-zone refining over horizontal zone refining is that the molten segment of the crystal is supported only by its own surface tension as it hangs between the two vertical, frozen sections of the crystal. This freedom of the molten zone from contact with any foreign surface eliminates any chance of contamination from such a surface. However, an unfavorable density-to-surface-tension ratio will make it difficult to maintain a stable zone. Under such conditions, it is necessary to inject the heat uniformly around the crystal but along as narrow a vertical segment as possible. Rotation of the sample while zoning increases the rate of purification and averages the angular variations of the heat source. To achieve a high degree of crystalline perfection, it is important that the scanning and rotating forces result in a minimum of vibration or other lateral motion of the molten zone.

OPPOSITE PAGE →

Fig. 3. Medical Nuclear Instrumentation. A plastic sphere – simulating a human head with internal blood vessels – is used in calibrating radiation scanning equipment in the Medical Spectrometry group. Radioactive solutions are inserted into the "blood vessels," and if the scanning equipment is working properly, it quickly maps the locations of the radioactivity, and it can then be applied in hospital use. The nickname for the sphere is "Alasper"; surname: Yorick.

PHOTO 71551

Both electron beam and induction heating are commonly used in zone refining semiconductor materials. The electron beam can be focused very tightly, but cannot be used to zone-refine materials that have a high vapor pressure when molten. Since neither method of heating is clearly superior to the other, relatively simple equipment has been constructed to gain practical experience with both. As a result of this work, design criteria have been formulated and equipment has been acquired which has the characteristics necessary to produce material of high purity and high crystalline perfection.

Charge-Sensitive Preamplifier

The design of a new pulse amplifier particularly suited for semiconductor detectors has been completed. The use of digital computer programs has permitted the study of network transfer functions prior to the determination of the form and component values of the pulse shaping network. The results of the study show the necessity of designing networks for specific applications. Particular attention has been given to the attenuator and to the pulse-shaping section of the amplifier.

Detailed formulas were derived for optimizing the input and filter sections of solid-state charge-sensitive preamplifiers that use field-effect transistors in the input stage. Gating techniques were developed to improve the signal-to-noise ratio of double-delay-line filters. An experimental charge-sensitive preamplifier, having an optimized input section and employing the new gating techniques in its double-delay-line filter, generated a symmetrical bipolar output pulse whose noise line width was 1.6 kev fwhm Si for a 5-pf simulated detector capacitance, a 4.2-μsec delay-line length, and a 1.4-μsec *RC* integrating time constant. A low-noise bipolar-transistor charge-sensitive preamplifier was developed. Its minimum noise line width was 8 kev fwhm Si for zero simulated detector capacitance and a 1-μsec *RC-RC* filter time constant.

Instrumentation for Photosynthesis Studies

In collaboration with the Photosynthesis Group of the Biology Division, we developed a mechanical phosphoroscope for a new measurement of the delayed light emission spectrum from the alga *Chlorella* at 1 msec after illumination. The spectrum, which was taken with an improvement of several times in resolution, confirmed older measurements made at 0.5 sec and again showed the identity of the fluorescent and delayed light emission spectra. We investigated several electronic light modulators and developed a phosphoroscope equipped with a Kerr-cell shutter. With this instrument we measured the delayed light emission at 5 μsec, which is one-tenth of the shortest delay reported a year ago. Using one of the phosphoroscopes, W. Bertsch (ORNL) and R. Clayton (Kettering Foundation) were able to show for the first time a direct connection between a photosynthetic reaction center and the delayed-light mechanism. When a mutant of a purple bacterium that contained no reaction center was used, the delayed light normally produced in the wild type was absent.

Two devices were developed for increasing the speed and accuracy with which microphotographic images of human chromosomes may be measured. The first device is a pair of dividers that translates distance into a proportional voltage. This voltage may be displayed or printed by a variety of readout devices. The second device is a pen that measures a curved image by generating a voltage pulse for each increment of distance traced (approximately 0.5 mm). The pulses may be counted and read out by conventional scalers. These devices are being evaluated by ORNL cytogeneticists in a study to determine the norms of human chromosome arm lengths and ratios.

NUCLEAR ENERGY CIVIL EFFECTS

DOSE DISTRIBUTION FUNCTIONS FOR NUCLEAR WEAPONS RADIATION IN JAPANESE DWELLINGS

The survivors of the nuclear bombings of Hiroshima and Nagasaki make up the largest and most important group of persons ever to receive high radiation exposures. This reservoir of radiobiological data can be used only when definitive dose values are available; a study to determine these doses has been under way in the Health Physics Division since 1956. A recent achievement of the dosimetry program was the development of the dose distribution equations for typical Japanese houses. These empirical equations were based on the experimental data from Operation BREN (a study in which a small fast reactor was mounted on a 1527-ft-high tower). Multiple regression analysis was used in conjunction with a digital computer to develop the equations, which were then tested by the application of the shielding data accumulated in nuclear weapons tests in 1958. Values predicted by the equations were within 6% of the measured values in 50% of the cases. Only 5% of the predicted values differed from the measured values by 15% or more. The equations are of the general form

$$\frac{\text{Dose}_{\text{House}}}{\text{Dose}_{\text{Air}}} = A_0 + A_1 G_1 + A_2 e^{G_2} + \ldots$$

to a maximum of eight terms. The A_i are numerical constants and the G_i are geometrical parameters (height above the floor, distance from front wall, etc.).

ACCELERATOR FOR OPERATION HENRE

A feasibility study was conducted to determine whether it is possible to build a monoenergetic neutron source, capable of an average yield of 10^{13} neutrons/sec for a period of 4 hr per target. It was concluded that an accelerator utilizing the duoplasmatron ion source, the $^3H(d,n)^4He$ nuclear reaction, and an acceleration potential of 150 kv was technically feasible and would have sufficient neutron yield. The purpose of constructing such a neutron source was to conduct a field experiment at the Nevada Test Site aimed at collecting data to verify theoretical results of machine computations for various shielding, activation, and transport phenomena. The source, which will provide a fiducial point for these computations, will be mounted on the 1527-ft BREN tower. The source has been constructed and is presently being tested.

CIVIL DEFENSE

The civil defense research project began at ORNL in September 1964, with the first month devoted to briefings by experts from other organizations. The initial research objectives were defined as an investigation of (1) the location of blast shelters in cities, (2) the interrelation of active and passive defense systems, and (3) the factors influencing the effect of various civil defense programs on the general population, public officials, and foreign countries. Shortly after the project began work, it was asked specifically to examine damage-limiting studies of the Department of Defense and to criticize their content constructively by direct communication with the Office of Civil Defense.

In the first problem, the location of blast shelters in cities, the group devised a scheme of blast-resistant tunnels, the so-called tunnel-grid shelter, which could be laid under the streets of a city with frequent entryways and underground emergency utility and life-support compartments attached. Some of the tunnels would extend to the suburbs, thus making it possible for the population to readjust its distribution, to reduce overcrowding, and thereby to minimize the effect of a bomb burst. A specific study of the installation of such a system in a 25-square-mile section of

Detroit was completed. The plan for entrance to the Detroit shelter is shown in Fig. 1.

Recognizing that interconnected tunnels under urban areas have considerable potential value for peacetime use, studies began of the dual use of underground highways and parking areas, subways, pedestrianways, and utility tunnels as blast shelters. A specific example was selected for conceptual design: six underground traffic lanes connecting the Lincoln Tunnel with Queens Midtown Tunnel plus 30,000 parking spaces. Other examples being reviewed are tunnels in an eastern city undergoing extensive urban renewal, a new subway system in Washington, D.C., and underground construction in a new city in California.

A mockup of a section of the tunnel-grid shelter was built at the Laboratory and equipped with cots, lights, and ventilating machinery. The ORNL mockup is shown under construction in Fig. 2. In shelter habitation studies, punkah-type hand-operated air movers were developed and given endurance tests which showed that, even with inexpensive construction, operation could be carried out for more than 1000 hr. Studies of air-moving capabilities of large check-valve-type punkahs showed that the air-moving capability was exceptionally high on a volume flow basis and exceeded by a considerable margin the air-handling capability of manually operated fans with small impellers. One such pump is shown in Fig. 3.

65-7412A

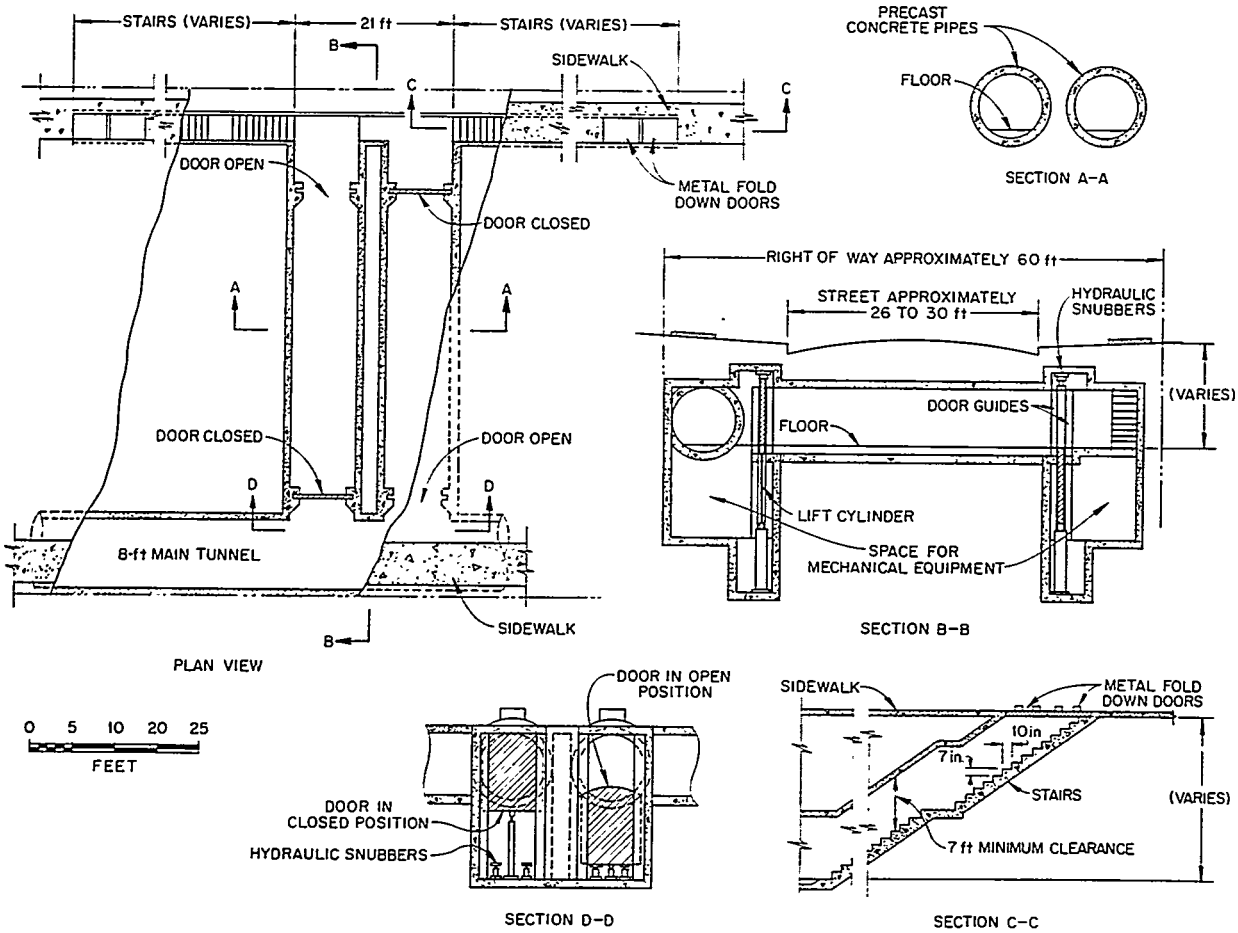

Fig. 1. Air-Lock-Type Entrance for Tunnel-Grid Shelter.

In studies of the interaction of active and passive defense and in the examination of the damage-limiting studies, the group has made less progress. In order to become familiar with the active defense situation, it is necessary to monitor a program in which approximately three quarters of a billion dollars is being spent annually. At the end of the first year, preliminary oral comments on damage limitation had been furnished the Office of Civil Defense, and a draft was being completed of a report containing a general description of missile defense systems, technical areas of special significance to passive defense systems, and several examples of complementary relationships between active and passive defense.

The social scientists in the group have participated in three ways. First, they have participated in the development of the underground tunnel-grid blast shelter system by evaluating the human factors and acceptability. These have included not only studies of likely acceptance and behavior in such a system, but also legal problems associated with acceptance on the part of municipal governing bodies. Second, they have set up two panels of experts to study problems which are pertinent to civil defense on a broader basis. The subjects for the panels are (1) the domestic and international effects of alternative active and passive defense programs and (2) the willingness of societies to sacrifice present rewards for uncertain future gains. Third, they have collected and reanalyzed previously obtained public opinion data on the attitudes of the United States public toward various national defense programs, with an emphasis on civil defense.

PHOTO 13034

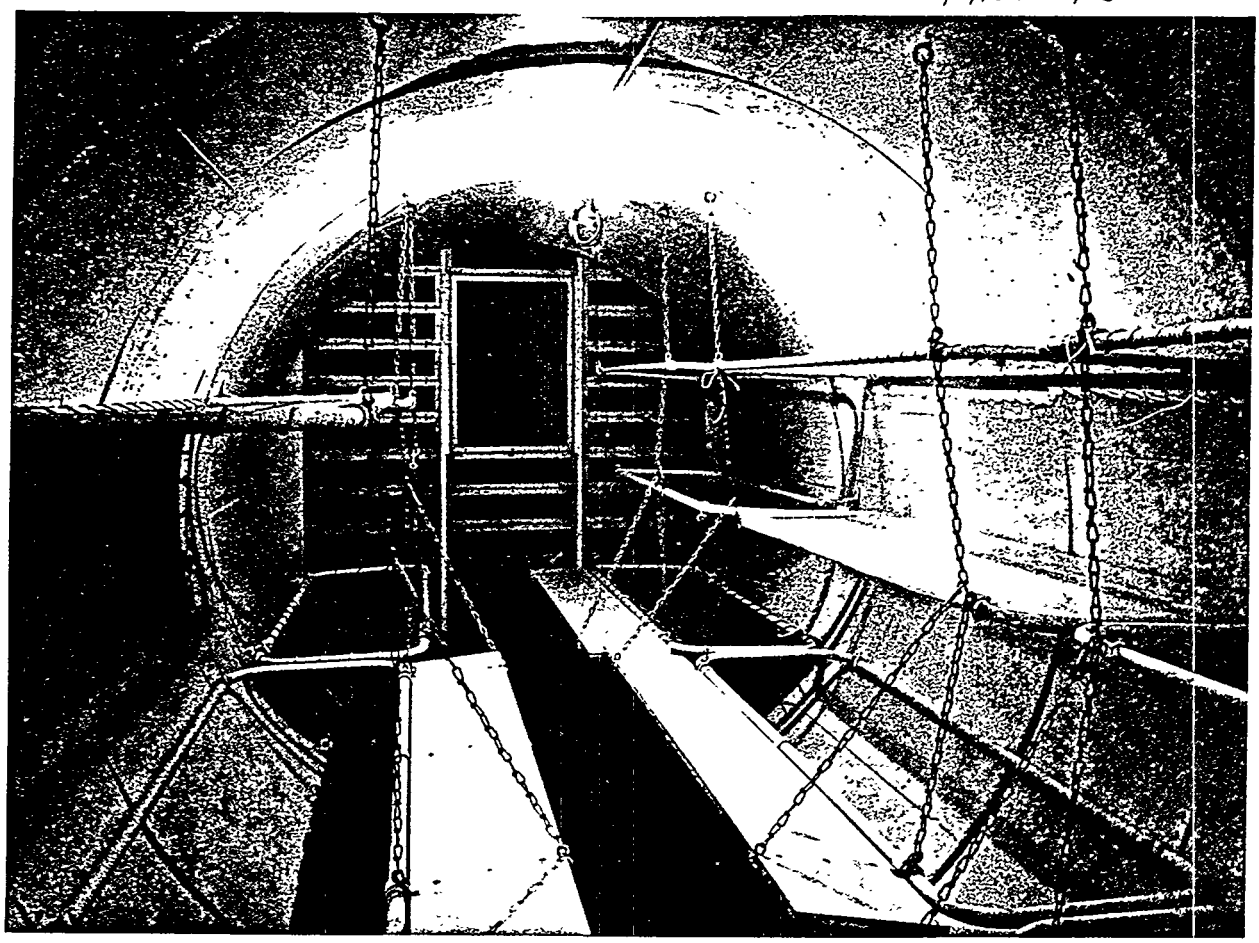

Fig. 2. Mockup of Tunnel-Grid Shelter.

65-4213

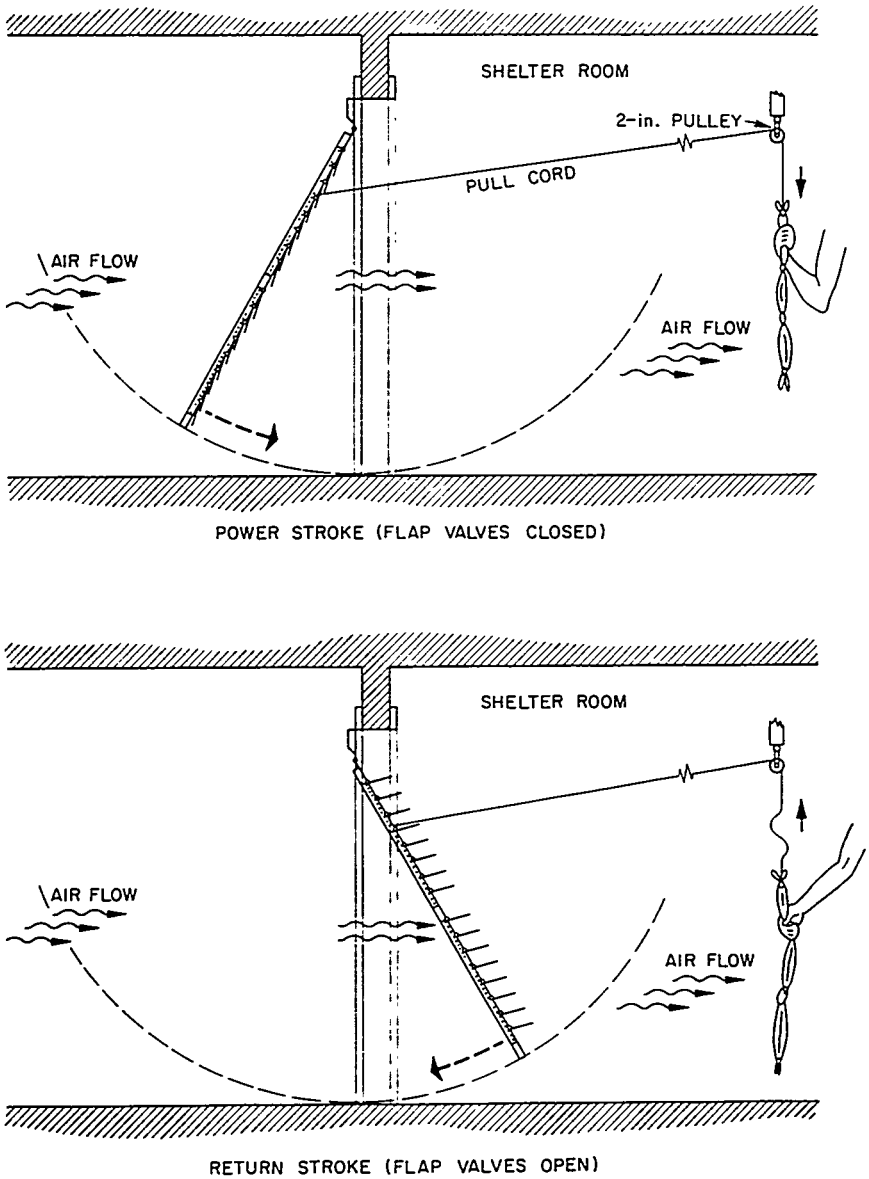

Fig. 3. Punkah-Type Air Pump. Vertical sections through doorway.

Research and Training in Biology.

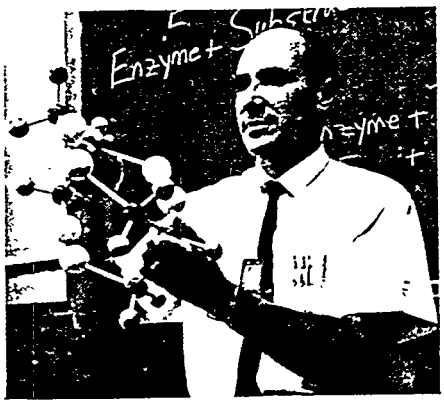

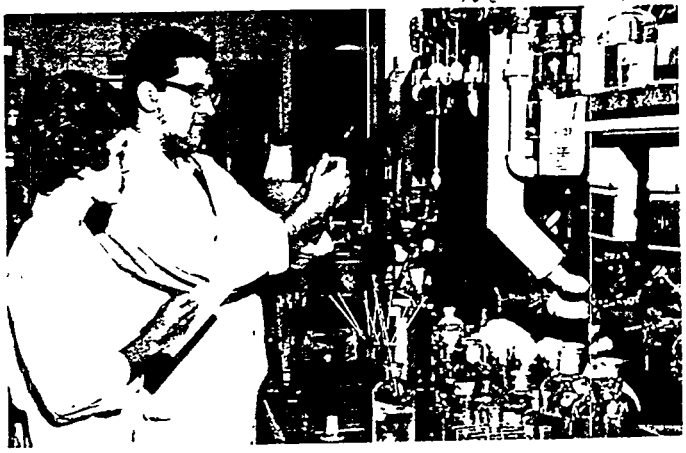

ART WORK - NO NUMBER

ISOTOPE DEVELOPMENT

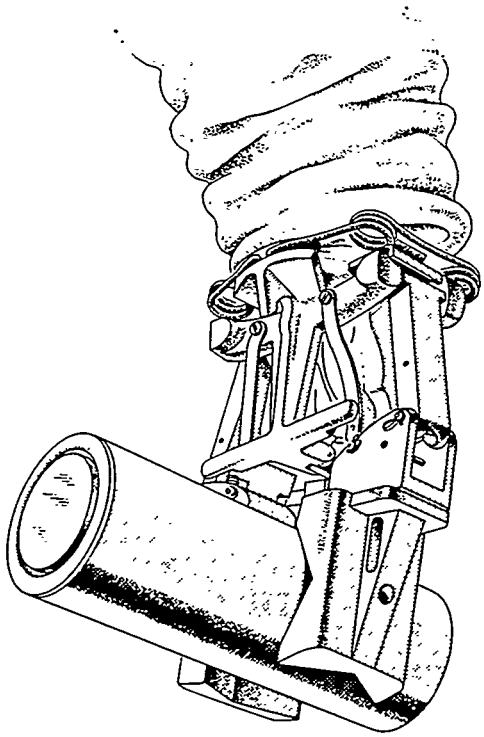

ISOTOPE DEVELOPMENT

NUCLEAR AND RADIOCHEMICAL ANALYSES

Branching-ratio measurements and decay-scheme studies were made on ^{141}Ce, ^{79}Kr, ^{99}Mo-^{99m}Tc, and a new isomer, ^{82m}Br. A study of successive neutron-capture reactions on lanthanum and cerium was begun. A search for new alpha emitters resulted in the discovery of alpha emission in ^{148}Eu. Nuclear levels were studied in a number of even-*A* nuclei, and neutron-deficient hafnium radionuclides produced in the Oak Ridge Isochronous Cyclotron (ORIC) by (α, xn) reactions were investigated. The use of lithium-drifted germanium diodes for such decay-scheme studies and the effect of spectrometer live time on precision were evaluated. A ^{137}Cs standard was assayed in connection with an interlaboratory comparison conducted by the International Atomic Energy Agency. An absolute determination of ^{125}I by the sum-coincidence method was made. A gamma-spectrometric determination of ^{232}U was developed and applied. New half-life values were obtained for ^{76}As, ^{137}Cs, ^{140}La, and ^{232}U. Trialkyl- and hexaalkylphosphorothioic triamides and metal di-*n*-butyl phosphorodithioates were studied as extractants for metals. Trivalent actinides were separated from lanthanides by liquid-liquid extraction with tricaprylmethylammonium thiocyanate. Technetium was separated by cyclohexanone extraction and determined by beta spectrometry. Cellulose column chromatography was used to separate trace quantities of 13 metals from uranium. Separation of tellurium isomers in different chemical media was studied; work continued on the determination of krypton and xenon fission yields from uranium. Studies relative to ore selection for Project Coach were made. A search for a naturally occurring transuranic radionuclide proved to be unsuccessful. Two new liquid scintillators, 1-methylnaphthalene and *N,N′,N″*-trimethylborazine, were studied. A liquid-scintillation method for absolute counting of beta emitters was developed. Several different computer techniques were applied to the resolution of gamma-ray spectra.

A radioactivity-release method was developed for the measurement of sulfur dioxide in the atmosphere. Radiotracers were used to study and to improve analytical procedures for sodium, lithium, and phosphorus. The problem of separating sodium from activated samples received continuing attention.

In applications of activation analysis to forensic problems, ammunition primer and gunshot residues, as well as hair and paper, were studied. Trace-element nutritional investigations in humans and animals were made, and a number of unusual samples, both biological and chemical, were analyzed. Analyses for trace elements in uranyl nitrate solutions and in high-purity Be, Al, and Fe were made by neutron activation. In addition, isotopic neutron sources were used for the analysis of organoboron compounds and high-cross-section materials in reactor fuel elements.

A rapid method of calculating the output spectra from the 14-Mev neutron generator was formulated; a catalog of 14-Mev neutron reactions for the elements having atomic numbers from 3 through 30 was prepared. Work on fast-neutron cross sections for titanium continued. An improved sample-irradiation and sample-handling system primarily for the determination of oxygen was designed. The neutron generator has also been used for the analysis of a number of materials and for the evaluation of neutron yields from experimental targets. Excitation functions and other nuclear data were gathered from experimental runs made with the 5.5-Mev Van de Graaff accelerator with ^{3}He particles; the potential usefulness of such procedures in activation analysis is being investigated further.

RADIOISOTOPE APPLIED RESEARCH

The purpose of the Radioisotope Applied Research Program is the preparation of radioisotopes useful in medical and research applications and the development of criteria for the recovery,

purification, and characterization of the preparations. The desired characteristics of radioisotope preparations such as half-life, purity, and specific activity are often so diverse that the needs can best be met by making available a spectrum of isotopes for a given element. The program is made more effective by maintaining a close liaison with workers in the physical and biological sciences to learn of their varied and unique requirements. The production facilities used are principally the Oak Ridge Research Reactor (ORR) and the ORNL 86-Inch Cyclotron.

Reactor-Produced ^{33}P

Millicurie quantities of 25-day ^{33}P were produced by the $^{36}Cl(n,\alpha)^{33}P$ and $^{33}S(n,p)^{33}P$ nuclear reactions for the first time. Potentially important uses for this radioisotope include autoradiography, studies of recoil energy, synthesis of complex organophosphorus compounds, and double labeling (together with ^{32}P) of phosphorus in complex molecules.

The reactor production of ^{33}P was made possible by the availability of enriched targets of ^{36}Cl [produced by the $^{35}Cl(n,\gamma)^{36}Cl$ reaction] and ^{33}S separated by the ORNL calutrons.

Radioisotope Generators

Radioisotope generator systems are particularly useful in medical diagnosis, treatment, and research work. Short-lived radioisotopes can be chemically separated from long-lived parent isotopes fixed on an ion exchange matrix, in the user's laboratory, thus eliminating the necessity for special production and shipping arrangements. Repeated separations or "milkings" of the daughter activity can be made throughout the useful life of the parent activity.

Successful generators were developed for 2.8-hr ^{87m}Sr, 6-hr ^{99m}Tc, and 1.7-hr ^{113m}In. Strontium-87*m* was separated from 80-hr ^{87}Y adsorbed on Bio-Rad AG-1 anion exchange resin by elution with 0.01 *M* $(NH_4)_2CO_3$ solution. Technetium-99*m* was separated from 67-hr ^{99}Mo adsorbed on Bio-Rad HZO-1 exchanger by elution with methyl ethyl ketone containing 5 vol % 0.01 *M* HCl. Indium-113*m* was separated from 118-day ^{113}Sn adsorbed on Bio-Rad HZO-1 by methyl ethyl ketone containing 5 vol % 0.01 *M* HCl. The product radioisotope from each of these generators was free of any detectable radioactive contamination.

The (n,γ) Burnup of ^{146}Pm in ^{147}Pm

Promethium-146 is a gamma-ray emitter which occurs in small but significant amounts with ^{147}Pm, which decays entirely by low-energy beta emission. These small amounts (1–5 ppm) are sufficient to cause shielding problems with very large (megacurie) ^{147}Pm power sources. Since the 4.4-year half-life of ^{146}Pm precludes complete decay or decay to negligible levels within a reasonable period in 2.6-year ^{147}Pm, it was desired to determine if the effective (n,γ) cross section were sufficiently large to deplete or reduce the ^{146}Pm content by reirradiating ^{147}Pm products in a reactor. Promethium-146 was produced by the $^{146}Nd(p,n)^{146}Pm$ reaction and irradiated in the ORR with the result that a burnup cross section of about 8400 barns was found, as compared with 230 barns for ^{147}Pm.

Other Radioisotope Production Studies

The yield, separation chemistry, and product characterization were investigated for each of the reactor-produced radioisotopes ^{67}Cu, ^{84}Rb, ^{54}Mn, and ^{109}Cd; similar studies were made on the cyclotron-produced radioisotopes ^{57}Ni, ^{57}Co, ^{7}Be, ^{87}Y, ^{88}Y, and ^{144}Pm.

Computer Programming for Isotopes Calculations

Two computer programs developed to handle reactor yield calculations are ISOTOPES and ISOCRUNCH. Program ISOTOPES was developed to calculate the optimum time of neutron irradiation for maximum yield, the specific activity of the product isotope in curies per gram of target material, and the combined specific activity of the target and product isotopes for any general first-order reaction or decay problem. The program ISOCRUNCH was developed by adding optional programs to the basic CRUNCH code and modifying the input and output data formats. ISOCRUNCH can be used to compute the amount of each isotope

in a reaction and decay chain for any specified neutron flux and time, to sum the contributions of various chains to the same isotope, to plot the yield of an isotope vs time for a given flux, and to find the optimum time for maximum yield of an isotope in a chain.

Cyclotron-Produced Radioisotopes

Target development work for the cyclotron has produced significant improvements in the preparation of ^{44}Ti, ^{55}Fe, and ^{132}Cs. The new targets do not materially increase production rates for these three isotopes, but for ^{44}Ti and ^{132}Cs they now give consistently reproducible results. The ease of fabrication for the modified ^{55}Fe target is an important contribution in the preparation of this radioisotope.

RADIOISOTOPE TECHNOLOGY

The radioisotope technology program includes beta and neutron source development, the preparation of high-specific-activity radiographic sources, improvement of currently used processes, and participation with industrial groups in cooperative test programs which include fueling and testing of radioisotopic power conversion devices.

Carbon-14 Process Improvement

The ^{14}C process was reviewed to determine yields from irradiated Be_3N_2 and the isotopic purity of ^{14}C produced under controlled conditions. The principal ^{14}C compound evolved during dissolution of the Be_3N_2 in H_2SO_4-H_2O_2 solution is methane, which indicates that ^{14}C produced by the $^{14}N(n,p)^{14}C$ reaction in the Be_3N_2 target is in the form of Be_2C. The CO_2, a minor component resulting from stable-carbon contamination, was separated from the ^{14}C methane by scrubbing the gas stream with caustic before the methane was converted to CO_2 by reaction with cobalt oxide at high temperature. Isotopic purity and yield of ^{14}C were greatly improved by this process change.

Xenon-133, Iodine-131 Process Improvement

An improved process was developed for recovery of ^{133}Xe, ^{131}I, and other short-lived fission products. All major objectives for which the process was designed were accomplished, for example, low release of ^{131}I into the plant waste gas system, reduction of ^{103}Ru contamination in ^{131}I product, and reduction in physical size of the plant to allow manipulator cell operation. Irradiated uranium-aluminum alloy targets dissolved in NaOH solution yielded a supernatant containing over 90% of the ^{131}I. This solution, when acidified with H_2SO_4, is sparged with air to produce elemental iodine for a primary separation from the radiochemical impurities in the solution. Final purification is accomplished by selective sorption of ^{131}I on platinum followed by desorption into a product solvent.

Krypton-85 Enrichment System

The installation of a thermal diffusion facility for isotopically enriching ^{85}Kr has begun. The system will have six column assemblies containing 36 electrically heated tubes each, a shielded transfer station, a cooling tower for column heat disposal, and remotely operated valves, pumps, and controls. With feed material containing about 5% ^{85}Kr, approximately 56 days will be required for batch operation through the two cascades to give an annual production rate of 3000 curies of 45% ^{85}Kr or correspondingly greater amounts of lesser enrichments.

Technetium-99 Source Preparation

Oxide-free ^{99}Tc metal was electrodeposited onto various metal foils from a dilute aqueous solution of ammonium pertechnetate containing ammonium oxalate, with a yield of more than 99%. This procedure should be useful for large-scale preparation of ^{99}Tc metal because of high yield, high purity, and simplicity of operation, and for the preparation of beta sources which are useful in the medical profession to coagulate blood and inhibit the formation of scar tissue from keloid-forming material. Examination of metallic deposits

64-10918

No Number

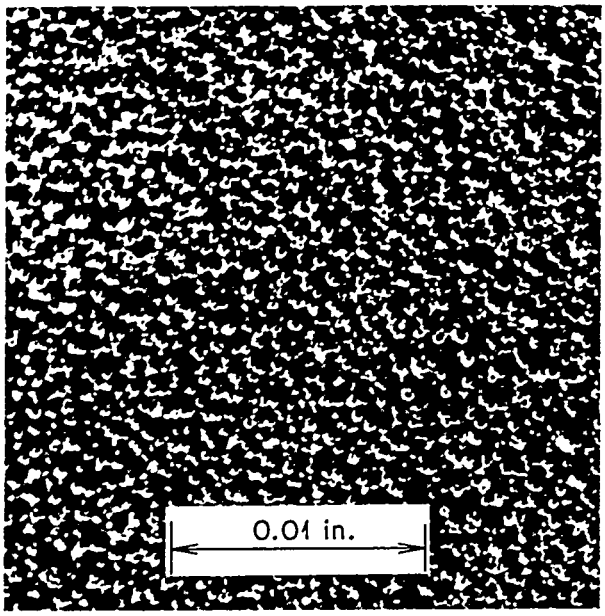

Fig. 1. Photomicrograph of Electrodeposited Technetium-99 on the Surface of Metal Foil in the Form of Microscopic Spheres.

under a 100-power microscope showed that technetium was deposited on the surface of the foil in the form of microscopic spheres (Fig. 1).

Americium-Beryllium-Curium Source

A method for fabrication of neutron sources composed of a mixture of ^{242}Cm, ^{241}Am, and beryllium was developed and tested. This unique system permits fabrication of the source without producing troublesome numbers of neutrons by encapsulating a pressed pellet composed of ^{241}Am oxide and powdered beryllium metal, followed by neutron irradiation in a reactor to produce ^{242}Cm by the ^{241}Am$(n,\gamma)^{242}$Am$(\beta)^{242}$Cm reaction. Neutron yields of 10^7 neutrons/sec have been obtained using 0.010 g of ^{241}Am. Some gamma activity is associated with the neutron yield due to fission products from the ^{241}Am (Fig. 2).

Iridium-192 Sources

High-specific-activity ^{192}Ir radiographic sources were prepared by irradiating thin (about 2-mil) iridium metal ribbons and then fusing them into

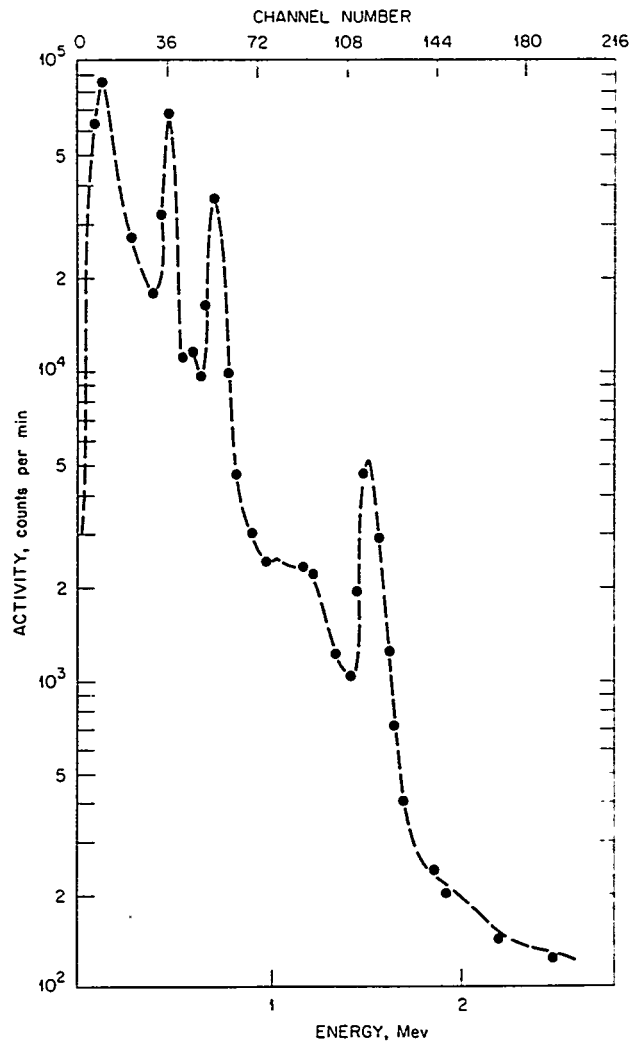

Fig. 2. Gamma Spectrum from 5.13-curie ^{241}Am-Be-^{242}Cm Neutron Source.

spheres about $\frac{1}{16}$ in. in diameter (Fig. 3). Iridium-192 sources with specific activities as high as 800 curies/g have been obtained by this method. Burnup of ^{192}Ir is of greater significance than decay in long-term irradiations to produce high-specific-activity sources; thus the specific activity achieved by irradiation of ordinary pellets in high-neutron-flux reactors is limited by its burnup cross section. By reducing the mass of iridium to thin sections, high utilization of the ^{192}Ir produced at or near the surface of the target can be obtained. Since the radiographic spherical source is formed after irradiation, a homogeneous concentration of ^{192}Ir is obtained in the form of a small point source.

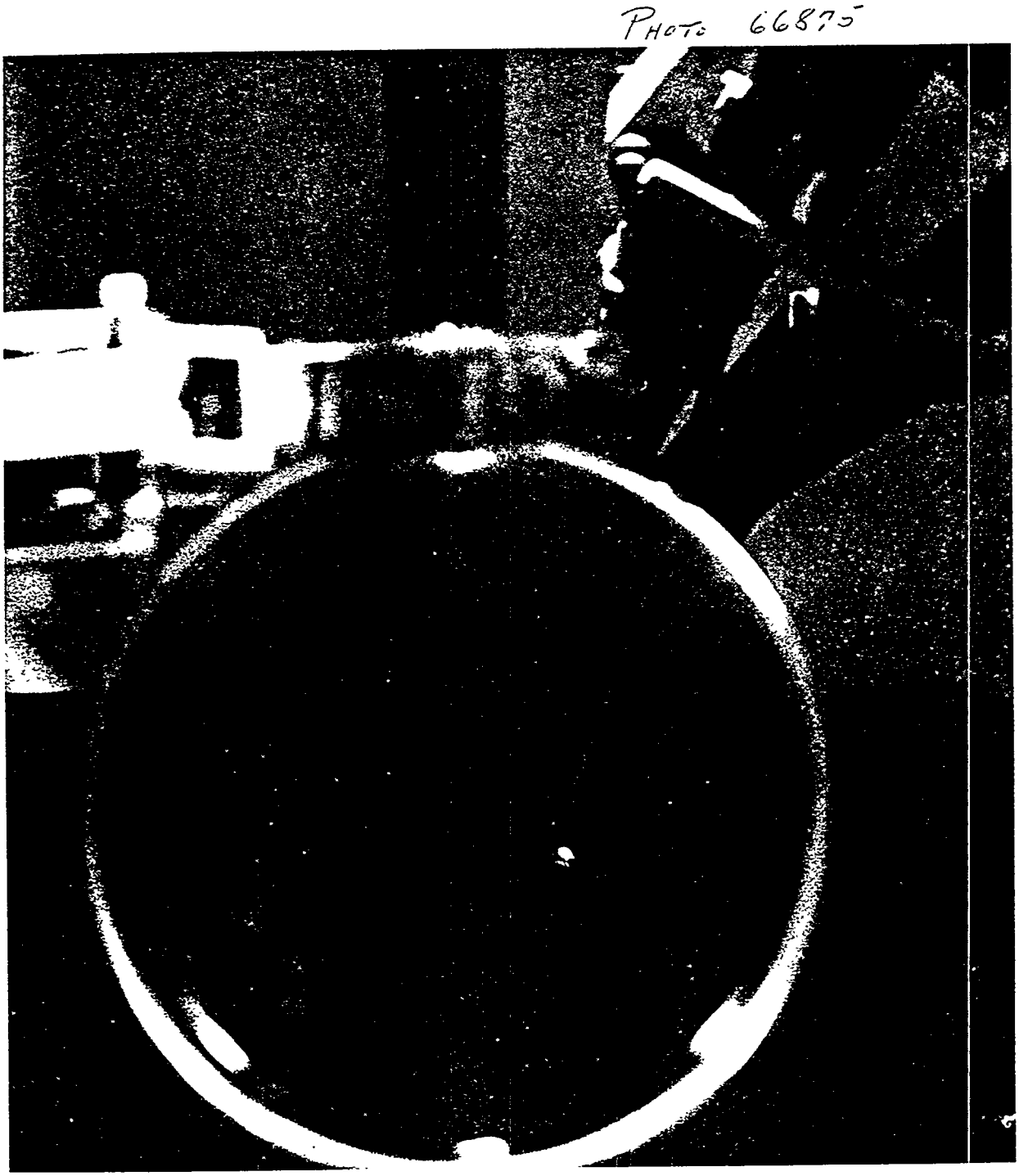

Fig. 3. Iridium-192 Radiographic Source Prepared by Fusion of Irradiated 2-mil Metal Ribbons into $\frac{1}{16}$-in.-diam Spheres.

65-3190 A

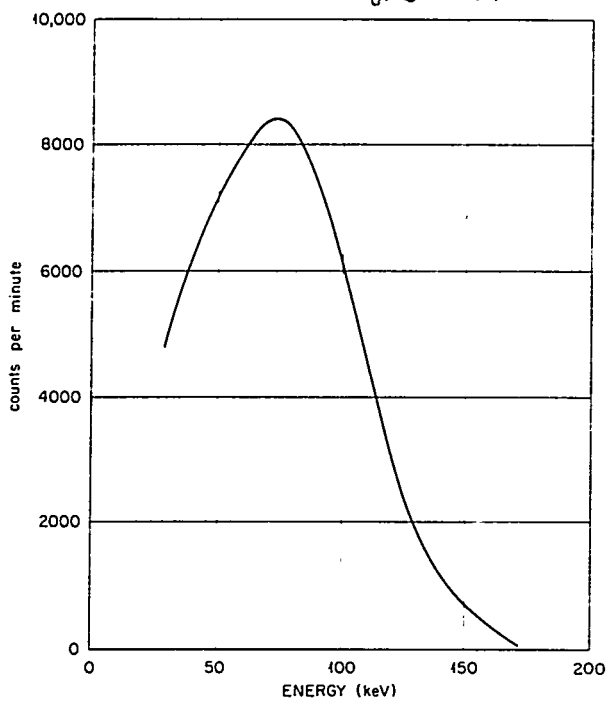

Fig. 4. Energy Spectrum of ^{147}Pm Source Used for Space-Radiation Simulations.

Promethium-147 Source

A 70-curie ^{147}Pm source, to be used in determining the damage to solar cells by 80-kev electrons, was prepared for space-radiation simulations. The source was fabricated by depositing a mixture of promethium oxide and potassium silicate onto a flat magnesium oxide disk about 2 in. in diameter and $\frac{1}{8}$ in. thick. A glass was formed by reacting this mixture at about 1100°C. To reduce smear contamination, a 5-mg/cm^2 Pyrex overlay was fused to the surface. The electron flux above 25 kev was about 4.6×10^{10} electrons cm^{-2} sec^{-1} at a distance of 2 cm (Fig. 4).

Phosphorus-32 Sources

About 200 ^{32}P sources were prepared to be used in a blood irradiator to study the synergistic effect of zero gravity and radiation on white blood cells. Since the experiment was designed for a manned capsule space flight, high-integrity sources were required. These high-integrity sources were prepared by bonding filter paper to platinum plaques and then saturating with ^{32}P solution. After drying, the paper was covered with dilute catalyzed epoxy resin, which dried to form a stable coating.

Simulation of Space Radiation Using the 86-Inch Cyclotron

The 86-in. cyclotron was used for the simulation of space radiation. Determinations of conductivity, temperature dependence, and other physical characteristics of semiconductors were obtained. The cyclotron beam was also used to determine space radiation effects on the human body, yeast cells, and bryozoan eggs.

Cooperative Programs with Industry

A prototype ^{60}Co-powered space vehicle propulsion unit was tested in a hot cell in cooperation with Marquardt Corporation and U.S. Air Force personnel. Heat is produced in heat exchanger plates by absorption of the gamma radiation from 50.000 curies of ^{60}Co metal in the form of 74 fuel pins. The heat is then transferred to hydrogen gas flowing between the plates and exiting through a rocket nozzle. The maximum temperature achieved during the tests was 1280°F under no-flow conditions at the exit nozzle. The fuel pins operated at a temperature only 50° lower than the heat exchanger exit temperature, because of inadequate insulation.

The largest $^{90}SrTiO_3$ pellets ever prepared were fabricated for an RCA thermoelectric generator test device which required 83,000 curies in a single unit. Green pellets 4.06 in. in diameter were pressed from calcined $^{90}SrTiO_3$ powder and sintered at 1400°C. The pressed pellets had diameters of about 3.5 in. and densities averaging 3.8 g/cm^3. Eight pellets were prepared, each containing about 16,000 curies of ^{90}Sr; five of the pellets were used in the final source. The pellets were doubly encapsulated in welded capsules to supply power for the converter. The fuel capsule was loaded remotely into the generator, which operated in a vacuum chamber for more than 1400 hr at a surface temperature of 1100°C. The overall thermal-to-electrical efficiency of the thermoelectric generator was 4.6%; there was no degradation of converter efficiency during the test.

Fission Products Development Laboratory Operations

During 1964, 1,200,000 curies of $^{90}SrCO_3$ was received. The first large-scale shipment (500,000 curies) of ^{144}Ce in the form of mixed rare-earth sulfates was made from Hanford to the Fission Products Development Laboratory in May. A shipment of fission product rare-earth solution containing 49,000 curies of ^{147}Pm was received. A total of 372,000 curies of ^{137}Cs was received in eight shipments of shielded transfer tanks.

RADIOISOTOPE SAFETY

The objectives of the safety testing program are to provide a system for classifying a wide variety of source designs into a few classes according to containment characteristics, to provide quantitative information on containment integrity that can be used by regulatory groups in evaluating licensing requests from manufacturers and users, and to provide a method of evaluating various types of source applications to assist regulatory groups in determining the class of source needed for a particular application. In addition, simple quality control tests are being developed which can be used by source manufacturers.

Source Classification System

The major accomplishments of the program during 1964 have been the completion of the source classification system and a draft of the test procedures for determining the class of a source. Sources are classified according to their ability to withstand requirements based on structural and environmental characteristics. Structural requirements are determined by internal pressure, puncture resistance, crushing force, shear strength, impact force, vibration, and abrasion tests of various degrees. Environmental requirements are determined by operating temperature resistance, operating temperature range, thermal shock range, and temperature-humidity cycling.

One hundred twenty sources representing 37 commercial designs were classified according to the proposed source classification system to determine if sources designed by different companies for similar applications would give consistent results. The trial classification results showed that 70% of the multicurie source capsule designs (teletherapy, radiography, and neutron sources) fell in the class III structural category, whereas 85% of the gaging-type sources, which normally contain less than 1 curie, were in the less demanding class II.

While these results are consistent with the intended use of the capsules, the temperature classes of the sources were less consistent. The same wide variation in temperature resistance of sources intended for similar applications was noted in earlier phases of the source safety testing program when more than 300 sources were tested to obtain values for the source classification system.

Evaluation of Test Methods

The only criterion determining failure of a classification test is the presence of a leak in the source capsule at the conclusion of the test that was not evident prior to the test. A simple leak test has been developed[1] for use with the classification tests and for potential use as a quality control procedure in source manufacture. The source to be leak-tested is immersed in ethylene glycol or isopropyl alcohol and the pressure above the liquid reduced to about 125 mm Hg abs; a leak is indicated by a stream of bubbles rising through the liquid. The sensitivity of the test was determined by preparing a number of calibrated leaks, measuring the hole sizes microscopically, and measuring the leak rates. Under the test conditions described above, leaks as small as 3×10^{-6} cm^3/sec can be readily detected; leaks of 1×10^{-7} cm^3/sec have been detected by subjecting the capsule to a higher gas pressure immediately before the test. The relationship between the leak diameter D, surface tension T of the immersion liquid, and pressure differential ΔP required to initiate bubbling can be expressed by the empirical equation $\Delta P = 4T/D$. Either isopropyl alcohol or ethylene glycol can be used as the immersion liquid because each has a relatively low vapor pressure and surface tension.

[1] C. R. King, *Vacuum Leak Testing of Radioactive Source Capsules*, ORNL-3664 (January 1965).

The vacuum leak test can be used only if there is a free volume in the capsule adequate to support a stream of air bubbles in the event of a leak. The test has been used successfully on samples having free volumes as small as 0.1 cm^3; however, this is considered the minimum volume at which it should be used. In cases where there is not sufficient free space in the capsule for the vacuum leak test, an alternative test can be used. This test involves adding a small amount of an easily soluble cesium or lithium salt (cesium or lithium chloride) to the nonradioactive source compound in the prototype capsule being tested and submerging the source in water in a vessel which is alternately evacuated and vented to atmospheric pressure for a period of 20 min. The water is then analyzed by a photometric technique capable of detecting cesium concentrations as low as 0.003 $\mu g/cm^3$. A soluble radioactive tracer ($^{137}CsCl$, $^{24}NaCl$) can be substituted for the nonradioactive tracer and standard counting methods used for analysis.

ISOTOPES INFORMATION AND QUARTERLY REVIEW

During 1964, the first volume of *Isotopes and Radiation Technology* was completed and three issues of Vol. 2 were published. Approximately 1600 documents and several hundred microfiches were accessioned. In addition, several thousand abstracts were placed on 5- by 8-in. cards for future accessioning. The Termatrex system was inaugurated, and most of the accessioned material has been indexed by punching addresses on the Termatrex cards. The indexed portion is now available for prompt retrieval. The following reports were issued:

ORNL-IIC-1, *Publications on Isotopes at ORNL, 1946–1963*

ORNL-IIC-2, *Production of Calcium-47 with Literature Review of Uses*

ORNL-TM-1047, *Research Materials Coordination and Planning Meeting, November 14–15, 1963*

TID-21620, *List of AEC Radioisotope Customers with Summary of Radioisotope Shipments, FY 1964*

The rough draft of a comprehensive brochure, *Isotopes in Industry*, was written for the AEC as part of their "Understanding the Atom" series. A number of translations of in-scope foreign articles were made available as part of the ORNL translation series. Numerous letters were also written to provide technical information and assistance in reply to letters of inquiry. The AEC Activation Analysis Display was exhibited and manned at four locations. Help was provided in administering the Library of Congress contract for obtaining isotopes information from foreign publications, and about 40 submissions to the *International Journal of Applied Radiation and Isotopes* were reviewed and edited.

TARGET PREPARATION

During 1964, more than 1700 isotope targets and other special materials were fabricated according to customer specification. These were used in sponsored AEC research conducted in the national laboratories, universities, and other organizations as well as for other federal agencies.

Chemical and isotopic purity of targets has been improved by development of ultrahigh vacuum systems, zone refining, electron bombardment vaporization sources, and limited single-crystal growing techniques. Chemical purification of starting materials – particularly evaporants – has been initiated. Pure magnesium, calcium, and rare-earth metals were prepared by distillation techniques. By using appropriate reducing agents such as La, Al, Zr, or Th, milligram quantities of various rare-earth metals were produced at temperatures below 1500°C by distilling the metal directly from a pressed compact mixture of the metal oxide and reductant. The resulting metal vapor could be condensed into thin-film form, polycrystalline "flowers," or even into single-crystal form. These metals varied in impurity levels between 30 and 500 ppm, most containing between 30 and 100 ppm. Since the metal vapor is condensed in a closed system under very high vacuum and the residual gases are mostly nonreactive, very low levels of oxygen, nitrogen, and carbon are contained in the product metal. The very low impurity levels obtained have allowed the rare-earth metals and even magnesium metal to be cold-rolled to thicknesses of less than 1 mg/cm^2.

A new compact heat source for use in target preparation by the vacuum evaporation technique was designed and constructed using electron bombardment of a refractory-metal crucible as the mode of heating. Temperatures in excess of 3000°C were achieved in this manner. By using refractory materials such as W, Ta, Mo, or C, most isotopes could be evaporated; if the particular isotope was incompatible with the crucible metal, ceramic liners were used, for example, BeO, MgO, Al_2O_3, or ZrO_2. When a crucible with tube length greater than internal tube diameter was designed and used, the vapor beam subtended an angle of less than 30° and mechanical vapor collimation resulted. As a result, vapor condensation efficiencies above 90% were achieved; for silicon isotopes (^{29}Si and ^{30}Si) the monetary saving amounted to about $3000 in preparing a 100-$\mu g/cm^2$ self-supporting film 0.75 in. in diameter. Using this technique, ^{252}Cf, as the oxychloride, was evaporated using only a few tenths of a milligram as starting material with condensation efficiencies of 2 to 10%. Further study of this process should result in even better efficiency.

Adaptation of this technique to special fabrications has been made. Cylindrical fission chamber components 2 in. high and 0.75 to 2.00 in. in diameter were coated with $^{239}PuO_x$ with a uniformity of ±10%. A special tungsten boat was fabricated which could be uniformly heated by electron bombardment. For both internal and external coating of the cylinders, the substrate was rotated at 100 rpm during the evaporation of PuO_2. Since PuO_2 evaporates at about 2600°C, electron bombardment offered the only suitable heating technique. Some cylinders were coated to an areal density of 100 μg of PuO_x per square centimeter and others to 1 mg/cm^2.

A special program involving high-energy neutron effects on ecological materials, Project HENRE, was instigated as a combined AEC–Defense Atomic Support Agency program. The ORNL Target Center was requested to fabricate the neutron generator targets to be used in these experiments. Criteria for these targets include capability of generating more than 10^{13} neutrons/sec for four consecutive hours under 150-kev deuteron bombardment; beam power was designated as about 75,000 w during bombardment. Targets prepared in this program were of the reactive metal coating type with tritium gas sorbed into a thin layer of Ti, Er, Y, Zr, or other hydrogen-reactive metals which had been evaporated onto a solid substrate, usually copper. Coatings having areal densities between 1 and 8 mg/cm^2 were evaluated. The results of these studies indicated that 4 mg/cm^2 was the optimum thickness and that titanium or erbium metal was suitable in terms of sorbing appropriate quantities of tritium to reach the desired neutron yield. Because of the greater resistance to thermal decomposition of the erbium tritide, erbium was chosen as the basic material for target fabrication. To date, neutron yields above 10^{11} neutrons sec^{-1} ma^{-1} have been obtained; extrapolation of this yield to deuteron beam conditions anticipated for the Project HENRE accelerator shows that yields greater than 10^{13} neutrons/sec will easily be attained. The accelerator will use a target having an active surface diameter of 14 in. The copper target substrate will weigh about 39 pounds.

Because the neutron yield (proportional to the tritium content of the target) has been found to be highly dependent upon the vacuum levels used during fabrication, all vacuum equipment employs combined titanium-sublimation and ion pumping to attain pressures of about 1×10^{-9} torr. With this type of pumping, residual gases contain inherently smaller amounts of reactive components than in diffusion-pumped systems because of preferential pumping of O_2, N_2, H_2O, CO, and CO_2; hydrocarbons are not encountered in this type of pumping. Similar pumping systems are now being employed in general fabrication of isotope targets to obtain ultrahigh purity.

ELECTROMAGNETIC ISOTOPE SEPARATIONS

The electromagnetic isotope separations facility at ORNL utilizes 40 separators (calutrons) for the isotopic enrichment of both stable and alpha-active materials. The capacity of the facility is 1 to 2 moles/day, depending on the element being processed, and four to six elements can be processed concurrently.

Techniques and equipment were developed which permitted the isotopes of americium to be separated for the first time. A 20-g sample of americium containing 1% ^{242m}Am was processed to yield a 74-mg sample of 20.5% ^{242m}Am. This run also

marks the first time that material having an appreciable quantity of gamma activity (65 curies) has been separated in the calutron.

The tungsten and silicon separations are examples of relatively large-scale process programs which were accomplished. Five pounds of ^{184}W was enriched to over 95% in a program which required the equivalent of six separators operating for one year. Several pounds of other tungsten isotopes separated concurrently with the ^{184}W were supplied for use in an NASA program concerned with the evaluation of the practicability of using enriched tungsten in nuclear reactors. About 90 g of ^{30}Si and 125 g of ^{29}Si were enriched to more than 95%. These isotopes will be formed into single crystals, which are to be used to fabricate lithium-coated silicon barrier-layer detectors for improving the counting efficiency of neutron spectrometers.

The electromagnetic isotope separator is also sufficiently versatile to provide milligram quantities of materials with isotopic purities that would be difficult or impossible to obtain by other separation methods. Approximately 50 mg of 70% ^{33}S was separated and has been irradiated in a reactor to prepare a sample of ^{33}P which will be relatively free of ^{32}P. Phosphorus-33 is useful in fundamental biological radiation-effect studies on viruses and microorganisms. Another important separated isotope, ^{196}Hg, is irradiated to produce ^{197}Hg, which is being used in research in the early identification of brain tumors.

Ion-bombardment techniques were developed for preparing specimens and targets by direct deposition in the calutron. This method permits mass separation and implantation in crystals or semiconductors in a one-step process under high-vacuum conditions so that chemical and isotopic contamination are minimized. Single-crystal silicon semiconductors with excellent junction characteristics were produced by implantation with phosphorus ions.

Studies of plasmas in a magnetic field resulted in the design of beam stabilizing plates which are mounted within the calutron tank. This development made possible a two-arc separation system which doubled the separation rate and greatly improved the mass separation previously attained for tungsten isotopes.

Improved magnetic focusing systems were developed for improved mass separations. A prototype 255° double-focusing isotope separator was found to give significant improvement in isotopic purities over those obtained in the standard calutron at the same production rate. As a further step toward improved isotopic purity, a 180° sector separator with a field inhomogeneity of 0.8 is being designed. The beam currents in this system will be low compared with the calutron, but the dispersion will be five times that of the calutron. These features make the separator desirable as a basic machine in the development program for the processing of the transplutonium elements and gamma-emitting radioisotopes.

Manipulator Cells in the Fission Products Development Laboratory.

Photo 43917

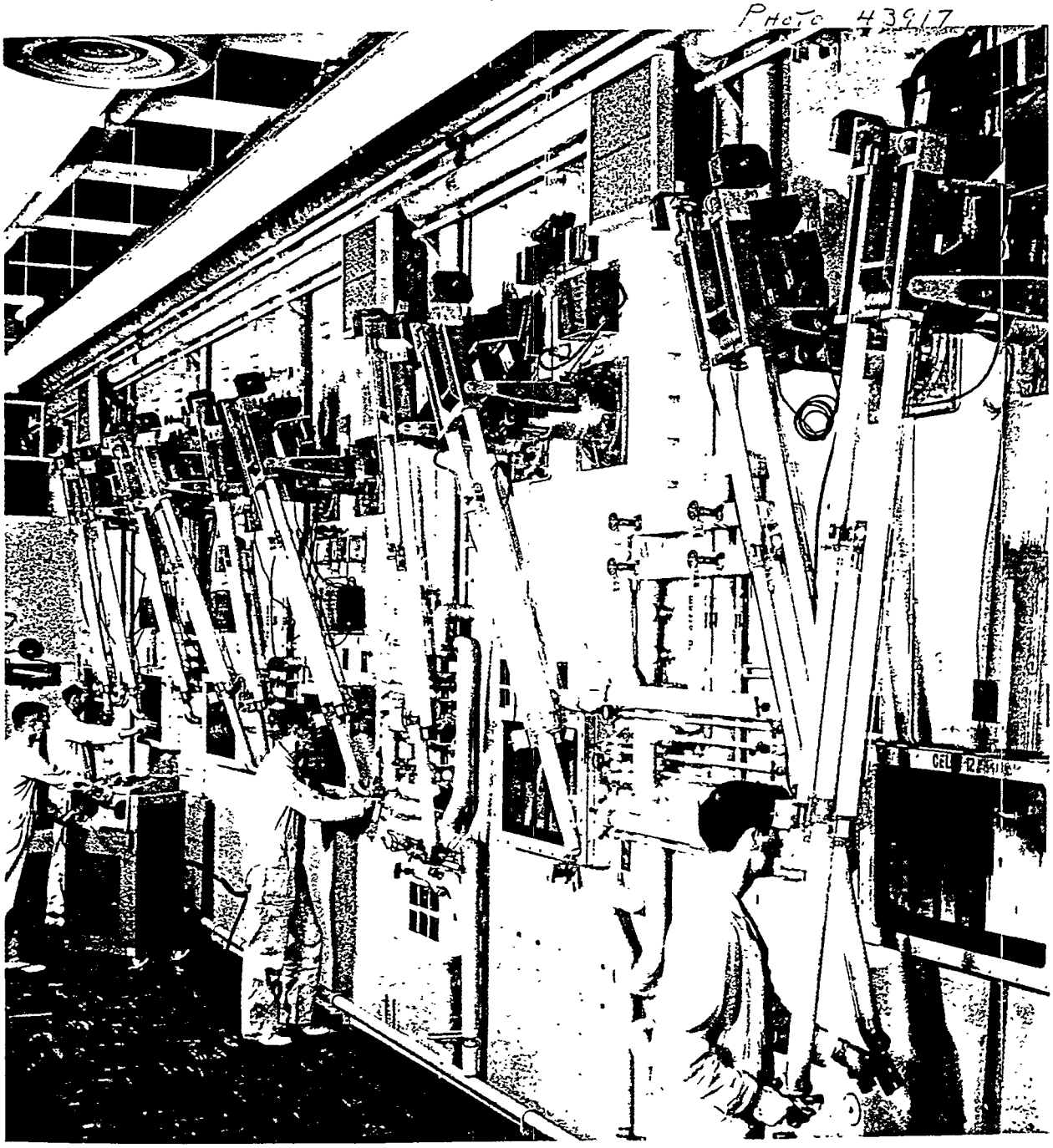

ART WORK – NO NUMBER

TRAINING, EDUCATION, AND INFORMATION

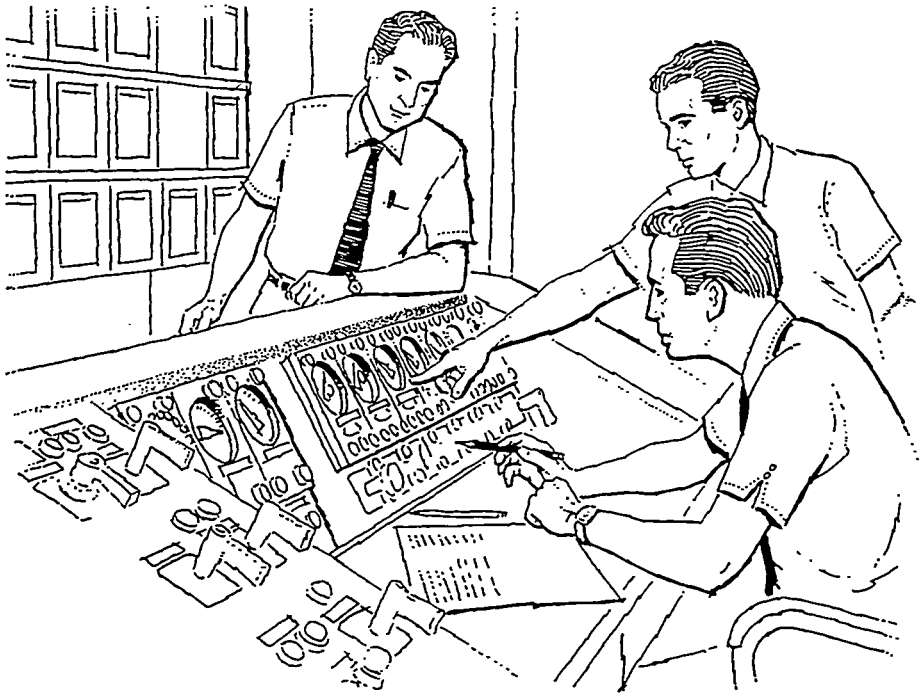

UNIVERSITY RELATIONS

University Relations activities at the Laboratory include several programs conducted in cooperation with the Oak Ridge Institute of Nuclear Studies. The Research Participation and Traveling Lecture Programs were established in 1950 to assist universities to expand the scope of training offered to undergraduate and graduate students and to stimulate in universities research which is of interest to the atomic energy program.

During 1964, 51 university faculty members spent the summer months at the Laboratory as Research Participants receiving advanced research and engineering experience in the sciences and arts associated with atomic energy. Participants were selected from applications submitted through ORINS on the basis of anticipated benefit to both the applicant and his home university and upon the available facilities and supervision at ORNL. A total of 39 institutions were represented under this program during 1964. In addition to the Research Participants, 35 other university faculty members were employed at the Laboratory as a part of the regular summer program.

Under the Traveling Lecture Program, Laboratory staff members deliver lectures before undergraduate and advanced university groups upon request as a part of the Commission's program of encouraging the dissemination of scientific and technical information. More than 80 speakers from the Laboratory visited 112 institutions during 1964, presenting a total of 250 lectures.

Oak Ridge Graduate Fellows at the Laboratory during 1964 numbered over 30. These Fellows, supported by ORINS, were assigned at the Laboratory to conduct thesis research, for the most part leading to the doctor's degree. Six AEC Postdoctoral Fellows, supported by ORINS-AEC funds, were at the Laboratory during 1964.

PHOTO 65815

Fig. 1. ORINS Trainee Assisting ORNL Chemist in X-Ray Diffraction Study.

OAK RIDGE SCHOOL OF REACTOR TECHNOLOGY

FORMAL PROGRAMS AT ORSORT

The Oak Ridge School of Reactor Technology is the primary function of the Education Division and provides training for four educational programs: Nuclear Reactor Operations Supervision, Nuclear Reactor Hazards Evaluation, Nuclear Engineering for AEC Employees, and Nuclear Engineering for AEC Contractor Employees.

The programs in Reactor Operations Supervision and Reactor Hazards Evaluation support the Atomic Energy Commission's efforts to assist foreign countries in training personnel. Seventeen students representing eight foreign countries completed their programs of study in 1964. The countries represented were Belgium, China, Greece, Germany, India, Italy, Japan, and Pakistan. Following the initial nine months of class work, the students in Operations Supervision spent three months participating in the Laboratory's reactor operations. This consisted of instruction by the operating personnel and personal experience with many of the problems of operation supervision. The Hazards Evaluation students worked in small groups under the guidance of senior Laboratory staff members and prepared a "Critical Review of Twenty-three U.S. Power Reactors," which is now being published as an ORSORT report. Both programs terminated on September 11, 1964. Seventeen students representing nine foreign countries enrolled in ORSORT programs on September 24, 1964. Countries represented were Australia, Japan, India, Israel, Netherlands, Pakistan, Philippines, South Africa, and Turkey. Their programs will end on September 10, 1965.

The ORSORT training programs used by the AEC to train Commission and Commission-Contractor employees include the AEC Nuclear Engineering Trainee Program for recent graduates, the AEC Inter-Discipline Professional Development Program for experienced employees, and the Nuclear Engineering Training Program for contractor employees. With the increased emphasis on nuclear operational safety within the AEC and with its requirement for trained personnel, the programs – especially the Hazards Evaluation course – are quite applicable to the Commission's training requirements. Twenty-four AEC employees and twenty-eight employees of Union Carbide completed courses in June 1964. Ten AEC employees and twenty-five Union Carbide employees enrolled for courses in September 1964.

Other government agencies make use of the programs at ORSORT to meet training requirements for their nuclear programs. These agencies include the Department of Health, Education and Welfare, the Department of Defense, and the National Aeronautics and Space Administration. Three students from the Defense Department and one from the National Aeronautics and Space Administration attended ORSORT programs in 1964.

ASSISTANCE TO EDUCATIONAL INSTITUTIONS

In addition to the formal programs at ORSORT, the Education Division conducts or supports several other activities which provide opportunities for university faculty and students to obtain training and experience of direct benefit to the individual and his institution. These activities include: (1) Summer Institutes on nuclear energy for engineering college faculty members, sponsored jointly by the American Society for Engineering Education and the Atomic Energy Commission, (2) the Nuclear Reactor Technology Training Program for university faculty members, (3) providing support for the ORNL-ORINS Summer Institute programs, and (4) conducting a program of reactor experiments for the senior class of nuclear engineering students at the University of Tennessee.

The 1964 ASEE-AEC Basic Summer Institute at North Carolina State College was given for eight weeks beginning June 29 and ending August 16, 1964. Twenty participants spent the last week of this period at ORSORT. The ORSORT work consisted of a series of experiments and lectures in instrumentation and controls and physics (including a criticality experiment at the Pool Critical Assembly), tours, and reports of their experiments.

Under the Nuclear Reactor Technology Training Program for university faculty members, ORNL accepts faculty members for one-year training programs at ORSORT. Participants of the program select courses in the standard curriculum and utilize the same facilities that the ORSORT faculty does. One faculty member from the University of Idaho completed the program in September 1964.

The ORNL-ORINS Summer Institute for physics teachers assists in the development of college courses, including laboratory experiments, devoted to the teaching of the principles and applications of nuclear energy and its associated fields of study. The Summer Institute for Discussion of Science in Society is designed to stimulate discussion among university faculty members of contemporary questions raised by modern science, with particular emphasis on nuclear science and technology. Forty-five participants, each representing a different college or university, participated in these Summer Institute programs in 1964.

A continuing cooperative effort between ORNL and the University of Tennessee has been worked out. It consists principally of providing computer time and arranging for access to critical assemblies and other unique equipment at ORNL for conducting a series of ORSORT-type experiments. The program will be expanded to include provisions for office space at ORNL for a University faculty member as a coordinator, use of research facilities, services by technicians and craftsmen, and a modest set of equipment. Twenty-two University of Tennessee students and three instructors participated in a series of reactor experiments during 1964.

Table 1. Activities of the Education Division

Classification of Students	Man-Months of Training	
	Fiscal Year 1964	Fiscal Year 1965
In-house		
ORNL scientists and engineers	119	126
AEC scientists and engineers	240	93
Subtotal	359	219
Foreign		
Students (participants)	192	184
Subtotal	192	184
Industry and other agencies		
Scientists and engineers	48	28
Subtotal	48	28
Educational cooperation		
Faculty at ORNL	22	15
Students at ORNL	6	4
Subtotal	28	19
Grand total	627	450

INFORMATION CENTERS

The ever-increasing volume of technical information is rapidly approaching the level of saturation for the individual scientist and engineer. In the past, abstract journals, monographs, and specialized reviews have been used as tools for coping with the voluminous output of technical information. Another tool, the technical information center, is not exactly new but has acquired considerable importance during the past few years; in particular, it received authoritative support from a panel of the President's Science Advisory Committee.[1] This report urged that more and better specialized information centers be established.

As befits its character as a large multipurpose institution, the Oak Ridge National Laboratory has provided a home for a number of such information centers. In several cases the initial impetus for the establishment of the centers was given by technical journals and reviews edited at the Laboratory. Other centers grew out of the more or less personal collections of individual experimentalists, who tried to organize the continuing stream of experimental data in fast-growing fields.

In order to ensure the high professional level of the centers, only areas in which the Laboratory has special technical competence are selected. Each information center is supervised by one of the research divisions of the Laboratory, and the staff includes active research workers whose main job assignment lies in theoretical or experimental studies in their chosen fields. In addition, each of the centers is backed up by other members of the division, who might be called on whenever the need arises.

The great variety in the backgrounds of the centers has resulted in the selection of a broad spectrum of storage and retrieval tools. The methods used include manual systems based on file cards containing an abstract or an extract of the material together with keywording; computer-operated storage and retrieval systems; optical coincidence methods; and automatic retrieval of the material contained on microfilm by means of photoelectric cells.

There is a certain amount of marginal overlap between the scopes of the centers; this is unavoidable, and it is not necessarily undesirable. The information center managers are aware of the coverage of fields of interest by their colleagues. The basic philosophy is that it does not matter who collects the information and who maintains the files as long as the potential recipients of the inquiries for a given subject know where they can find the most up-to-date answer.

The centers collaborate closely when considering the purchase of new hardware. The Termatrex system used by one of the centers is shared by others whose volume does not yet justify the purchase of equipment; similar cooperative arrangements will be made with the newly purchased Flexowriter. This cooperation is especially marked in the field of computer services. The Central Data Processing facility of the Union Carbide Nuclear Division provides assistance to all the centers who might need it. The personnel of Central Data Processing have acquired considerable proficiency in programming for this particular field, and the software developed for one center may often be adapted for another one with similar problems.

Assistance with the input of material represents another important area of collaboration between centers. The Central Research Library is the chief procurement agency for information, and an experienced professional librarian serves as procurement coordinator for routine accessions of the centers.

With the exception of the Nuclear Data Project, which has been in existence for more than 15 years, most of the information centers have an age of less than 3 years. It is therefore very difficult to estimate their impact on the scientific community. Most of the effort until now has consisted in organizing the activities, recruiting the

[1] Panel on Science Information (A. M. Weinberg, Chairman), *Science, Government, and Information: The Responsibilities of the Technical Community and the Government in the Transfer of Information. A Report of the President's Science Advisory Committee*, U. S. Govt. Printing Office, 1963.

staff, and establishing a pattern for work. Some of the centers maintain a special answering service; in such cases, a definite increase in the number of inquiries has been noted as the centers become better known among the scientists served. In other cases the chief purpose of the center is to collect the material, organize it, and make the compilation available to the technical community.

At the present time there are many efforts to strengthen the bonds between the information centers and the scientific community. This is achieved by preparing exhibits at technical meetings and organizing special symposia on information center programs.

A list of the information centers currently organized at the Oak Ridge National Laboratory is given below:

Information Center	Sponsoring Division	Head
Accelerator Information Center	Electronuclear	F. T. Howard
Atomic and Molecular Processes Information Center	Thermonuclear	C. F. Barnett
Charged-Particle Cross-Section Information Center	Physics	F. K. McGowan
Criticality Data Center	Neutron Physics	A. D. Callihan
Engineering Data Collection	General Engineering and Construction	C. E. Burchsted
Information Center for Internal Exposure	Health Physics	S. R. Bernard
Nuclear Data Project	Director's	K. Way
Nuclear Fuel Technology Information Center	Metals and Ceramics	R. L. Pilloton
Nuclear Instruments Information Center	Instrumentation and Controls	C. J. Borkowski
Nuclear Safety Information Center	Reactor	W. B. Cottrell
Photographic Reference Collection	Technical Information	N. T. Bray
Radiation Shielding Information Center	Neutron Physics	S. K. Penny
Research Materials Information Center	Solid State	T. F. Connolly
Space Materials Information Center	Reactor	H. W. Hoffman
Water Desalination Collection	Director's	K. A. Kraus